Novel application forms and setting mechanisms of mineral bone cements

Dissertation zur Erlangung des naturwissenschaftlichen Doktorgrades der Julius-Maximilians-Universität Würzburg

vorgelegt von

Theresa Brückner geb. Christel

aus Würzburg

Würzburg 2017

Eingereicht bei der Fakultät für Chemie und Pharmazie am

_____

Gutachter der schriftlichen Arbeit

1. Gutachter: Prof. Dr. Jürgen Groll

2. Gutachter: Prof. Dr. Matthias Lehmann

Prüfer des öffentlichen Promotionskolloquiums

1. Prüfer: Prof. Dr. Jürgen Groll

2. Prüfer: Prof. Dr. Matthias Lehmann

3. Prüfer: Prof. Dr. Uwe Gbureck

Datum des öffentlichen Promotionskolloquiums

_____

Doktorurkunde ausgehändigt am

_____

„Tue es oder tue es nicht.

Es gibt kein Versuchen!“

1980 | Krieg der Sterne

Das Imperium schlägt zurück

Content

Abbreviation index

abbreviation	meaning	annexe
1-way ANOVA	one way analysis of variance	
2-HEMA	2-hydroxyethyl methacrylate	
AA	acrylamide	
ADHP	ammonium dihydrogen phosphate	
APS	ammonium persulfate	
BET	Brunauer-Emmet-Teller	
BMP	bone morphogenic protein	
bMSC	bone marrow stromal cells	
BPO	benzoyl peroxide	
BSA	bovine serum albumin	
CaP	calcium (ortho)phosphate	
CDHA	calcium deficient hydroxyapatite	
CPA	calcium polyacrylate	
CPC	calcium phosphate cement	
CSD	calcium sulfate dihydrate	
CSH	calcium sulfate hemihydrate	
DAHP	diammonium hydrogen phosphate	
DCPA	dibasic calcium phosphate anhydrate	monetite
DCPD	dibasic calcium phosphate dihydrate	brushite
DHEPT	N,N-dihydroxyethyl-p-toluidine	
DMEM	Dulbeccos's Modified Eagle's Medium	
e.g.	example given	
ECM	extracellular matrix	
EDS	Energy dispersive X-ray spectroscopy	
EDTA	ethylenediaminetetracetic acid	
EGDMA	ethylene glycol dimethacrylate	
etc.	et cetera	and so on
FDM	fused deposition modeling	
FRCPC	fiber reinforced calcium phosphate cement	
FTIR	Fourier-Transformation infrared spectroscopy	
GIC	glass ionomer cement	
HA	hydroxyapatite	
HPMC	hydroxypropyl methylcellulose	
i.e.	*id est*	which means
JCPDS	The Joint Committee on Powder Diffraction Standards	
KDHP	potassium dihydrogen phosphate	
LB	lysogeny broth	
MBAA	N,N'-methylenebisacrylamide	
MCPA	monocalcium phosphate anhydrate	
MCPM	monocalcium phosphate monohydrate	
MEW	melt electrospinning writing	
MgP	magnesium phosphate	

abbreviation	meaning	annexe
MOC	magnesium oxychloride cement	MOC
MPC	magnesium phosphate cement	
n.a.	not available	
NDHP	sodium dihydrogen phosphate	
OCP	octacalcium phosphate	
PAA	poly(acrylic acid)	
PBS	phosphate buffered saline	
PCL	poly(ε-caprolactone)	
PDF	powder diffraction file	
PEG	poly(ethylene glycol)	
PEI	poly(ethylene imine)	
PEO	poly(ethylene oxide)	
PLA	polylactide	
PLGA	poly(lactide-co-glycolide)	
PLR	powder-to-liquid ratio	
PMMA	poly(methyl methacrylate)	
PS	polystyrene	
RT	room temperature	
SBF	simulated body fluid	
SEM	scanning electron microscopy	
SES	solution electrospinning	
TEGDMA	triethylene glycol dimethacrylate	
TEMED	N,N,N',N'-tetramethylethylene diamine	
TEOS	tetraethyl orthosilicate	
TTCP	tetracalcium phosphate	hilgenstockite
v.	*versus*	as opposed to
VEGF	vascular endothelial growth factor	
VP	N-vinyl-2-pyrrolidone	
XRD	X-ray diffractometry	
α-TCP	α-tricalcium phosphate	
β-TCP	β-tricalcium phosphate	

Symbol index

symbol	meaning	context
Q	flow rate	Hagen-Poiseuille
ΔP	pressure drop	relationship
d	inner diameter	
μ	viscosity	
L	length	
Φ	Lennard-Jones potential	Lennard-Jones potential
ξ, β	constants	
x	distance	
M_t	released drug amount after time t	Higuchi's model
D	diffusion coefficient	
ε	porosity	
τ	tortuosity	
C_S	solubility	
t	time	
A	initial drug amount	
σ_C	compressive strength	compressive strength
F_{max}	maximum force	
A	cross-sectional area	
a	heigth	
b	width	
σ_b	4-point-bending strength	4-point-bending strength &
l_A	span length	modulus
l_B	length of reference bar	
F_{max}	maximum force	
a	height	
b	width	
E	4-point-bending modulus	
F_L	end force of bending modulus calculation	
F_H	beginning force of bending modulus calculation	
X	bar bending	
σ_s	shear strength	shear strength
F_{max}	maximum force	
F_0	stamp net force	
A	cross-sectional area	
d	diameter	

symbol	meaning	context
Φ	porosity	porosity
m_w	wet mass	
m_d	dry mass	
δ	density	
V	volume	
$m_{\%}$	percentual residual mass	mass loss
m_c	current mass	
m_i	initial mass	
l	crystal length	Scherrer equation
k	shape factor	
λ	wave length	
$FWHM$	full width at half maximum	
θ	diffraction angle	
I	net area in 2-component powder with CDHA	quantitative XRD evaluation
I_{100}	net area in 100 % CDHA	
f_{CDHA}	CDHA weight fraction	
M_t	released drug amount after time t	Korsmeyer-Peppas model
M_∞	released drug amount after infinite time	
K	shape factor	
t	time	
n	release exponent	

1. Motivation

According to the opinion of experienced clinicians from trauma and maxillofacial surgery, the market for biomaterials does not provide ideal solutions for the treatment of bone bleeding (bone wax), the fixation of small bone fragments by bone adhesive or complicated fractures that require cement augmentation of the fragments followed by screw osteosynthesis (drillable bone cement) [1]. Either the existing products from synthetic biomaterials do not work properly especially under moist conditions [1], are linked to severe biological effects [2], or the availability of suitable materials is strongly limited. The need for such materials is demonstrated by approximately 2,000,000 surgeries taking place per year to repair defects of the bone tissue in consequence of trauma, tumor or hereditary diseases [3]. Here, autologous bone is considered as „gold standard“ as it is the only replacement material which complies with all main requirements of bone substitution: osteogenesis (a), osteoinductivity (b), osteoconductivity (c) and osteointegration (d) [3, 4] comprising:

a) the formation of new bone [5],
b) the induction of new bone formation also at a heterotopic implantation site [4],
c) the ability to serve as a template for the newly forming bone [5],
d) and the direct contact between native bone and bone substitute without an interface from connective tissue [5].

The limited availability and donor site morbidity due to the need for a second surgery are unavoidable issues of autografts [3, 5]. Thus, synthetic replacement materials represent a promising alternative including all material classes i.e. polymers (e.g. polylactide), metals (e.g. magnesium alloys) and ceramics (e.g. β-tricalcium phosphate) [6]. Besides the above mentioned requirements, synthetic bone grafts should fulfil further demands including biocompatibility, sterilizability, easy handling [7], reproducibility, high availability, cost-efficiancy, a long shelf-life [8] and mechanical properties which are comparable to those of the native tissue at the implantation site [5]. Additionnally, the second generation of biomaterials necessitates biodegradability such that the implant is completely replaced by autologous bone over time [9] without loosening its mechanical integrity [6].

Since their discovery in the 1980’s, calcium phosphate cements belong to the most common bone graft substitutes for non-load-bearing applications. Mechanistically, calcium phosphate cement raw materials dissolve in an aqueous phase and precipitate at supersaturation in relation to the reaction product. As the reaction proceeds, the malleable paste gains rigidity due to the growth and entanglement of precipitated crystals and shows a brittle ceramic-like fracture behavior which is its weightiest detriment [10-12]. Also, the setting reaction starts immediately after mixing of all components which restricts the surgical processing window to few minutes [13]. The essential benefits of calcium phosphate cements are that they are self-setting, freely moldable, biocompatible, osteoconductive [11, 12] and, when hydroxyapatite is the setting product, also their composition is similar to the mineral phase of human cortical bone and tooth mineral [14]. In contrast to its high-temperature equivalent (“sintered hydrox-

[1] Personal communication from PD Dr. med. Stefanie Hölscher-Doht; University Hospital Würzburg, Trauma surgery and Prof. Dr. Dr. Alexander C. Kübler; University Hospital Würzburg, Maxillofacial surgery.

yapatite ceramic"), hydroxyapatite from wet-chemical precipitation is nanocrystalline which additionnally renders it biodegradable to a certain degree, as it might be resorbed by osteoclastic cells, even though not being chemically soluble under physiological conditions [10]. Since few years, a new trend in mineral bone cement's research came up: magnesium phosphate cements. They likewise harden through a dissolution-precipitation reaction, but have a higher degradation potential *in vivo*, exhibit high initial strengths and release biologically valuable magnesium ions among setting and degradation [15]. Currently, mineral bone cements are applied in different forms such as injectable or moldable pastes and putties, as prehardended granular bulk material or in shape of solid macroporous blocks [6].

Some modifications to classic cement formulations have to be undertaken to overcome the issues of their brittleness and the narrow processing time frame. Here, different approaches are possible, e.g. dual setting cements which simultaneously form a hydrogel phase, as well as calcium / (magnesium) binding systems that predominantly form chelate complexes instead of crystalline products and were displayed to be advantageous for the fracture mechanics of the hardened cement [16-18]. The use of premixed formulations, whereat the raw powder is dispersed in a non-aqueous carrier liquid, allows the stabilization of the cement system in its pasty status until the cement is injected into an aqueous environment [19, 20]. Those alternative setting mechanisms are particularly transferable to hydroxyapatite forming calcium phosphate cements [16-20], as they have a long shelf-life, neutral setting and only water is necessary for the setting reaction [12, 21]. Thus, this thesis aimed to achieve the following goals:

1) The application of hydroxyapatite forming calcium phosphate cements in different paste formulations, to generate novel application forms improving handling and biological properties (chapter 3.1; *Calcium phosphate cement based approaches*). For instance, this affects drillable cements which are hardly represented in current literature (chapter 3.1.1; *A systematic study of a drillable, injectable and fast-setting cement system*) or classic bone waxes that presently deal with infection, inflammation and hindered osteogenesis [2] (chapter 3.1.2; *Bone wax from poly(ethylene glycol)-calcium phosphate cement mixtures*). The development of a freely moldable ceramic mat for cranial implantation has not been described so far, but it solves the problem that cements usually need a confining bone structure which actually rules out the treatment of flat cranial defects (chapter 3.1.3; *Prefabricated laminates*).

2) The transfer of the calcium phosphate cement paste design principles to magnesium phosphate cements (chapter 3.2; *Magnesium phosphate cement based approaches*). This step is challenging, as magnesium phosphate cements require a foreign ion source, set at acidic pH [15] and multiconstituent formulations are not storage stable. Presumably, these issues might interact with other ingredients of non-classic paste systems such as dual setting or premixed cements. Though the creation of an adequate receipt (chapter 3.2.1; *Chelate bonding mechanism in a novel magnesium phosphate cement*) and consequently valuable application forms, such as drillable cements (chapter 3.2.2; *In vitro study of a degradable & drillable farringtonite based bone cement*) and bone adhesives (chapter 3.2.3; *A mineral cement for the application as bone and metal adhesive agent*), generated from

a degradable cement, builds the basis of the second part of this thesis. Both application forms represent a niche within the field of mineral bone cements with high novelty.

Table 1 summarizes the developed applications forms, clinical purposes and current issues with assimilable (commercial) products.

Table 1: Novel applications forms which are introduced in the present thesis, their clinical purposes and reasons for the need for further development.

application form	clinical purpose	current issues
drillable bone cement	augmentation of bone fragments treated with screw or plate osteosythesis [22, 23]	only one commercial calcium phosphate cement based product whose availibilty is limited to the US market [2]
bone wax	sealing of osseous wounds (e.g. after sternotomy) [2, 24]	infection, inflammation, hindered osteogenesis of beeswax / vaselin based products [2]; niche application for mineral bone cements
prefabricated laminates	treatment of flat defects (e.g. cranial defects)	thermal conductivity and heat development of commercial treatment approaches [25, 26]; no comparable development in current literature; need of classic cements for a confining, cavity-like, surrounding bone structure
bone adhesive	bonding of small bone fragments [1]	commercial products mostly not well working under moist conditions and non-biodegradable [1]; niche application for mineral bone cements

[2] www.depuysynthes.com/hcp/biomaterials/products/qs/Norian-Drillable-US (11.10.2017).

2. State of knowledge

2.1 Types of mineral bone cements

Mineral bone cements are actually termed “bone void fillers” to distinguish them from poly(methyl methacrylate) (PMMA) based “bone cements” [15]. The latter mostly consists of a 2-component system of organic PMMA powder [27, 28] - technically known from Perspex [29] - enriched with radiopacifier and initiator and a liquid phase from monomer, accelerator and initiator of the polymerization [27, 28]. PMMA bone cements exemplarily enable anchoring of implants and transfer of high loads after cemented total knee or hip joint replacement surgery [27]. As currently no other material compound fulfills the mechanical demands, PMMA cements are widespread in clinical applications such as subcutaneous vertebroplasty, kyphoplasty [28] or the as-mentioned endoprosthetics, though they come along with severe drawbacks. Those include toxic activators, particle abrasion [27], volume shrinkage and extreme heat development while polymerization [27, 28] as well as their not being biodegradable [27]. The exothermic reaction sets free 52 kJ/mol of monomer which locally leads to temperatures of up to 120 °C. This might provoke tissue necrosis in form of collagen denaturation and damaged bone tissue at the cement-bone interface [28]. The release of unreacted monomers can have similar effects [30]. Proceeding tissue resorption can affect the prosthesis such that it fails [31] i.e. in terms of aseptic loosening [28].

Usually, many of the demonstrated disandvantages do not occur with mineral bone cements. These include calcium and magnesium containing phosphate compounds which form a moldable, self-hardening paste among contact with an aqueous solution [10, 15]. Special formulations are even very similar to the mineral phase of bone [14]. Besides common demands for ideal biomaterials, just like biocompatibility [7], reproducibility, cost-efficiency, shelf-life etc. [8], mineral bone cements should further meet the following requirements:

They should be

- injectable for minimally invasive surgery [12]
- cohesive in an aqueous environment to avoid blood clotting
- radio-opaque such that they can be distinguished from the native bone tissue [13]
- setting in an adequate time frame such that the physician is able to prepare and apply the cement before hardening has progressed too far [32].

Even if the brittle mechanical behavior of mineral bone cements stays a relevant issue limiting its usage to non-load-bearing defect sites [15], the present thesis will show, that they offer a lot of other application forms to meet current clinical demands. The following chapter 2.1 will give an overview of two mineral bone cements which are actually interesting for biomedical usage, including calcium phosphate cements, their general characteristics and improvement strategies (chapter 2.1.1) and magnesium phosphate cements as a quite new research field in bone replacement purposes (chapter 2.1.2).

2.1.1 Calcium phosphate cements, general characteristics and improvement

2.1.1.1 Cement formulations and setting principles

Calcium phosphate cements (CPC) were firstly described by Brown and Chow [10, 33] in the 1980's as a hydroxyapatite (HA, $Ca_5(PO_4)_3OH$) forming cement system that is based on tetracalcium phosphate (hilgenstockite, TTCP, $Ca_4(PO_4)_2O$) and monetite (DCPA, dibasic calcium phosphate anhydrate, $CaHPO_4$) (Equation 1) [10, 33, 34].

The reaction mechanisms for all CPC are subject to the following dissolution and precipitation principles [35]: one calcium orthophosphate (CaP) or a blend of more CaP powders is mixed with an aqueous solution [10, 21, 35, 36]. The raw powders dissolve and a CaP with a lower solubility precipitates [10, 36] as a consequence of supersaturation [11, 21] with respect to the reaction product [11]. Crystal growth and entanglement of the resulting CaP provide its mechanical stability [10, 35, 36] and the observed transition from a viscous, moldable paste into a hardened implant enables the application of CPC as self-setting bone void fillers [12]. Solubility phase diagrams may be consulted to predict the resulting precipitation product [11, 37, 38] (Figure 1).

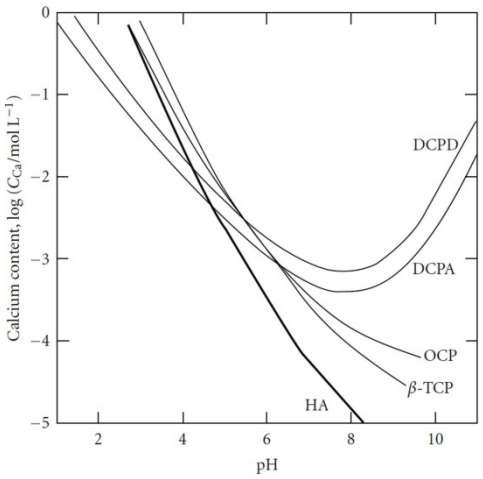

Figure 1: Solubility phase diagram of different calcium orthophosphates reprinted from [38] and adapted. Copyright (2012), K. Kuroda and M. Okido.

Those isotherms (Figure 1) reveal the total amount of calcium in saturated solutions of different CaP with varying pH at constant temperature and pressure. Even if a couple of formulations are known in CPC chemistry, solely two CaP are stable over a broad pH range. At a pH value of <4.2, brushite (DCPD, dibasic calcium phosphate dehydrate, $CaHPO_4 \cdot 2H_2O$) or its dehydrated equivalent monetite (pH <4.4) have the lowest solubility. As monetite sets in an endothermic reaction, the exothermic precipitation of brushite is typically favored [39, 40]. Alterations to the setting reaction can promote monetite precipitation, including low water availability [40], pH [39, 40] and controlled supersaturation by an increased ionic strength [41, 42]. Alternatively, set brushite can be dehydrated e.g. *via* thermal hydrolysis [40, 43, 44]. At pH >4.2, HA is the most stable CaP [11].

Therefore, neutrally setting CPC mainly form stoichiometric HA with a molar Ca/P ratio of 1.67 ($Ca_5(PO_4)_3OH$, $Ca_{10}(PO_4)_6(OH)_2$) or HA derived formulations like non-stoichimetric HA (CDHA, calcium deficient hydroxyapatite, $Ca_{10-x}(HPO_4)_x(PO_4)_{6-x}(OH)_{2-x}$ with $0<x\leq1$ and a Ca/P

ratio of 1.50-1.67) [12, 21] and carbonated HA [11]. The HA forming cement system proposed by Brown and Chow [33] (Equation 1) represents an acid-base reaction between basic TTCP and slightly acidic monetite [12]. Brown *et al*. [45] suggested that octacalcium phosphate (OCP, $Ca_8H_2(PO_4)_6 \cdot 5H_2O$) with a theoretical Ca/P ratio of 1.33 was a precursor of biological apatite [45, 46]. Simultaneously, Fukase *et al*. [47] supposed the transitional formation of OCP during this reaction proposed by Brown and Chow [12, 47], as its precipitation occurs faster [21, 47]. Therefore, the term of OCP forming CPC can be found in early publications as well [21]. Alternatively to acid-base reactions, hydrolysis of a metastable CaP is the existing setting mechanism [12, 21] when the Ca/P ratio is identical for raw powder and precipitate [10, 12, 36]. Exemplarily, mixing α-tricalcium phosphate (α-TCP, $\alpha\text{-}Ca_3(PO_4)_2$) with water forms CDHA whereat both minerals have a Ca/P ratio of 1.5 (Equation 2). The solid phase of such systems is called single-component cement powder [12, 48].

$Ca_4(PO_4)_2O + CaHPO_4$ *TTCP* *DCPA*	→	$Ca_5(PO_4)_3OH$ *HA*	[10, 33, 47]	**(1)**
$2Ca_4(PO_4)_2O + 2CaHPO_4$	→	$Ca_{10}(PO_4)_6(OH)_2$	[12, 21]	
$3\alpha\text{-}Ca_3(PO_4)_2 + H_2O$ *α-TCP*	→	$Ca_9(PO_4)_5(HPO_4)(OH)$ *CDHA*	[12]	**(2)**

In contrast, brushite precipitates at a pH value of <4.2 [21, 33, 35, 37, 47]. All brushite cements set in an acid-base reaction such as the equimolar combination of β-tricalcium phosphate (β-TCP, $\beta\text{-}Ca_3(PO_4)_2$, basic) and monocalcium phosphate monohydrate (MCPM, $Ca(H_2PO_4)_2 \cdot H_2O$, acidic) (Equation 3) [10, 12] which was proposed by Lemaître *et al*. [49]. Alternatively, brushite is obtained by mixing β-TCP with phosphoric acid (H_3PO_4) (Equation 4) [12, 21, 50].

$\beta\text{-}Ca_3(PO_4)_2 + Ca(H_2PO_4)_2 \cdot H_2O + 7\ H_2O$ *β-TCP* *MCPM*	→	$4CaHPO_4 \cdot 2H_2O$ *DCPD*	[10, 12, 21, 50]	**(3)**
$\beta\text{-}Ca_3(PO_4)_2 + H_3PO_4 + 6H_2O$ *phosphoric acid*	→	$3CaHPO_4 \cdot 2H_2O$	[50]	**(4)**

Monocalcium phosphate anhydrate (MCPA, $Ca(H_2PO_4)_2$) instead of MCPM [12, 21, 40, 51] and α-TCP [12, 21, 40] or CDHA [12, 21] instead of β-TCP were successfully applied to form brushite, as well [12, 40]. Both α- and β-TCP have the same chemical composition, but α-TCP is the high-temperature formulation with different crystal structure which makes it more soluble [10, 52]. It is formed when β-TCP is treated >1130 °C [52] and quenched to room temperature (RT) afterwards to avoid reconversion [10]. Table 2 represents the CaP com-

pounds that are most relevant in CPC chemistry including their solubility at 25 °C and corresponding Ca/P ratio.

Table 2: CaP compounds and their corresponding chemical formula, solubility product constants and solubilities at 25 °C and Ca/P ratios. The * labeled CaP cannot be obtained *via* precipitation from aqueous solutions [12, 21, 53].

shortcut	CaP compound	chemical formula	solubility -log(K_{sp})	solubility in mg/L	Ca/P ratio
MCPM	monocalcium phosphate monohydrate	$Ca(H_2PO_4)_2 \cdot H_2O$	1.14	~ 18.000	0.5
MCPA	monocalcium phosphate anhydrate	$Ca(H_2PO_4)_2$	1.14	~ 17.000	0.5
DCPD	dibasic calcium phosphate dihydrate (brushite)	$CaHPO_4 \cdot 2H_2O$	6.59	~ 88	1.0
DCPA	dibasic calcium phosphate anhydrate (monetite)	$CaHPO_4$	6.90	~ 48	1.0
OCP	octacalcium phosphate	$Ca_8H_2(PO_4)_6 \cdot 5H_2O$	96.6	~ 8.1	1.33
α-TCP *	α-tricalcium phosphate	$\alpha\text{-}Ca_3(PO_4)_2$	25.5	~ 2.5	1.5
β-TCP *	β-tricalcium phosphate	$\beta\text{-}Ca_3(PO_4)_2$	28.9	~ 0.5	1.5
CDHA	calcium deficient hydroxyapatite	$Ca_{10-x}(HPO_4)_x(PO_4)_{6-x}(OH)_{2-x}$	~ 85.1	~ 9.4	0<x≤1, 1.5-1.67
HA	hydroxyapatite	$Ca_5(PO_4)_3OH$	116.8	~ 0.3	1.67
TTCP *	tetracalcium phosphate (hilgenstockite)	$Ca_4(PO_4)_2O$	38-44	~ 0.7	2.0

2.1.1.2 Setting kinetics

HA cements have long intrinsic setting times [10, 12, 21] that can be reduced down to 10 to 15 min when the pastes are appropriately modified [10]. Accelerating the setting is possible with an increase in powder-to-liquid ratio (PLR) meaning a reduction of the liquid phase [10, 12, 13] which can impair their injectability [10, 12, 54]. An alternative is the reduction in particle size [13, 55-59] which leads to an enlarged surface area [57, 59] or amorphization of the raw powder *via* high-energy milling which would increase its thermodynamic solubility [55, 56, 58, 59]. The same effect is achieved when acidic components just like phosphoric acid or MCPM [10, 21] are supplemented. Fast accessible calcium or phosphate ions can accelerate initial setting [13, 57] but elongate the total reaction as precipitation is promoted while dissolution is confined (common ion effect) [57]. Soluble orthophosphates such as Na_2HPO_4 [21, 60-63] prevent early precipitation of CDHA on undissolved DCPA surfaces which would segregate the acidic reaction partner and decelerate the quantitative conversion to CDHA [21, 63]. Precipitated HA can serve as seed crystals for an accelerated hydration [13, 57, 60, 64]. Among all these possibilities it should also be mentioned that an increase in temperature from RT to physiological conditions of 37 °C likewise reduces the setting time [13, 60, 62, 65].

In contrast, brushite forming CPC have short intrinsic setting times which vary between few seconds (α-TCP + MCPM) and several minutes (HA + MCPM). Here, the solubility of the basic component is the crucial factor [10, 21]. Sulfate [66-69], pyrophosphate [50, 66, 67, 70]

and citrate ions [66, 71] were shown to have a setting retarding effect on brushite CPC. All three supplements are known to decrease the brushite crystal growth rate [66], but exceeding a critical concentration sulfates form calcium sulfate dihydrate (CSD, $CaSO_4 \cdot 2H_2O$) which act as seed crystals for brushite precipitation [40, 66]. A setting retarding effect is also obtained by addition of α-hydroxyl carboxylic acids such as citric [71-74], tartaric [73] or glycolic acid [72, 73] whereat this concept did not work for hydroxyl group free carboxylic acids [40, 72]. Proteins with carboxylic acid residues or calcium chelating sites have an adsorption and hence setting retarding potential [40] which applies exemplarily to fibrinogen [75]. In a quite new study from 2017, Meininger *et al.* [76] revealed the suitability of phytic acid as setting retarding agent [76]. Phytic acid was shown to form chelates with α- and β-TCP derived calcium ions [77, 78] and to effectively inhibit the crystallization of brushite [79]. Lastly, the substitution of CaP raw powders with strontium [80], magnesium [81] or silicon ions [82] can lead to a prolonged setting, as well [40, 80-82]. Incidentally, the concept of setting retarding supplements also works for HA forming CPC in terms of magnesium [62, 83, 84] and carbonate ions, pyrophosphates [62] or citric acid [85, 86].

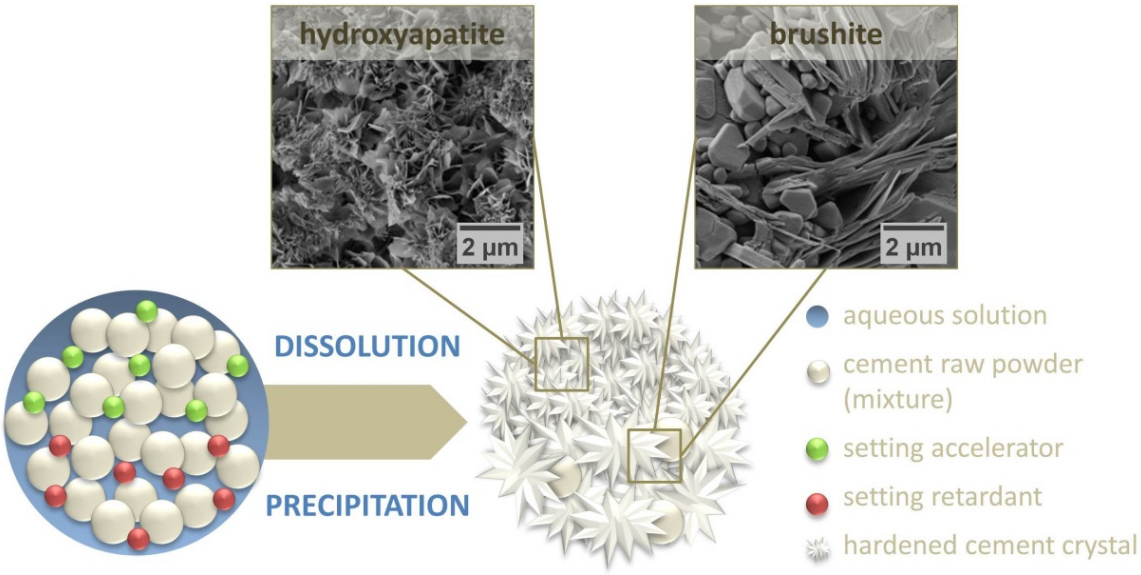

Figure 2: Scheme of a classic dissolution and precipitation reaction of a hydroxyapatite or brushite forming cement system. The scheme shall illustrate the fundamental differences that exist during the setting of hydroxyapatite and brushite what concerns setting time, conversion and crystal size. Scanning electron micrographs are reprinted from [87] and adapted. Copyright (2012), with permission from Elsevier.

HA crystals are generally nano- [11] to submicrometer-sized [10] whereas brushite forms microcrystals [11]. Ferreira *et al*. [88] were able to trace the different phases of brushite formation which is similar to Oswald ripening: larger brushite particles grow at the expense of dissolving low-crystalline HA intermediates [88]. An associated dynamical model was developed by Oliveira *et al*. [89]. Set brushite might be blended with some unreacted β-TCP residues [40, 87, 90] and MCPM was observed to fully dissipate within 20 min [40, 90]. In contrast, HA forming CPC set within a more prolonged time span of >24 h [91, 92]. Fundamental setting differences between HA or CDHA and brushite are depicted in Figure 2. Certainly, the crystallite size of the hardened mineral can be affected as well by different parameters such as setting retardants [40], zinc [93-95], magnesium [93, 94, 96, 97], strontium [94, 98], carbonate [94, 99] and antibiotic [69, 87, 100] supplementation, grinding time of the raw powder [56, 92] or addition of fillers [101].

2.1.1.3 Mechanical properties

CPC typically show a brittle mechanical behavior [11, 12, 21, 37, 102] with small fracture deformation [103], a low fracture toughness [37, 102] and they are noticeably susceptible to tension [12, 21] as crack propagation is eased under this kind of stress [37]. Thus, the tensile or bending strengths are observed to be much lower compared to the corresponding compressive strengths [12, 21, 37]. The application of CPC is therefore limited to low- [37] or non-load-bearing defect care [12, 21, 37, 102] such as cranio-maxillofacial surgery [11, 12, 21, 102] or non-load-bearing orthopedic defect sites [12, 21]. Further crucial aspects are the poor reliability [37] and dependency of the mechanical performance on the surgeon [11, 13, 35]. A combination of CPC with metal implants enables their use in load-bearing defect sites [10, 21]. Zhang *et al*. [37] sketched the correlation between HA and brushite forming CPC in matters of compressive strength [37]. A higher porosity generally results in a lower strength [10, 12, 13, 21, 37, 102, 104] and is mainly caused by the unreacted, excessive liquid phase [102]. Brushite formulations might solely reach a fraction of which is possible for HA systems with comparable porosity [10, 37]. Exemplarily, brushite samples with a porosity of approximately 30 % resulted in compressive strengths of 13 to 23 MPa under wet conditions [71, 105, 106] whereas the values for HA specimens with similar porosity lay between 37 and 131 MPa [107-109]. In brief, a wide range of CPC with compressive strengths in the range of cancellous (4-12 MPa) as well as cortical human bone (130-180 MPa) can be fabricated [37, 110]. Beside porosity and setting product, the final amount of product in the set cement affects the mechanical performance, as well [102].

As already mentioned, a reduction in porosity [10, 12, 13, 21, 37, 102, 104] as well as pore size [37, 111] can improve the compressive strength. Due to the smaller crystal size of HA forming CPC, the pores are usually smaller [102]. A decrease in porosity can be enabled *via* PLR increase [71, 104-106], pre-compaction of the cement to press out excessive liquid [71, 108, 109] or incorporation of fillers [62, 101, 112]. Porosity can further be minimized without pre-compaction for water-consuming cement systems (e.g. brushite) [40, 105], but Bohner *et al.* [54] defined the so-called plastic limit as a minimum amount of liquid which is still necessary to form a workable cement paste [54, 57, 102]. Precursor particle size [55, 56, 113, 114] or setting conditions such as temperature and humidity [60, 62] that lead to a faster conversion can result in smaller crystals and form a more dense crystal texture [37]. Reasons for some additives to control the strength in a positive manner mainly result from the possibility to obtain workable cement pastes in spite of a low liquid amount [37, 71, 73, 85, 108, 109]. The plastic limit might be decreased by either a high surface charge (i.e. zeta potential) to prevent particle agglomeration or by choosing a bimodal particle size distribution such that small particles fill the voids which would elsewise be occupied with excessive water [54, 101, 102]. However, specific setting accelerating agents were observed to impair the mechanical properties [60-62, 64, 115] whereas supplements that decelerate the setting [66, 67, 82, 100, 116, 117] might provoke a more homogeneous microstructure and consecutive ameliorated strength [37]. All those approaches affect the strength but the resulting material is still brittle [102]. Further, some of those strategies are actually non-practicable for minimally invasive treatments (e.g. pre-compaction) and also from a biological point of view (e.g. low porosity).

Table 3: General correlations between FRCPC design options and tendencies/effects on the resulting composite properties. The information below was taken from [103]. The * labeled characteristics might be detrimental for the mechanical outcome of the FRCPC, the ** labeled characteristics are needed for a positive mechanical outcome under the mentioned conditions.

fiber		
volume content	>20 vol.-%:	increase of bending strength
	high:	potential fiber aggregation* & problems with processability (injectability)
aspect ratio	high:	increase of strength & potential fiber aggregation*
	4 to 10 mm:	mostly used length in FRCPC research
orientation & architecture	options:	single fibers, fiber bundles, woven, mesh; random, (an)isotropic
	continuous, aligned:	lower volume content required**
	discontinuous, random:	higher volume content required**
mechanical properties	high elastic modulus:	more load worn by fibers
degradability	often low elastic modulus:	less load worn by fibers*
		time-dependent mechanical behavior
interface		
design & functionalization	options:	form-fit (roughness) or chemical (coating) bonding
	sufficient bonding strength:	proper load transfer between matrix and fiber**
	bonding too high:	potential fiber disruption*
	bonding too low:	potential fiber pull-out*, higher volume content required**
matrix		
compositon & mechanical properties	high toughness:	higher volume content required**
	densification:	increase of binding within interface possible**

Alternative reinforcement strategies are aimed at circumventing the brittle mechanical fracture behavior that is characteristic for classic CPC formulations. Within fiber reinforced CPC (FRCPC) the occurring load is partially transferred to the fibers [103]. Whiskers, i.e. single crystals (e.g. HA [118, 119], SiC [120], silicate [121], carbonate [122]), discontinuous non-degradable (e.g. aramid, E-glass [123], carbon [123, 124], polypropylene, polyamide [124, 125]) or discontinuous degradable fibers (e.g. chitosan [126, 127], poly(ε-caprolactone), PCL [128], poly(lactide-co-glycolide), PLGA [123, 129-137]) as well as continuous fibers (wovens) or fiber meshes (e.g. chitosan [138, 139], PLGA [140-142]) have already been implemented mostly in HA forming CPC [102, 103] whereas brushite forming FRCPC represent an exception [103, 129]. The mechanical performance of the resulting FRCPC is affected by several fiber characteristics such as volume content, aspect ratio (length/diameter), orientation and architecture, mechanical properties (elastic modulus, strength, strain at failure) and degradability. In terms of processability, only the use of short fibers seems reasonable and the fiber volume content is limited as the cement paste viscosity increases with increasing amount. The interaction between fiber surface and cementitious matrix, as well as the mechanical properties of the latter component are also considerable factors [103]. Table 3 reveals some

general correlations between FRCPC design options and tendencies/effects on the resulting composite properties. The work of fracture which is a measure for composite toughness can increase by to two orders of magnitude [103, 141].

The addition of reactive polymers is another approach for the improvement of the cement toughness. The underlying mechanisms are either the incorporation of Ca^{2+} chelating compounds [102] (e.g. polyacrylic acid [18, 143-148]) or the supplementation with monomers that polymerize simultaneously to the dissolving and precipitating of the cementitious phase [102] (e.g. acrylamide [124, 125, 149, 150]). Consecutively, an interpenetrating network of organic and inorganic components is formed. The latter concept was introduced in 1999 by Dos Santos *et al.* [149] as a so-called dual-setting cement system [149]. Both approaches frequently showed their ability to improve the mechanical performance of CPC [18, 102, 143-145, 149, 150] and are discussed in detail in chapter 2.2 dealing with different setting strategies for mineral bone cements. The addition of non-reactive polymers (e.g. collagen [151-153], chitosan [154-156], hyaluronic acid [157, 158], cellulose derivates [159, 160]) is also numerously described in literature, but mainly serves as an improvement of handling and biological properties of the cements [102]. Combinations of reactive [124, 125] or non-reactive [126, 127, 130, 131, 133, 134, 136, 141] polymers with FRCPC systems were yet investigated and partly caused synergistic effects on the composite toughness [133, 141]. Exemplarily, Xu *et al*. [141] showed an increase in work of fracture from 0.007±0.002 kJ/m² for CPC control to 0.092±0.009 kJ/m² for CPC with chitosan alone, 5.29±1.02 kJ/m² for CPC with PLGA fiber mesh alone or 9.77±0.75 kJ/m² for CPC with both chitosan and PLGA, respectively [141].

2.1.1.4 Rheological properties

To benefit from the self-setting character of CPC and for application in minimally invasive surgeries (e.g. vertebroplasty, kyphoplasty), injectability is essential [11]. CPC have been observed to be barely injectable as solid and liquid phase separation (i.e. filter-pressing) might occur [10, 13, 37, 54]. It is important not to confuse injectability with the “ease at injection” [54]. Analyzing the extrusion of a cement paste at a constant low force might lead to the false conclusion that the paste would be non-injectable [54]. Therefore, Bohner and Baroud [54] defined injectability as the ability of a paste not to phase-separate during injection through a needle irrespective of the injection force. Exemplarily, the extruded fraction can serve as a measure for injectability. To facilitate the ease at injection one can make use of so-called injection guns in clinical daily routine [54]. A regular raw powder morphology [161, 162], a bimodal [101] or broad particle size distribution, smaller, de-agglomerated particles [54] and a lower PLR [108, 161-163] can lead to an improved injectability of CPC [54]. An alternative promising approach is the addition of citric acid [71, 85] or citrate ions [71, 108] which adsorb on the CaP particle surfaces to reduce inter-particular attraction due to a high negative surface charge [71, 85, 108]. The addition of viscosity promoting polymers such as lactic acid [154], chitosan [154, 155], glycerol [154], hyaluronates and hyaluronic acid [157, 158, 164] or cellulose derivates [165, 166] has yet been proved to have beneficial effects on handling as a result of CaP particle immobilization [159]. Positive results of an injectability test further depend on distinct setting parameters just like a smaller flow rate Q and needle length L with a major inner diameter d. This correlation is well approximated by the Hagen-

Poiseuille relationship (Equation 5) considering that this law actually applies not to non-Newtonian fluids such as CPC [54].

$$Q = \frac{\Delta P \cdot \pi \cdot d^4}{128 \cdot \mu \cdot L} \quad \textbf{(5)}$$

ΔP describes the corresponding pressure drop in the injected paste and μ the cement paste viscosity. Experimentally, the effects of needle diameter were shown by Burguera *et al*. [163] who observed an 18-fold maximum injection force of 144±17 N when decreasing the external needle diameter from 3.4 (10 gauge) to 0.8 mm (21 gauge) for a HA forming CPC based on TTCP/DCPA and hydroxypropyl methylcellulose (HPMC) [163]. This indicates the crucial role of the needle diameter which is also visible in the Hagen-Poiseuille relationship where the diameter is attended by fourth power. In terms of clinical application, needle sizes up to 10 gauge are realistic [167]. A distinct experimental setup was performed by Habib *et al*. [168] who achieved significant injectability improvements *via* ultrasound supported extrusion [168]. The Hagen-Poiseuille relationship does not simply consider external parameters but also the cement paste viscosity which behaves in inverse proportion to the flow rate. Due to the cement setting, the viscosity (and consecutively flow rate) are time-dependent [169]. The use of premixed CaP pastes is one option to create time-stable injectable cement systems [11]: the liquid phase usually contains non-aqueous liquids that can be water-miscible (e.g. glycerol [160, 170-172], poly(ethylene glycol) (PEG) [172, 173]) or water-immiscible (e.g. synthetic triglycerides [19, 20]). Ideally, the paste does not harden before it is injected into the defect were physiological fluids of the moist environment induce cement setting [35]. The principles of premixed CPC will be reviewed more precisely in chapter 2.2.3. It has to be mentioned that the factors of a suitable injectability might impair other cement properties such as mechanical performance or cohesiveness and *vice versa* [21]. Exemplarily, a decrease of the paste viscosity *via* PLR diminution would favor an enhanced injectability [108, 161-163] and reduce the compressive strength [71, 104-106], while cohesion of the paste in an aqueous environment is promoted for higher viscous cement pastes [54]. According to Bohner and Garoud [54], it is therefore recommended to predominantly use alterations that do not reduce the cement paste viscosity such as the use of viscous polymer solutions [54], especially as too low viscosities result in a defect leakage. An ideal viscosity was found to be in the range of 100 to 1000 Pa·s [174].

Besides injectability, cohesion is a further requirement of CPC for injection *in vivo*. Cohesion is the ability of a cement paste not to disintegrate upon contact with physiological fluids [10, 12, 21, 174] and is described as “washout resistance” / “anti-washout ability” [159, 160, 164, 170, 172, 175-178], “cohesiveness” [160, 170, 179] or “non-decay” [164, 180, 181] in literature. Cohesion is of crucial importance as released CaP particles might be responsible for inflammatory reactions [178] or blood-clotting [182] which is detrimental for the biological outcome of a CPC paste [13, 37]. Bohner *et al*. [183] performed a theoretical and experimental study to predict the effects of different parameters on the cohesion of aqueous non-setting CaP pastes and how they can be altered in a controllable manner.

$$\Phi = \frac{\xi}{x^{12}} - \frac{\beta}{x^6} \quad \textbf{(6)}$$

The Lennard-Jones potential Φ joins attractive Van der Waals with repulsive electrostatic forces between two identical molecules in vaccum (Equation 6) which is likewise adaptive for particles in liquid whereat ξ and β are constants. The equation depicts the inverse proportional dependency of attractive interactions on the particle distance x. Thus, a decrease of PLR might enlarge the particle distance and impair the resulting cohesiveness. An increase in Van der Waals attraction might also be gained with a decrease in particle size. Both predictions could be confirmed experimentally for CaP pastes [183]. Bohner *et al*. [183] further claimed that the adsorption of charged molecules, e.g. citrate ions, on the particle surface would compromise the cohesion due to electrostatic repulsion of the particles. This effect could be proven, as well. However, it has to be considered that the as-mentioned study did not include self-setting cement pastes with time-dependent viscosity and that not every assumption was definitely verified in experiments, e.g. the impact of steric stabilization or osmotic pressure [183].

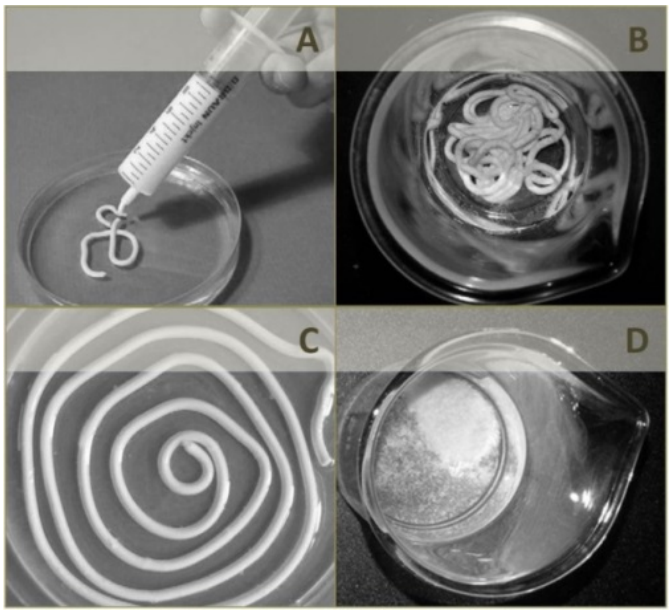

Figure 3: Examples of CPC with adequate injectability and cohesiveness either on the basis of a premixed paste (a, c) or by addition of polysaccharides (b). The as-shown CaP control paste showed insufficient anti-washout ability (d). The photographs a, c and b/d are reprinted and adapted from [20], [19] and [176], respectively. Copyright (2013 & 2015), with permission from Elsevier.

For self-setting CPC pastes, cohesion seems to be mainly associated with viscosity [21]. The incorporation of viscosity increasing polymers (gelling agents), such as cellulose [159, 160, 170], chitosan [159, 170, 176], alginate [180], polylactide [175], hyaluronate [158, 164] or hyaluronic acid [157] and starch [158] in both conventional [157-159, 164, 176, 180] as well as premixed [160, 170, 175] CPC pastes led to an improved washout resistance. The effect of an increased PLR [158] which was anticipated by Bohner *et al*. [183] for non-setting CaP pastes is equally valid for self-setting CPC [21, 158, 184]. In contrast, a smaller particle size elevates the plastic limit [54] and thus the amount of liquid which is necessary for a moldable paste. The resulting cohesion can yet be appropriate [21, 184]. Lastly, the composition of the immersion liquid seems to play a certain role as cohesion was significantly enhanced by using phosphate buffered saline (PBS) instead of water [13].

Pooling both injectability and cohesion adequately seems to be possible with the addition of the mentioned polysaccharide solutions to the pastes which mostly have a thixotropic rheo-

logical behavior. Their viscosity decreases with increasing shear rate which promotes a good injectability and simultaneously preserves an appropriate anti-washout ability when no shear stress is applied [184]. Examples from literature for CPC with suitable injectability and cohesion are depicted in Figure 3.

2.1.1.5 Intrinsic biological properties

CPC are attributed to good biocompatibility and bioactivity [12, 21, 37]. HA forming CPC typically set at neutral pH conditions which is adjuvant in terms of biocompatibility [12, 21] while cement formulations which set at acidic pH might be detrimental [12, 21, 50]. *In vivo* studies of HA-CPC proved that such cements can be implanted without any toxic or inflammatory response, infections, foreign body reactions or connective tissue formation [185-191]. Equally, inflammation or immunogenic reactions did not occur in case of brushite CPC [192], but an excess of β-TCP is conducive, as less protons are released [51]. Higher amounts of the acid reactant as well as final brushite content (>50 to 95 %) were shown to have an adverse impact on biocompatibility *in vivo* [51] including foreign body reactions [187, 193] and fibrous, unmineralized tissue growth [192-197]. Osteoconductive materials operate as templates to direct the deposition of new, native bone matrix [4] at an orthotopic i.e. osseous implantation site [198] which has been frequently verified in animal experiments [188-191, 196, 199, 200]. Some CPC research also shows indications of osteoinductivity [189, 201] which implies bone formation in heterotopic such as subcutaneous and intramuscular tissues [4, 198], but this ability is controversially discussed and might be “intrinsic” (e.g. due to an interconnecting macro- and microporosity) or “engineered” (e.g. due to the incorporation of osteogenic cells and growth factors) [4] (see “engineered biological effects”).

Formerly, implants applied in orthopedics should have stayed permanently at the implantation site but the introduction of tissue engineering and regenerative medicine deals with the full recovery of functional native tissues which is enabled by biodegradable materials [202]. The process of being replaced by newly formed bone is the so-called osteotransductivity [21]. Products of CPC degrade *via* two converse mechanisms: passive and active degradation. Passive degradation occurs by chemical dissolution or hydrolysis of the CaP which mainly depends on its solubility (Table 2) [12, 21, 87, 202], but it must not be confused with a mass loss of the cement specimen caused by cement disintegration [40], especially as Pioletti *et al*. [203] revealed a possible negative impact on the function of osteoblasts caused by CaP particles [203].

By means of the solubility phase diagram from Chow [11] the solubility related degradation rate of different CaP can be estimated as follows at a pH of 7.0:

$$\text{TTCP} > \alpha\text{-TCP} > \textbf{DCPD} > \textbf{DCPA} \approx \text{OCP} > \beta\text{-TCP} > \textbf{HA}$$

In general, CaP are biodegradable when their solubility exceeds the solubility of the mineral phase of bone [10]. In theory, brushite complies with this requirement and an initial resorption rate of 0.25 mm/week was revealed [10, 204]. However, cell-free *in vitro* studies showed that brushite can undergo hydrolysis to form HA [187, 205, 206] or its precursor OCP [206] as a consequence of supersaturation [206] which implies preceding dissolution [205] as illustrated

via Equation 7 and 8 [206]. The as-shown release of phosphoric acid might be detrimental in concerns of biocompatibility [10, 21]. Noticeably, hydrolysis was not seen in case of monetite cements [206] and pure chemical dissolution for brushite was equally observed [187, 207]. *In vivo*, the reprecipitation of brushite as apatite [187, 197, 206, 208], OCP [206, 209, 210] or whitlockite [209] was demonstrated.

$$CaHPO_4 \cdot 2H_2O \rightarrow Ca^{2+} + HPO_4^{2-} + 2H_2O \quad \textbf{(7)}$$

$$10CaHPO_4 \cdot 2H_2O \rightarrow Ca_{10}(PO_4)_6(OH)_2 + 4H_3PO_4 + 18H_2O \quad \textbf{(8)}$$

According to Grover *et al*. [205] different parameters such as immersion fluid composition, liquid-to-cement-volume ratio and immersion protocol (static v. dynamic) inhibit or promote brushite dissolution and HA precipitation *in vitro*. A basic requirement for dissolution to occur is the undersaturation of the immersion fluid with calcium and HPO_4^{2-} ions which was exemplarily the case for large amounts of the immersion fluid under dynamic conditions. These assumptions might be transferred to *in vivo* experiments [205]. For instance, Constantz *et al*. [187] observed differences in HA transformation depending on the implantation site (cancellous v. cortical bone) which was associated with differences in body fluid supply [187]. Hydrolysis can decelerate the resorption rate, as possible reprecipitation products have lower solubilities compared to brushite. Incidentally, the same applies to unconverted β-TCP [40]. Successful confinement of HA formation is realized by the addition of HA setting retarding agents such as pyrophosphoric acid [211], magnesium ions [212] / poorly soluble magnesium salts [208] or when using albumin [213] and serum [205] containing immersion fluids. Boskey [214] gave a survey of several bone and dentin matrix proteins which function detrimentally towards apatite formation [214]. *In vivo*, proteins tend to form complexes with calcium and phosphate ions an thus increase the brushite solubility [208]. An alternative approach is the supplementation with highly soluble calcium sulfate hemihydrates (CSH) [40, 204]. Promoting the setting reaction towards monetite would likewise be beneficial in this context [215] as no phase transformation of monetite was observed both *in vitro* [206, 216] and *in vivo* [217].

The second degradation mechanism for CPC is of active nature and implies cell-mediated resorption. Großardt *et al*. [218] showed that cellular resorption predominated passive degradation on both brushite and monetite surfaces using murine monocyte cell line derived osteoclasts. Those are able to locally decrease the pH value which promotes the solubility of the underlying CaP [218]. *In vivo*, phagocytosis of disintegrated cement particles by macrophages was mainly observed [187, 192, 193, 196] even though osteoclasts are able to resorb brushite cements *in vitro* [218, 219] and it was shown to likewise occur at the implantation sites [192, 196]. Constantz *et al*. [187] asserted that macrophage mediated resorption predominantly took place before brushite reprecipitation as HA [187]. Overall, promising results in concerns of implant resorption and new bone formation in animal experiments are reported [192, 193, 204]. Those are in the range of 52 to 98 % degradation within 12 months [218]. Moderate outcomes were equally observed [196, 209, 210] which was due to occurrent phase transformations into less soluble minerals [209, 210] or maybe derived from the

potential inhibited cell attachment caused by cement supplements such as citric acid [210, 220]. Thus, phytic acid was recently proposed as a possible alternative [76]. Lastly, degradation of brushite is linked to a decrease in mechanical performance [205, 207, 209-211] and mass [205-207, 211] and to an increase in porosity [210, 211]. Thus, degradation and bone growth might be concerted exemplarily *via* slowly soluble β-TCP particles to avoid too fast resorption and thus immature bone growth. The β-TCP then serves as bone anchors [12, 21, 40, 221].

Among all CaP, low-temperature HA is most similar to the mineral phase of bone. In contrast to its high-temperature equivalent, it might have a high specific surface area of >100 m²/g resulting in a higher bioresorption rate [184]. However, cell-mediated dissolution is the only resorption mechanism that is observed for low-temperature HA [6] and the *in vivo* depletion can take several years [10]. Klammert *et al.* [209] emphasized the significance of cell-mediated resorption implanting CDHA cylinders intramuscularly in rats to trail chemical dissolution in the absence of bone cells. After 15 months, the implant area was unaltered [209]. However, even implanting HA in bony defect sites showed no resorption within 8 weeks [200] and merely slight resorption of the outer zones after 3 months or longer time periods of 6 to 10 months whereat the cement bulk was still present [188-191, 199, 210]. In some cases, histological sections demonstrated the presence of osteoclastic cells near the implant border [188-191] but the active *in vitro* CDHA resorption of murine monocyte cell line derived osteoclasts was revealed to be <0.01 % within 13 d [218]. Thus, a crucial factor for an effective degradation is the porosity [184]. If specified, the porosities for HA cement surfaces and implants in the above mentioned examples were in a range of 42 to 50 % [199, 210, 218]. Introducing porosities of 71 to 75 %, a complete critical size defect bridging [222] and degradation of up to 65 % [199] was verified. In a cell-free study at least, degradation rate increased with increasing pore size despite of invariant porosity [111]. However, no obvious effect of macropore sizes was observed concerning the *in vivo* response [223].

Intrinsic microporosity (<10 µm) [36] is mainly controlled by the PLR and enables the flow of physiological fluids through the implant [37]. Besides, the surface area of the implant is increased *via* micropores which promote interactions with ions or proteins [202]. The incorporation of interconnected macropores (>100 µm) [36, 224] further facilitates accelerated cement resorption and substitution with newly formed bone [37], as smaller pores do not allow adequate vascularization and bone cell migration [36] or bone ingrowth [225-227]. Notably, Klawitter and Hulbert [227] revealed a minimum pore size of 100 µm being necessary for bone ingrowth whereas smaller pores between 5 and 15 µm caused the growth of fibrous tissue in calcium aluminate ceramics [227]. Dorozhkin [36] recommended an interconnected network of >60 % macropores (150 to 450 µm) and >20 % micropores [36] and Tamai *et al*. [228] exemplarily showed that cells were able to migrate through interconnecting channels of at least 10 µm in diameter [228].

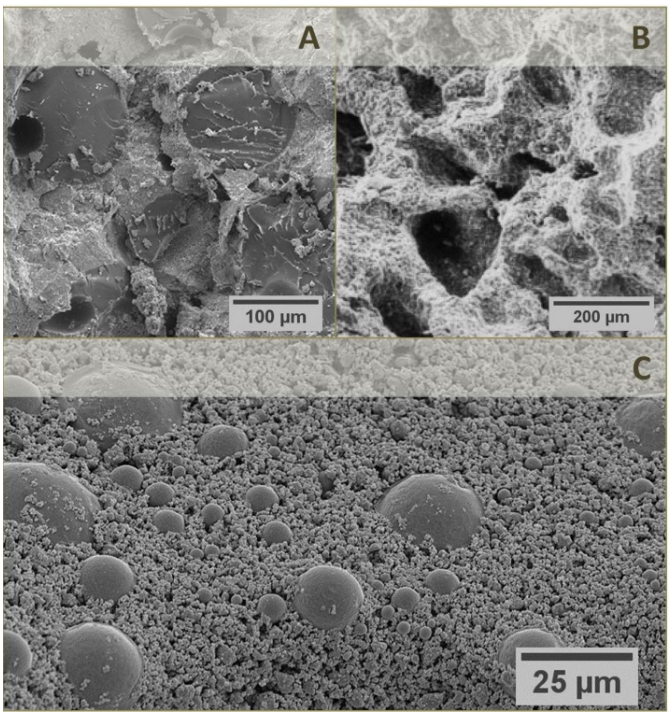

Figure 4: Scanning electron micrographs of CPC with increased porosity *via* porogen leaching (PLGA beads) (a), gas foaming (CO_2) (b) or a mixture of both (c). The micrographs were reprinted and adapted from [229], [230] and [231]. PLGA microbeads were not yet resorbed and still visible in the corresponding figure. Copyright (2009), with permission from Elsevier. Copyright (2007), with permission from John Wiley and Sons. Copyright (2006), with permission from Mary Ann Liebert, Inc.

As already mentioned the PLR belongs to the essential parameters to control (micro)porosity but the liquid component of the cement must not necessarily be exclusively water-soluble. Exemplarily, creating an oil-in-water emulsion by means of surfactant molecules whereat droplets of a hydrophobic liquid (e.g. paraffin oil with sorbitan monooleate) are dispersed in the aqueous cement slurry leads to a macroporous scaffold after hardening [35, 232]. The addition of water-soluble particles also results in the formation of macropores after their dissolution [12, 21, 35]. Highly soluble mannitol crystals [104, 131, 233-236], sucrose [237] and glucose microparticles [179], sodium chloride [111, 238, 239], sodium phosphate salts [237] and frozen solutions thereof [107], as well as carbonates [237] have yet been utilised for porogen leaching of HA forming CPC. Fast soluble porogens lead to poor initial mechanical properties which for resorbable polymer microspheres with longer durability on the basis of PLGA [229, 231, 240-244], gelatin [245, 246] or alginate/fibrin [247] have been implemented, as well. This further offers the possibility to use such fillers for a controlled release of drugs such as bone morphogenic proteins (BMP) [241, 242] or even for cell encapsulation [247]. A major drawback of porogen leaching is the need for high amounts of the soluble substances to ensure interconnectivity [35, 37] which simultaneously was shown to impair injectability [229]. Gas foaming is a well-known alternative to porogen leaching whereat macropores are formed before cement hardening [35, 37]. Common representative gas foaming agents are hydrogen peroxide [248], $NaHCO_3$ in combination with an acidic component [230, 244, 247, 249] or the incorporation of surfactants like polysorbate 80 [207, 250] and proteins with foaming capacity such as albumen [199, 251], gelatin [250] and gelatin/soybean mixtures [252, 253]. To avoid possible damages to the body as a consequence of gas evaporation, Ginebra *et al*. [251] developed a cement system whereat a HA forming cement paste was mixed with a pre-prepared albumen foam [251]. Combinations of foaming agents with degradable mi-

crobeads for an improvement of the initial mechanical performance could also be found in literature [231, 244, 247]. Examples of leached, foamed and mixed CPC scaffolds are given by Figure 4.

2.1.1.6 Engineered biological effects

The existing (intrinsic micro)porosity of CPC enables the admixture of biologically relevant substances (e.g. drugs) [87] or even cells *via* degradable micro-particular capsules [235, 247]. As the cements usually set at room or body temperature, it is not expected that those supplements are damaged thermally, but changes in terms of pH and ionic strengths still have to be considered [87]. Drugs can be dissolved in the liquid phase [69, 254, 255] or added as solids to the powdery phase of the cement paste [105, 256-262]. Schnitzler *et al*. [263] doped their CaP raw powders by mechanical stirring in a drug solution for several days [263]. Some authors describe the encapsulation of drugs in resorbable polymer beads such as PLGA [264, 265] or polysaccharide microcapsules made from pectin derivates [266]. Those are then embedded in the inorganic matrix. This strategy serves to manipulate and retard the drug release which is oftentimes observed to have an initial burst [87, 264, 265]. Most research focused on the incorporation of antibiotics such as gentamycin crobefate or sulfate [69, 254, 255, 259, 260, 265] and vancomycin hydrochloride [105, 256-258, 264]) that are applied prophylactically or for the treatment of specific infectious diseases [87]. At times, the initial release profile of different drugs fitted the so-called Higuchi's model (as specific case of the Korsmeyer-Peppas model) (Equation 9) [87, 255, 266, 267] which was actually introduced for flat geometries with interconnected pores. It is only valid under restrictive conditions such as the initial drug amount A has to be much higher than its solubility C_S and that the drug has to be distributed homogeneously and be much smaller compared to the diffusion distance. Lastly, the matrix or its ingredients must not dissolve. The released drug amount M_t after time t can be estimated as follows [268]:

$$M_t = \sqrt{\frac{D \cdot \varepsilon}{\tau} \cdot C_s \cdot t \cdot (2A - \varepsilon \cdot C_s)} \quad \textbf{(9)}$$

D is the diffusion coefficient, ε the matrix porosity and τ its tortuosity [268]. In case of brushite CPC, cement degradation or recrystallization to form a less soluble CaP might accelerate or decelerate the release kinetic, but especially at the beginning the release of drugs is exclusively diffusion mediated. Diffusion can be controlled by different cement characteristics such as crystallinity, crystal size and porosity, but at the same time these parameters are affected by interactions with the drug itself. Those interactions modulate setting (e.g. in terms of mineralization or crystal growth inhibition) and thus rheological, microstructural and mechanical properties of the resulting mineral [87]. Exemplarily, Bohner *et al*. [66] monitored positive effects on the properties of brushite forming CPC using sulfuric acid as liquid phase. Small amounts of sulfate ions (0-0.1 M) decreased the crystal growth of brushite, thus they prolonged the setting time and promoted a finer microstructure leading to an improved mechanical performance [66]. Substituting sulfuric acid with an antibiotic solution of gentamicin sulfate, they could reproduce their observations, but the effects on the cements microstructure lowered corresponding drug release rates [69].

Beside antibiotics, anti-inflammatory agents (e.g. ibuprofen [266]), drugs against cancer (e.g. doxorubicin [261]) or osteoporosis (e.g. alendronate [262, 263]), growth factors such as BMP [241, 242, 269-272] and other biologically active substances have yet been analyzed in combination with CPC [87]. Ionic modification of CPC is also a crucial topic in terms of engineered biological effects, because numerous ions are elements of native hard tissues and have a proven impact on bone remodeling processes [87]. This includes strontium [80, 94, 98, 273-277], silicon [82, 278, 279], zinc [280, 281], magnesium [212, 282] and antimicrobial active dopings with silver [283] or alkali ions [284]. Table 4 recaps the main function of these ions in bone metabolism and other biological effects, respectively. Their occurrence in human hard tissues is given for comparison.

Table 4: Biological impact of different ions (on bone metabolism) and occurrence in different human hard tissues according to [94]. For comparison, calcium represents 37.6, 40.3 and 36.6 wt.% and phosphor represents 18.3, 18.6 and 17.1 wt.% of human enamel, dentin and bone, respectively.

ion	effect & application	portion in human enamel, dentin & bone
effects on bone metabolism		
strontium	stimulates osteoblast differentiation & inhibits osteoclastogenesis → treatment of osteoporosis [285]	0.03, 0.04 and 0.05 wt.%
silicon	assumed to take part in early bone calcification [286]	n.a., n.a. and 500 ppm
zinc	stimulates osteoblast differentiation & inhibits osteoclastogenesis → treatment of osteoporosis [287]	263, 173 and 39 ppm
magnesium	stimulates osteoblast differentiation & inhibits osteoclastogenesis [288]; inhibits HA crystal growth [289]	0.2, 1.1 and 1.6 wt.%
other effects		
silver	binds to cellular components (e.g. cell membrane) through complexation mainly with phosphor and sulfur donor ligands → antibacterial activity [290]	0.6, 2 ppm and n.a.
sodium potassium	elevates pH as basic products form during setting of sodium and potassium substituted CaP → antibacterial activity [284]	0.7, 0.1 and 1.0 wt.% 0.05, 0.07 and 0.07 wt.%

2.1.1.7 Résumé

A summary of the previous chapter, of general CPC characteristics and how they can be enhanced for clinical applications is given by Table 5.

Table 5: Summary of essential properties of CPC and suitable improvement strategies.

setting time
- PLR
- reactivity of raw powders
  - particle size / amorphization
  - pH
- setting accelerating / retarding effects
  - fast accessible calcium or phosphate ions
  - seed crystals
  - sulfate / pyrophosphate / citrate ions
  - α-hydroxyl carboxylic acids
  - proteins with carboxylic acid residues / calcium chelating sites
  - ionic substitution with strontium / magnesium / silicon / carbonates
- temperature / humidity

mechanical properties
- porosity
  - PLR / plastic limit
  - pre-compaction
  - inert fillers / bimodal particle size distribution
  - water-consuming cement systems
  - pore builders
  - zeta potential
- degree of conversion
- crystal size & microstructure
  - setting kinetic affecting parameters
  - inert fillers
  - bimodal particle size distribution
- temperature / humidity
- user-dependent
- reinforcement strategies
- biodegradability

injectability
- cement paste composition
  - particle morphology / size (distribution)
  - PLR / plastic limit
  - particle interaction
  - citrate ions
  - viscous polymer solutions e.g. chitosan
- experimental setup
  - flow rate
  - needle diameter / length
  - special settings e.g. ultrasonication
- premixed cement pastes

cohesion
- Van der Waals attraction
  - particle size
  - particle distance: PLR
- electrostatic repulsion
  - citrate ions
- viscosity
  - gelling agents e.g. cellulose, chitosan
  - particle size / PLR
  - plastic limit
- composition of the immersion medium

biological properties
- biocompatibility
- osteoconductivity
- osteoinductivity
  - intrinsic (interconnected macro- & micropores) v. engineered (osteogenic cells & growth factors)
- biodegradability
  - phase composition and solubility
  - recrystallization: pyrophosphoric acid, magnesium ions
  - immersion conditions: proteins, body fluid supply
  - porosity: PLR, O/W-emulsion, porogen leaching (e.g. mannitol, sodium chloride, PLGA, gelatin), gas foaming (CO_2, albumen)
  - micropores v. macropores
  - passive v. active
- drug delivery
  - addition to the solid or liquid phase, doping, encapsulation
  - pH or ionic strength alterations might affect biological functionality
  - reciprocal interactions between drugs / proteins / ions and cements
  - antibiotics, anti-inflammatory agents, drugs against cancer and osteoporosis, growth factors (e.g. BMP), ionic modifications (Sr, Si, Zn, Mg, Ag, alkali ions) , stem cell encapsulation *via* microbeads

2.1.2 Magnesium phosphate cements for biomedical applications

Parts of the following section 2.1.2 were reused from the rewiew article M. Nabiyouni, T. Brückner, H. Zhou, U. Gbureck, S.B. Bhaduri. Magnesium-based bioceramics in orthopaedic applications. Acta Biomaterialia. (2017). The article has been submitted and accepted for minor revision, but not published by the time of the submission of this thesis. N. Nabiyouni and T. Brückner hold shared first authorship. Each section and figure from chapter 2.1.2 which correspond to a large extent to parts of the as-mentioned review article were exclusively written by T. Brückner and firstly manifested within the present thesis.

In contrast to CPC, magnesium-based cements are already known since 150 years [291]. In 1966, a specific utilization of magnesium phosphate cements (MPC) as refractory coatings on oven surfaces was proposed by Limes and Pozanti [292]. Since the 1970's, MPC have especially been noted for their application in civil engineering as rapid repair concrete of damaged roads, highways, runways, pavements and bridges or for nuclear waste immobilization [291]. According to a recent review of Ostrowski *et al*. [15], Driessens *et al*. [293] were the first to recognize the feasible potential of MPC to likewise be applied in the biomedical sector [15, 293]. In addition to their high early strength [294], the following characteristics make them superior (or at least equal) to classic CPC:

- The human bone consists of 1.6 wt.% magnesium [94] and 50 to 60 % of the overall magnesium in the body is stored in calcified tissues [295]. It is well known that Mg^{2+} ions influence bone remodeling [87]: Beside the observed enhanced bone regeneration around degradable magnesium alloys [296-298], detailed *in vitro* studies proved the ability of Mg^{2+} ions to stimulate osteoblast differentiation [288, 299] and to inhibit osteoclast formation [288, 300] in a dose-dependent manner.

- The products of MPC have a superior degradation potential to CPC [15]. The dissolution rates of hardened MPC are higher compared to HA forming CPC [301, 302] and their advantage over brushite CPC are the Mg^{2+} ions which should avoid recrystallization into less soluble mineral phases (e.g. apatitic reprecipitates). This could be confirmed *in vivo* [210]. Actually, the addition of magnesium salts to brushite CPC is performed on purpose to prohibit such phase transformations [208, 212].

- Antibiotics are usually incorporated into CPC to provide them with antibacterial properties [87]. In contrast, specific sodium containing MPC formulations were shown to be intrinsically antimicrobial against variable bacterial strains that are related to implant infections (e.g. *Escherichia coli*) [303] or dental plaque (e.g. *Streptococcus sanguinis*) [294]. This feature was mainly ascribed to the basic pH development during setting [294, 303], which was equally the case for alkali doped CPC [284].

- CPC are not known for their bonding ability on bone [1]. In fact, there is only one research article published which deals with promoting the adhesive potential of brushite CPC *via* substitution of orthophosphoric with pyrophosphoric acid [304]. Indeed, MPC were successfully used *in vivo* as adhesives for bone-implant interfaces [305] and tendon-to-bone healing [306]. These results seem quite promising.

2.1.2.1 Cement formulations and setting principles

So far, most of the raw materials for successful MPC compositions are crystalline, such as magnesia (magnesium oxide, MgO) [294, 301, 303, 307-309] and farringtonite (trimagnesium phosphate, $Mg_3(PO_4)_2$) [210, 218, 310-313]. Of late, the use of brucite (magnesium hydroxide, $Mg(OH)_2$) has also been reported (Table 6) [314]. Usually, the crystalline compounds react *via* an exothermal acid-base reaction [315] which is comparable to that of brushite forming CPC [15]. Diammonium hydrogen phosphate (DAHP, $(NH_4)_2HPO_4$) [210, 218, 310-313], ammonium dihydrogen phosphate (ADHP, $NH_4H_2PO_4$) [210, 294, 301, 303, 308, 309, 312], sodium dihydrogen phosphate (NDHP, NaH_2PO_4) [294, 303, 308], potassium dihydrogen phosphate (KDHP, KH_2PO_4) [307, 316, 317] and phosphoric acid (H_3PO_4) [314] among others have already been used as possible reactants for MPC in biomedical applications. The phosphate salts can either be dissolved in the aqueous phase [210, 218, 310-313] or supplemented as solids to the powdery phase [294, 301, 303, 307-309, 316].

Wagh and Jeong [318] clarified the acid-base reaction mechanism of MPC with magnesia as raw powder *via* an intermediate aquosol and gel formation [318]. The dissolution of the phosphate salt results in an initial decrease in pH [319]. Thereupon, MgO dissolves in the acid aqueous environment to form Mg^{2+} and OH^- ions [318], in turn, elevating the MPC paste pH value [319]. This dissolution step is proposed as dissociation of an intermediate brucite mineral as a consequence of the stepwise adsorption of water molecules (Equation 10-12) [315]. Subsequently, the magnesium cations interact with water and generate positively charged aquosols which further react with the dissolved phosphate ions from the acidic reacting agent to hydrophosphate salts (Equation 13-14) and form a gel. With the progress of the reaction, the gel gains viscosity and precipitates as a layer of the final hydration product on the surface of undissolved MgO grains [318] which was confirmed by Ding *et al*. [317] through microscopic observations [317] (Figure 5). The hydration product introduced *via* Equation 14 is newberyite (dibasic magnesium phosphate trihydrate, $MgHPO_4 \cdot 3H_2O$) [15].

$MgO + H_2O$	→	$MgOH^+ + OH^-$	**(10)**
$MgOH^+ + 2H_2O$	→	$Mg(OH)_2 + H_3O^+$	**(11)**
$Mg(OH)_2$	→	$Mg^{2+} + 2OH^-$	**(12)**
$Mg^{2+} + H_2O$	→	$[Mg{\leftarrow}OH_2]^{2+}$	**(13)**
$[Mg{\leftarrow}OH_2]^{2+} + HPO_4^{2-} + 2H_2O$	→	$MgHPO_4 \cdot 3H_2O$	**(14)**

The setting mechanism of MPC is not yet completely understood, but most researchers agree with a dissolution and precipitation reaction as described above [315] still including the work of Neiman and Sarma [320] who described the mechanism through a formation of colloidal structures which assembled on unreacted MgO grains followed by setting initiation [320]. The mechanical stability of the hardened cement is provided *via* mechanical interlocking of the hydration products [315].

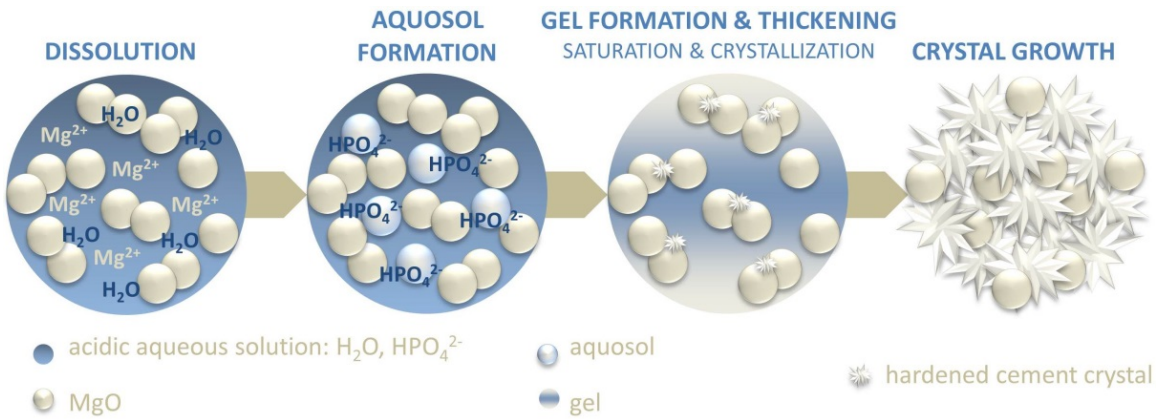

Figure 5: Scheme of the acid-base reaction which underlies the setting mechanism of MPC systems on the basis of MgO. It describes intermediate aquosol and gel formation as proposed by [318].

Using an ammonium phosphate salt (DAHP, ADHP), hydrated ammonium magnesium phosphates such as struvite (magnesium ammonium phosphate hexahydrate, $NH_4MgPO_4 \cdot 6H_2O$) [210, 218, 294, 301, 303, 308-311, 313, 321], dittmarite ($NH_4MgPO_4 \cdot H_2O$) [321], schertelite ($(NH_4)_2Mg(HPO_4)_2 \cdot 4H_2O$) [294, 303, 308] and more seldom hannayite ($(NH_4)_2Mg_3(HPO_4)_4 \cdot 8H_2O$) [312, 321] are formed, among which struvite is the most frequent product [315, 322]. Possible reaction routes for the struvite generation on the basis of either MgO or farringtonite and DAHP are proposed as follows wherein magnesia causes the vaporization of ammonia and farringtonite releases phosphoric acid (Equation 15-16):

$MgO + (NH_4)_2HPO_4 + 5H_2O \rightarrow NH_4MgPO_4 \cdot 6H_2O + NH_3\uparrow$	[15]	**(15)**
magnesia *DAHP* *struvite* *ammonia*		
$2Mg_3(PO_4)_2 + 3(NH_4)_2HPO_4 + 36H_2O \rightarrow 6NH_4MgPO_4 \cdot 6H_2O + H_3PO_4$	[323]	**(16)**
farringtonite *phosphoric acid*		

The utilization of the corresponding primary phosphate slightly alters the above out-pointed stoichiometry [309], whereby with MgO (Equation 15) no ammonia will form and with farringtonite the amount of phosphoric acid (Equation 16) will increase.The substitution of DAHP with the potassium containing equivalent KDHP leads to the formation of K-struvite (magnesium potassium phosphate hexahydrate, $KMgPO_4 \cdot 6H_2O$) [307, 316, 317, 324]. While magnesia based MPC typically show an initial pH drop (phosphate dissolution) with successive pH increase (OH^- release) [319], farringtonite based cements exhibit a continuous pH decrease because of the phosphoric acid side product [210].

As already mentioned struvite is the most frequent setting product of MPC [315, 322] which has mainly to do with the fact that struvite - among all possible products within the MgO-H_3PO_4-NH_3-H_2O system - has the lowest solubility product constant [315]. However, (reciprocal) transformations are possible (Figure 6): Dittmarite can be found as an early intermediate product of struvite formation or when the reaction is very fast [291, 322]. Besides, Sarkar [325] showed that struvite is unstable at temperatures >55 °C and forms dittmarite at ~60 °C in excess water wherein hydration at RT regains struvite [325]. Thus, low amounts of water

as well as the high heat development, followed by dehydration might trigger dittmarite setting [326]. Through precipitation, Frazier *et al*. [327] obtained schertelite and hannayite. Schertelite was highly soluble in water and formed struvite. Similar results were observed after aging in air for several months [327]. Schertelite was further assumed to be an intermediate mineral in struvite formation [291]. Hannayite would also dissolve in water - but more steadily compared to schertelite - and form a mixture of struvite and newberyite. It further represents an intermediate mineral phase during the formation of schertelite when struvite (or newberyite) is immersed in saturated ADHP solution [327]. Conditions, such as heating struvite in dry air results in the loss of water of crystallization and ammonia and might lead to the formation of amorphous magnesium phosphate (MgP) such as e.g. $MgHPO_4$. This phase can be rehydrated to form newberyite or struvite which depends on the remaining ammonium quantity [291, 325]. Using a primary sodium phosphate (NDHP) as reactant is an alternative approach to generate amorphous MgP phases as shown by Mestres *et al*. [294, 303, 308].

$MgO + H_3PO_4 + 2H_2O$ *magnesia* *phosphoric acid*	→	$MgHPO_4 \cdot 3H_2O$ *newberyite*	[318]	**(17)**
$Mg(OH)_2 + H_3PO_4$ *brucite*	→	$MgHPO_4 \cdot 3H_2O + H_2O$		**(18)**

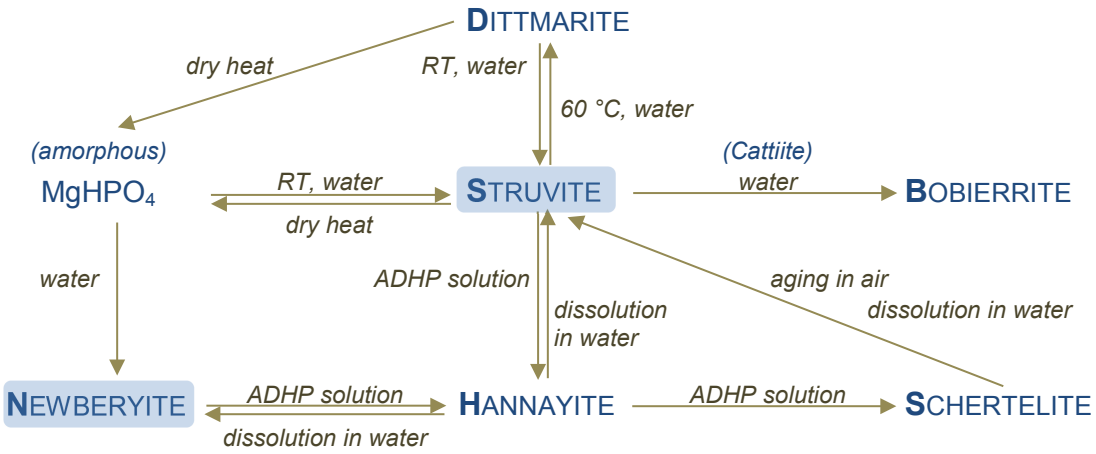

Figure 6: Scheme of the correlations between different MgP within the $MgO\text{-}H_3PO_4\text{-}(NH_3)\text{-}H_2O$ system. The main hydration products struvite and newberyite are highlighted with blue boxes.

Ammonium- and potassium-free hydrated products of MPC comprise mainly of newberyite and to a lesser extent bobierrite (trimagnesium phosphate octahydrate, $Mg_3(PO_4)_2 \cdot 8H_2O$). Both can be found as side products in the $MgO\text{-}H_3PO_4\text{-}NH_3\text{-}H_2O$ system [315, 321]. However, a selected precipitation of newberyite is possible when using phosphoric acid as a reactant with MgO [318, 328] or brucite [314] (Equation 17-18). According to Frazier *et al*. [327], bobierrite is the product of the slow transformation from struvite in water *via* cattiite (trimagnesium phosphate hydrate, $Mg_3(PO_4)_2 \cdot 22H_2O$) [327]. Including ammonium containing compounds in the above mentioned context reveals relationships being illustrated by Figure

6. A summary of the mentioned crystalline MgP phases with corresponding chemical formula and solubility product constants and solubilities at 25 °C is given by Table 6. Comparing the solubilities provides the following chronology:

newberyite > **(K)-struvite** > brucite > cattiite > farringtonite > bobierrite > magnesia

Table 6: MgP compounds, their corresponding chemical formula and solubility product constants and calculated solubilities at 25 °C. The * labeled MgP is metastable in water [329-334].

MgP compound	chemical formula	solubility -log(K_{sp})	solubility in mg/L
bobierrite (trimagnesium phosphate octahydrate)	$Mg_3(PO_4)_2 \cdot 8H_2O$	25.2	1.46
brucite (magnesium hydroxide)	$Mg(OH)_2$	11.2	6.79
cattiite (trimagnesium phosphate hydrate) *	$Mg_3(PO_4)_2 \cdot 22H_2O$	23.1	6.20
dittmarite	$NH_4MgPO_4 \cdot H_2O$	unknown	unknown
farringtonite (trimagnesium phosphate)	$Mg_3(PO_4)_2$	23.4	2.15
hannayite	$(NH_4)_2Mg_3(HPO_4)_4 \cdot 8H_2O$	unknown	unknown
K-struvite (magnesium potassium phosphate hexahydrate)	$KMgPO_4 \cdot 6H_2O$	10.6	78.0
magnesia (magnesium oxide)	MgO	25.0	$1.27 \cdot 10^{-8}$
newberyite (dibasic magnesium phosphate trihydrate)	$MgHPO_4 \cdot 3H_2O$	5.51-5.82	$(1.69\text{-}2.54) \cdot 10^{3}$
schertelite	$(NH_4)_2Mg(HPO_4)_2 \cdot 4H_2O$	unknown	unknown
struvite (magnesium ammonium phosphate hexahydrate)	$NH_4MgPO_4 \cdot 6H_2O$	9.94-13.4	8.38-119

Apart from MPC, magnesium oxychloride cements (MOC) - also called Sorel cements after their discoverer Stanislas Sorel [335] - were equally proposed as biomaterial by Tan *et al*. [336, 337] in 2014 [336]. MOC were formerly used in diverse applications like stucco or flooring, as they have a high strength and resilience when properly filled [338]. Nowadays, MOC are rather considered for niche applications such as nuclear waste immobilization [291]. Basically, MOC describe all formulations within the $MgO\text{-}MgCl_2\text{-}H_2O$ system [335] whereas the resulting hydrate phase and its properties depend on factors such as precursor molar ratio [339-342], MgO reactivity [339, 340, 343, 344] and temperature [335]. Examples of possible reaction routes are given by Equation 19-20 [291]. Similar to the acid-base mechanism described above for MPC the magnesia raw powder dissolves in an acid ~1.5 to 3.0 M solution of magnesium chloride ($MgCl_2$) [291] *via* neutralization reactions, followed by hydrolysis of the resulting Mg^{2+} ions with free OH^- and subsequent bridging of the as-formed mononuclear to form polynuclear complexes $[Mg_x(OH)_y\text{-}(H_2O)_z]^{2x-y}$ with unknown composition. The resulting amorphous gel consists of polynuclear complexes, Cl^- and water and quantitatively precipitates [345] to form a basic crystalline hydrated magnesium chloride salt with the general formula $x Mg(OH)_2\ y MgCl_2 \cdot z H_2O$ [291]. The research of Lukens [346] in 1932 for example revealed the formation of the 5-phase (x/y=5) precipitate and its gradual transformation into the 3-phase (x/y=3) modification in $MgCl_2$ solution [346]. Both are considered being the main reaction products that are responsible for the mechanical rigidity of hardened MOC [345].

$$3MgO + MgCl_2 + 11H_2O \rightarrow 3Mg(OH)_2\,MgCl_2{\cdot}8H_2O \quad \textbf{(19)}$$

magnesia — *magnesium chloride* — *"3-phase", 3-1-8*

$$5MgO + MgCl_2 + 13H_2O \rightarrow 5Mg(OH)_2\,MgCl_2{\cdot}8H_2O \quad \textbf{(20)}$$

"5-phase", 5-1-8

Because of their poor water resistance, the MOC experienced degradation, which is not desirable in construction [291]. However, this degradability actually makes them interesting for biomedical applications, as MOC dissolve to form brucite under moist conditions [336]. Tan *et al*. [336, 337] used a 5-phase forming MOC system in combination with phosphoric acid to promote its water resistance and to have a better control over its degradability [336, 337]. The addition of phosphoric acid decreased the concentration of Mg^{2+} ions being necessary for a longer-term stable 5-phase-formation [347] and it stimulated the precipitation of the less soluble magnesium phosphate hydrate bobierrite on the cement surfaces after deposition in phosphate buffered saline (PBS) for 50 d [336, 337].

2.1.2.2 Setting kinetics

Table 7: Reaction equations of possible dry and wet routes for the synthesis of MPC raw powders magnesia and farringtonite.

MAGNESIA	
dry route	wet route
$MgCO_3 \xrightarrow{630-710\,°C} MgO + CO_2$ [348]	$MgCl_2 + Ca(OH)_2 \rightarrow CaCl_2 + Mg(OH)_2$ [291] $Mg(OH)_2 \xrightarrow{T} MgO + H_2O$ [348]
FARRINGTONITE	
dry route	wet route
$2MgHPO_4 \cdot 3H_2O + Mg(OH)_2 \xrightarrow{>1000\,°C,\ >5\,h} Mg_3(PO_4)_2 + 7H_2O + H_2$	$3MgCl_2 + 2Na_3PO_4 \rightarrow Mg_3(PO_4)_2 + 3NaCl_2$

MPC are generally known for their fast setting character which was the main reason for their use in diverse civil engineering applications such as rapid repair concretes since the 1970's [291]. Depending on the exact cement formulation, the initial setting times of MPC with biomedical purpose range between <1 min and >90 min [15, 310, 312]. Many factors which concern setting kinetics are comparable to the findings of CPC research (e.g. particle size, PLR, setting solution, reacting salt concentration etc.), but the most crucial parameter seems to be the dissolution step of the MgO and farringtonite, respectively [15]. The corresponding synthesis routes affect properties like crystal size, surface area and thus reactivity [291]. Usually, both magnesium compounds experience a high-temperature treatment before application. For example, MgO can be synthesized by grinding calcined magnesite ($MgCO_3$) [348, 349]. Alternatively, it can also be synthesized through the precipitation of $Mg(OH)_2$ from hy-

drolyzed limestone ($Ca(OH)_2$) in a $MgCl_2$-rich brine with subsequent calcination [291]. For farringtonite as raw material, researchers mostly chose the high-temperature solid reaction route of commercial $MgHPO_4 \cdot 3H_2O$ and $Mg(OH)_2$ [210, 218, 310, 311, 313], but precipitation is equally possible [312]. Corresponding reaction equations are recapped in Table 7.

With increase in duration [350-352] as well as height of the temperature treatment [343, 350-354] the surface area [343, 351, 354] and thus reactivity [351-354] of MgO is decreased, while crystal size increases [350, 352, 353]. Hence, magnesia which has been calcined at comparably low temperatures between 600 to 1300 °C (700 to 1000 °C) is called reactive or caustic-calcined (light-burned), respectively. Caustic-calcined magnesia might be too reactive for its use in MPC, but it is acceptable for MOC, as less reactive MgO requires lesser amount of water, which alters the ionic strength of the $MgCl_2$ solution. Thus, the composition and stability of the resulting hydrated phases can also be altered [291]. Bates and Young [340] showed that a calcination temperature of 800 °C provided the best results in terms of setting time and mechanical properties in a MOC system [340]. In case of MPC, calcination at 1500 °C which is called dead-burning [291] is a current method to decelerate setting [294, 303, 308, 309] to comply with clinical requirements. In contrast, farringtonite which is mostly produced *via* sintering [210, 218, 310, 311, 313], is intrinsically less reactive and might be additionally grounded to regain reactivity and ensure short setting times [81]. It is conceivable that blends of reactive magnesia and farringtonite could be useful for special applications such as 3D-powder printing, where a fast-setting of 1-2 min is an indispensable requirement to ensure selected spreading of the binder liquid [355].

As already known for CPC [60, 62, 63], an increase in temperature equally accelerates the setting of MPC [15, 291, 315, 321]. According to Yang and Wu [321] setting of a MPC at -10 °C was still possible within less than 30 min [321] and autogenous heating occurs due to the exothermic reaction [291]. The heat release might be reduced by the addition of setting retarding agents [294], but controversial effects were equally observed [310]. For example, Mestres and Ginebra [294] found a temperature decay from 110 to 42 °C using 3 wt.% sodium borate decahydrate (borax, $Na_2B_4O_7 \cdot 10H_2O$) as a setting retarder [294], while Moseke *et al*. [310] found the reaction to be more exothermic when adding 1.5 M diammonium citrate ($(NH_4)_2C_6H_6O_7$) [310]. In MPC research with biomedical purpose, only the as-mentioned compounds were used as setting retarders, so far [294, 303, 308, 310]. While citrates are known from CPC chemistry [66, 71], borates and boric acid were frequently used in MPC of civil engineering applications [321, 356-358]. Diverse theories exist in trying to understand the setting retarding mechanism: either Mg^{2+} ions are chelated by $B_4O_7^{2-}$ ions [291, 358] or alternatively, Hall *et al*. [358] suggested that under the existing pH conditions tetraborate ions would rather dissociate into $B(OH_3)_3$ and $B(OH)_4^-$ which then adsorb on the surface of magnesia grains [358]. The formation of a crystalline boron and magnesium containing phosphate lüneburgite ($M_3B_2(PO_4)_2(OH)_6 \cdot 6H_2O$) was supposed by Wagh and Jeong [318]. In all three cases, a layer of amorphous or crystalline composition surrounds undissolved magnesia which hinders or retards a further dissolution [291, 318, 358].

Even though the mechanism is not absolutely clear yet, borax and boric acid seem to be very effective in retarding of MPC setting [291]. However, they both are believed to be toxic at high dosages [359, 360]. Finally, strategies to alter setting kinetics, which are well-known

from CPC research and have already been positively evaluated *in vivo* can also be considered. These strategies include parameters like raw material particle size [81, 294, 311], surface area [307, 312], composition [294, 311], PLR [210, 307, 310-312] and P/Mg ratio [321]. In these situations, additives are generally not necessary, but might help in handling and workability related properties such as injectability [310]. As indicated before phosphoric acid can serve as a setting retarder in MOC research [336].

2.1.2.3 Mechanical properties

Table 8: Rating of the wet compressive strengths of different MPC and MOC with selective examples from literature with biomedical purpose. * Bi_2O_3 is a radiopaque supplement. ** High compressive strengths after 24 h were achieved without phosphoric acid which resulted in cements with low water-resistance and would not be suitable for biomedical applications. *** No details about hardening conditions were revealed.

compressive strength after 24 h under moist conditions at 37 °C			
struvite MPC >	**amorphous MPC** >	**MOC** >	**newberyite MPC**
examples from literature with biomedical context			
Mestres, 2011: ~50 MPa **solid phase:** MgO, ADHP, borax **liquid phase:** water PLR: 7.7 g/mL, cylindrical specimens stored in Ringer's solution [294]	**Mestres, 2011: ~50 MPa** **solid phase:** MgO, NaH_2PO_4, borax **liquid phase:** water PLR: 7.7 g/mL, cylindrical specimens stored in Ringer's solution [294]	**Tan, 2014: 20-66** MPa** **solid phase:** MgO **liquid phase:** $MgCl_2$ with or without H_3PO_4 PLR: 1.0 g/mL, cylindrical specimens*** [336]	**Zhou, 2013: ~13 MPa** **solid phase:** $Mg(OH)_2$ **liquid phase:** H_3PO_4 PLR: 0.6 g/mL, cylindrical specimens stored at 100 % humidity [314]
Kanter, 2014: 58-66 MPa **solid phase:** $Mg_3(PO_4)_2$ **liquid phase:** ADHP/DAHP PLR: 2.0-3.0 g/mL, rectangular specimens stored in PBS [210]	**Mestres, 2014: ~40 MPa** **solid phase:** MgO, NaH_2PO_4, borax, Bi_2O_3* **liquid phase:** water PLR: 7.7 g/mL, cylindrical specimens stored in Ringer's solution [308]	**Tan, 2015: 20-66** MPa** **solid phase:** MgO **liquid phase:** $MgCl_2$ with or without H_3PO_4 PLR: 1.0-1.7 g/mL, cylindrical specimens stored in PBS [337]	**Zhou, 2013: ~30 MPa** **solid phase:** $MgHPO_4 \cdot 3H_2O$ **liquid phase:** water PLR: 2.5 g/mL, cylindrical specimens stored at 100 % humidity [314]

MPC are likewise not suitable for load-bearing applications due to their brittle mechanical fracture behavior [15]. Some authors observed that MPC were superior from the perspective of their mechanical performance when directly compared to CPC [210, 294, 301, 314]. Indeed, maximum compressive strengths of 85 MPa [361] are reported in the literature on MPC with biomedical context without applying common reinforcement strategies such as precompaction or ceramic fillers. Such high values can equally be achieved with HA forming CPC [102]. The fact which really points out MPC in direct comparison to CPC is that they are gaining those high values quite fast after initiating the setting reaction. Mestres and Ginebra [294] showed that 60 % of the final compressive strength of a struvite forming MPC was already reached after 1 h under physiological conditions while the final strength of ~50 MPa was obtained 1 h later. The same study revealed that the compressive strength of an apatitic control still increased after 15 d [294]. Other groups only analyzed the mechanical properties after 24 h of setting or after longer periods to observe degradation in an aqueous environment [210, 301, 307, 309, 310, 312-314, 324, 361], but the phenomenon of high early strength is well-known in MPC research for civil engineering applications [321, 357] and constitutes one of the main reasons for their use as rapid repair concretes [291, 315]. Comparing

the wet compressive strengths after 24 h observed for different MPC and MOC with biomedical purpose, one could set up the rating shown by Table 8. However, it has to be kept in mind that different experimental approaches were performed to obtain the results of the as-mentioned examples and that the shown trend is not definite. To be annotated, most research actually focused on compressive strength while bending or (diametric) tensile strength of biomedical MPC were barely explored. The systematic study of Meininger *et al*. [362] about the strength reliability of 3D-printed MgP represents an exception [362].

The compressive strength of MPC can be influenced by different parameters such as P/Mg ratio, particle size, PLR and curing conditions [315]. In magnesia based cement systems it was found to be beneficial in concerns of compressive strength when an excess of MgO is available [315, 321, 357]. In theory, a 1:1 molar ratio from MgO and ADHP would be sufficient for a quantitative conversion, but from a practical standpoint, this does not quite work out [315]. On the one hand, it is known that hydrated MgP precipitate on the surfaces of magnesia grains [317, 318] which are blocked for further reaction. An excess of MgO thus provides more reactant for the present phosphates [291] and residual MgO might serve as a ceramic filler in the gaps of the hydrated products [315]. However, MgO slowly degrades to form $Mg(OH)_2$ on heat release followed by crack formation which again deteriorates the mechanical performance [291, 315]. On the other hand, an excess of unreacted soluble phosphate would disturb the mechanical integrity of the hardened cement specimen as well [315]. Yang and Wu [321] depicted that decreasing the P/Mg ratio from 1:2 (35.5 MPa) to 1:5 (74.4 MPa) more than doubled the resulting compressive strength after 24 h in a struvite forming MPC. The P/Mg ratio equally affected the initial as well as the long-term strength values. Therefore, an optimum P/Mg ratio was found to be 1:5 while lower ratios led to a decrease in compressive strength [321]. Similar results were obtained for K-struvite systems with an optimum P/Mg ratio of 1:4. In this context, the major conversion to K-struvite (~85 %) using a 1:1 ratio did not result in the best mechanical properties [324] for the above defined reasons. Le Rouzic *et al.* [363] confirmed the negative impact of a KDHP excess in K-struvite systems [363]. According to the knowledge about MPC for civil engineering, most magnesia-based research with biomedical purpose deals with MgO excesses [294, 301, 303, 307-309, 361]. The used primary phosphate/MgO ratio ranged between 1:3.4 [307] and 1:4 [361]. Concerning farringtonite as a raw material, a systematic study with regard to the influence of the P/Mg ratio on the mechanical properties of the hardened specimens was not found in current literature. However, currently available farringtonite based formulations have used an excess of the raw material. For instance, Vorndran *et al*. [311] used a molar DAHP/farringtonite ratio of approximately 1:3.3 when mixing farringtonite with 3.5 M DAHP solution at a PLR of 3.0 g/mL [311] and compositions of related publications reported similar ratios [210, 310]. In theory, a molar DAHP/farringtonite ratio of 1:0.7 should be sufficient for a quantitative reaction (Equation 16).

The particle size or surface area of the used raw materials not only affect setting kinetics, but additionally have an impact on the strength properties of the hardened cement [315]. This was indeed shown frequently in farringtonite based cement systems either by applying different calcination temperatures on the precipitated raw powder with subsequent milling [312] or by differently grinding the uniformly sintered raw powder [81, 311]. Ostrowski *et al*. [312]

generated hannayite cements with a 15-fold increase of the wet compressive strength to ~30 MPa after 48 h by decreasing the surface area from 81.19 m²/g (amorphous) to 0.65 m²/g (crystalline). This behavior is contrary to the common wisdom. It has to be mentioned that the used PLR are not comparable because of handling reasons [312]. Generally, the common knowledge in CPC research points out to an increase in compressive strength with increasing reactivity [55, 58]. In this case, the usage of amorphous raw powders seemed to be non-suitable for the generation of viable formulations with appropriate mechanical performance [312]. Vorndran *et al*. [311] and Klammert *et al*. [81] reported that smaller-sized raw materials led to increased compressive strengths in both struvite- and newberyite-based MPC formulations [81, 311]. Yang and Wu [321] found an almost 4-fold increase in compressive strength to 36.5 MPa after a hardening time of 1 h when they used a MgO with a higher surface area of 0.35 m²/g instead of 0.13 m²/g. However, with longer hardening periods, the compressive strengths approximated each other [321]. The influence of calcination temperature and grinding of magnesia was already observed by Bates and Young [340]. Mestres and Ginebra [294] tested the fineness of their second reactant (ADHP, NaH_2PO_4) on the temperature evolution of the setting cement, but the impact on the resulting mechanics is unknown [294].

When the reactants of MPC are split in both the solid and the liquid phase, a change in the PLR results in an altered amount of the liquid component which causes opposite effects: A decrease in PLR increases the water amount which promotes the product formation, as water is consumed during reaction [307, 326]. Simultaneously, the amount of second retardant is increased as well equally supporting the formation of hydrated MgP [324]. An excess of water would have the same effect as in CPC which is to serve as a pore builder [105, 109, 307]. In this regard, MPC are less susceptible to PLR alterations [210, 310]. However, in reality, the influence of porosity increase with decreasing PLR seems to predominate the effect of product quantity [210, 307, 310, 311, 321, 324, 326, 357]. This was clearly shown by Kanter *et al*. [210], who observed an increase in compressive strength from 58 to 66 MPa when increasing the PLR from 2.0 to 3.0 g/mL. In this case, the change in the liquid amount accompanied a decrease in porosity from 7 to 5 % with a simultaneous decrease in struvite content from 41 to 34 % [210]. Similar results were obtained by Wang *et al*. [324] who produced K-struvite on the basis of magnesia. With an increase in PLR from 2.0 g/mL to 6.0 g/mL, a 5.5-fold improvement of the moist compressive strength (55±3.5 MPa) after 24 h was reached. Simultaneously, the crystallinity diminished and the packing density gained 21 % [324]. A minor compressive strength at a definite PLR is also possible due to handling reasons. When the cements set too fast, they cannot be molded properly and do not result in cohesive specimens with suitable mechanical rigidity and resilience [312]. As indicated, porosity seems to play a key role, even though the dependency of the compressive strength on the porosity is stronger in case of CPC [210]. In literature with biomedical context, a porosity range between 4.2 [308] and 22 % [307] are reported, which is mostly below the values known for CPC [37, 102].

As already described, the environmental temperature alters the setting kinetics of MPC [315, 321]. At high temperatures, the early strength characteristic is reached faster, but there is no impact on the final strength. In contrast, setting in dry atmosphere seems to be more effective in terms of long-term stability compared to setting in water due to degradation processes

[315]. However, most MPC researchers with biomedical background analyzed the compressive strength of their cement formulations at 37 °C under wet or at least moist conditions. This practice to simulate biological setting conditions is highly recommended. This should also be considered for the analysis of MOC for biological applications: It was found that the 3-phase modification tends to form a chlorocarbonate phase with atmospheric CO_2 which serves as a less soluble layer on top of the MOC [364, 365]. In addition, Sugimoto *et al*. [366] revealed the susceptibility of this phase towards changes of humidity which leads to crystal water exchange and density alterations followed by a possible damage to the matrix [366].

The incorporation of high concentrations of setting retarding agents mostly led to a deterioration of the mechanical properties in both MPC as well as MOC systems [310, 321, 336, 358], while little amounts can improve them [310, 358]. A consistent increase of the flexural strength with a borax content of up to 10 wt.% was observed by Yang and Qian [316]. In this case, the adjustment of the PLR for workability reasons is probably the main cause of the monitored strength development [316].

The aforementioned parameters have a detrimental or enhancing impact on the strength properties of the hardened MPC. However, addressing the problem of brittle mechanical fracture behavior actually would require the use of composite systems either by fiber reinforcement or by an interpenetrating polymeric phase [102]. This area of research is highly "underexplored", but offers a lot of possibilities according to the know-how from CPC research [15]. Indeed, fiber reinforcement has already been investigated for rapid repair concrete applications [367, 368] and a report about cement-polymer-composites with an initial rubber-like behavior followed by a gain in stiffness while setting in an aqueous environment for sealing applications was equally found in current concrete literature [369]. Presumably, solely Krüger *et al*. [370] published their results about the mechanical improvement of a biomedical MPC. They successfully improved the fracture behavior by the implementation of degradable magnesium alloy wires. Beside an enhancement of the bending strength with up to ~140 MPa, an increase in non-linear behavior was observed [370].

2.1.2.4 Rheological properties

The basic information about rheological properties (injectability, cohesion) of cementitious systems has been discussed in detail in chapter 2.1.1.4. In MPC research, only few publications deal with those cement characteristics. In terms of injectability, most publications give rather a statement of the cement system used being injectable [306, 371] or they provide a subjective and qualitative evaluation of the cements' handling properties [302, 303, 312]. In general, it seems that the workability becomes better by decreasing the PLR [302, 310, 312], by increasing the raw material crystallinity [312], when amorphous products are formed [303, 308] or by adding liquefying agents [310]. Quantitative evaluation of the injectability was performed by Mestres *et al*. [308] and Moseke *et al*. [310]. Mestres *et al*. [308] improved the injectability of their struvite forming MPC system from 36 to 90 % by substituting half of the ADHP salt with the sodium containing equivalent to promote the formation of an amorphous product together with the crystalline struvite precipitate [308]. Moseke *et al*. [310] even obtained injectabilities of up to 99 % when adding adequately high concentrations of diammonium citrate which maintained a negative Zeta potential of the raw material particles while re-

action leading to the electrostatic repulsion of those particles [310]. The performance of this liquefying effect can be easily evaluated considering that the first study used needles with a 14 mm inner diameter [308] while the latter used needles with a smaller inner diameter of 0.8 mm [310]. According to Equation 5 (Hagen-Poiseuille relationship), the flow rate of the paste goes along with the fourth power of the needle diameter [54]. With respect to cohesion of MPC, it was solely investigated by Mestres *et al*. [303] who found cohesion times of less than 7 min [303]. This lies exactly within the given range for clinical requirements [372].

2.1.2.5 Combinations of magnesium and calcium phosphate cements

As already mentioned, research on MPC with biomedical applications is much less mature as compared to that on CPC research. It is, therefore, well-worth the effort to develop formulations with controllable properties by combining CPC with their well-proven clinical track records with MPC with superior characteristics (e.g. high early strength, higher degradation kinetics etc.).

Table 9: List of exemplified formulations from literature where up to four components known from MPC and CPC research were used to fabricate a combined cement system.

2-component systems	3-component systems	4- component systems
MgO + MCPM [282, 373, 374]	MgO + ADHP + HA [375]	MgO + ADHP + TTCP + DCPA [301, 376]
$Mg_3(PO_4)_2$ + MCPM [81]	MgO + ADHP + CSH [309]	MgO + MCPM + TTCP + DCPA [282]
$Ca_xMg_{(3-x)}(PO_4)_2$ + DAHP [209, 311]	MgO + $MgHPO_4 \cdot 3H_2O$ + DCPA [293, 373]	MgO + ADHP + HA + CSH [375]
$Ca_xMg_{(3-x)}(PO_4)_2$ + MCPM [81]	MgO + $MgHPO_4 \cdot 3H_2O$ + DCPD [373]	

In the past, certain amounts of magnesium containing compounds have already been implemented in CPC to affect setting kinetics [62, 83, 84], to eliminate the crystallization of insoluble reprecipitates in brushite cements [208] or to enhance the degradation and biological outcome [282]. Ginebra *et al*. [371] were the first to investigate a vast spectrum of different cement formulations on the basis of newberyite and/or MgO with regard to their suitability as bone substitution materials. Among all CaP compounds used (e.g. MCPM, DCPA, DCPD, α-/β-TCP, TTCP), DCPA together with a combination of MgO and newberyite seemed to be the most promising reaction partners leading to cements with adequate setting kinetics (4 to 7 min) and mechanical properties (~11 MPa compressive and ~2 MPa tensile strength) [371].

An examination of formulations of combinatory systems shows that there generally exist two different preparation methods: raw materials known from both CPC and MPC research are mixed to a certain extent (2-4 components) [81, 282, 293, 301, 309, 373-376] as it was the case in the previously mentioned publication of Ginebra *et al*. [371]. Alternatively, calcium containing compounds (e.g. calcium carbonate, $CaCO_3$ and DCPA) are added to magnesium containing ones (e.g. newberyite, brucite) prior to high-temperature treatment leading to a calcium and magnesium containing sintering cake (e.g. mixtures of farringtonite and stanfieldite, $Ca_3Mg_3(PO_4)_6$, generally described as $Ca_xMg_{(3-x)}(PO_4)_2$) before cement reaction is

applied [81, 311]. In the latter case, the resulting calcium doped MgP might be handled as a conventional MgP and can be mixed with DAHP solution to result in struvite as the main setting product [311] (Table 9).

Some researchers systematically studied the properties of combinatory cements in comparison to the single components and partially found synergistic effects depending on the exact cement preparation. Klammert *et al*. [81] mixed $Ca_xMg_{(3-x)}(PO_4)_2$ with MCPA and 0.5 M citric acid as equivalent to brushite forming CPC. For x=0.75 and at a defined milling time and PLR, the combination showed the best mechanical properties (~40 MPa compressive strength after 24 h) versus x=0 (pure farringtonite) and x=3 (pure β-TCP) [81]. Similar results were obtained by Yang *et al*. [309] who mixed CSH with different amounts of MPC consisting of MgO and ADHP and water whereat CSD and struvite were the main reaction products [309]. At small amounts, sulfates are known to be applied as setting retarders in brushite forming CPC [66-69]. Here, concentrations not exceeding 50 % CSH likewise led to hardened cements with better compressive strengths of ~70 MPa after 4 weeks as compared to the pure CSH or MPC (~30 MPa). Simultaneously, the slow setting of the CSH (25 min) and the fast setting of the MPC control (3 min) were balanced and reached proper setting times between 7 and 12 min [309]. Yet another paper dealing with mixtures of TTCP, DCPA (CPC), MgO and ADHP (MPC) arrived at similar conclusions [301]. Pijocha *et al*. [375] found positive effects on the heat evolution during setting using combinatory systems of MgO, ADHP, HA and CSH [375]. Besides setting characteristics and mechanical performance, the biological outcome and degradability are other properties that seem to be well controllable by adjusting the composition of combinatory cement formulations [282, 301, 309, 311, 374, 376] (see “biological properties”).

2.1.2.6 Biological properties

As already mentioned before, half of the total magnesium amount in the body (~25 g in a healthy adult) is stored in bone [295, 377, 378]. It is supposed that magnesium which is found on the bone surface (⅓ of the skeletal magnesium) serves as a nutrient reservoir in case of magnesium depletion leading to a decrease in skeletal magnesium content. Magnesium is found in every intracellular compartment in which cells with a high metabolic activity generally contain more magnesium [378]. Magnesium participates in the activity of over 300 enzymatic systems [295, 378] so that the cause of magnesium depleted diseases is oftentimes linked to the malfunctioning of enzymatic processes [378]. Examples striking the bone metabolism are hypocalcaemia and osteoporosis [295, 378]. Kenney *et al*. [379] and Rude *et al*. [380] found that a magnesium poor diet led to a slower growth, reduced bone strength [379] as well as reduction in bone mass and volume in rats. A further observation was an increased osteoclast activity without the additional activation of osteoblasts disturbing the natural balance between bone resorbing and bone forming cells [380]. Thus, a magnesium deficiency might lead to osteoporosis [378].

On the contrary, enhanced bone regeneration was observed around degradable magnesium alloys [296-298] which corresponds to an additional Mg^{2+} ion supply. Thus, some *in vitro* studies explicitly analyzed the effect of Mg^{2+} ions on different bone cells to simulate magnesium alloy degradation [288, 299, 300]. Yoshizawa *et al*. [299] cultured human bone marrow

stromal cells in Mg^{2+} supplemented medium. At concentrations of 10 mM $MgSO_4$, mineralization of the extracellular matrix (ECM) was enhanced and an increased expression of the collagen type X protein as well as the vascular endothelial growth factor (VEGF) and other osteogenic ECM proteins and transcription factors was equally observed. At higher concentrations of >20 mM, Mg^{2+} ions appeared being cytotoxic [299]. This concentration dependency of the metabolic activity was likewise observed by Wu *et al*. [300] for human osteoclasts as cell proliferation and differentiation were increased at low and decreased at rather high Mg^{2+} concentrations. They further recognized the significance of the Mg^{2+} origin (magnesium chloride solutions v. magnesium extracts) [300]. Using co-cultures of bone forming and bone resorbing cells, the susceptibility of monocytes towards high Mg^{2+} concentrations is eased [288].

The biological applications of magnesium raised the interest in MPC for similar applications as well. However, relatively lower maturity of the research in this field is probably the reason for the limited number of published animal studies concerning both MPC and combinatory systems (Table 10-Table 11). In cell studies, the cytocompatibility and positive effects of MPC on cell proliferation were frequently shown for bone-linked cells such as murine osteoblast-like cell line MC3T3-E1 [81, 314] and human osteoblast cell line MG-63 [301, 309, 311, 313, 374, 376]. However, Burmester *et al.* [381] emphasized the importance to use bone-derived primary cells or at least more suitable cell lines during examinations of the osteoinductivity of magnesium containing implant materials as MG-63 behaved completely different to primary osteoblasts when exposed to Mg^{2+} extracts [381]. Nevertheless, the biocompatibility of MPC and the combinatory systems was affirmed *in vivo*, as no inflammatory reactions [209, 210, 301, 361], formation of fibrous tissue [361], foreign-body response [301], inflammation [209], rejection [209, 210] or toxic [361] and adverse effects in general [382] were reported. Besides, all non-heterotopic animal models indicated the osteoconductive character of MPC and the combinatory systems [195, 301, 361, 382-384]. Interestingly, mixtures of MPC and CPC often showed superior biological properties compared to the single components *in vitro* [301, 374]. Direct comparisons of the *in vivo* behavior of combinatory systems with both pure MPC and CPC have not been found in common literature. In terms of biocompatibility, the pH and temperature development while setting have also to be considered. While the pH exemplarily depends on the chosen raw powder and might be controlled over a wide pH range [210, 319], the commonly high heat release during the reaction of MPC was shown to be confined by adding setting retarding agents [294].

The products of MPC have a superior degradation potential to CPC [15] and their dissolution rates are higher compared to HA [301, 302]. For example, the chemical dissolution was shown by Klammert *et al*. [209] who implanted pre-hardened cylinders of struvite and newberyite in the absence of bone cells [209]. According to Großardt *et al*. [218] this chemical dissolution of struvite MPC dominates the active resorption by murine monocytic cell line RAW 264.7 derived osteoclasts at a factor of 3. Simultaneously, the total resorption was almost 20-times higher compared to CaP formulation monetite and at least 8-times higher compared to brushite [218]. In contrast, Blum *et al*. [385] found the active resorption to be the predominant degradation mechanism of struvite wherein the amount of released Mg^{2+} and PO_4^{3-} ions could additionally be enhanced through calcium doping of the cement raw material. In some *in vivo* studies, presence of osteoclasts was detected at the MPC implantation

site, leading to the conclusion that active resorption mechanism might be the principal degradation mechanism [383, 384]. The work of Klammert *et al*. [209] demonstrated that such MgP compounds do not only chemically dissolve in a physiological environment, but also present remarkable changes of their phase composition, in which both struvite and newberyite converted into low-crystalline whitlockite [209]. In two other cases, the formation of nanocrystalline apatite was reported, but as a nearly quantitative implant degradation within 10 months took place, the detected apatite probably was due to the attended new bone growth [210, 293]. Porosity is another parameter which affects biodegradability in addition to the pure chemical solubility. Increasing the initial porosity from 5 to 7 % by varying the PLR in a struvite forming cement, Kanter *et al*. [210] observed a drop in implant diameter by 60 to 80 % within 10 months. In both cases, the early pore diameter was below 1 µm [210]. By introducing differently sized micropores *via* soluble salt leaching on purpose, Kim *et al*. [384] observed a faster degradation in rabbit calvarial defects, while forming a better quality of the regenerated bone and numerous blood vessels [384].

To equip them with special biological properties, biologically active ions such as strontium [362, 386], enzymes such as lysozyme [387], radio-opaque additives such as bismuth oxide [308] and even bone marrow stromal cells (bMSC) [383] have already been incorporated in MgP scaffolds, coatings and cement systems. Interestingly, specific amorphous sodium containing MPC were shown to have intrinsic antimicrobial properties due to the alkaline pH development while setting [294, 303].

Table 10: List of MPC and combinatory systems that have already been implanted in animal models.

source	cement paste composition	set cement composition	application form	animal model	defect model	examination time point
magnesium phosphate cements - implantation in bone						
Yu, 2010 [361]	powder: MgO, ADHP, unknown retarder liquid: unknown	unknown; probably struvite	pre-hardened cylinders	New Zealand white rabbits (~3 kg)	distal condyle of the femur; hole defect of Ø 3.2 mm, 10 mm depth	0.5, 1, 2, 3 and 6 months
	outcome: no inflammatory response or fibrous tissue growth, degradation with simultaneous new bone ingrowth within 6 months, osteoblast layer at the interface					
Zeng, 2011 [374, 383]	powder: MgO liquid: phosphoric acid (+ bMSC)	unknown; probably newberyite	granules	New Zealand white rabbits (2-2.5 kg)	maxillary sinus floor elevation	2 and 8 weeks
	outcome: amount of newly formed bone less, when no cells were used; 7(14) % new bone formation within 8 weeks (with cells); 22(14) % residual material (with cells)					
Kanter, 2014 [210]	powder: farringtonite liquid: DAHP, ADHP solution	struvite, farringtonite	paste	merino sheep (~94 kg)	medial condyle of the femur; hole defect of Ø 10 mm, 15 mm depth	3, 7 and 10 months
	outcome: no inflammation or rejection, nearly quantitative cement degradation (<2 mm in diameter) and new bone formation after 10 months, loss of mechanical performance, increase in porosity and pore size and apatite formation					
Kim, 2016 [384]	paste: farringtonite, NaCl, HPMC, ethanol post-hardening liquid: DAHP solution	struvite, farringtonite, HPMC	3D printed post-hardened micro-porous discs	white rabbits	cranial bone defect à Ø 4 and 6 mm	4 and 8 weeks
	outcome: faster dissolution in the smaller defect and new bone formation, better bone regeneration and blood vessel formation in microporous structures depending on the pore size with maximum 85(50) % regenerated bone within 8 weeks for the 4(6) mm defect					

Table 11: List of MPC and combinatory systems that have already been implanted in animal models - prosecution.

source	cement paste composition	set cement composition	application form	animal model	defect model	examination time point
magnesium phosphate cements - heterotopic implantation						
Yu, 2010 [361]	powder: MgO, ADHP, unknown retarder liquid: unknown	unknown; probably struvite	pre-hardened cylinders	New Zealand white rabbits (~3 kg)	subcutaneously, dorsal muscle pouch implant size of Ø 3.2 mm, 10 mm length	1, 2 and 3 months
	outcome: no toxicity, degradation indicated by increasing surface roughness and decreasing compressive strength					
Kim, 2016 [384]	paste: farringtonite, NaCl, HPMC, ethanol post-hardening liquid: DAHP solution	struvite, farringtonite, HPMC	3D printed post-hardened micro-porous blocks	Sprague-Dawley rats	femoral extensor muscle, implant size of 4x4x8 mm	1 and 6 weeks
	outcome: faster dissolution for micropores containing scaffolds					
magnesium calcium phosphate cements - implantation in bone						
Wu, 2008 [301]	powder: MgO, DAHP / DCPA, TTCP liquid: water	struvite, MgO, HA, TTCP	pre-hardened cylinders	New Zealand white rabbits (~3 kg)	distal part of the femur, hole defect of Ø 4 mm, 3 mm depth	1, 2, 3 and 6 months
	outcome: no inflammatory or foreign-body response, nearly quantitative cement degradation and new bone formation after 6 months, good biocompatibility and osteoconductivity					
Schendel, 2009 [382]	OsteoCrete®	unknown	paste	New Zealand white rabbits	cranial bone defect à 1.5 cm²; bone flap repositioned with cement paste	2, 12 and 24 weeks
	outcome: no adverse effects, 50 % replaced after 12 weeks with new bone ingrowth, good adhesion to the bone surface and good bone flap position and apparent stability					
Zeng, 2011 [374, 383]	powder: MgO, MCPA liquid: water (+ bMSC)	farringtonite	granules	New Zealand white rabbits (2-2.5 kg)	maxillary sinus floor elevation	2 and 8 weeks
	outcome: amount of newly formed bone less, when no cells were used; 26(31) % new bone formation within 8 weeks (with cells); 30(22) % residual material (with cells); moderate biodegradability and excellent osteoconductivity					
magnesium calcium phosphate cements - heterotopic implantation						
Driessens, 1995 [293]	powder: MgO, newberyite, DCPA liquid: unknown	bobierrite, brucite, monetite	pre-hardened cylinders	Wistar rats (150-200 g)	subcutaneously, implant size of Ø 6 mm, 12 mm length	1, 2, 4 or 8 weeks
	outcome: slow dissolution of the magnesium phosphate with decrease in mechanical performance and apatite formation					
Klammert, 2011 [209]	powder: $Ca_{0.75}Mg_{2.25}(PO_4)_2$ liquid: DAHP solution	struvite, farringtonite	pre-hardened cylinders	Sprague-Dawley rats (~318 g)	femoral extensor muscle implant size of Ø 5 mm, 10 mm length	1, 2, 6, 10 and 15 months
	outcome: no indication for infection, inflammation or rejection; chemical dissolution by surface, changes of the phase composition into whitlockite and decrease in mechanical performance					
Klammert, 2011 [209]	powder: $Ca_{0.75}Mg_{2.25}(PO_4)_2$, MCPM liquid: citric acid	newberyite, brushite	pre-hardened cylinders	Sprague-Dawley rats (~318 g)	femoral extensor muscle implant size of Ø 5 mm, 10 mm length	1, 2, 6, 10 and 15 months
	outcome: no indication for infection, inflammation or rejection; chemical dissolution by volume, changes of the phase composition into whitlockite and decrease in mechanical performance					

2.2 Alternative setting mechanisms of mineral bone cements

Beside the classic hydraulic reaction mechanism of mineral bone cements, diverse alternatives have been launched to ameliorate either handling characteristics of the cement paste or different properties of the hardened ceramic (i.e. mechanics).

Dual setting cements enable the simultaneous taking place of two parallel processes: the cementitious dissolution/precipitation reaction (inorganic) and the gelation of a second component, either organic (e.g. water soluble monomers with reactive double bounds) [16, 17, 149, 150, 388, 389] or inorganic (e.g. pre-hydrolyzed silicates) [215] without chemical interactions between both phases. This design enables the loading with high polymer amounts [102] which results in advantages for the mechanical performance [16, 17] as well as a better control over drug release kinetics [17, 215].

In **calcium binding cement** systems, one takes advantage of the carboxylic acid or organic phosphate compartments in polymers [102], mostly poly(alkenoic acids). Following the cross-linking of the binding sites *via* CPC precursor released calcium ions, the cementitious reaction usually to form HA successively takes place [146]. The usage of poly(alkenoic acids) enables the formulation of composite materials with a ductile-like mechanical behavior, but simultaneously might impair working characteristics [18]. When monomeric chelating agents (e.g. phytic acid) were used instead, mechanical benefits over classic CPC have not been achieved, so far [77, 78].

In contrast, **premixed CPC** do not supply any mechanical benefits. They consist of either one or more aqueous and non-aqueous liquids where the reactive specimens of the CaP system are dissolved or dispersed in. The noteworthiness about such pastes is that they can be used immediately without classic powder and liquid mixing in the operating theater which is very time-saving. In the ideal case, premixed pastes are long-term storage stable and do not harden until they are mixed with their second liquid phase or directly delivered in the moist defect milieu which both initiates the setting reaction [35].

2.2.1 Dual setting cement systems

The introduction of the term “dual/double setting” can be ascribed to a publication of Dos Santos [149] in 1999 with the intention to improve the compressive strength of CPC. The general principle was a parallel reaction of the cementitious dissolution/precipitation and crosslinking reaction of water-soluble monomers [149].

Dos Santos *et al*. [149] chose a mixture of 5 to 20 % monofunctional acrylamide (AA) as the main constituent of the resulting hydrogel and 0.5 to 2.0 % N,N’-methylenebisacrylamide (MBAA) as a bifunctional crosslinker in the aqueous phase of the α-TCP cement paste. The polymerization initiating system consisted of ammonium persulfate (APS) as the radical former as well as N,N,N’,N’-tetramethylethylene diamine (TEMED) which were split onto the solid (APS) and the aqueous (TEMED) phase of the cement. Mixing both phases, the radical polymerization reaction was initiated resulting in an interpenetrating network of organic and inorganic components. With this principle, Dos Santos [149] gave rise to a new category of composite materials.

Actually, Sugawara *et al*. [388] published a study with a quite similar principle already in 1989 using an initiator system of benzoyl peroxide (BPO) and N,N-dihydroxyethyl-p-toluidine (DHEPT) for the radical polymerization of monofunctional 2-hydroxyethyl methacrylate (2-HEMA) together with bifunctional bisphenol A glycidyl methacrylate (BisGMA) and triethylene glycol dimethacrylate (TEGDMA). The essential difference towards nowadays dual setting systems was the intermediate coating of the CPC raw powders (TTCP/DCPA) with the radical former BPO and subsequent prevention of HA formation [388].

2.2.1.1 Inorganic/organic systems

The main finding of the dual setting cement system introduced by Dos Santos *et al*. [149] was a considerable increase in the initial compressive strength which was not measurable for the control group and anyhow 6.8 MPa for the polymer containing formulation. With increasing immersion time in simulated body fluid (SBF), the effect of continuous cement mineralization likewise increased such that the mechanical properties assimilated. However, the polymerization reaction retarded the conversion from α-TCP into HA [149]. One attempt to effectively improve the long-term mechanical performance of dual setting cements consisted in the addition of 1 % polyacrylate as a liquid reducer to previous cement formulations which enabled an increase in PLR thus reducing the porosity of the hardened cement. Consequently, an outstanding increase in compressive strength by 149 % (55 MPa) and in tensile strength by 69 % (21 MPa) was reached. Simultaneously, a reduction in crystal size was observed [150]. Abandoning the liquid reducing agent and using small fractions of polyamide fibers (0.8 %) instead for additional reinforcement only led to modest amendments of the compressive strength [125]. Taking a step further, Dos Santos *et al*. [124] combined their primary dual setting system with both polyacrylate and fiber reinforcement (carbon, nylon and polypropylene fibers). Though the compressive strength of the reinforced double setting cement was reduced through up to 4 % fiber addition as a consequence of elevated porosity, especially the use of carbon fibers resulted in outstanding bending strength and toughness: The former was increased by 133 % (29 MPa) while the toughness was increased by 2800 % (1.72 $MPa \cdot m^{1/2}$) [124]. Analyzing the diametric tensile strength, Rigo *et al*. [389] showed that

this positive effect on the mechanical properties could equally be transferred onto HA forming CPC which were based on the TTCP/DCPA system. However, the attempt to create working dual cements with alternative water soluble monomers such as 2-HEMA and N-vinyl-2-pyrrolidone (VP) at concentrations between 5 to 20 % failed [389]. According to Christel *et al*. [17] much higher concentrations of at least 50 % of 2-HEMA in the aqueous solution and the omission of crosslinkers indeed resulted in α-TCP based dual setting cements with enhanced mechanical fracture behavior. The study systematically showed that an increase in 2-HEMA concentration resulted in a decrease of crystal size and HA-conversion [17] affirming the observations of Dos Santos for AA/α-TCP-systems [149, 150]. Christel *et al*. [17] further revealed that concentrations of just 2.5 % of a crosslinker (ethylene glycol dimethacrylate, EGDMA) operated detrimentally on the bending strength and reduced the bending modulus. However, the absorbed fracture energy was more than doubled [17]. A further benefit using 2-HEMA instead of AA is the toxicity of possibly unreacted monomer residues [102]. Furthermore, Wang *et al*. [16] introduced a biodegradable alternative which was glycidyl methacrylated natural polysaccharide dextran. Again, the cement system was based on TTCP/DCPA and the initiators were APS and TEMED. This study reassured the performance of only high monomer amounts between 45 and 75 % in terms of fracture energy [16]. The research which has already been performed on inorganic/organic HA systems was ever based on monomers with reactive double bounds in such as acrylate and methacrylate functionalities (Figure 7). Recently, Schamel *et al*. [390] demonstrated the use of *in situ* forming hydrogels as a possible alternative. In an aqueous environment, six arm star-shaped terminally isocyanate functionalized poly(ethylene oxide) (PEO) crosslinked *via* simple hydrolysis simultaneously to the hydrolysis of incorporated α-TCP fillers [390].

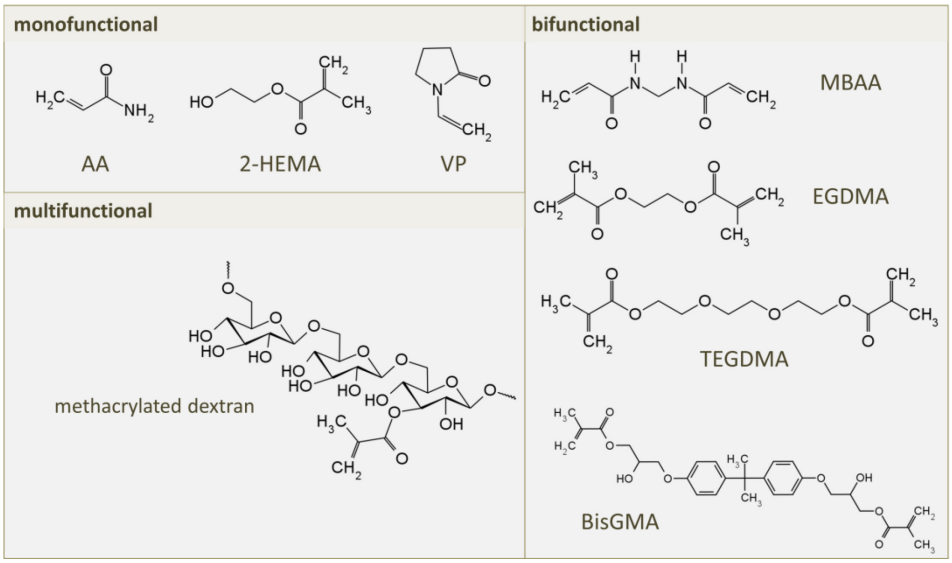

Figure 7: Chemical structures of all building blocks with reactive double bonds that have already been applied in inorganic/organic dual setting HA cement systems.

As just shown, most of the double setting research has been performed on HA forming CPC. One challenge in transferring dual systems on brushite forming CPC might be the acidic setting pH which could be detrimental to polymerization. This obstacle could be overcome by Schamel *et al.* [391] who cunningly took advantage of this, as the conversion of *Bombyx mori* derived silk fibroin from its random coil into the more ordered β-sheet structure was promoted by the presence of brushite educt descending acid phosphates. The parallel process of

brushite precipitation and silk fibroin β-sheet formation resulted in an extraordinary mechanical outcome for the final interpenetrating inorganic/organic matrix such that the composite could be nailed and cut without failure [391].

2.2.1.2 Inorganic/inorganic systems

A further example turning the setting events of brushite CPC into account was described by Geffers *et al*. [215]. Mechanistically, the condensation of hydrolyzed tetraethyl orthosilicate (TEOS)-presursors to form porous silica networks *via* sol-gel-process is promoted at pH changes and during water consumption whilst brushite formation. This fact enabled the simultaneous taking place of the cementitious dissolution/precipitation reaction of β-TCP and the gelation of pre-hydrolyzed TEOS-sols resulting in an interpenetrating network of macroporous (brushite) and microporous (silica-gel) inorganic compartments. Beside a positive impact on compressive strength, this system further displayed a smart possibility to foster monetite instead of brushite formation [215].

2.2.2 Calcium binding cement systems

TenHuisen and Brown [146] were the first to transfer the mechanistic principles of glass ionomer (polyalkenoate) cements (GIC) to CPC systems. The reaction principle of GIC is generally described as an acid-base and sol-gel reaction between ion-leachable glasses (especially calcium and aluminium ions) and poly(alkenoic acids) such as poly(acrylic acid) (PAA). Initially, the alumino silicate glass superficially dissolves in the acidic environment and is predominantly depleted of calcium ions. During gelation, a crosslinking reaction between calcium ions and the carboxylic acid groups of the poly(alkenoic acid) molecules takes place, followed by a successive incorporation of less mobile depleted aluminium ions which provides the matrix with its mechanical rigidity. Their reaction mechanism allows chemical bonding to mineralized tooth tissue [392].

The idea of TenHuisen and Brown [146] consisted in using CPC precursor materials instead of alumino silicate glasses for calcium leaching and interacting with the carboxylic acid groups of PAA. Though they used both TTCP and DCPA as raw materials, predominantly TTCP was consumed and tended to form a calcium poylacrylate (CPA) network [146]. DCPA is generally not involved in CPA formation, but in the consecutive precipitation and growth of HA crystals [145]. Since then, a multitude of publications dealt with the combination of HA precursor CaP and PAA [18, 143-145, 147, 388], but brushite and monetite were equally found as possible mineral setting products within the polymer matrix [18, 148]. Setting kinetics and mechanical properties are affected by the inserted PAA concentration [145, 146] and molecular weight [144, 145] and by the chosen TTCP/DCPA ratio [144]. Exemplarily, Chen *et al*. [18] reported the transition from brittle (Young's modulus of 300 to 1000 MPa) to ductile (Young's modulus of 30 to 200 MPa) mechanical behavior when increasing the PAA amount from 25 to 67 % in relation to the CPC raw powder. Simultaneously, they critically evaluated the linked high paste viscosity regarding cement application [18]. In terms of avoiding the usually fast reaction between TTCP and PAA, Watson *et al*. [147] found the prehydration of TTCP precursors to be an adequate option in slowing down the reaction and enhancing the workability of the resulting cement paste [147]. Alternatively and in the context of GIC, Wilson, Crisp and Ferner [393] proposed the implementation of acidic chelating co-monomers such as tartaric or citric acid to improve the cement setting behavior. They assumed that this would facilitate the depletion of the powder phase with ions and simultaneously confine PAA ionization and uncoiling to prolongate workability [393]. Additionally, such small chelating agents might act as bridging molecules when PAA crosslinking is lowered for steric reasons which can be beneficial for the final mechanical properties [392]. This principle was indeed adapted by Chen *et al*. [18] using tartaric acid for TTCP/DCPA/PAA systems [18] and itaconic acid was used for PAA copolymerization [143, 388]. Poly(methyl vinyl ether maleic acid) [148, 394], poly(vinyl phosphonic acid) [395] and poly[bis(potassium carboxylatophenoxy) phosphazene] [396] were equally successfully established instead of PAA in CPC systems (Figure 8). In contrast to conventional GIC, mixtures of CPC and polymers with carboxylic acid or organic phosphate moieties have the advantage that crosslinking of the polymer through interactions with CPC precursor powder released calcium ions occurs parallel to a conventional dissolution and precipitation reaction of the inorganic component. Thus, it is probably not necessary to choose a polymeric compound with numerous binding sites to obtain a composite material with a certain mechanical stability. In GIC exemplarily, it is not pos-

sible to create stable formulations by using small chelating molecules (e.g. tartaric acid) alone [392]. This is not the case for CPC formulations, even if small amounts of chelating agents (e.g. phytic or citric acid, 0.1 to 0.5 mol/L, Figure 8) mainly act as setting retarders [76].

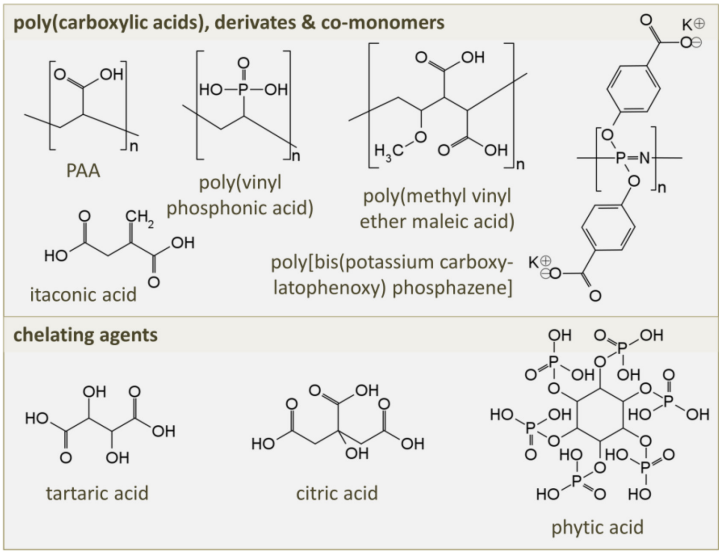

Figure 8: Chemical structures of poly(carboxylic acids) and chelating agents that have already been applied in inorganic/organic CPC systems.

Sporadically, phytic acid was also tested in this context [77, 78, 394, 397] whereat much higher amounts of ~20 % were necessary to get a mechanically relevant output [397]. Adding small amounts of phytic acid into the aqueous phase of a TTCP/DCPA system, Matsuya *et al*. [394] mainly observed the setting retarding effect and even a mechanical weakening compared to the control [394]. Instead of adding phytic acid into the aqueous component, Takahashi *et al*. [78] surface-modified their precursor β-TCP powder by dispersion in a neutralized 3000 ppm phytic acid solution for 24 h. For cement preparation, they simply mixed the as-prepared powders with water and obtained a maximum compressive strength of 23 MPa which was a >10-fold amelioration in comparison to the control group. However, Takahashi *et al*. [78] chose a wet ball-milling routine in water leading to a partial prehydration of the β-TCP powder to form almost equal amounts of HA. Secondly, the milling process resulted in high specific surface areas of up to 64 m²/g. As the authors missed providing strength results of convenient milled and biphasic β-TCP powders without phytic acid modification [78], it is not clear, whether the presence of precipitated HA, the elevated packing density of β-TCP by milling or a possible chelation due to the surface modification is the reason for the enhanced mechanical performance. A similar procedure was described by Konishi *et al*. [77] for the surface modification of HA powder with sodium phytate (sodium salt of phytic acid). Indeed, an increase in sodium phytate concentration led to slight ameliorations in compressive strength, but the values stayed in a single-digit MPa range [77]. In both cases, an increase in Zeta-potential was observed [77, 78] which generally enables the realization of processible cement pastes with low liquid amounts [54]. In contrast to the GIC principle, the main output of using small chelating agents in CPC was not an enhancement of the mechanical properties such that this subject provides the basis for continuing explorations.

2.2.3 Premixed cement systems

The main wanted effect of the already presented alternative setting mechanisms (dual setting and calcium binding systems) was an improvement of the brittle mechanical behavior of classic cement formulations [102]. In contrast, premixed cements have the major task to enhance simplicity of handling and thus optimize the life span and reproducibility of hardened implants [35].

2.2.3.1 Multi-component systems

Lemaitre [398] and Chow [399] both tried to overcome the handling issues of conventional cement pastes by segregating the reactive species from one another within at least two separate systems. In contrast to powder-liquid formulations, the components should be provided in liquid or pasty form and the reaction should be initiated not before mixing [398, 399]. The approach from Lemaitre [398] mainly included water-based ingredients i.e. the two reactive species are either dissolved or suspended in an aqueous solution [398]. Going a step further, Chow [399] described the so called “dual-phase cement precursor systems” whereat at least one of the two liquids should be on a water basis and the second could be non-aqueous, but water-miscible i.e. contains glycerol, ethanol, PEG and so on. The principle of two separated liquids can be applied either on dual setting as well as on calcium binding cement formulations and is equally covered by the as-mentioned patent [399]. The main advantage of such multi-phase systems is that adequate homogenization of liquids is easier compared to powder-liquid formulations [35]. Examples of such cement formulations mostly included CPC systems with more than 1 reactive species [398, 399].

Alternatively, Bohner *et al*. [400] came up with the idea of a cation exchange dual paste being suitable for cements where one single specimen reacts with water solely (e.g. α-TCP-cements). The early precipitation of HA within an α-TCP containing aqueous paste has to be suppressed while a second phase provides setting accelerators for a fast reactivation after stocking. Indeed, the authors succeeded in creating a CPC-paste which stayed stable for at least one year by the following procedure: 1) The α-TCP raw powder was calcined at 500 °C for 25 h to reduce its reactivity [400]. In an earlier publication, Bohner *et al*. [401] showed that the calcination step diminished the number of surface defects and the amount of amorphous constituents of α-TCP thus postponing the reaction with Na_2HPO_4 solution [401]. 2) The dissolution of α-TCP and subsequent nucleation and precipitation of HA was hindered by choosing 0.1 M $MgCl_2$ solution as dispersant of the pre-treated α-TCP-powder. A major challenge was to regain the reactivity of this system. As conventional accelerating agents such as seed crystals or phosphate salts did not work out, Bohner *et al*. [400] tried to prosper by adjusting the magnesium-to-calcium ratio [400]. According to Aoba *et al*. [402] the interaction of magnesium with synthetic apatites and diverse mineralized tissues such as enamel, dentin and bone followed the composition of experimental electrolytes in terms of calcium and magnesium content, i.e. the higher the magnesium-to-calcium ratio, the higher the adsorption of magnesium on the corresponding surface [402]. Thus, Bohner *et al*. [400] chose $CaCl_2$ as activator dissolved in the second phase of the dual paste. Above a critical magnesium-to-calcium molar ratio of 1, full conversion of the inhibited α-TCP paste was enabled. Interestingly, this task was equally undertaken by other divalent cations. Mechanistically, the addition

of $CaCl_2$ leads to a displacement of the corresponding cation from the raw powder surface with calcium ions to finally initiate the dissolution/precipitation reaction. The following order of efficiency was stated whereat nickel blocked the reaction even in the presence of calcium ions while copper and zinc only delayed the reaction [400].

$$Ni^{2+} > Ba^{2+} > Mg^{2+} > Str^{2+} > Cu^{2+} \approx Zn^{2+}$$

2.2.3.2 1-component systems

1-component premixed cements are available in single pre-prepared paste form and hence are known as “ready-to-use” cement pastes in literature. Generally, hardening starts not until the paste is extradited to an aqueous environment, i.e. physiological fluids [35]. Such cement pastes join the following advantages: The homogenized cement paste is yet available in a syringe or other package and remains there until its use without hardening [170]. No blending of the powder and liquid phase is necessary. The cement setting starts as soon as the raw powder is exposed to the aqueous environment. Homogenization of the cement paste is not user-dependent and will not affect the resulting implant properties [35]. The surgeon has enough time to feed the paste and to correct the filling which is especially benefiting in case of irregularly shaped bone defects. Also, the overall surgical time is reduced [170]. The preparation under more controlled conditions results in an increased implant performance [35].

2.2.3.3 Aqueous systems

A special challenge is the generation of storage stable aqueous cement formulations which inherently contain all reactive species. One approach was initiated by Grover *et al*. [403]. Conventional aqueous brushite CPC were prepared and frozen immediately after premixing at -20 to -196 °C (liquid nitrogen) and stored for up to 4 weeks before further processing. Depending on the cement composition, the shelf-life of the pastes could be maintained over the whole period and freezing at temperatures of -80 °C actually had positive effects on the mechanical performance [403]. However, this variation impedes the ease of handling due to the indispensable defrosting procedure.

2.2.3.4 Non-aqueous, (non)-water-miscible systems

The reaction mechanism of non-aqueous cement formulations is based on the following principle: The cement raw powder is mixed with a biocompatible water-miscible (e.g. glycerol) [160, 170-172, 404-407] or water-immiscible (e.g. triacylglycerol) [19, 20] liquid to form a homogeneous and workable paste. When the paste is exposed to an aqueous environment, an increase in water amount either by gradual mixing of the water-miscible liquid with physiological fluid [160, 170], or by discontinuous diffusive exchange between the water-immiscible liquid and the physiological fluid [19, 20] will initiate the cementitious dissolution/precipitation reaction. Often, the delayed water supply was observed to prolong hardening time [160, 175], reduce mechanical properties [19, 160, 175] and diminish product [160, 170] or promote water-free CaP (i.e. monetite instead of brushite) formation [171, 406, 407], respectively. Both a reduced HA or promoted monetite formation is able to simultaneously elevate the overall biodegradability [10].

In 1990, Sugawara et al. [405] were the first to combine CaP raw powders (TTCP/DCPA or TTCP/DCPD) with glycerol as a vehicle liquid for root canal sealing, but the term of "premixed" cement pastes was used not before 2003 by Takagi *et al*. [160]. Beside glycerol which was adapted by a few other publications [170-172, 404, 406, 407], poly(propylene glycol) [170] PEG [172, 173] and N-methyl-2-pyrrolidone [175] (Figure 9) were used as water-miscible vehicle materials for both HA [160, 170, 173, 175, 404, 405] as well as acidic CPC [171, 172, 406, 407].

As premixed cement pastes have a prolonged setting and tend to disintegrate upon exposure to an aqueous environment, Takagi *et al*. [160] proposed the addition of gelling agents (e.g. HPMC) and setting accelerators (e.g. Na_2HPO_4) [160] which was pursued in other publications [170, 173, 404]. Beside HPMC which is a well-known supplement in terms of ameliorated cement handling properties [37], Carey *et al*. [170] analyzed a combination of chitosan malate and $Ca(OH)_2$. The dissolution of $Ca(OH)_2$ would increase the pH and activate chitosan gelling [170]. A further mechanism to improve washout resistance was proposed by Wu *et al*. [175] who dissolved polylactide (PLA) in their carrier liquid (N-methyl-2-pyrrolidone). By exchange of N-methyl-2-pyrrolidone with water, the hydrophobic PLA precipitated and probably unified disintegrated CaP particles. The enhanced washout resistance of the fresh paste derived from the thickening effect of the PLA solution [175]. However, the authors did not consider the high toxicity of N-methyl-2-pyrrolidone which is detrimental for biomedical applications. As Na_2HPO_4 was shown not to be an ideal setting accelerator in non-aqueous cement systems [170], MCPM [170, 404] and tartaric [170, 173], malic, malonic, citric as well as glycolic acid [173] were also investigated. The use of tartaric acid showed the best results with an excellent washout resistance [170] and in terms of hardening time (8.2±0.2 min) and diametric tensile strength (6.5±0.8 MPa) [173].

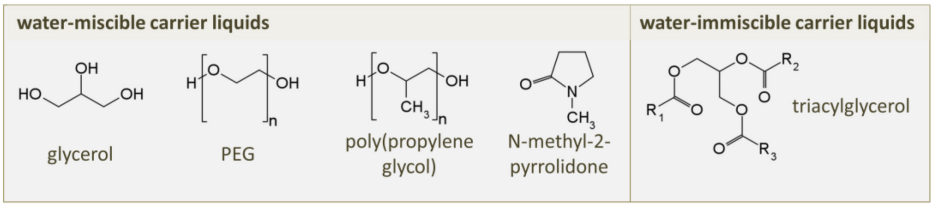

Figure 9: Chemical structures of (non-)water miscible vehicle molecules that have already been applied in premixed CPC systems. R_1-R_3 derive from esterification of glycerol with 8 to 12 C saturated fatty acids.

When CaP raw powders for brushite/monetite formation were used, mostly no gelling or accelerating agents were added [171, 172, 407], as acidic cements are known for their intrinsic fast-setting ability [10]. Though, Han *et al*. [172] described their formulations to have tolerable cohesiveness which became worse at correspondingly higher paste amounts [172]. Thus, the use of both gelling and accelerating supplements seems to be indispensable for usually fast setting formulations, too. This was realized by Aberg *et al*. [406] who combined β-TCP/MCPM with glycerol carrier liquid, HPMC as gelling agent and a surface active polysorbate to improve glycerol diffusion [406]. Even though the principle of premixed cement pastes seems to work also for brushite/monetite forming systems, the shelf-life of such pastes should be considered critically. According to Gbureck *et al*. [408], as-prepared mixtures of β-TCP and MCPM as well as the corresponding anhydride MCPA did not harden with sodium citrate solution already after 1 d of ageing at ambient conditions [408]. This is not the only issue in reference to storage stability of premixed cement pastes. According to

Ginebra *et al*. [35] it is insufficiently thought of the negative influence of water bearing contaminations [35]. Rather, none of the as-mentioned publications dealt with the shelf-life of non-aqueous water-miscible systems and one might assume that analysis was each performed on freshly prepared cement pastes. The research from Engstrand and Engqvist [171] is an exception. Actually, they demonstrated that small water impurities of only 1.7 % were enough to heavily alter both handling as well as characteristics of hardened cement specimens. The working time while stocking under elsewise dry conditions at RT was reduced from 14 d to 5-6 h being linked to an increased extrusion force since 3 h of storage compared to the water-free control. Simultaneously and quite logical, the setting time was reduced by 10 min (19±2 min) and the wet compressive strength after 24 h nearly doubled (11.2±1.5 MPa) [171]. Appending to that, a shelf-life of 2 weeks for the water-free control is still not adequate for clinical applications. In terms of workability, the analysis of premixed cement pastes focused either on the proof of washout resistance [160, 170, 172] or on injectability [171, 406, 407], but the successful complying of both requirements was merely demonstrated once [175]. However, it is known from classic CPC research that an adequate cohesiveness can be linked to a poor injectability and *vice versa* [184].

The gradual increase of water within the premixed cement paste after delivering is connected to a continuous change in paste composition and consecutive setting reaction to which the quality of the hardened ceramic is very susceptible. Thus, Heinemann *et al*. [19] proposed the usage of a water-immiscible carrier liquid instead of the conventional formulations with glycerol or PEG. This would lead to a discontinuous replacement of the liquid with physiological fluids resulting in a more controllable and reproducible setting reaction and thus product quality. Heinemann *et al*. [19] combined 85 % carbonated HA forming raw powders (60 % α-TCP, 26 % DCPA, 10 % $CaCO_3$, 4 % HA) with 15 % oil phase. The latter consisted of a water-immiscible synthetic triglyceride (Figure 9, Mygliol 812 with 8 to 12 C saturated fatty acids) and a mixture of two surface reactants (14.7 % castor oil ethoxylate 35 and 4.9 % hexadecyl phosphate) to facilitate paste homogenization. Small amounts of K_2HPO_4 were supplemented to the solid phase as setting accelerator. With this concept, the authors succeeded in creating a smooth, homogeneous paste without phase separation (even during centrifugation), with short setting time (2.5 min), with adequate cohesiveness (only 0.2 % CaP released under aqueous conditions within 24 h) and injectablity (extrusion force from ~20 N on not exceeding 100 N). After 4 d of setting the compressive strength was even better compared to the aqueous CaP control [19]. In a subsequent research article [20], the suitability of this paste for controlled release of diverse antibiotics (vancomycin, gentamycin) dispersed either within the paste or dissolved in a second aqueous component was shown. The opportunity to individually design the composition of this second phase using half-filled double-chamber cartridges would be ideal for customized needs [20]. In principle, this double-chamber application is related to the multi-component formulations which were successfully applied by Chow [399].

2.3 Application forms of mineral bone cements

The following chapter shall give an overview (Figure 10) about how the just presented different cement systems and setting mechanisms might be used to create structures for varying applications in medicine.

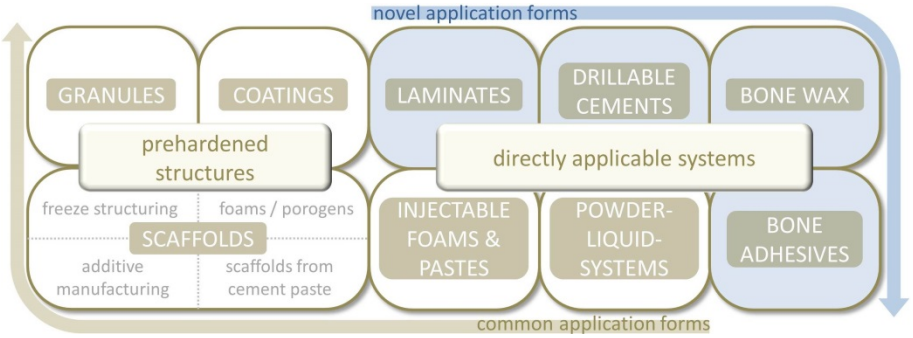

Figure 10: Schematic overview about different application forms on the basis of mineral bone cements.

Basically, one can distinguish between prefabricated implants in form of granules, cuboids, cylinders, plane, customized structures or coated implants and systems which have a pasty or waxen texture after preparation and might be delivered minimally invasive or by means of a spatula. The broad range of already existing literature in matters of different application forms such as granules and 3D-printed, freeze structured or foamed scaffolds is large, so the main focus of the present work will be directed on rather uncommon and novel opportunities to make use of the possibilities given by the diversity of mineral bone cement systems.

2.3.1 Common application forms

Below, common application forms of CPC and MPC are divided into loose granules and compact scaffolds. It has to be mentioned that the methods to generate both of these application forms partially overlap and that powders naturally form the basis of bulk implants. Thus, a strict separation is difficult. Coatings will not be considered in the present work but it is referred to a review article from Paital and Dahodre [409] including different techniques and their corresponding principles and features for the generation of CaP coatings on implant surfaces [409].

2.3.1.1 Granules and particulates

Ceramic particles can be nano- to millimeter sized and are used as raw powders in mineral bone cement systems or other processing techniques such as 3D-printing, pressing or plasma spraying, as (inactive) inorganic fillers in cement pastes and putties with a cementitious, aqueous or organic binder phase or as independent bone graft substitutes in orthopedic and dental surgery [410]. Embedded in a suitable gel-like liquid (e.g. solutions from gelatin, HPMC), granules might be applied minimally invasively through injection [35] and used for drug delivery and even as cell carriers [410]. Regularly shaped microspheres allow the filling of irregularly shaped defects with high packing density [35]. The main advantage of particles compared to dense ceramics with the same composition is probably the biological outcome: The intergranular space enables a rapid material resorption and invasion of the bone substitute with newly formed bone through the overall implantation site [410]. According to theoretical calculations of Bohner and Baumgart [411], (dense) microporous ceramic particles which

cannot be invaded by cells should be in a size range of 100 to 200 µm to adjust a fast resorption with a fast new bone ingrowth. This size range is an agreement of small particles which increase the surface area and enable fast resorption and large particles which increase the interparticular gaps leading to an accelerated invasion with blood vessels. Even though conformity of 80 % with literature data was reached, this model does not implement alternative or disturbed resorption mechanisms such as disintegration and reprecipitation [411]. Gauthier *et al*. [412] analyzed the performance of differently sized (40-80 or 200-500 µm) biphasic CaP (β-TCP/HA) particles in HPMC solution as vehicle liquid in the femurs of New Zealand white rabbits. For the smaller diameter, 50 % of the original material was resorbed within 12 weeks whereas it was only around 70 % for the larger granules. Simultaneously, the smaller particles fostered novel bone ingrowth to a greater extent within 8 weeks [412]. However, other research showed that the high resorption rate of still smaller powders (10-20 µm) - despite the overall best result in terms of bone ingrowth - was linked to comparably distinct early inflammation reactions [413]. A poor mechanical stability of granular implant materials and a possible particle migration from the implantation site are further issues [36].

The following methods include cementitious reactions for the production of ceramic particles: Tamini *et al*. [414] pestled preset brushite monoliths and gained size-classified granules with a diameter of 0.2 to 1 mm by sieving [414]. This method was later on adapted to obtain monetite granules through autoclaving of preset, milled and sieved brushite particles [43, 415]. These granules were successfully implanted in rabbit calvariae [43, 414] and even human alveolar bone defects [415]. The simple preparation method leads to irregularly formed sharp-edged granules which might be offending to soft tissues of the implantation site [416]. A comparative *in vivo* study with round and sharp-edged HA particles was performed by Misiek *et al*. [417] by submucosal insection in the mouths of beagle dogs. They observed a moderate inflammatory response in both cases which was resolved earlier in the case of round particles while sharp ones were prone to irritate the surrounding soft tissue [417]. One approach to gain non-irritative spherical particles is the so-called emulsion technique which was firstly described by Bohner [232]. In brief, the cement paste or slurry is mixed with a hydrophobic liquid (e.g. paraffin oil [232, 416, 418], food-grade oil [416, 419-422]) and surface-active agents (e.g. polyethoxylated castor oil [232], sorbitan monooleate [232, 416, 418, 422]) for stabilization and then homogenized. Depending on the ratio of the components and type of emulsifier used, two kinds of cement emulsions (either oil droplets in cement paste or cement paste droplets in oil) are possible which result in porous cement blocks (oil-in-water emulsion) or spherical granules (water-in-oil emulsion) [232]. By continuous hardening through dissolution/precipitation reaction, the granules turn from cement droplets into solid particles whose size can be adjusted by different parameters such as emulsifier type [422] and concentration, oil viscosity [416, 422] and temperature [416], stirring velocity and geometry of the stirring tool [422] or cement composition [416, 422]. This method was successfully applied to form spherical granules from hydroxyapatite [232, 421, 423], brushite [416] and struvite [422] within a clinically relevant size range which is 425 to 1000 µm for oral clinical applications [418]. In one special case, the hydration of CSH was used for an aqueous cement slurry which formed spherical granules under stirring in an oil phase. The resulting CSD particles transformed to carbonated HA through hydrothermal immersion in a phosphate and carbonate rich solution [423]. Kim *et al*. [424] used the pH increase while thermal urea de-

composition for the reprecipitation of dissolved HA to form HA granules from aqueous solution in mineral oil [424].

The emulsion technique is not only applied for self-setting cement pastes. Ceramic particles, mostly HA [418-420, 425-427], were suspended in a polymer solution from chitosan [418], gelatin [419-421, 426, 428] or polyvinyl butyral [427, 429] which was dispersed in a second, with the first phase immiscible liquid. Depending on the hydrophobic character of the binder solution, both water-in-oil [418-421, 426, 428] and oil-in-water [425, 427, 429] emulsions were possible. The addition of crosslinking agents (e.g. glutaraldehyde for chitosan) [418], cooling [421, 426, 428] or evaporation of the solvent [427, 429] led to the chelation of the vehicle liquid. The formed microspheres could be post-treated by additional crosslinking [421], high temperatures to get rid of the organic binder and to consolidate the structure [418-420, 425-429] or autoclaving [428] to obtain phases of low crystallinity. The granules were loaded with diverse (model) drugs and proteins (e.g. alendronate, albumen) [418, 419, 424] and coated with a protective layer e.g. from PLA [426] to evaluate drug delivery and drug release kinetics or they were equipped with internal cavities for an improved bone conduction [427, 429]. Most of them ranged in a µm-size range from 100 to 2000 µm [418, 419, 425-427, 429] (Figure 11).

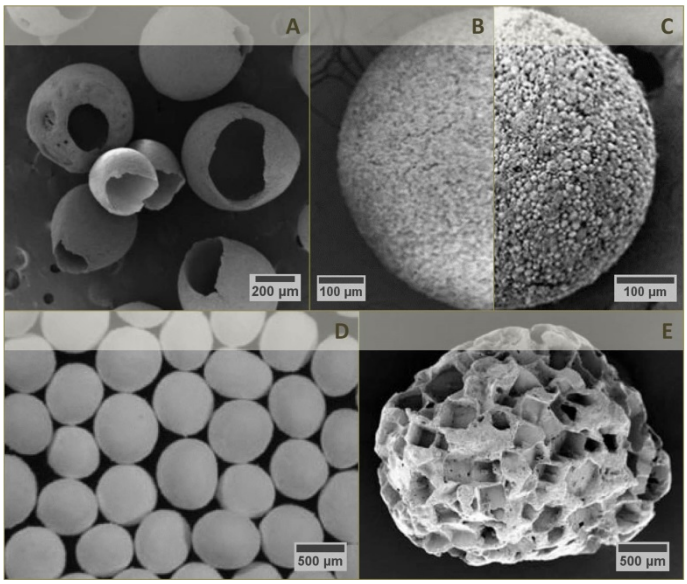

Figure 11: Scanning electron micrographs of CaP microspheres prepared by oil-in-water emulsion with subsequent solvent evaporation and thermal consolidation (a), by water-in-oil emulsion with subsequent autoclaving (b) or thermal consolidation (c), by drip-casting of a CaP-alginate-slurry in $CaCl_2$ solution with subsequent thermal consolidation (d) and by sieve-shaking of a CaP-ethanol slurry with subsequent cement reaction and porogen leaching (e). The micrographs were reprinted and adapted from [429],[428], [430] and [239]. Copyright (2010), with permission from Mary Ann Liebert, Inc. Copyright (2009), with permission from Elsevier. Copyright (2008), with permission from John Wiley and Sons. Copyright (2007), with permission from Springer Science+Business Media, LLC.

Beside emulsification, there are alternative techniques to gain spherical particles from pasty systems which must not necessarily be self-setting. Sieving and extruding a mixture of powder and binder liquid equally enables the fabrication of spherical structures, but the resulting diameters are limited to stay within a mm-range, as the pores of the used pelletizing tool (e.g. sieve) might be clogged easily with the used paste system [410]. Exemplarily, Cortez *et al*. [431] fed a paste of HA and hydrated cellulose in an extruder with attached 1 mm sieve fol-

lowed by spheronization. The resulting particles were burned for removal of organic components and consolidation [431]. Tas [239] presented a system on the basis of carbonated HA raw powder mixed with ethanol and brought in granular form through sieve-shaking. The cement reaction was initiated by immersion of the dried granules in water [239].

Further methods which are not described here in detail, but enable the formation of spherical granules in a sub-mm-range for instance include drip-casting [430, 432, 433] and lost-wax method [434, 435]. Bohner [410] proposed 3D-powder printing for the production of CaP microspheres [410]. Nano- to microparticles are gained exemplarily *via* flame-synthesis [436, 437] or classic precipitation [438, 439]. A particularly approach in this regard has been presented by Tas [440] who simply aged modified SBF solution to obtain *in situ* formed nanosized, monodisperse, amorphous CaP spheres [440]. The above described emulsion technique is likewise transferable to nano- to micronsized particles (precipitation-emulsification) [441, 442]. Regarding most of the mentioned techniques, it is referred to the well-arranged review article about the synthesis of granular materials on a CaP basis written by Bohner *et al*. [410].

The fabrication techniques and size ranges of CaP particles are broad and they are frequently handled for diverse intended uses [410]. Beside their application as MPC raw powders in cement systems (chapter 2.1.2), in additive manufacturing processes such as 3D-powder printing [323, 362] and in CaP/MgP nano-precipitates exemplarily for gene delivery [443-445], little information is available about the use of MgP-particles and granules as independent bone grafts. Zeng *et al*. [383] implanted cell-seeded MgP granules (probably newberyite) for maxillary sinus floor augmentation in New Zealand white rabbits, but the fabrication manner, size and composition of those granules is vague [383]. Christel *et al.* [422] used the water-in-oil emulsion technique to generate spherical struvite granules within a size range of 200 to 1000 µm for dental applications [422]. A special particle-based formulation was proposed by Laurenti *et al*. [446] who prepared MgP nanosheets (similar to newberyite) *via* precipitation. In water, those formed long-term stable, injectable, physically crosslinked hydrogels with outstanding biological properties for bone regeneration [446, 447].

2.3.1.2 Scaffolds

The presumably easiest way to generate prefabricated cement-based scaffolds is casting of the cement paste in a specific mold. As already mentioned in a previous chapter (2.1.1.5) porosity is a key property in terms of the biological outcome as it decides about degradation and cell invasion, especially in the case of materials with low chemical solubility (HA). To generate interconnecting macropores [36], the addition of leachable porogens with short (e.g. mannitol, sodium chloride) [104, 111] or longer durability (e.g. PLGA, gelatin) [231, 245] or supplementation with foaming agents (e.g. $NaHCO_3$ and acid, surfactants, proteins with foaming capability such as albumen) [199, 207, 244] is one option to circumvent this issue. Oil-in-water emulsions equally create scaffolds with additional porosity [232]. All three strategies (porogen leaching, gas foaming and oil-in-water emulsions) are very common in CPC research. As MPC research with biomedical purpose is quite new and perhaps due to the higher *in vivo* resorption potential of MPC hydration products, the need for macroporous MgP scaffolds is potentially minor. When applying one of these techniques, solely sodium chloride

was used as water-soluble porogen in MPC or mixtures with CPC [376, 384, 448]. In this context, it should be mentioned that microporous scaffolds are not restricted to prefabricated implants, as injectable foams are also in the focus mostly of HA-CPC research [199, 250-253, 449]. Alternatively, organic foams might be impregnated with CaP [450-453] or MgP [454] followed by cauterization of the foam template, but this method only provides high-temperature phases.

Going a step further, freeze-casting is a possibility to obtain at least unidirectional lamellar channels within a ceramic matrix. In principle, a slurry of ceramic powder (e.g. HA), solvent (e.g. water), dispersant (e.g. ammonium polymethacrylate) and organic binder (e.g. polyvinyl alcohol) [455, 456] is frozen followed by ice crystal formation of the solvent whereat the cooling conditions (e.g. cooling gradient) will have a large impact on the crystal growth. Afterwards, the solidified solvent sublimates i.e. directly passes into the gas phase at low pressure. The remaining pores are a negative replica of the ancient ice crystals and the walls oftentimes are consolidated *via* high-temperature treatment [457] or freeze-drying [458-460] in case of retaining the organic component. For detailed information, see the review article of Deville [457]. Water (solidification point of < 0 °C) [455, 456, 458, 459, 461-470] and camphene (solidification point of 44 to 48 °C) [471-476] are typically used as solvents for ice-templating in which the latter enables processing at RT [457]. Usually, inactive HA [455, 456, 461-466, 469-473, 475] or β-TCP [468] particles were used as solid constituents of the slurry, but reports about composites with glasses [467, 476] and polymers such as PLGA [460], poly-L-lactide [477], collagen [458], alginate [459], gelatin [460] and chitosan [477] can also be found in common literature. Obviously, most research in this field focused on the usage of non-reactive CaP particles and only little information is available in terms of freeze-structured reactive cement systems. Exemplarily, a purely inorganic system was presented by Hesaraki [478] who prepared an aqueous suspension from TTCP and DCPA which was freeze-templated and -dried, followed by immersion in SBF solution for HA conversion [478]. In contrast, Qi *et al*. [479] dispersed HA forming CPC raw powder in 2 % alginate solution and froze the cement paste with a temperature gradient from -30 °C to RT to create unidirectional macropores. After freeze-drying, the scaffolds formed HA at 37 °C and 100 % relative humidity and were infiltrated with PLGA [479]. He *et al*. [480] plasma-treated those scaffolds for additional collagen immobilization [480]. Such or similar scaffold design could not be found in MgP or MPC research.

To obtain scaffold with even more manageable pore size and distribution, one can make a detour of computer-aided negative moulds exemplarily from wax (*via* ink-jet printing) [453, 481-484] or epoxy resins (*via* stereolithography) [485] with periodic pore structure. Those can be impregnated with the corresponding cement paste, mostly non-reactive HA-slurries, followed by removal of the organic template through high temperature treatment [453, 481-487]. One big advantage of the negative mould technique is its independency from the casting process and thus from any possible material composition of the finished scaffold which cannot be processed with direct methods [481, 482].

Direct additive manufacturing techniques offer the possibility to straightly generate reproducible scaffolds with controllable architecture. Among all existing methods, only few can take advantage of the setting principles of mineral bone cements [35]. In contrast to other ap-

proaches such as selective laser sintering or fused deposition modeling (FDM), 3D-powder printing works at RT which is beneficial for the possible incorporation of temperature sensitive additives (biologically active substances e.g. growth factors, antibiotics) and enables the use of low-temperature phosphate powders. Basically, a binder liquid is printed selectively and computer-aided onto a ceramic powder bed which leads to a bonding of the particles within the layer. A new powder film is deposited and the binder liquid is anew spread on top to link both layers and so forth. The predetermined construct is built in a layer-by-layer manner. The consolidation of the resulting 3D-construct occurs physically when the binder liquid contains water-swellable polymers (e.g. cellulose, starch) or chemically when the binder liquid initiates hydraulic dissolution/precipitation reaction. The two main requirements for exact results are: 1) an adequate powder size (15 to 35 µm) which is smaller than the layer thickness (< 80 to 150 µm) and large enough not to form agglomerates (> 5 µm) and 2) the setting time should ideally be within 1 to 2 min as either unregulated spreading of the binder liquid or inexistent fusion between the layers would impair the accuracy and stability of the resulting 3D-construct [355]. This method can be used to take computed tomography scans as templates for the fabrication of patient-specific replacements. Klammert *et al*. [26] descriptively demonstrated the feasibility of this process by means of human cadaver skulls [26].

Beside finding out ideal basic printing parameters concerning the particle size, flowability, compaction rate and surface roughness of the powder bed [488], Butscher *et al*. [488-490] discovered further interesting optimizing strategies: Plasma treatment of the raw powder can improve the powder flow- and wettability [488], printing under moist conditions can improve the accuracy and resolution of the printed structures [490] and printing of special scaffold designs (cages with loose fillers) can improve the depowdering results [489].

In cementitious systems, the powder bed mostly consisted of monophasic or biphasic mixtures of α- and β-TCP and the binder liquid was a diluted phosphoric acid with concentrations between 5 to 40 % to form brushite as resulting hydration product [26, 217, 488-499]. Alternative formulations comprehend the addition of HA fillers, the addition of surfactants for an improved printing process, the addition of collagen [500] or alginate for an ameliorated mechanical and biological outcome [500, 501], TTCP with phosphoric acid and diluted phosphate salts [497, 498] mixtures of CSH and pregelatinized starch with water [502], mixtures of TTCP/β-TCP, TTCP/CSD [503] or TTCP/DCPA/TCP with citric acid [496, 503] and farringtonite with ammonium phosphate solution [323, 504]. For unreactive systems, powders from biphasic TCP [496, 499], coarse and fine HA [505], HA/β-TCP granules [506] and farringtonite [362] were composed with organic binders such as HPMC [496, 499], starch [505], dextrin and saccharose [506].

Common post-treatment approaches are sintering to get rid of organic residues, for mechanical consolidation and to obtain glass-like phases (e.g. from calcium pyrophosphate) [362, 492, 493, 503, 505, 506], immersion in binder or other adequate solution for higher conversion and mechanical consolidation [26, 217, 323, 362, 491, 492, 494, 495, 497, 498], hydrothermal treatment (i.e. autoclaving) [26, 217, 491, 494, 497, 502] or heating [498] to obtain anhydrides (e.g. monetite from brushite) and infiltration with biologically active substances (e.g. VEGF, antibiotics) [497, 498] or biopolymers for a better biological outcome (e.g. collagen, alginate) [500, 501] and synthetic soluble polymers (e.g. PLGA) [493, 498] or insoluble

systems (e.g. dianhydro-D-glucitol [bis(dilactoylmethacrylate)] and 2-HEMA) [503] for a mechanical improvement. The research of Vorndran *et al*. [499] shall be notably pointed out, as the use of a multijet 3D-printing head enabled the simultaneous process of powder printing and drug incorporation with variable drug distribution (homogeneous, depot-like, gradual or with an outer polymer barrier) [499].

Premixed cement systems seem to be the ideal candidate for computer-operated extrusion processes through thin moving nozzles which directly “write” the desired paste scaffold on a building platform. This technique is also known as 3D-dispense-plotting [453, 483, 484, 507-509], 3D-plotting [510-515] or robocasting [516-524] amongst others. Just as in the case of 3D-powder printing, the extrusion process is performed under mild conditions and allows the simultaneous incorporation of biologically active substances such as (encapsulated) VEGF [510, 513] or bovine serum albumin (BSA) [510, 512]. However, only few publications were found dealing with the 3D-plotting of premixed cement pastes, all based on the same non-aqueous formulation which consisted of carbonated HA forming raw powders and an oil phase, stabilized *via* surfactant molecules [510-513]. This is probably due to the demands which are made on such a paste: it has to be injectable through a thin needle which requires a low viscosity while extrusion but simultaneously retain its shape and concurrently fuse at the contact points of different layers until the hardening process is finished [525]. Using premixed formulations, the setting reaction can be initiated by storing the printed scaffold under aqueous conditions [510-512] or at least high humidity [510]. Luo *et al*. [512] even showed the feasibility to print biphasic scaffolds of a non-aqueous CaP paste and an alginate solution using a multi-channel plotter which deposited alternate layers of both. In this case, the aqueous setting solution additionally contained $CaCl_2$ for crosslinking of the alginate and direct loading of both pastes with BSA for protein delivery purpose was likewise possible [512]. Recently, this concept was transferred onto a combination of CPC paste and VEGF laden alginate or alginate-gellan gum blends [513]. Maazouz *et al*. [516] used a self-setting ink from reactive α-TCP in 10 % gelatin solution for 3D-dispense-plotting. While α-TCP formed HA in water through dissolution/precipitation, gelatin was chemically crosslinked and equipped the scaffolds with viscoelastic properties and simultaneously improved the biological outcome [516].

Indeed, mostly HA [453, 483, 484, 507, 514, 515, 517, 518, 520-523, 526-529], β-TCP [517, 519, 521, 524] or mixtures of both [508, 509, 521, 523, 524] were simply used as ceramic fillers in viscous solutions of chitosan [526], alginate [514, 515], maltodextrin [514], HPMC [517, 519, 522, 524, 529], Pluronic® [521, 523], polyvinyl butyral [527] or polyacrylate [522, 528, 529]. The ceramic inks were gelled adequately (e.g. by adding the flocculent poly(ethylene imine) (PEI)) [517, 519, 520, 524, 528] and after printing them onto a building platform [483, 484, 507-509, 514, 515], in a gelling liquid (in case of not being gelled before) [514, 526] or in an oil bath [517, 519-524, 528, 529], the 3D-printed scaffolds were usually sintered [453, 483, 484, 507-509, 514, 517-524, 527-529] for mechanical consolidation and removal of organic residues, but more rarely post-gelled (e.g. alginate in $CaCl_2$ solution) [515] or freeze-dried to preserve the organic component (e.g. chitosan, alginate) [514, 526].

Dispense-plotted formulations on the basis of MPC or at least with MgP fillers could not be found in common literature. Anyway, some related projects were discovered such as the one

of Richard *et al*. [524] who used magnesium doped TCP as a filler for a HPMC based ink [524] and Casas-Luna *et al*. [530] who infiltrated a plotted TCP scaffold with pure magnesium [530]. Examples of CaP scaffolds fabricated by different additive manufacturing methods can be seen in Figure 12.

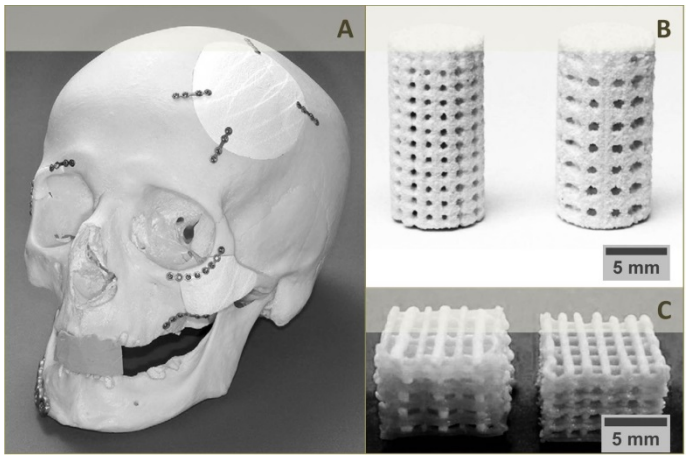

Figure 12: Photographs of CaP scaffolds prepared by 3D-powder printing (a-b) and 3D-plotting. *Via* 3D-powder printing, customized implants for a human cadaver skull from biphasic TCP powder and 20 % phosphoric acid (a) and cylindric scaffolds with high accuracy and variable pore size from the same composition (b) were gained. 3D-plotting enabled the fabrication of biphasic CaP/alginate (left) or composite CaP/alginate (right) constructs from premixed cement paste and alginate solution using a multi-channel plotter (c). The photographs were reprinted and adapted from [26], [495] and [512]. Copyright (2010), with permission from Elsevier. Copyright (2013), with permission from IOP Publishing Ltd. Copyright (2013), with permission from Royal Society of Chemistry.

2.3.2 Novel application forms

The following chapter will focus more on such application forms which seem to be vastly under-explored in mineral bone cement research including drillable bone cements, bone waxes, prefabricated laminates and bone adhesives. All the experiments on this thesis were performed with the purpose to fill the gaps and solve the issues that exist within this research area.

2.3.2.1 Drillable bone cements

The following section 2.3.2.1 is likely to be used in the introduction of a publication manuscript, which is however not submitted or published by the time of the submission of this thesis.

One method of bone fracture fixation are plate and screw fixations which shall supply the affected bone area with adequate stability, reduce and spread loads and thus reduce occurring strains without impair the natural bone healing process. In some cases those fixation systems must additionally be structurally augmented whereat the stabilization of comminuted or metaphyseal fractures or poor bone quality are the main indications, as well as augmentations of exemplarily the tibial plateau or vertebral bodies [531].

Table 12: Augmentation techniques of screws with mineral bone cements.

	technique		
no.		*1st step*	*2nd step*
1	[532-534]	cement application	screw embedding before cement sets
2	[535]	screw insertion	cement application through surgery accession
3	[534]	screw insertion	cement application through cannulated screw
4	[23, 535]	cement application	cement tapping/drilling and screw insertion after cement has set

Doht *et al*. [23] analyzed the treatment of lateral depression fractures of the tibial plateau in a biomechanical fracture model and showed that the combination of a screw osteosynthesis technique (jail technique) with a mineral bone cement behaved superior compared to the bone cement or screw system solely. In brief, the combination of both lowered the displacement of bone fragments under partial weight bearing conditions [23]. Charles *et al*. [536] examined pull-out forces for augmented and non-augmented percutaneous pedicle screws in spines of cadavers (82-100 years old) and observed elevated values of up to 944 N in case of cement augmentation. In their study, the authors used conventional PMMA bone cement for screw augmentation [536], which is commonly linked to severe drawbacks such as elevated temperatures and volume shrinkage while setting as well as a bioactivity deficit [27]. For the combined augmentation of screws and mineral bone cements, there generally exist four options (Table 12). Hoelscher-Doht *et al.* [535] compared cases 2 (screw insertion and cement application through surgery accession) and 4 (cement application and cement tapping/drilling and screw insertion after cement has set) for the treatment of a model tibial head depression fracture. They asserted that the application of the cement before screw insertion

led to a minor secondary loss of reduction, as this technique enabled a complete defect filling [535].

Because of their brittle mechanical nature, CPC as well as MPC are not suitable for load-bearing applications [15]. Special mechanical demands are therefore made on a cement system when the cement shall stabilize bone fragments and be taped and drilled afterwards, as brittle materials are known to craze while screw insertion [397]. Only one commercially available product was found that consists of mineral bone cements and deals with drillability (Norian® drillable, DePuy Synthes) [103, 531, 537]. Norian® drillable is based on CPC chemistry and gains its resistance to tapping and drilling by reinforcement of the cementitious matrix with bioresorbable fibres [21, 531]. The embedment of fibres can improve the composite toughness [103] as well as its tensile and flexural strength because of crack bridging, but this often impairs the cements' workability [37] and interface compatibilization stays one of the most challenging tasks in fibre reinforcement research [103].

2.3.2.2 Bone wax

The following section 2.3.2.2 is reused from the research article: T. Brückner, M. Schamel, A.C. Kübler, J. Groll, U. Gbureck. Novel bone wax based on poly(ethylene glycol)-calcium phosphate cement mixtures. Acta Biomaterialia. 33 (2016) 252-263. T. Brückner holds first authorship. She designed and executed the whole experimental study alone except for the mercury porosity measurements, which were conducted by M. Schamel. She further wrote the whole manuscript, whilst J. Groll and U. Gbureck were involved in supervision, submission and proof-reading. A.C. Kübler came up with the idea of the study.

Since its introduction in 1886 by V. Horsley [2, 538] bone wax is used as mechanical hemostatic agent in the case of bone injury without having intrinsic hemostatic properties [539]. From a historical point of view, bone wax was a mixture of beeswax, salicylic acid and almond oil [538]. Nowadays, sterilized [539] mixtures of beeswax, isopropyl palmitate and softening agents are used [2, 538]. Bone wax is getting soft and malleable when warmed [2] and can be pressed onto an osseous wound to create a physical barrier (tamponade) to bleeding [539]. It is easy to handle and cost-effective [539], but its suitability as bone sealant should be considered critically.

Beside allergic reactions [2], several clinical case reports recovered foreign body reactions with fistula [540], abscess [541] or granuloma [542] formation, serous discharge [543] and inflamed fibrous tissue [24] after treatment of cranial defect [540], mastoid [541], iliac crest [543] or sternum [24, 542] with bone wax. Furthermore the risk of infection increases when bone wax is used as sealant agent as it serves as nidus for bacteria [2] such as *Staphylococcus aureus*, that might promote diseases like osteomyelitis [544]. Damages of the surrounding tissue are also reported in terms of inferior alveolar nerve morbidity [545] and cord compression [546]. Bone wax further hinders osteogenesis as it is not resorbable under physiological conditions [2, 538]. These adverse effects on bone regeneration could be seen in animal models with defects at iliac crest [547], tibia [548] and sternum [549, 550] associat-

ed with inflammation and reduced mechanical integrity [549]. For those reasons, bone wax is only recommended as a first-line treatment [539] in non-infected defect sites [2] and a reconsideration of the classical bone wax composition should be performed urgently.

Some efforts were made to improve the properties of bone wax formulations. The use of resorbable polymers as for example alkylene oxide copolymers [550, 551], PEG [552], PEG/microfibrillar collagen composites [553], PEG-poly(propylene glycol)-PEG copolymers [554, 555] or chitosan [556] may improve osteogenesis. As they dissolve in the body, no interferences with bone healing take place and infection rates might be reduced [550, 551, 555]. The supplementation with hemostatic agents, as for example pregelatinized starch [557], is an approach to promote liquid sealing ability of bone wax as it absorbs water and low molecular weight components from blood. Starch is a natural polysaccharide [554] being composed of two glucose polymers [558] amylopectin and amylose (Figure 13) [554, 558, 559] with varying amylose contents between 0 and 80 % [559]. Gelatinization of native starch with subsequent dehydration leads to the formation of pregelatinized starch [558, 559], which is known to form gels in cold water whereas native starch is water-insoluble [558]. Pregelatinized starch is known to be biodegradable [560], non-toxic, nonirritating and cost-effective [554] and was found to be suitable for controlled release matrices [558, 559] and tissue engineering scaffolds [561, 562].

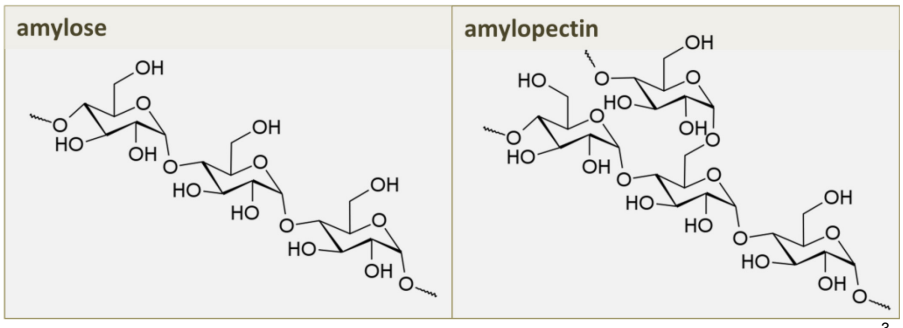

Figure 13: Chemical structures of starch basic modules amylose and amylopectin [3].

Incorporation of osteoconductive particles into the above mentioned bone wax like systems is rather described in literature. Chen *et al*. [563] analyzed bioactive glass, chitosan and carboxymethyl cellulose composites. Hoffmann *et al*. [556] used starch and chitosan modified HA particles to form a water-based slurry that could be suitable as substitute for classic bone wax. It would be supposable to exchange these osteoconductive, but non-reactive CaP particles by reactive CPC precursors and directly incorporate them into a resorbable polymer matrix. Such a system could not be found in current literature, so far.

[3] This figure is not contained in the article T. Brückner *et al*., Acta Biomater. 33 (2016) 252-263.

2.3.2.3 Prefabricated laminates

The following section 2.3.2.3 is likely to be used in the introduction of a publication manuscript, which is however not submitted or published by the time of the submission of this thesis.

As a consequence of trauma, neurological surgery or infection of the cranium, autologous (if available) or synthetic flaps are secured with screws, miniplates and clamps or sutures from titanium on the healthy skull surface (cranioplasty). Nowadays, titanium meshes or PMMA cements are mostly considered as substitutes, but major issues of titanium are its low malleability [25] and its comparably high thermal conductivity [26], while PMMA leads to heat necrosis and inflammation due to its exothermic reaction. In both cases, chemical bonding to the native bone tissue is not enabled [25]. Pure CaP or MgP pastes alone might not be able to replace those synthetic allografts for such plane defects and stay in place. To broaden the application range for unset mineral bone cements to non-cavity-like defects, the following requirements must be fulfilled: Mineral bone cements have a pasty consistency and tend to flow as long as they are uncured when being not confined *via* an external barrier, i.e. surrounding bone. For plane defects, it would be necessary to equip the bone substitute with an internal stabilizing structure, e.g. a polymer-based fiber mesh with a geometry allowing an optimal paste penetration and distribution. An alternating lamination of cement paste and the fibrous structure would form a 2-dimensional construct for the cover of corresponding defects. As the cranium is not of flat, but of curved geometry, the cement-fiber-construct should be flexible and adaptable while surgery and harden afterwards. This problem represents an ideal application for premixed cement pastes (chapter 2.2.3). No reports about this kind of application form neither for CPC nor MPC could be found in current literature. For the mentioned reasons, such constructs were termed “prefabricated” laminates.

2.3.2.4 Bone adhesives

The following section 2.3.2.4 is likely be used in the introduction of a publication manuscript, which is however not submitted or published by the time of the submission of this thesis.

There are two main indications for the application of bone adhesives: One is to joint bone fragments of comminuted fractures as a bone-to-bone interface. This allows the complete substitution of fracture fixation metal components like wires, screws and plates which also circumvents a second surgery for the removal of those implants. Further, bone adhesives can serve as an additional bone-to-metal interface for metallic alloys (e.g. stainless steel). To be applied at both indication sites, appropriate adhesion to bone, as well as metal compartments is necessary. Especially in the first case, the adhesive material must not impair fracture healing which is enabled while applying the bone adhesive only selectively or by using biodegradable materials. Most synthetic materials that have been tested as bone bonding agents do not fulfill the requirement of biodegradability, as for example PMMA and its associated formulations [1].

In contrast, mineral bone cement formulations just like CPC and MPC can be degraded *in vivo* [209, 210] but were actually not developed for the application as bone adhesives, but simply as bone substitutes or bone void fillers, respectively. Unfortunately, especially CPC are considered to have relatively low bone adhesiveness [1]. Indeed, CaP are described as osteoinductive materials which indicates their ability to induce bone formation at heterotopic defect sites [198] and when implanted in cortical bone, a narrow contact between a HA forming CPC and bone was observed [190, 304]. However, an instant bone bonding which would be desirable for their use as bone adhesives is not the case [304]. In the field of CPC, there are little examples which directly prove the ability of those cements to glue on bone surfaces. Grover *et al.* [304] substituted orthophosphoric by pyrophosphoric acid in a brushite forming cement system to improve its bonding on cortical bone and on different biomaterial surfaces [304]. This is why most research with respect towards mineral bone cement for application as bone bonding agents focused on the implementation of CaP fillers such as MCPM [564] or β-TCP into methacrylated polymer-based composite systems just like biodegradable methacrylated PLA [564-566]. However, because of their similarity to the mineral phase of bone [1, 36], CPC are still promising for applications where bone bonding is required [1]. In general, MPC seem to have the higher bonding potential [1] as they were already used in an adhesive manner *in vivo* for a successfully improved tendon-to-bone-healing [306] and it was shown that MPC are more effective in stabilizing bone fragments to native bone compared to CPC [567]. Gulotta *et al*. [306] exemplarily used a commercially available MPC [566] which was composed of reactive MgO, potassium as well as sodium phosphate and tricalcium phosphate. Though, this formulation has not been approved as bone adhesive so far [1].

3. Results and discussion

3.1 Calcium phosphate cement based approaches

The subsequent chapters refer to **Project 1** *in the experimental section and describe different possible application forms of HA forming CPC such as drillable cements, bone waxes and prefabricated laminates (chapter 2.3.2). They are based on the concept of either dual setting or premixed cement systems presented in chapter 2.2.1 and 2.2.3, respectively.*

When it comes to alternative setting mechanisms for mineral bone cements, they are initially applied in HA forming CPC which has well-defined reasons: Beside the fact that these cements - regardless of their being based on α-TCP, TTCP/DCPA or carbonated formulations - have been studied for decades, they are comparably easy to apply in different paste systems. Even if the raw powder consists of more than one single component, these raw materials are considered being storage stable. This is especially important for premixed formulations which have to be resistant towards conversion for months. Water is sufficient for setting and the system does not require any additional compounds which are possibly not compatible with the setting mechanism. To accelerate the slow conversion of HA, besides the common approach of adding orthophosphate ions, other options likewise optimize the non-decay of the cement paste in an aqueous environment such as fast gelling monomers (e.g. 2-HEMA in dual setting cements) and polymers (e.g. pregelatinized starch in premixed cements) which entrap unreacted raw powder particles or the use of surfactant molecules (e.g. castor oil ethoxylate 35 in premixed cements) which stabilize solid and liquid phase. Those options are each compatible with the corresponding setting mechanism and maintain the cohesion of the paste as long as the HA conversion slowly proceeds. The setting reaction is neutral such that compounds of alternative setting systems which are susceptible to low pH are not impaired by the cementitious reaction (e.g. 2-HEMA in dual setting cements). Those arguments partially exclude brushite forming CPC and MPC for their use in diverse alternative setting formulations, but it has to be kept in mind that all presented systems are more or less model formulations for biodegradability issues when it comes to application *in vivo*. The different feasible paste systems for HA forming CPC further enable a vast spectrum of varying application forms among which three examples are presented in the following chapters (Table 13).

Table 13: Setting concepts, paste compositions, application forms and intended use cases for CPC.

chapter	setting concept	paste composition	products	application form	indication
3.1.1	dual	α-TCP & APS; 2-HEMA, Na_2HPO_2 & water	CDHA poly-2-HEMA	drillable cement	augmentation of bone fragments followed by screw fixation
3.1.2	premixed	TTCP, DCPA, Na_2HPO_2, NaH_2PO_4, (starch & vancomycin); PEG 1,500 & 400	HA	bone wax	osteoconductive sealing of osseous wounds
3.1.3	premixed	electrospun PCL scaffolds & α-TCP; biocement D, triglyceride & surfactants	carbonated HA	prefabricated laminates	osteoconductive covering of non-cavity-like curved defects

3.1.1 A systematic study of a drillable, injectable and fast-setting cement system

The subsequent application form describes the application of a model dual setting system (chapter 2.2.1.1) as a drillable mineral bone cement (chapter 2.3.2) and refers to **Project 1A** *in the experimental section.*

Single results of the following section 3.1.1 are reused from the research article: K. Hurle, T. Christel, U. Gbureck, C. Moseke, J. Neubauer, F. Goetz-Neunhoeffer. Reaction kinetics of dual setting α-tricalcium phosphate cements. Journal of Materials Science: Materials in Medicine. 27(1) (2015) 1-13. T. Brückner (née T. Christel) holds second authorship and provided the results of mechanical testing and scanning electron microscopy (SEM) and she wrote the concerned sections of the as-mentioned article. C. Moseke supported her in SEM imaging, whilst U.Gbureck was involved in proof-reading of the concerned parts. No other parts of the article, for which the collaboration partners K. Hurle, J. Neubauer and F. Goetz-Neunhoeffer were responsible, were used for chapter 3.1.1 unless to discuss the results. Concerned sections were specifically marked.

3.1.1.1 Abstract

The application of dual-setting cement systems is one sophisticated approach to overcome the brittle nature of CPC. In the present study, the dissolution of α-TCP raw powder with subsequent precipitation to form CDHA was combined with the simultaneous polymerization of the organic hydrogel component poly-2-HEMA. It was the main ambition 1) to gain detailed comprehension about the occurring setting mechanism with respect to setting kinetics, crystal size, specific surface area and conversion rate, how it is affected by different parameters such as 2-HEMA content (0 to 50 %), hardening in an aqueous environment (2 h to 7 d) and PLR (1.6 to 3.0 g/mL) and how these parameters further influence the mechanical outcome and 2) to adjust the formulation in a way such that it would be suitable for clinical application in terms of injectability, setting time and drillability. With increasing monomer amount, the conversion to CDHA was steadily confined resulting in minor CDHA extents and polycrystal sizes. Smaller crystals are known to form a more dense and thus more strengthened texture, but a minimum concentration of 50 % of 2-HEMA in the liquid phase of the cement paste was necessary to see imposing effects on the overall performance including the introduction of a pseudoplastic mechanical behavior (low bending modulus of at least 5.5±1.7 GPa and high adsorbed fracture energy of at most 13.3±5.8 mJ/mm² at improved bending strength). It further seemed to be beneficial to simultaneously increase the amount of water within the system i.e. decrease the used PLR to 1.6-2.0 g/mL. Such formulations were considered being injectable with injection forces of at least 75 N and drillable with screw pull-out forces of up to 260 N.

3.1.1.2 Introduction

A major drawback of CPC is the brittleness of their setting product, so that their application range is restricted to non-load-bearing usage. There are versatile approaches to improve the mechanical performance of CPC by addition of permanent as well as resorbable short and continuous fibers or fiber meshes [102]. Degradable fibers increased composite toughness

[128, 132, 141], mostly accompanied with an increased bulk porosity after fiber degradation [128, 132]. A more sophisticated mechanism to overcome the brittleness of CPC is the creation of a dual setting cement system whereby water soluble monomers are supplemented to the aqueous phase of the cement paste. Their polymerization is initiated simultaneously to the conventional cement dissolution/precipitation setting reaction resulting in an interpenetrating network of inorganic and organic compartments. The concept of dual setting cements was firstly described by Dos Santos *et al.* [149] in 1999 who used poly(acryl amide) cross-linked hydrogels for the improvement of CDHA forming CPC [149]. To overcome the toxicity of acrylamide residues [102], investigations with methacrylated dextran derivates [16] or 2-HEMA [17] were undertaken. In a former study, it was shown that the addition of 50 % of the water soluble monomer 2-HEMA to the aqueous phase of a CDHA forming cement matrix led to a composite with comparably high fracture strength, pseudoplastic behavior and accelerated initial setting [17]. It is further assumed that these - for a ceramic material - extraordinary mechanical properties enable drilling shortly after initiation of the setting reaction without failure.

Drillable bone cements could play a certain role in clinical applications when surgical screws are used for bone fracture management. Several screw fixation and plate osteosynthesis techniques are discussed for the treatment of calcaneus fracture exemplarily in case of intraarticular fracture with joint displacement of >2 mm [568]. The operative treatment of such complicated fracture appearances *via* plate osteosynthesis can be accompanied with damage of soft tissue, loss of reposition, posttraumatic arthrosis, infection and revision [569]. Additional augmentation of the fragments with an autograft from the iliac crest or alternative bone substitutes can be recommended when the fragments are greatly unstable [568]. Presumably, the augmentation with CPC could improve calcaneus treatment quality [4]. For fracture fixation, surgical screws can be embedded in the cement matrix, and, when screws are cannulated, the cement paste can be injected through the canal into the defect [531]. Clinical and biomechanical studies of Jones fractures fixations revealed that small screws of 4 mm fail earlier when being cannulated compared to solid screws [22]. If non-cannulated screws are used, drillable CPC are required, whereat little is known from literature. Detailed information about the clinical need for drillable mineral bone cements might be taken from chapter 2.3.2.1. The current chapter shall address the following goals:

1) Beside its good mechanical performance and fast setting time, the previously studied cement [17] had short workability and high viscosity due to its likewise high PLR of 3.0 g/mL what limits its range for clinical application. However, it was a prior aim to understand more the mechanisms and setting kinetics of the known dual setting model system on CDHA/poly-2-HEMA which was a cooperation project with the Department of Mineralogy in Erlangen [5].

[4] Personal communication from PD Dr. med. Stefanie Hölscher-Doht and Dr. med. Martin Jordan, University Hospital Würzburg, Trauma surgery.

[5] K. Hurle *et al*., J. Mater. Sci. - Mater. Med. 27(1) (2015) 1-13. This was a cooperation project whereat Theresa Brückner holds 2nd authorship for performance of the mechanical tests and providing scanning electron micrographs.

2) Secondly, certain modification would be necessary to transfer the model cement to clinical relevance as for example the treatment of calcaneus fractures with osteosynthesis techniques and simultaneous augmentation of the fragments with the drillable CPC. Thus, a lower PLR between 1.6 and 2.0 g/mL was chosen as varying parameter. In a systematic study, where mechanical performance, injectability and drillability were key features for evaluation, the clinical significance of this dual setting cement system is demonstrated.

3.1.1.3 Results

Table 14: Time for which cement pastes from α-TCP and 50 % 2-HEMA with varying PLR of 1.6, 1.8 or 2.0 g/mL were manually injectable. Samples from pure α-TCP with a PLR of 2.0 g/mL were taken as controls.

	cements with 50 % 2-HEMA			reference, no 2-HEMA
PLR	1.6 g/mL	1.8 g/mL	2.0 g/mL	2.0 g/mL
injectable for	4.5±0.0 min	3.7±0.3 min	3.0±0.5 min	>30 min

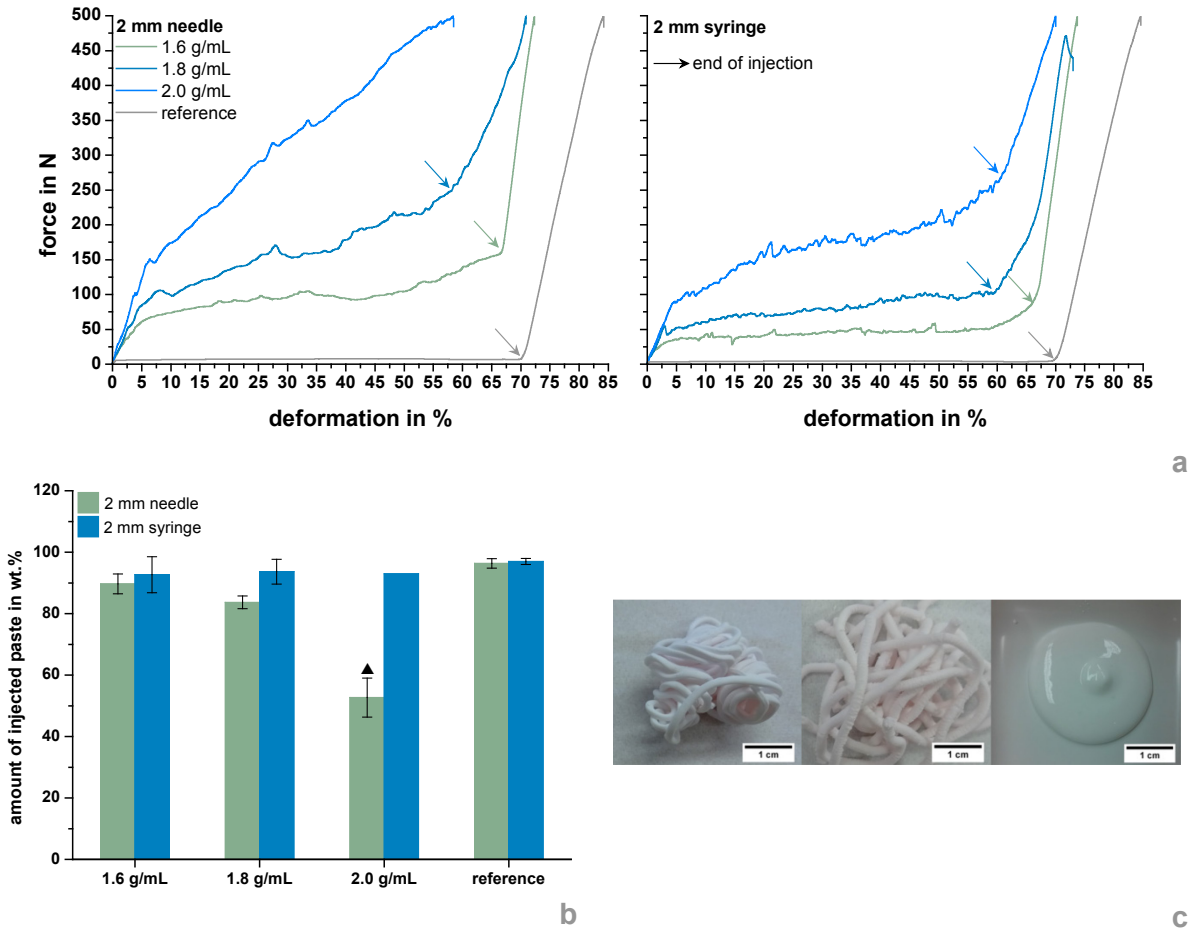

Figure 14: Injectability. Injection force of CDHA / poly-2-HEMA mixtures with a PLR of 1.6, 1.8 or 2.0 g/mL while injection trough a 5 mL syringe with or without a needle with a 2 mm inner diameter 150 s after mixing of the solid and liquid phase (a) and amount of injected paste during this test setup (b). Arrows indicate the end of injection when stress was applied on empty syringe. Photos of the injection product of the paste with a PLR of 1.8 g/mL trough a needle (c, left) or a syringe only (c, middle) and photo of the injected reference paste (c, right). The ▲ marked formulation showed significant difference ($p<0.001$) towards all others.

With increasing PLR, the time for which the 50 % 2-HEMA containing cements were manually injectable trough a syringe with a 2 mm inner diameter decreased from 4.5 min (1.6 g/mL)

to 3.0 min (2.0 g/mL). In contrast, reference paste without 2-HEMA was injectable for at least 30 min (Table 14). The force needed for this injection was measured by applying compression onto the syringe with or without a 14 G needle. High injection forces of at least 75 N for 2-HEMA-containing samples can be seen in Figure 14 a. Measurements without the application of injection needles led to a bisection of the injection force increasing with increasing PLR. In contrast, no difference could be monitored while injection of the reference paste and besides, injection forces of at least one magnitude lower were necessary. With the exception of 2.0 g/mL samples with needle, the cement paste could almost completely be injected trough the syringe (Figure 14 b), as amounts of at least 84 % were extruded. Despite high injection forces, the usage of needles additionally to syringes resulted in more homogeneous surface structures of extruded cement paste strands. The reference measurements again are an exception, as no cohesive strands were formed, but a low viscous unhardened paste without retaining its shape (Figure 14 c).

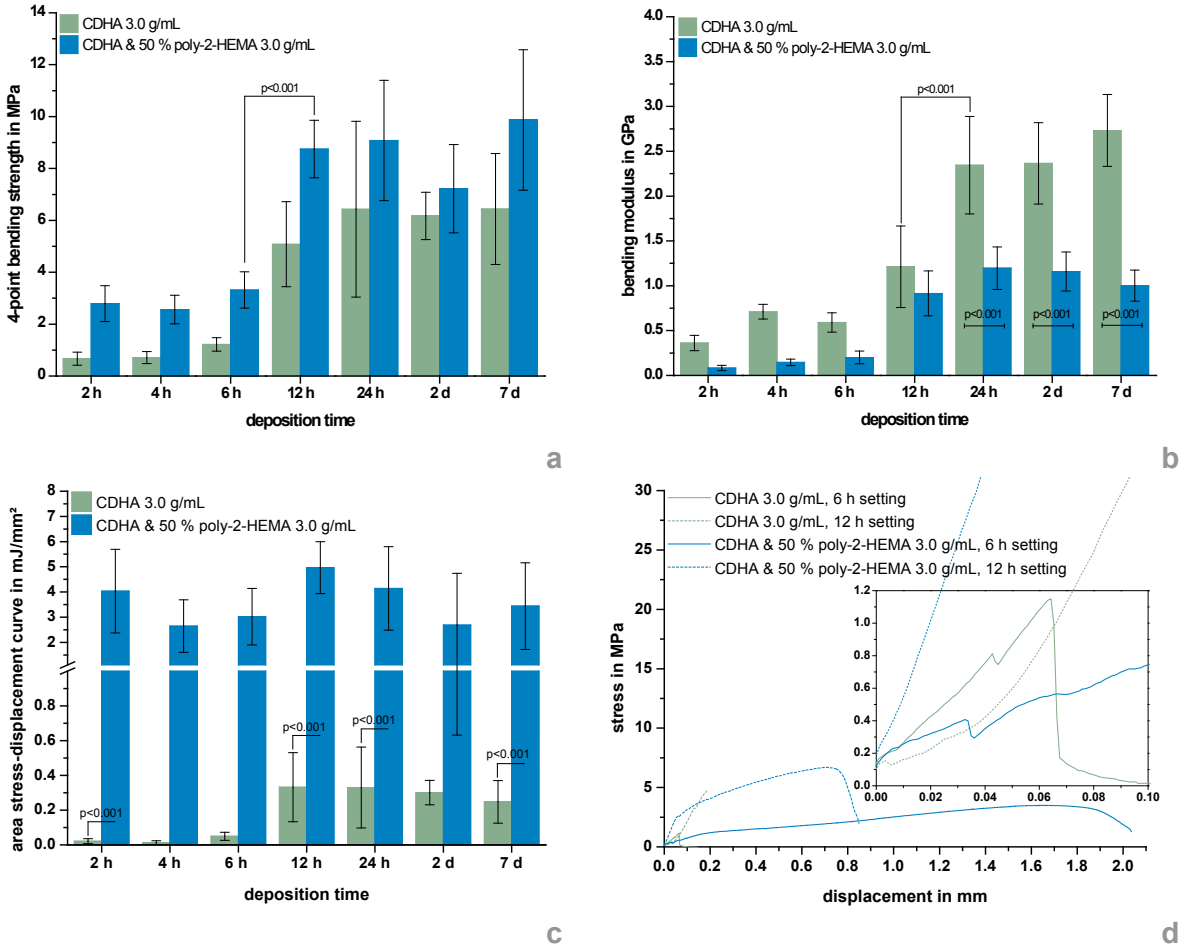

Figure 15: Mechanical performance I. 4-point bending strength (a), bending modulus (b), area under the stress-displacement curves (c) and stress-displacement curves of cements from CDHA and 50 % poly-2-HEMA with a PLR of 3.0 g/mL after 2 h, 4 h, 6 h, 12 h, 24 h, 2 d and 7 d of setting in water at 37 °C. Samples from pure CDHA with the same PLR were taken as controls [6].

For evaluation of the mechanical properties, three different parameter sets were analyzed: Initially, the dependency of the mechanical behavior was investigated in a time-resolved manner for constant formulations from α-TCP with 50 % 2-HEMA at a PLR of 3.0 g/mL

[6] Figures based on these results have already been presented in the shared publication K. Hurle *et al.*, J. Mater. Sci. - Mater. Med. 27(1) (2015) 1-13., but were exclusively produced by Theresa Brückner.

(Figure 15). Secondly, the impact of different 2-HEMA concentrations (Figure 16) was examined and in a final step, varying PLR of 1.6 to 2.0 g/mL with a constant 2-HEMA concentration of 50 % should reveal eligibility of cement formulations with adjusted workability (Figure 17).

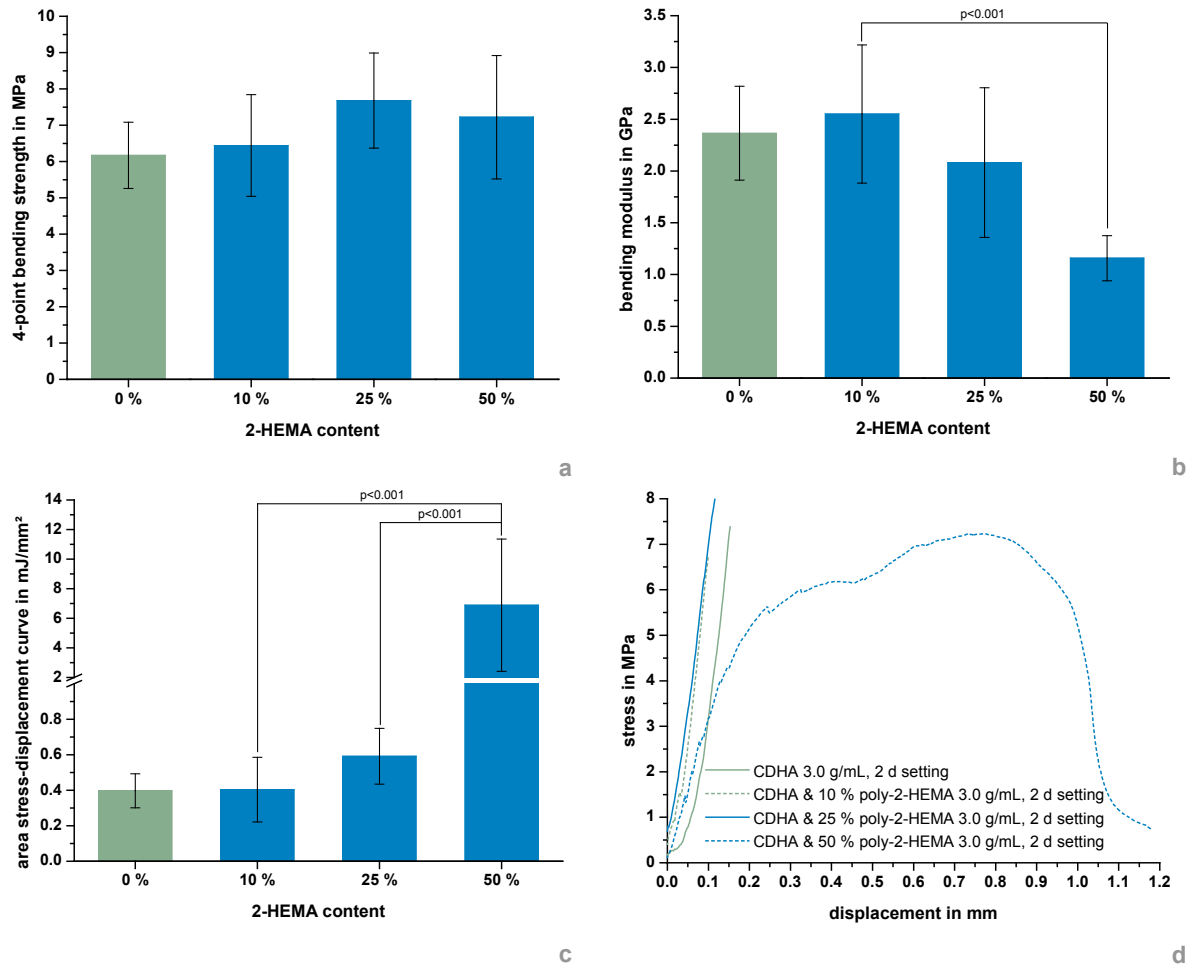

Figure 16: Mechanical performance II. 4-point bending strength (a), bending modulus (b), area under the stress-displacement curves (c) and stress-displacement curves of cements from CDHA and 10, 25 or 50 % poly-2-HEMA with a PLR of 3.0 g/mL after 2 d of setting in water at 37 °C. Samples from pure CDHA with the same PLR were taken as controls [7].

Figure 15 depicts the mechanical behavior of cements from α-TCP and 50 % 2-HEMA with a PLR of 3.0 g/mL and its time-dependent development by deposition in an aqueous environment for 2 h up to 7 d. For the 2-HEMA free control, a continuous increase of the 4-point bending strength from 0.7±0.3 MPa after only 2 h to 6.4±2.1 MPa after the whole examination period was observed. The strongest improvement of 316 % occurred between 6 and 12 h of deposition in water. Even though the general trend was similar for composites with 50 % 2-HEMA, the initial bending strength was about four times higher compared to the reference and the 1-week strength added up to 9.9±2.7 MPa. Equally, the composite material experienced a significant increase in bending strength by 164 % between 6 and 12 h (Figure 15 a). Both cement formulations demonstrated a time-dependent increase in bending modulus from initially 0.36±0.09 (no 2-HEMA) and 0.08±0.03 GPa (50 % 2-HEMA) which seemed

[7] Figures based on these results have already been presented in the shared publication K. Hurle *et al.*, J. Mater. Sci. - Mater. Med. 27(1) (2015) 1-13., but were exclusively produced by Theresa Brückner.

to stagnate after 12 (50 % 2-HEMA) to 24 h (no 2-HEMA) and resulted in 2.7±0.4 (no 2-HEMA) and 1.0±0.2 GPa (50 % 2-HEMA) after 7 d. At the same time, the reference experienced a significant doubling between 12 and 24 h and it showed higher values and thus more brittle behavior at every measured time point (Figure 15 b).

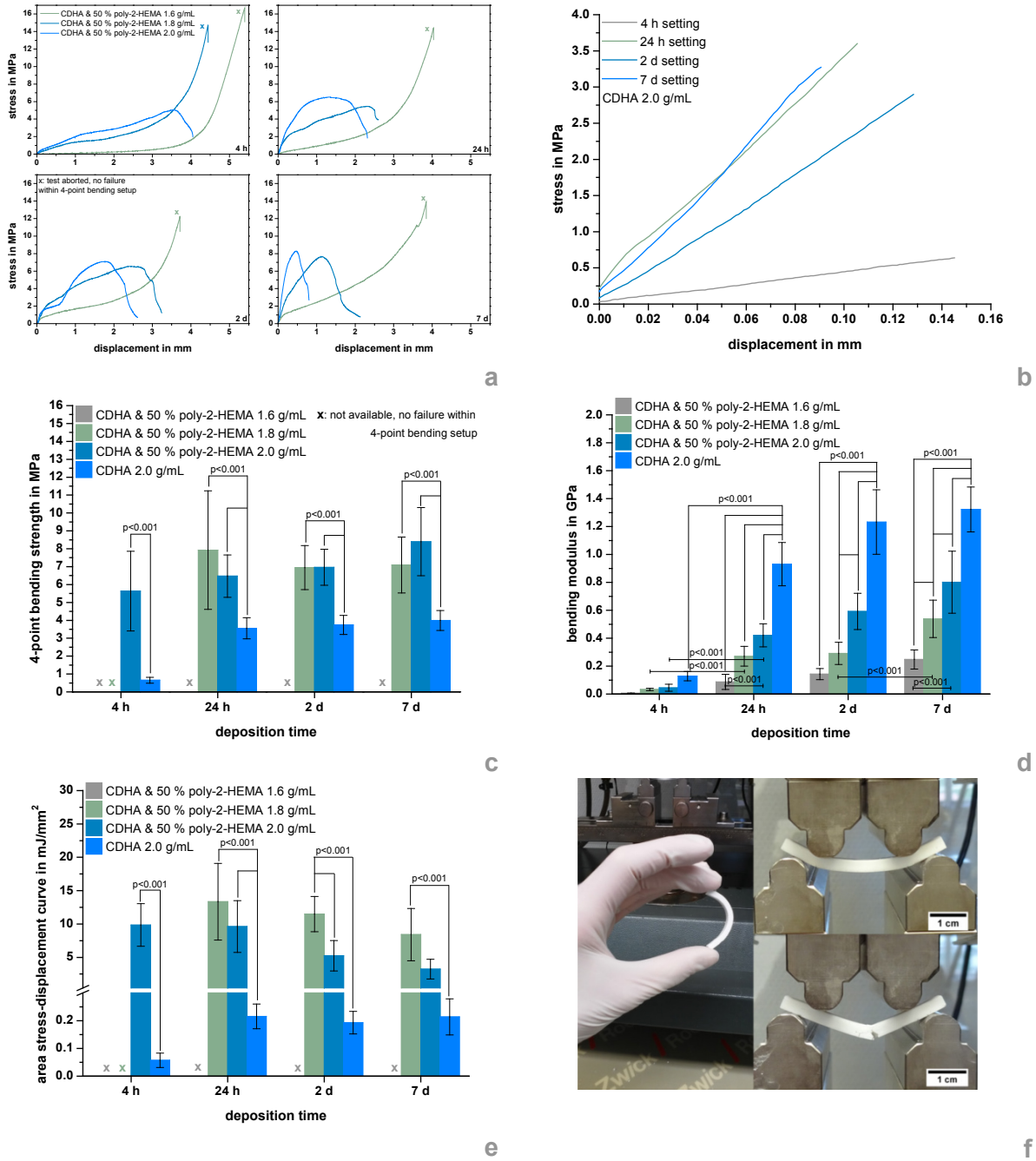

Figure 17: Mechanical performance III. Stress-displacement curves (a-b), 4-point bending strength (c), bending modulus (d), area under the stress-displacement curves (e) of cements from CDHA and 50 % poly-2-HEMA with varying PLR of 1.6, 1.8 or 2.0 g/mL after 4 h, 24 h, 2 d and 7 d of setting in water at 37 °C. Samples from pure CDHA with a PLR of 2.0 g/mL were taken as controls. Photo of the pseudoplastic behavior of a 1.6 g/mL rod after 4 h of setting (g, left) and photo of the test setup of a 1.8 g/mL rod after 24 h (f, right, above) and 7 d of setting (f, right, below).

Evaluating the area under corresponding stress-displacement curves, which might serve as a measure for the absorbed energy until fracture, a major discrepancy between the polymer-free and polymer-containing samples was visible. While the reference experienced an increase from 0.02±0.01 to 0.33±0.20 mJ/mm² within the first 12 h and showed comparable

values afterwards, the values of the 2-HEMA containing samples were around one order of magnitude greater and fluctuated between 2.6±1.0 (4 h) and 5.0±1.0 mJ/mm² (12 h) (Figure 15 c). A demonstrative summary of bending strength, bending modulus and area as a measure for the absorbed fracture energy in dependency of cement composition and deposition time is given by chosen stress-displacement curves. Pure CDHA depicted a fracture behavior which is characteristic for brittle ceramics while the addition of a polymer was able to implement a certain plasticity (Figure 15 d).

Reducing the 2-HEMA amount in the liquid cement paste from 50 to 25 and 10 % at the same PLR of 3.0 g/mL revealed that a certain monomer concentration was necessary for effective reinforcement of the cementitious matrix (Figure 16). While no significant differences were visible after 2 d of setting in water in matters of 4-point bending strength (Figure 16 a), only the cement formulation with the highest 2-HEMA amount did not behave similar towards the control group both in case of bending modulus (Figure 16 b) and stress-displacement course (Figure 16 d) as well as area under this curve (Figure 16 c).

Table 15: Initial setting times of cement pastes from α-TCP and 50 % 2-HEMA with varying PLR of 1.6, 1.8 or 2.0 g/mL. Samples from pure α-TCP with a PLR of 2.0 g/mL were taken as controls.

	cements with 50 % 2-HEMA			**reference, no 2-HEMA**
PLR	1.6 g/mL	1.8 g/mL	2.0 g/mL	2.0 g/mL
initial setting time	18.2±1.0 min	10.3±0.8 min	6.5±0 min	>30 min

As it was shown by Table 14 and Figure 14, the workability of dual-setting CDHA/poly-2-HEMA composites in terms of injectability became better with decrease in PLR. Simultaneously, higher amounts of cement liquid within the formulations would increase the total monomer amount despite unaltered 50 % 2-HEMA solution. Thus, the mechanical performance of composites containing 50 % 2-HEMA at reduced PLR of 1.6, 1.8 and 2.0 g/mL were also tested after limited deposition time points (Figure 17). Within this series, pure CDHA with a PLR of 2.0 g/mL was used as control. Figure 17 a describes stress-displacement curves of the three different 2-HEMA containing cements after 4 h, 24 h, 2 d and 7 d of setting. Obviously, all samples showed a pseudoplastic mechanical behavior characterized with high displacement. Partially, the measurements even had to be aborted as displacement passed the limits of the 4-point bending setup without failure of the rods. With increasing PLR and increasing immersion times, the brittle influence of the inorganic component increased (Figure 17 a), being characterized by increased maximum stress and increased curve gradient. A typical pure brittle fracture behavior could only be noticed in the case of control samples (Figure 17 b). With values reached between 5.6±2.2 and 8.4±1.9 MPa, PLR and deposition time further showed a minor impact on the bending strength of the test specimens, but a maximum improvement of 700 to 800 % compared to the CDHA control (Figure 17 c). The bending modulus, being higher with increasing brittle behavior, increased for all samples by the course of time and with decrease in 2-HEMA content. At the end of the study, values between 0.25±0.07 (50 % 2-HEMA, 1.6 g/mL) and 1.3±0.16 GPa (no HEMA, 2.0 g/mL) were reached (Figure 17 d). A 2.5-fold area under stress-displacement curves at most could be seen with decrease in PLR from 5.0±2.3 (2.0 g/mL) to 12.2±5.4 mJ/mm² (1.8 g/mL) on day 7 whereas no significant difference between samples of the same composition was visible by

the course of time. The lowest area, corresponding to the lowest material toughness, was even one magnitude higher compared to the reference (Figure 17 e).

The tested cement pastes had an increasing initial setting time from 6.5 min (2.0 g/mL) to 18.2±1.0 min (1.6 g/mL) with decreasing PLR (Table 15). However, after 10 min, setting was as progressed such that they could be drilled without damaging the dual set constructs. In contrast, a 2-HEMA free cement paste with a PLR of 2.0 g/mL had an initial setting time of >30 min and was hence not drillable after 10 min. For reference, screw pull-out experiments (Figure 18) could only be performed *via* embedding of the screw in the liquid cement paste. The stress while pulling-out led to a disruption of the reference specimen (Figure 18 a, below) which has not been observed for the dual setting cement systems (Figure 18 a, above). Figure 18 b shows exemplarily monitored force-displacement courses while screw pull-out for screws being drilled as well as embedded. Corresponding pull-out forces are depicted in Figure 18 c. The maximum load was always approximately as double as high for embedded compared to drilled specimens and increased with increasing PLR from 110±20 N (drilled, 1.6 g/mL) or 320±60 N (embedded, 1.6 g/mL) to 260±40 N (drilled, 2.0 g/mL) or 450±50 N (embedded, 2.0 g/mL). As already mentioned, the reference cement was not drillable after 10 min and the maximum load while pull-out of embedded surgical screws only reached values similar to drilled, 2-HEMA containing samples with corresponding PLR.

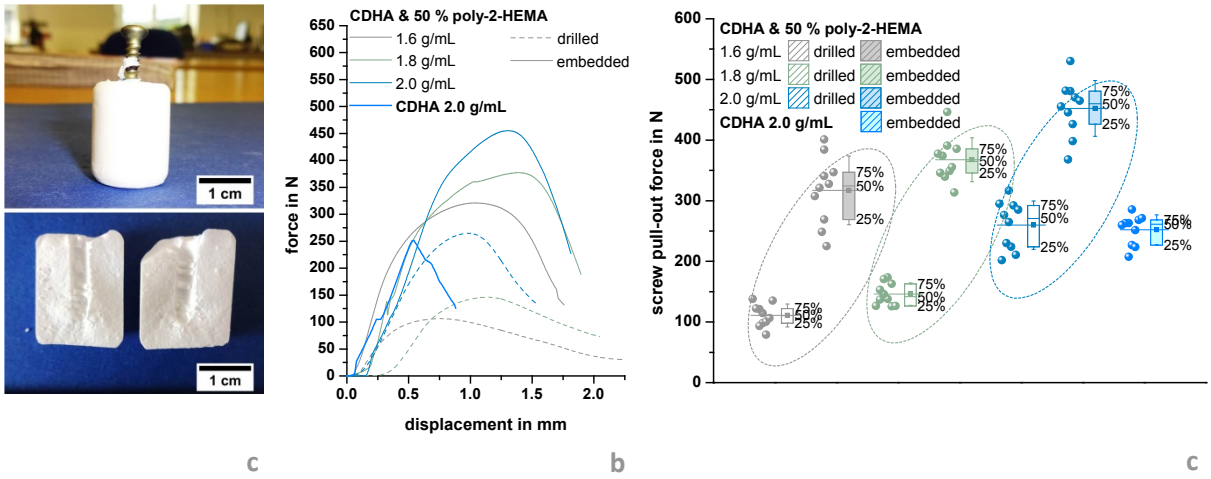

Figure 18: Drillability. poly-2-HEMA containing specimen with a PLR of 1.6 g/mL (a, above) and reference specimen (a, below) after testing, force-displacement curves (b) and screw pull-out force (c) of cylindrical test specimens from CDHA and 50 % poly-2-HEMA with varying PLR of 1.6, 1.8 or 2.0 g/mL after 24 h of setting in water at 37 °C. The screws were drilled 10 min after mixing the cement paste or directly embedded into the cement matrix.

Figure 19 illustrates the impact of deposition time in the aqueous environment, 2-HEMA amount in the liquid phase of the cement paste and PLR on the size and morphology of resulting CDHA crystals. Independently from the PLR, a prolonged immersion in water resulted in a crystal growth from 300 nm (no 2-HEMA, Figure 19 a) and 185 to 285 nm (HEMA containing samples, Figure 19 b-e) after 4 h to 1 µm (no 2-HEMA, Figure 19 f, k) and 360 to 460 nm (HEMA containing samples, Figure 19 g-j, n) after 2 d, respectively. As seen before, the addition of 50 % 2-HEMA at varying PLR led to overall smaller CDHA crystals whereat the PLR seemed to make only a marginal difference as long as the monomer concentration stayed unaltered. With decrease in PLR the whole amount of monomers in the liquid phase, but also the water amount increased which enabled slightly bigger CDHA crystals. Similar tendencies were observed, when smaller concentrations of 2-HEMA were used without alter-

ing the PLR (Figure 19 l-m): already amounts of 10 % in the liquid phase of the cement paste reduced CDHA crystal size by half compared to the control group without polymer. In all cases, entangled, needle-like crystals with partly flower-like accumulations were observed. Some bigger grains within a µm-size range, as they insularly appeared after short deposition (Figure 19 c-d), might be assigned to unreacted α-TCP raw powder. In case of high PLR of 3.0 g/mL in combination with a high 2-HEMA concentration of 50 % after 2 d of setting in water (Figure 19 g, n), the surface topography of the resulting cements differed widely from the residual samples as no characteristic CDHA-like aggregations were visible, but the mineral surface seemed to be embedded in a kind of amorphous matrix while single platelets of approximately 500 nm lay flatly within the existing gaps.

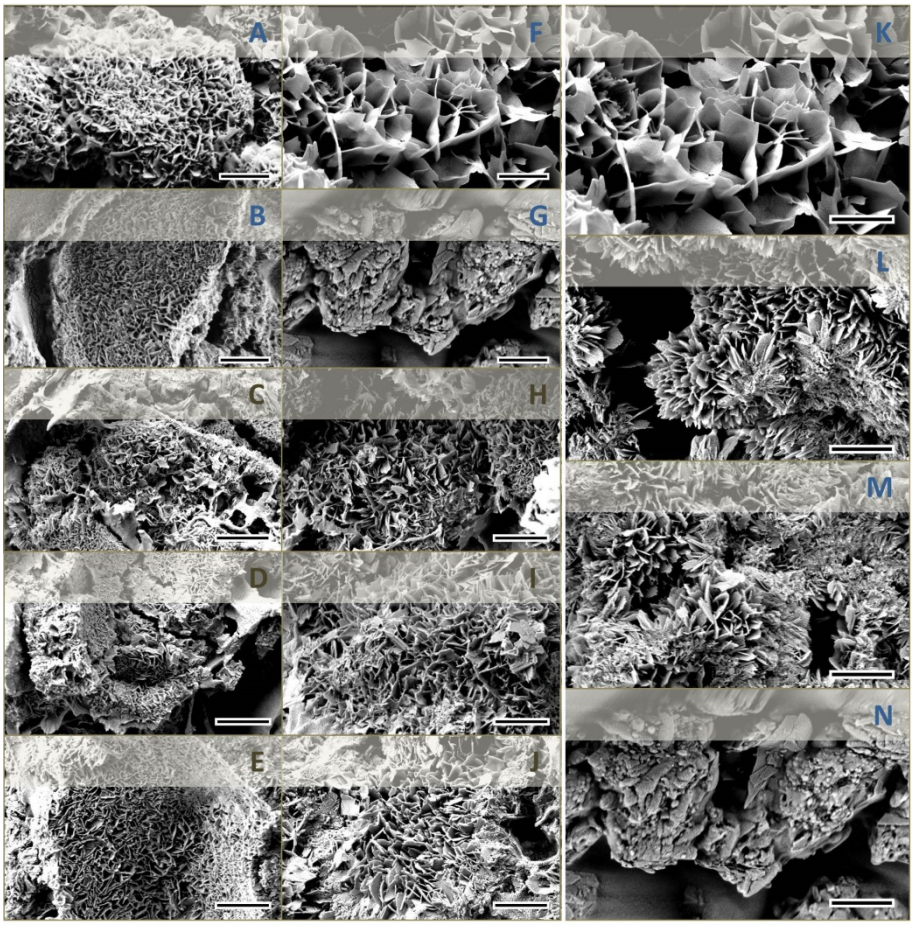

Figure 19: Scanning electron micrographs of fracture surfaces with a 20,000 fold magnification from CDHA without (a, f, k) and with 10 (l), 25 (m) or 50 % (b-e, g-j, n) poly-2-HEMA with varying PLR of 1.6 (e, j), 1.8 (d, i), 2.0 (c, h) or 3.0 g/mL (a-b, f-g, k-n) after 4 h (a-e) or 2 d (f-n) of setting in water at 37 °C. The scale bar of all micrographs is 1 µm. Already published micrographs are labelled in blue [8].

The results of measuring the BET specific surface area showed the following tendencies: Firstly, the size of the surface area was confined by the presence of the polymer such that initially, with a surface area of 15.23±0.01 m²/g, the control surface had a 2.7- to 3.4-fold value compared to the 2-HEMA containing ones and with 22.26±0.02 m²/g at least a 2.2- to 2.5-fold surface area after 7 d. Generally, no obvious differences were seen between samples of

[8] Figures based on these results have already been presented in the shared publication K. Hurle *et al*., J. Mater. Sci. - Mater. Med. 27(1) (2015) 1-13., but were exclusively produced by Theresa Brückner and SEM analysis was supported by Dr. Claus Moseke.

different PLR and the specific surface area steadily increased by time. In contrast, the reference without polymer seemed to reach its maximum already after 24 h (Table 16).

Table 16: BET specific surface area of cements from CDHA and 50 % poly-2-HEMA with varying PLR of 1.6, 1.8 or 2.0 g/mL after 4 h, 24 h, 2 d and 7 d of setting in water at 37 °C. Samples from pure CDHA with a PLR of 2.0 g/mL were taken as controls.

	specific surface area *via* BET in m²/g			
deposition time	**50 % 1.6 g/mL**	**50 % 1.8 g/mL**	**50 % 2.0 g/mL**	**0 % 2.0 g/mL**
4 h	4.48±0.01	5.09±0.02	5.72±0.01	15.23±0.01
24 h	7.37±0.03	6.57±0.01	6.80±0.01	23.13±0.01
2 d	5.33±0.01	8.09±0.03	7.72±0.02	20.58±0.06
7 d	9.93±0.05	10.21±0.04	8.97±0.02	22.26±0.02

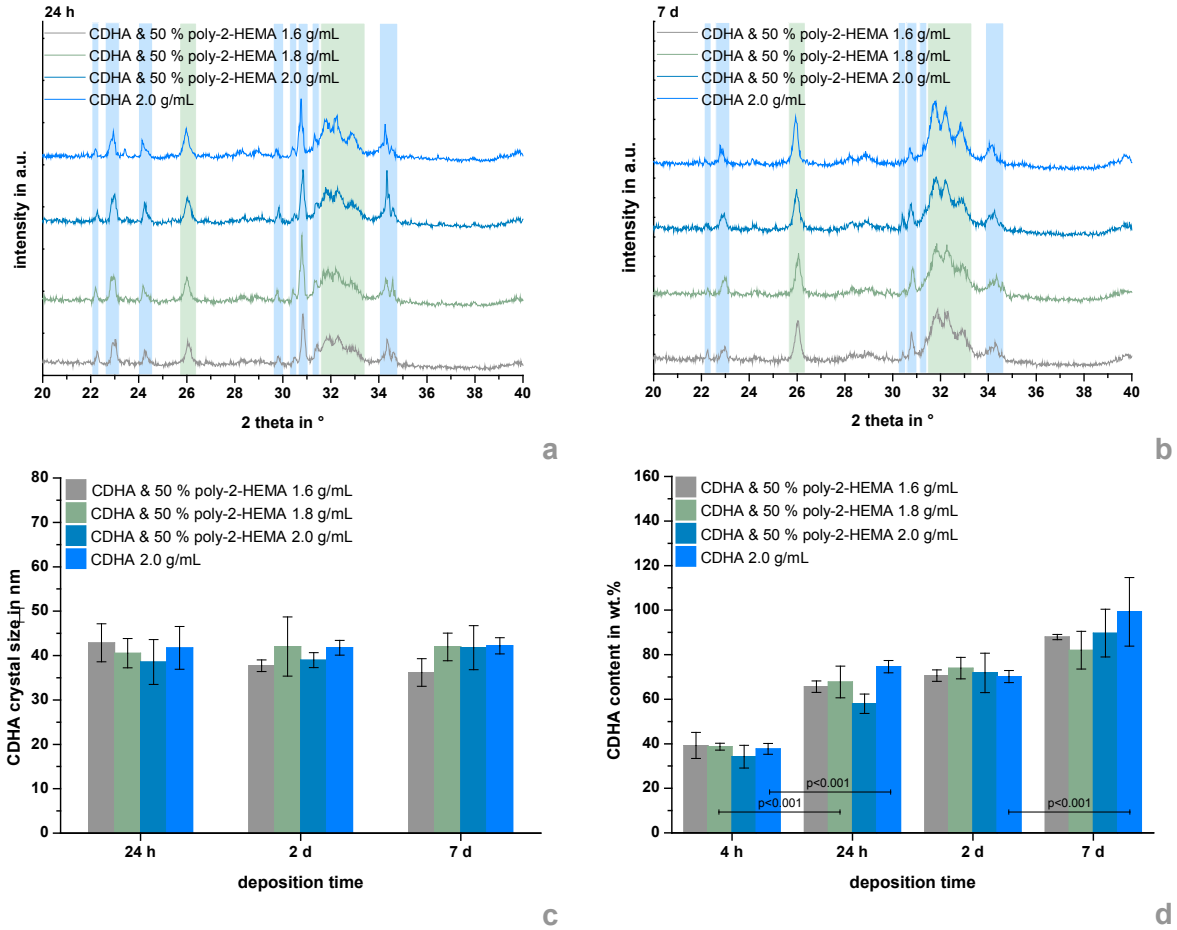

Figure 20: X-ray diffractograms (XRD) of samples from CDHA without and with poly-2-HEMA with varying PLR of 1.6, 1.8 or 2.0 g/mL after 24 h (a) or 7 d (b) of setting in water at 37 °C whereat characteristic reflexes of α-TCP and CDHA are labeled in blue or green, respectively. Quantitative evaluation of the XRD by means of the Scherrer Equation (Equation 29) and by reference to a calibration curve revealed CDHA crystal size (c) and amount (d). Do to small initial CDHA reflexes, crystal size could not be evaluated after 4 h of deposition.

Phase composition and quantitative analysis of the samples with reduced PLR was performed by intermittent X-ray diffractometry with subsequent Scherrer calculation (Equation 29) to determine the crystal size. Comparison with a calibration curve should reveal the extent of conversion into CDHA. Exemplarily, recorded diffractograms of the different cement formulations after 24 h and 7 d of setting are depicted in Figure 20 a-b. All represented sam-

ples contained quantitative amounts of the raw powder α-TCP whereat characteristic diffraction reflexes at 2θ=22.3 °, 30.7 ° and 34.3 ° decreased in intensity and reflexes at 2θ=24.2 °, 29.8 °, 38.4 ° and 34.6 ° partially fully disappeared within one week, respectively. After 24 h of setting in an aqueous environment, the CDHA diffraction reflexes seemed to be more distinctive compared to the corresponding reflexes in the residual patterns. Calculations of the crystal size by Scherrer Equation (Equation 29) showed no obvious dependencies on cement composition and deposition time and added up to approximately 40 nm (Figure 20 c). Comparing specific reflex net area ratios of the patterns with a calibration curve (Figure 57 b) revealed the absolute amount of CDHA after certain time points. While no differences were observed within the first 4 h of setting under aqueous conditions, the extent of reaction confinement was obvious after 7 d as the polymer free cement showed an at least 10 % higher CDHA amount of 99 % compared to the poly-2-HEMA containing samples. During the whole examination period, a steady increase in CDHA content from initially approximately 40 % was depicted (Figure 20 d).

3.1.1.4 Discussion

Conventional CPC are well-established bone substitution materials in clinics as they are osteoconductive, biocompatible [35] and similar to human bone concerning their structure and chemical composition [36]. However, their application is limited to non-load-bearing defect sites because of their brittle mechanical nature. Beside higher fracture toughness [102], further properties that are required from clinicians are adequate setting time, cohesiveness and injectability for minimally invasive treatments [13].

Nowadays, open surgery is replaced by more preservative minimally invasive treatments [12]. Therefore, defect filling materials have to be injectable, but CPC often undergo a so-called filter-pressing effect while injection, when the liquid phase of the cement paste separates from CaP particles and is solely extruded through the needle [13]. Some efforts have been made to overcome this problem: To reduce the paste viscosity of a CDHA forming cement system, Gbureck *et al*. [101] supplemented the cement raw powder with unreactive fillers forming a bimodal particle size distribution [101]. Alternatively, an ionic modification of the cement liquid had the same effect [108]. In both cases, complete injectability was possible in spite of a quite high PLR from 3.3 to 3.5 g/mL. Further improvements include the usage of round-shaped cement particles, low PLR and viscous polymeric solutions [54]. In the present study, a CDHA forming cement system was modified with *in situ* hydrogel forming water-soluble monomers (2-HEMA). This system reached an injectability of at least 84 % using a 14 G (2.11 mm) needle and a PLR of 1.6 to 1.8 g/mL. Complete injectability (>95 %) was feasible for cement pastes with a PLR of up to 2.0 g/mL when performing the test without needle, but with syringe only (Figure 14 b-c). Therefore, no further modification with fillers or ions was necessary. As the 2-HEMA modified cement pastes are of fast-setting nature (Table 15) concerning their polymeric phase, a fast increase in paste viscosity led to high injection forces of at least 75 N for a PLR of 1.6 g/mL with the usage of a 14 G injection needle (Figure 14 a). However, the injection took place without observance of any filter-pressing and homogenously textured and cohesive strands were extruded (Figure 14 d). For clinical applications, lower injection forces and complete injectability would be preferable. Exemplary, injection needles down to 10 G are used for osteoplastic surgeries [167] corresponding to

a diameter of 3.40 mm. An increase in needle diameter would improve injectability and reduce the force needed for injection, as it was shown by Burguera *et al*. [163]. According to Bohner *et al*. [54] the "ease of injection" is only limited to 100 N, if manual injection without the use of injection guns is practiced [54]. For all these reasons, the presented cement pastes are considered being injectable when appropriate injection equipment is used.

CPC are mainly applied in non-load-bearing defects because of their brittle nature. As previously shown, the implementation of *in situ* hydrogel forming water-soluble 2-HEMA monomers can increase toughness of the cement and provide it with a pseudoplastic mechanical behavior [17]. A more systematic study in cooperation with the Department of Mineralogy in Erlangen [9] (Figure 15-Figure 16) revealed detailed dependencies of the mechanical properties from immersion time in an aqueous environment and 2-HEMA concentration in the liquid phase of the cement paste at a constant PLR of 3.0 g/mL. Varying the 2-HEMA concentration between 10 and 50 % did not show any significant effects on the material's 4-point bending strength (Figure 16 a), but obvious changes in stress-displacement curves (Figure 16 d) were visible for the highest monomer concentration leading to an improved fracture behavior in terms of bending modulus (Figure 16 b) and absorbed energy until fracture (Figure 16 c). Hence, it seems to be necessary working with a minimum amount of the organic, ductile component which again confirms previous results from literature: Christel *et al*. [17] analyzed CDHA forming cement systems with 30 to 70 % of 2-HEMA in the liquid phase of the cement paste. Even if bending modulus and work of fracture steadily altered with increasing monomer amount, only the 50 % samples showed positive effects on the bending strength [17]. Wang *et al*. [16] came to a similar conclusion using methacrylated dextran for the organic component, as a strong improvement of the fracture energy was seen not until using monomer concentrations of >45 % [16]. Of course, the principle of dual setting cement systems was introduced about one decade earlier [149], but a former 2-HEMA related publication dealt with minor monomer contents and little impact on the mechanics, as the brittle character of the ceramic component dominated the overall behavior [389]. Low amounts of the monomer might act detrimentally on the strength properties as incoherent hydrogel networks presumably disturb the cement structure. Thus, we focused on using a 50 % concentrated 2-HEMA solution for all residual experiments.

To evaluate the impact of deposition time in an aqueous environment, 4-point bending test setup was performed on the as-mentioned cement formulation in comparison to a pure CDHA control with similar PLR after 2 h to 7 d of setting. For longer time points, the positive effect of poly-2-HEMA within the cement matrix on the bending strength was only minor while long-term deposition showed vast discrepancy in terms of bending modulus and absorbed fracture energy reflecting the less brittle and more plastic fracture behavior of 2-HEMA modified samples. In contrast, the obvious advantage of the dual setting system with respect to 4-point bending strength is the higher values already after short setting (Figure 15).

In terms of actual application, cement formulations with lower PLR and consequently higher monomer content were equally tested in this study. Even if work of fracture and bending

[9] K. Hurle *et al*., J. Mater. Sci. - Mater. Med. 27(1) (2015) 1-13. This was a cooperation project whereat Theresa Brückner holds 2nd authorship for performance of the mechanical tests and providing scanning electron micrographs.

strength were not available for all cement compositions and time points within a 4-point-bending test setup, it can be assumed: The higher the monomer content, the more coherent is the resulting hydrogel network. The hydrogel immediately forms upon mixing the liquid and the solid phase of the cement paste resulting in both hydrogel and hygroscopic cement powder competing for water molecules. A more coherent hydrogel network can bind more water, so that less of it is available for cementitious dissolution and precipitation reactions. Thus, the plastic fraction predominates the brittle fraction of the composite. Resultant is a decrease of bending modulus with increasing monomer content. By time, water molecules from the immersion media can advance the cementitious reaction and lead to an increased bending modulus. In contrast, the fracture energy stayed relatively constant by time and was at least one order of magnitude higher compared to the control group. As already observed for higher PLR of 3.0 g/mL, the time influence on the bending strength was only minor. All in all, the pseudoplastic mechanical behavior occurred in a greater extent at low PLR (Figure 17).

The remarkable mechanical behavior of this cement system i.e. the strong impact of the plastic component especially in the initial phase of cement setting is connected with a drillability of the hardened cement already 10 min after mixing both the liquid and the solid phase. It was shown that the analyzed 2-HEMA modified cement systems were drillable, but the screw pull-out forces increased with increasing PLR i.e. decreasing monomer content from 110 N (1.6 g/mL) to 260 N (2.0 g/mL) after 24 h (Figure 18 c). However, cements without *in situ* hydrogel forming monomers were not drillable after 10 min and disrupted while testing because of their brittle nature when screws were embedded in the unhardened cement matrix (Figure 18 a). Few is known about drillable CPC from literature, but there are some concepts for bone augmentation with CPC in conjunction with surgical screws: Usually, screws are embedded in an unhardened CPC matrix [570-572], CPC paste is injected through cannulated screws [573, 574] or screws are inserted in prehardened CaP scaffolds fabricated *via* 3D powder printing [26]. As a common outcome, those publications suggested an enhancement of screw osteosynthesis by using CPC for augmentation [570, 572, 574]. This demonstrates the need for drillable cement systems which are compatible with screw insertion. It was rarely tried to optimize CPC in this direction. Probably, a carbonated apatite forming cement being reinforced with resorbable fibers is the only commercially available and drillable cement system (Norian® drillable, DePuy Synthes). It was analyzed in biomechanical studies of tibial depression fracture [23, 535] whereat the authors stated noticeably lower displacement when a defect was filled firstly with the cement paste and drilled afterwards [535].

The setting kinetics of a dual setting cement system based on α-TCP with a 10 to 50 % concentrated 2-HEMA solution and a PLR of 3.0 g/mL were revealed by Dr. Katrin Hurle from the Department of Mineralogy in Erlangen [10] using *in situ* X-ray diffractometry with subsequent Rietveld refinement and the so-called G-factor method to trail α-TCP diminution and simultaneous CDHA conversion online and in the presence of the water-soluble monomer, considering potential amorphous constituents and water loss during measurements. The observed developments can be used for adequate correlation with the particular mechanical

[10] K. Hurle *et al.*, J. Mater. Sci. - Mater. Med. 27(1) (2015) 1-13. This was a cooperation project whereat Theresa Brückner holds 2nd authorship for performance of the mechanical tests and providing scanning electron micrographs.

properties of this cement system. Combining the dissolution/precipitation with the simultaneous polymerization reaction takes the following effects:

1) The presence of 2-HEMA in the initial cement paste both slowed down and restricted the hydration from α-TCP to CDHA. Though, the monomer did slightly affect the reaction rate, but strongly the overall level of conversion. With increase in 2-HEMA concentration from 10 to 50 %, the total amount of CDHA after 2 d of setting was steadily reduced by up to 37 % (34 % CDHA, 75 % conversion) compared to the control group (54 % CDHA, 91 % conversion), but a notable portion was formed quite early. The fact that the overall CDHA amount seemed to be restricted still after 7 d in a wet environment was attributed to the non-availability of penetrating water, which was probably physically bound to the hydrogel, and hence limited dissolution and ion transport [10]. Despite of constant influence on the setting reaction, the mechanical benefit did not show up before using 50 % concentrated 2-HEMA solution (Figure 16). Decreasing the PLR in subsequent examinations down to 1.6 g/mL equally increased the total amount of 2-HEMA in the original cement paste such that one would anticipate a likewise reduction in CDHA formation. As seen in Figure 20 d, this prospect was not fulfilled. In contrast, calculated CDHA amounts, which increased with advancing deposition time, were comparable for all three PLR variations and the 2-HEMA free control for up to 2 d. The impeding effect of the polymer did not appear until day 7. In contrast, corresponding measurements of the BET surface area indeed showed a difference between the samples such that the final area was doubled from approximately 9 to 10 m²/g (with 2-HEMA) to 22.26±0.02 m²/g (without 2-HEMA, Table 16) indicating a higher amount of nanocrystalline product within the reference during the whole study.

At high liquid amounts, not only the monomer, but equally the absolute water content increases and both hydrogel and unreacted cement raw powder compete for this water. Obviously, enough water was available for consistent α-TCP hydration independently from the PLR/2-HEMA amount. Consecutively, an increasing monomer concentration with reduced water supply has a stronger influence on the hydration reaction than an increasing monomer concentration with sufficient water supply. In the latter case, the reaction kinetics stay unaffected, while only the final CDHA amount is restricted. However, as seen in Figure 15-Figure 17, both opportunities overcome the brittleness of classic cement formulations in such a way that low PLR/high 2-HEMA amounts reduce bending modulus and improve fracture toughness. Although the highest CDHA conversion rate was shown to occur already after 1 h of setting [10], the weakness of the initial mechanical performance of the controls anew proves the ability of the dual setting concept as a suitable improvement strategy.

2) The size of CDHA monocrystals was only marginally affected by the presence of 2-HEMA as seen in published data [11] as well as results based on Scherrer Equation (Equation 29, Figure 20). In contrast, corresponding scanning electron micrographs revealed a continuous decrease in the size of CDHA polycrystals with increased monomer concentration and unaltered PLR presumably due to space issues (Figure 19 k-n). Using increased 2-HEMA amounts together with an increased water amount seemed to have no impact on the

[11] K. Hurle *et al.*, J. Mater. Sci. - Mater. Med. 27(1) (2015) 1-13. This was a cooperation project whereat Theresa Brückner holds 2nd authorship for performance of the mechanical tests and providing scanning electron micrographs.

polycrystal size (Figure 19 g-j). Some reports presume positive effects of smaller crystal sizes on the mechanics of purely inorganic cement systems [37] such that 2-HEMA, beside its filling up of pores within the CDHA matrix and plastic character, leads to additional mechanical benefits.

3.1.1.5 Conclusion

In the present study, the setting mechanism of a dual setting CPC system based on α-TCP and 2-HEMA was systematically examined. This encloses the confinement of crystal growth and conversion to CDHA whilst simultaneously enabling the cement to be drilled already 10 min after mixing due to a pseudoplastic fracture behavior and *in situ* stable organic matrix. With decrease in PLR at constant 2-HEMA concentration this reduction was less distinctive, but the brittle character of the mineral component was confined all the more. Long-term deposition of the injectable composite revealed a constant bending strength and absorbed fracture energy even though the bending modulus steadily increased as reaction of the brittle fraction proceeded. All the results provided now help to understand more the principles of dual-setting as a step forward as regards clinical application of a functional biomaterial.

3.1.2 Bone wax from poly(ethylene glycol)-calcium phosphate cement mixtures

The subsequent application form describes a possible alternative for conventional bone waxes (chapter 2.3.2.2) and takes advantage of the concept of premixed cement systems as presented in chapter 2.2.3.

The following section 3.1.2 is reused from the research article: T. Brückner, M. Schamel, A.C. Kübler, J. Groll, U. Gbureck. Novel bone wax based on poly(ethylene glycol)-calcium phosphate cement mixtures. Acta Biomaterialia. 33 (2016) 252-263. It refers to **Project 1B** in the experimental section. T. Brückner holds first authorship. She designed and executed the whole experimental study alone except for the mercury porosity measurements, which were conducted by M. Schamel. She further wrote the whole manuscript, whilst J. Groll and U. Gbureck were involved in supervision, submission and proof-reading. A.C. Kübler came up with the idea of the study.

3.1.2.1 Abstract

Classic bone wax is associated with drawbacks such as the risk of infection, inflammation and hindered osteogenesis. Here, a novel self-setting bone wax on the basis of hydrophilic PEG and HA forming CPC was developed to overcome the problems that are linked to the use of conventional beeswax systems. Amounts of up to 10 wt.% of pregelatinized starch were additionally supplemented as hemostatic agent. After exposure to a humid environment, the PEG phase dissolved and was exchanged by penetrating water that interacted with the HA precursor (TTCP/DCPA) to form highly porous, nanocrystalline HA *via* a dissolution/precipitation reaction. Simultaneously, pregelatinized starch could gel and supply the bone wax with liquid sealing features. The novel bone wax formulation was found to be cohesive, malleable and after hardening under aqueous conditions, it had a mechanical performance (~2.5 MPa compressive strength) that is comparable to that of cancellous bone. It withstood systolic blood pressure conditions for several days and showed antibacterial properties for almost one week, even though 60 % of the incorporated drug vancomycin hydrochloride was already released after 8 h of deposition by diffusion controlled processes. It is expected that the described bone wax formulation outmatches conventional bone waxes, as it circumvents the detriments being associated with the term ‘‘bone wax”. The presented formulation has a novel composition and would broaden the application of CPC and besides, the general interest in bone waxes will increase, as they were long considered as a ‘‘first-line treatment” to avoid.

3.1.2.2 Introduction

The study investigated the development of alternative bone waxes on the basis of a HA forming CPC system. Conventional bone waxes are composed of non-biodegradable beeswax/vaseline mixtures that are often linked to infection, inflammation and hindered osteogenesis [2]. Here, the usage of bioresorbable polymers and the supplementation with hemostatic agents was combined with the incorporation of a mineral component to overcome those drawbacks. The implementation of HA forming precursor powders into a water-soluble polymer matrix prevents a setting reaction of the cement before contact with physiological

fluids. Cement systems based on this principle are known from literature as ready-to-use [19, 20] or premixed [160, 170-173, 175, 404] cement pastes, but they have a lower viscosity for minimal invasive application and are probably not suitable for non-cavity-like bone defects.

The present study evaluated a novel bone wax system based on HA forming precursor powders TTCP/DCPA that were implemented into a plastic PEG matrix. To improve its liquid sealing ability up to 10 wt.% pregelatinized starch from corn were supplemented and the cohesion, compressive strength, mass loss, phase composition, morphology, PEG and ion release, porosity and water sealing duration were analyzed. As infection with *S. aureus* is a well-known problem with classic bone wax, antibiotic release and antibacterial properties were also tested *via* vancomycin hydrochloride incorporation.

3.1.2.3 Results

Table 17: Relevant parameters of bone wax composition changing for the cohesion study (Figure 21) and correlating compressive strengths after 24 h in water. All samples were prepared with a CPC:PEG ratio of 5:3.

fixed parameters	varying parameters	weight ratio/content of parameters				
	(parameter number)	compressive strength in MPa				
(2)=4:1, (3)=2:1	PEG1,500:PEG400	2:1 (a)	3:1 (b)	4:1 (c)	5:1 (d)	
(4)=0 wt.%	(wt.) (1)	1.36±0.21	1.25±0.26	1.59±0.26	1.65 ± 0.38	
(1)=4:1, (3)=0.008:1	TTCP/DCPA: NaH_2PO_4	1:0.004 (e)	9:1 (f)	4:1 (g)	7:3 (h)	
(4)=0 wt.%	(wt.) (2)	0.20±0.04	0.79±0.24	2.03±0.38	1.44 ± 0.22	
(1)=4:1, (2)=4:1	Na_2HPO_4:NaH_2PO_4	1:0.004 (i)	2:1 (j)	1:1 (k)	1:2 (l)	0.008:1 (m)
(4)=0 wt.%	(molar)(3)	too weak	1.59±0.26	1.38±0.24	1.48±0.22	2.03±0.38
(1)=4:1, (2)=4:1	starch content	0 (n)	1.0 (o)	10 (p)		
(3)=0:1	in wt.% (4)	2.03±0.38	2.10±0.41	1.81±0.35		

Table 17 shows that different compositions were tested to find an ideal bone wax composition where workability, cohesiveness in an aqueous environment (Figure 21) and adequate compressive strength after 24 h under aqueous conditions (Table 17) were favored. Formulations with a CPC to PEG ratio <5:3 showed no adequate cohesiveness (data not shown) and disintegrated shortly after being placed in water. An increase in PEG 1,500 led to an improvement of the bone wax cohesiveness (Figure 21 a–d). With a PEG 1,500 to PEG 400 ratio of 2:1 or 3:1, respectively, cuboidal bone wax samples strongly disintegrated after 10 min in water, while samples maintained their cuboidal shape at higher amounts of the higher molecular weight PEG. Having a look at the compressive strength of those samples after 24 h, a slight tendency to higher values from 1.36±0.21 to 1.65±0.38 MPa could be seen. As an increase in PEG 1,500 simultaneously reduced workability, further experiments were performed with a 4:1 PEG 1,500 to PEG 400 ratio. To promote the desired properties, NaH_2PO_4 powder was added to the cement system as a soluble phosphate source to accelerate the cement setting reaction. Without or with a high loading of NaH_2PO_4, a strong disintegration of prepared bone wax cuboids was observed (Figure 21 e–h). Only with the addition of 1 g NaH_2PO_4 to 4 g TTCP/DCPA raw powder, an appropriate cohesiveness was ob-

tained. This composition came along with the best compressive strength of 2.03±0.38 MPa after 24 h. Using a mixture of primary and secondary sodium phosphates did not alter the cohesiveness (Figure 21 i–m), but an entire abdication of primary sodium phosphates led to a disintegration of the cuboids. Additionally, supplementing pregelatinzed starch to the bone wax slightly promoted cohesiveness with increasing starch content as seen in Figure 21 n–p. For those reasons, continuous work was performed with a bone wax composition that contained a PEG 1,500 to PEG 400 ratio of 4:1, a TTCP/DCPA to NaH_2PO_4 ratio of 4:1 and varying amounts of pregelatinized starch of up to 10 wt.%.

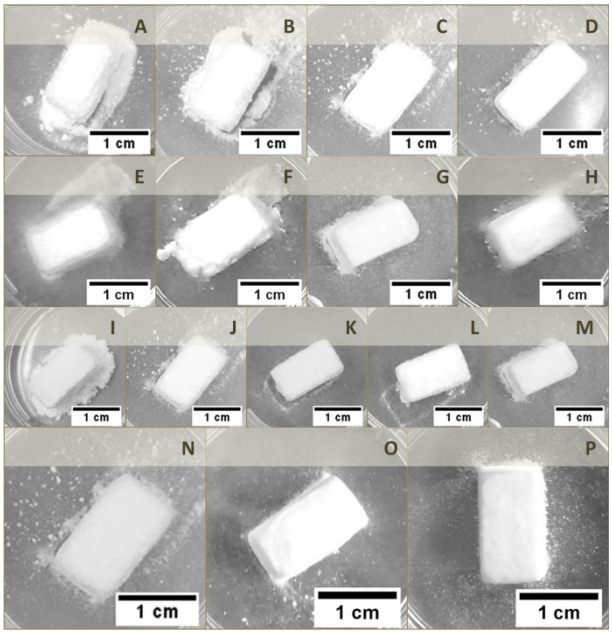

Figure 21: Cohesion. Influence of bone wax composition on sample cohesion after 10 min in water. Pictures (a-d) show the effect of increasing poly(ethylene glycol) 1,500 content, (e–h) the effect of increasing NaH_2PO_4 content, (i–m) the effect of increasing NaH_2PO_4 at a constant sodium phosphate content and (n–p) the effect of increasing starch content. Detailed composition information can be found in Table 17.

Figure 22 [12] illustrates that those novel bon wax formulations are indeed malleable and smearable, exemplarily shown with artificial bone.

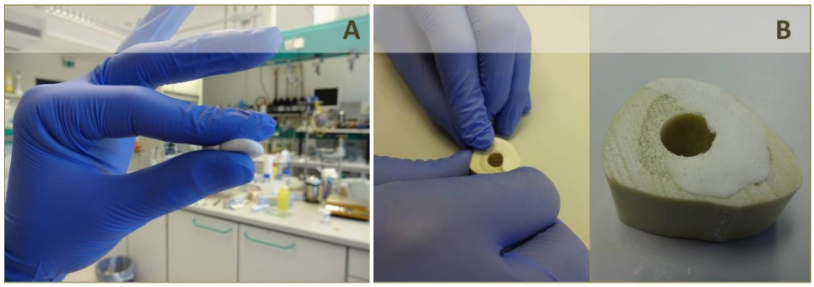

Figure 22: Handling. (a) illustrates the malleability and (b) the smearability of novel bone wax formulations [12].

Cuboidal bone wax samples with pregelatinized starch contents between 0 and 10 wt.% were deposited in PBS for 24 d at 37 °C and their compressive strength development (Figure 23 a), mass loss (Figure 23 b) and phase composition (Figure 23 c and d) was studied during this time period. The mechanical properties of the tested bone waxes did not change significantly by time with a compressive strength of 2.0 to 2.9 MPa for starch-free samples, 2.4 to

[12] This figure is not contained in the article T. Brückner *et al*., Acta Biomater. 33 (2016) 252-263.

2.6 MPa for samples with 1.0 wt.% starch and 1.9 to 2.2 MPa for samples with 10 wt.% starch (Figure 23 a). Concerning the mass loss, all samples behaved similar during the first four days of the immersion study. They lost about 2 % of their weight firstly measured after 2 d of deposition in a wet environment. During the next 20 d, additional mass loss of only 1 % took place for starch containing samples. For starch-less samples, a continuous mass loss of about 0.2 to 0.3 % per day could be seen by day six such that a final mass of 91 % was reached (Figure 23 b). Figure 23 c shows the time-dependent development of the bone waxes' phase composition. It has to be mentioned that there were similar tendencies for any bone wax type (Figure 23 d). After 2 d, characteristic reflexes of both raw powders (TTCP and DCPA) and product (HA) could be seen. By time, there was an increase of product reflex intensities accompanied by a decrease of raw powder reflex intensities. At the end of the release study, monetite seemed to be completely converted, while there were still some TTCP residues left (Figure 23 c).

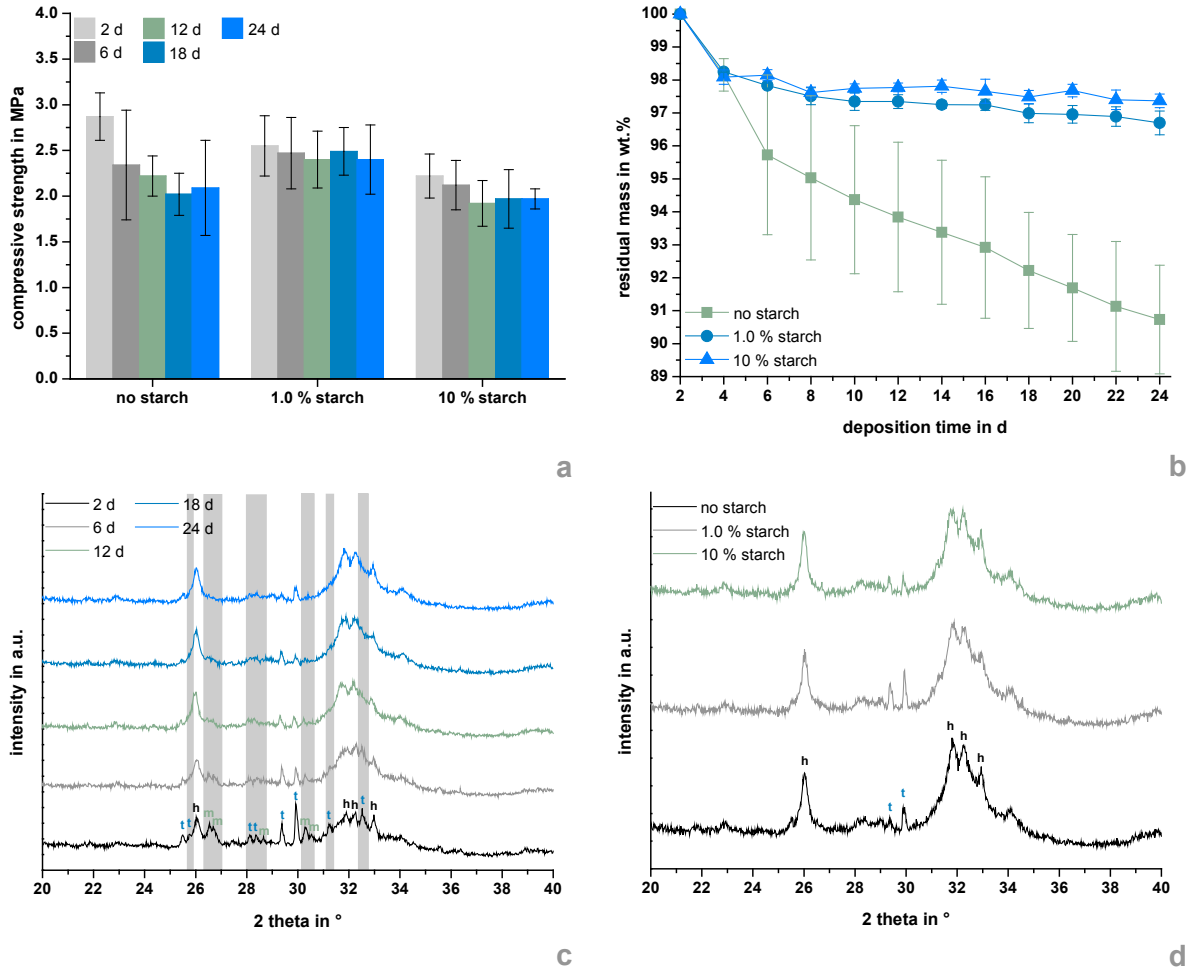

Figure 23: Mechanical properties and composition. Development of compressive strength (a) and mass loss (b) of cuboidal bone wax samples without starch or with 1.0 or 10 wt.% starch during 24 d setting in PBS at 37 °C. X-ray diffractograms of bone wax without starch after 2, 6, 12, 18 and 24 d setting (c) and of bone wax without starch or with 1.0 or 10 wt.% starch after 24 d setting (d) in PBS at 37 °C. Characteristic reflexes of HA, TTCP and DCPA are labeled with h, t and m, respectively. Reflex intensities that disappear by time (c) are pointed grey.

Calculated crystal sizes of the product HA according to Scherrer equation varied between 18 nm (no starch) and 20 nm (10 wt.% starch) after 24 d (Table 18). Figure 24 shows the scanning electron micrographs of the three different bone wax types after 2, 12 and 24 d of deposition in PBS at 37 °C. Bone wax without starch showed a quite inhomogeneous and

porous surface topography after 2 and 12 d consisting of a mixture of flaky crystals with a diameter of about 2 µm (Figure 24 a and b) and larger grains with diameters up to 17 µm. At the end of the release study, the topography appeared more homogeneous with lacerated flake-shaped crystals with diameters up to 2 µm sticking out of a smooth surface consisting of 1 µm large polished grains (Figure 24 c). The surface of bone wax with 1.0 wt.% starch again seemed inhomogeneous and porous after 2 d in PBS (Figure 24 d), but a surface homogenization took place during the next 10 d where it was consistently covered with up to 4 µm sized flaky crystals (Figure 24 e). After 24 d, the surface seemed grazed and less, but lacerated crystals could be seen (Figure 24 f). For the bone wax with a 10 wt.% starch content, the surface seemed to be largely covered with a smooth film (Figure 24 g). After 12 and 24 d, the surface structure looked quite similar, but beside flaky 2 µm crystals, additional needle-like crystals sized <1 µm could be detected (Figure 24 h and i).

Table 18: Full width at half maximum (*FWHM*) and length (*d*) of HA crystals in bone wax calculated *via* Scherrer equation (Equation 29) and Figure 23 d at a diffraction angle 2θ=26 ° after 24 d in PBS at 37 °C.

starch content (wt.%)	FWHM in °	d in nm
0	0.46	18
1.0	0.43	19
10	0.40	20

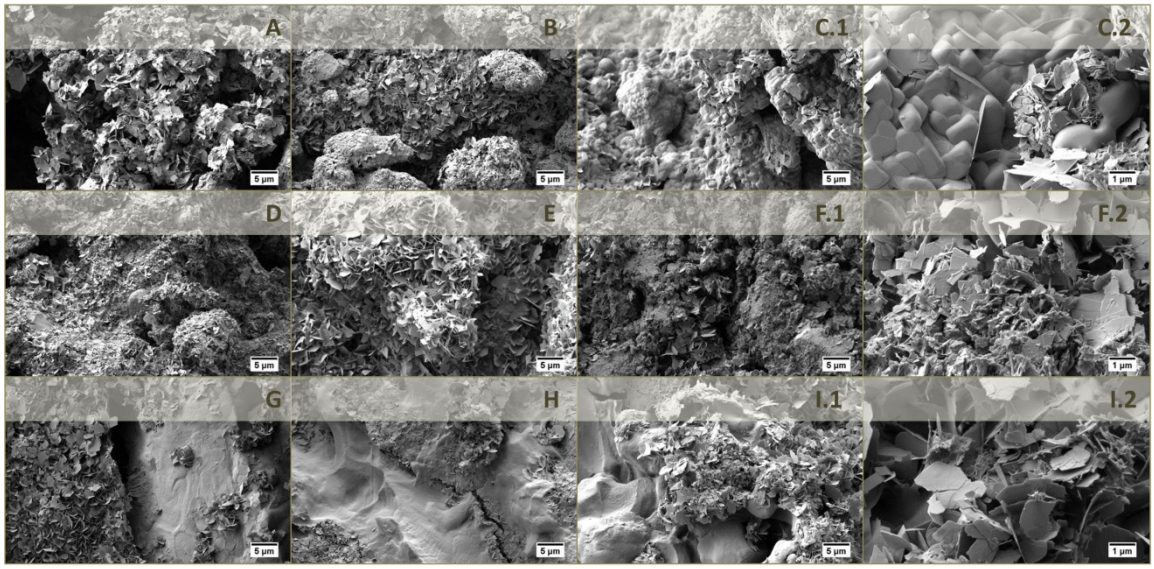

Figure 24: Morphology. Scanning electron micrographs of bone wax without starch (a–c) or with 1.0 (d–f) or 10 wt.% (g–i) starch after 2 (a, d, g), 12 (b, e, h) or 24 d (c, f, i) setting in PBS at 37 °C.

Figure 25 illustrates the PEG, Ca^{2+} and PO_4^{3-} release, as well as the pH development during deposition of bone wax with varying starch content for 24 d in PBS at 37 °C. The PEG release is exemplarily shown for the bone wax samples without starch, but the other wax types behaved comparably. Comparing the Fourier-Transform-Infrared (FT-IR) spectrum of pure PEG 1,500 with 10 µL of dried PBS supernatant after 2, 4 and 6 d release, characteristic vibrational bonds of PEG – CH-stretching, CH-bending and CO-stretching – were visible only after 2 and 4 d and continuously decreased in transmission intensity. After 6 d, possible PEG residues in 10 µL PBS were beyond the detection limit of the FT-IR spectrometer (Figure 25

a). As a counter evidence, we additionally performed FT-IR spectroscopy with dried and pestled bone wax samples that were stored for 2, 6 or 12 d in PBS. In this case, only the development of CH-stretching and CH-bending could be traced, as CO-stretching intensely overlapped with characteristic vibrational bonds of the inorganic bone wax component. Solely after 2 d, PEG could be certainly detected since at later time points, the cement to PEG ratio was too large (Figure 25 b).

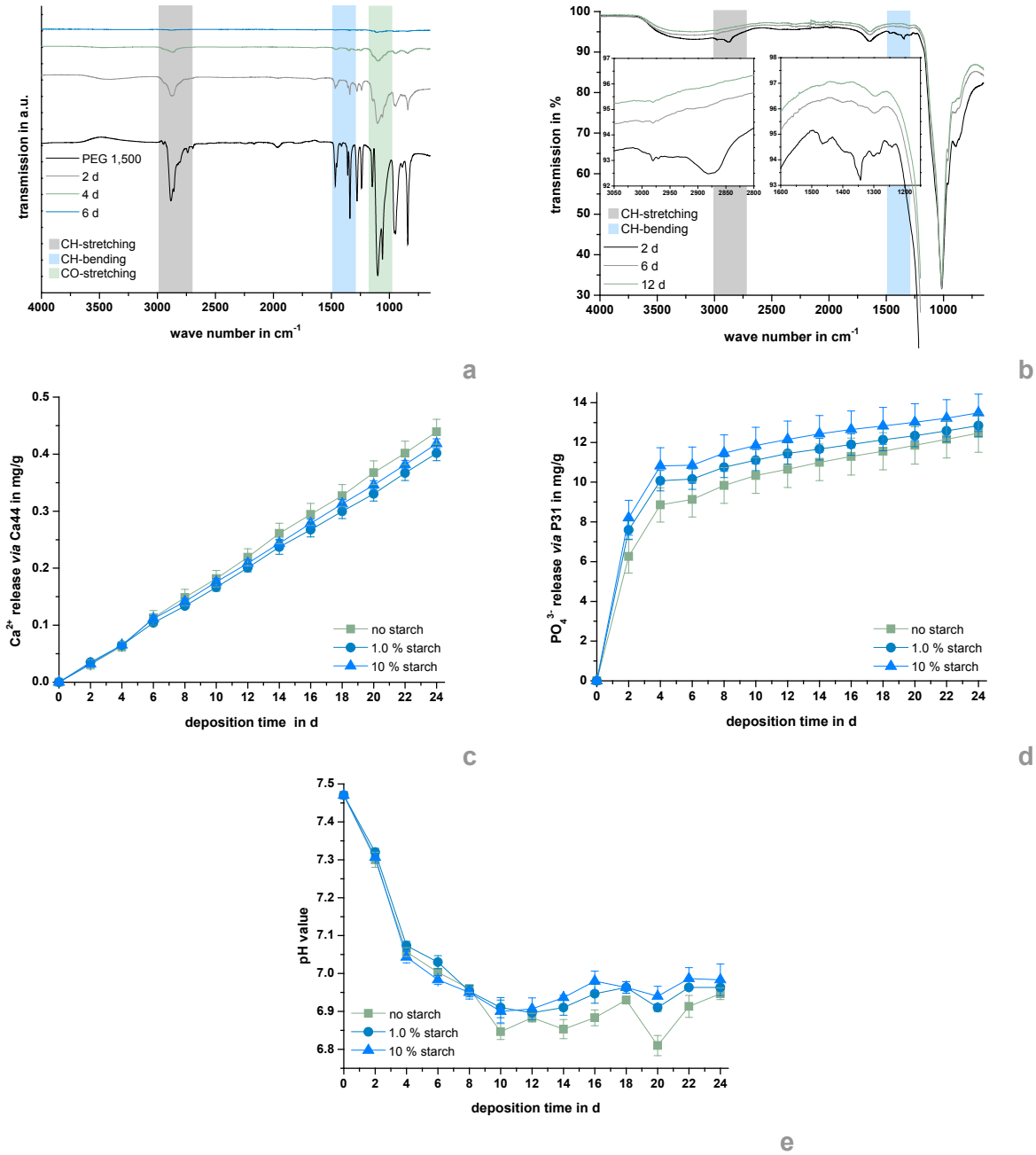

Figure 25: Release behavior. FT-IR of 10 µL dried PBS in which bone wax without starch was deposited (a) and FT-IR of dried bone wax samples without starch (b). Cumulative Ca^{2+} (c) and PO_4^{3-} (d) release from cuboidal bone wax samples without starch or with 1.0 or 10 wt.% starch and pH development of PBS in which bone wax without starch or with 1.0 or 10 wt.% starch was deposited (e). All samples were stored for 24 d in PBS at 37 °C.

Figure 25 c and d show the release of Ca^{2+} and PO_4^{3-} ions being analyzed *via* mass spectrometer with inductively coupled plasma (ICP-MS). All bone wax types showed a similar release. Over the whole period, a constant Ca^{2+} concentration of 0.017 (1.0 wt.% starch) to 0.019 mg/g per day (no starch) with a final amount of 0.40±0.01 to 0.44±0.02 mg/g was re-

leased (Figure 25 c). Concerning the PO_4^{3-} release, all bone waxes showed a similar burst release up to day 4 of the release study with least being released by bone wax without starch fallowed by bone wax with 1.0 or 10 wt.% starch. Afterwards, the PO_4^{3-} ion release converged and seemed to gain a certain saturation. Within 24 d, bone wax without starch, with 1.0 or 10 wt.% starch released 12.46±0.96, 12.84±0.56 or 13.49±0.94 mg/g of phosphorous in PO_4^{3-} (Figure 25 d). The pH-development of PBS supernatants where the different bone wax specimens were deposited in also behaved independently from starch content. In the first 10 d, the initial pH value dropped from neutral conditions (~7.5) to slightly acidic conditions (~6.8–6.9), where it stayed stable for the residual time (Figure 25 e).

The composition of the bone waxes had no influence on their porosity properties. Porosity after immersion for 24 d ranged between 63 % (with starch) and 66 % (no starch) according to Hg porosimetry and about 10 % fewer according to Equation 27 (Table 19). Simultaneously, the specific surface area marginally ranged from ~17 to 20 m²/g with increasing content of pregelatinized starch. Exemplarily, Figure 26 shows the relative and cumulative pore volume of a bone wax sample without starch before and after 24 d in PBS with a bimodal pore size distribution. After kneading, an increase in the minimal pore size could be observed indicating the existence of even smaller pores that could not be measured *via* Hg porosimetry. At the end of the immersion study, those pores disappeared and shifted to more large pores with a first maximum in the range of 0.05 and 0.07 µm and a second between 0.9 and 1.1 µm. Simultaneously, the porosity increased from 8 % to 66 %.

Table 19: Porosities of bone wax according to Hg porosimetry and Equation 27 before and after setting and specific surface area [13] after setting in PBS at 37 °C for 24 d.

starch content	**initial porosity** *via* **Hg porosimetry**	**porosity after 24 d** *via* **Hg porosimetry**	**porosity after 24 d** *via* **Equation 27**	**specific surface area** *via* **BET**
in wt.%	**in %**	**in %**	**in %**	**in m²/g**
0	8.21	66.18	55.88±0.27	20.36±0.02
1.0	9.04	63.36	55.89±0.77	19.66±0.02
10	7.97	63.38	53.97±0.76	17.25±0.02

Figure 27 visualizes the water sealing ability of cone-shaped bone wax samples at RT under a pressure of 140 mm Hg. The results of different samples of same composition were not reproducible; however, a liquid sealing duration of at least 18 h for all bone waxes was possible. Samples with 10 wt.% starch featured a comparably small time frame from 18 to 47 h, whereas the remaining samples had a twice as long liquid sealing time frame from 26 to 70 h (no starch) and 21 to 72 h (1.0 wt.% starch), respectively.

[13] Measurement of specific surface area *via* BET-method was performed after publishing the article T. Brückner *et al*., Acta Biomater. 33 (2016) 252-263.

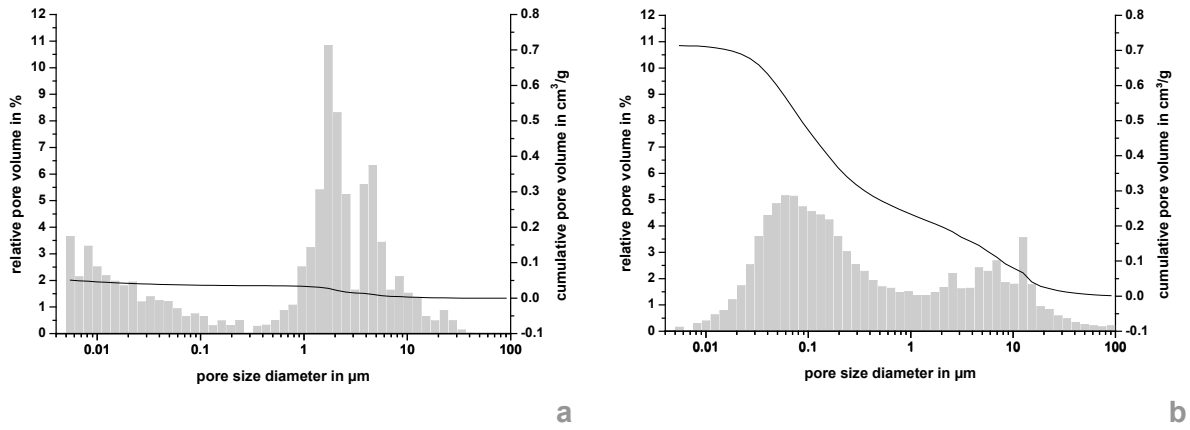

Figure 26: Porosity. Relative and cumulative pore volume as a function of pore size diameter measured via Hg porosimetry of cuboidal bone wax samples without starch before (a) and after 24 d of setting in PBS at 37 °C (b).

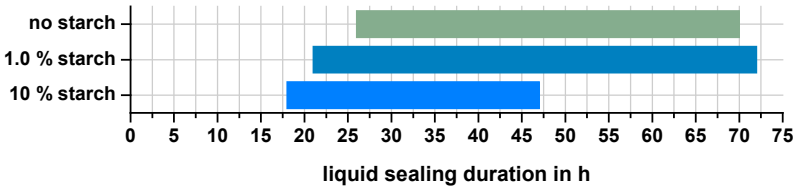

Figure 27: Liquid sealing duration. Water sealing ability of cone-shaped bone wax samples without starch or with 1.0 or 10 wt.% starch at RT and 140 mm Hg.

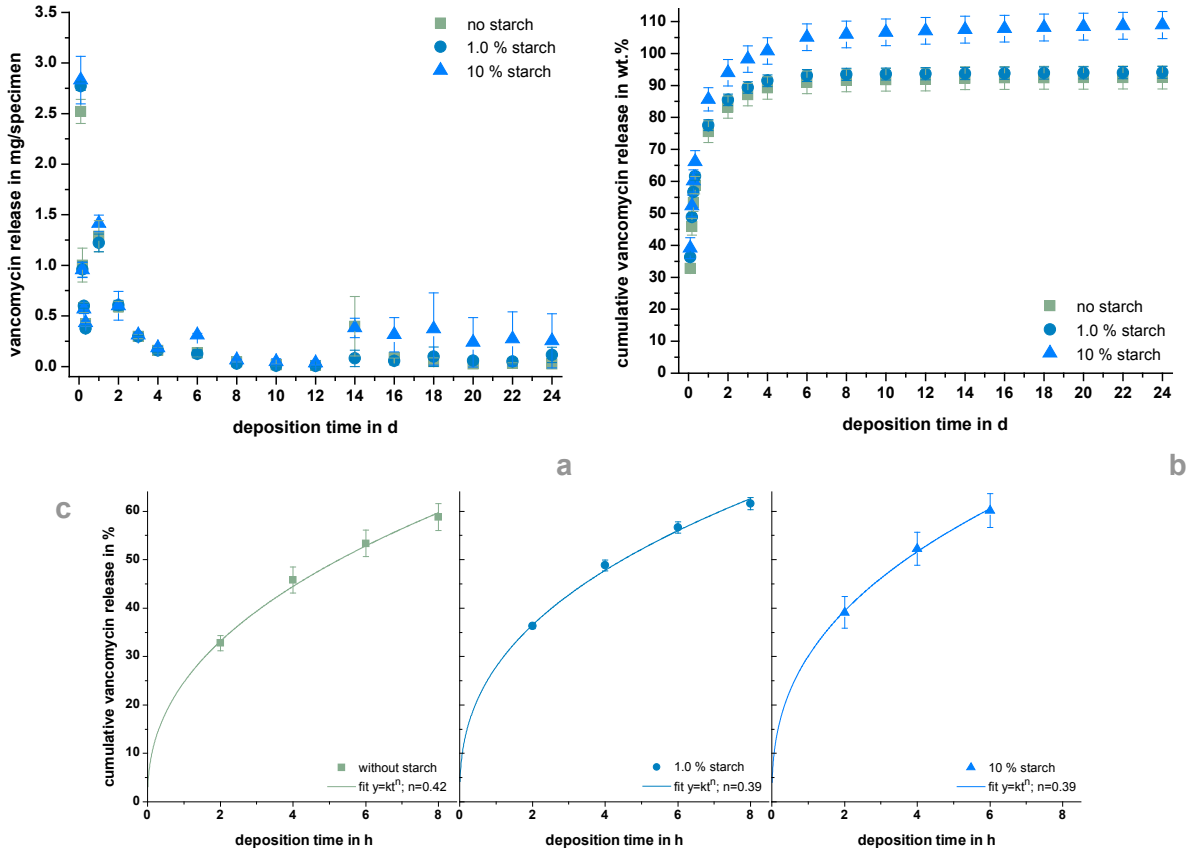

Figure 28: Antibiotic release behavior. Release behavior of vancomycin hydrochloride from cuboidal bone wax samples without starch or with 1.0 or 10 wt.% starch during a deposition in PBS at 37 °C for 24 d. Release per day (a), cumulative release (b) and alignment with the Korsmeyer–Peppas model (c) are shown.

To provide the bone waxes with antibacterial properties, 1.24 % vancomycin hydrochloride was supplemented and the release in PBS for 24 d at 37 °C was studied (Figure 28), whereat most vancomycin (2.5 to 2.8 mg/specimen) was released during the first 2 h. Afterwards, the vancomycin content in supernatant PBS continuously decreased and from day 3 on, the daily release was always below 0.5 mg/specimen. Except samples with a 10 wt.% starch content, the bone waxes seemed to behave similar. Especially after 2 h, 6 d and from day 14 on, slightly more vancomycin was released by the 10 wt.% starch containing samples. The curves for the first 60 % of released antibiotics were adjusted by the Korsmeyer–Peppas model (Figure 28 c; Equation 31): 60 % of released vancomycin was reached after 6 to 8 h of deposition in PBS. Fitting parameters k, n=24.70±0.84 %, 0.42±0.02 (no starch) up to k, n=30.05±0.95 %, 0.39±0.02 (10 wt.% starch) were calculated according to Table 20.

Table 20: Fitting parameters of the release profiles according to the Korsmeyer-Peppas model.

starch content in wt.%	k in %	n	release mechanism
0	24.70±0.84	0.42±0.02	diffusion
1.0	27.88±0.68	0.39±0.02	diffusion
10	30.05±0.95	0.39±0.02	diffusion

The pharmacological activity of released vancomycin was tested against *S. aureus* in an agar diffusion test. Figure 29 a illustrates the size of daily inhibition zones that resulted from vancomycin release from the three different bone wax types for 6 d. The size of inhibition zones continuously decreased from 10.4±1.0 mm (no starch), 11.6±0.4 mm (1.0 wt.% starch) and 11.7±0.1 mm (10 wt.% starch) on day 1 and approximated 1 to 2 mm after 6 d. Exemplarily, photographs of the daily inhibition zones are shown for one starch-free specimen from day 1 to day 3 *via* Figure 29 b.

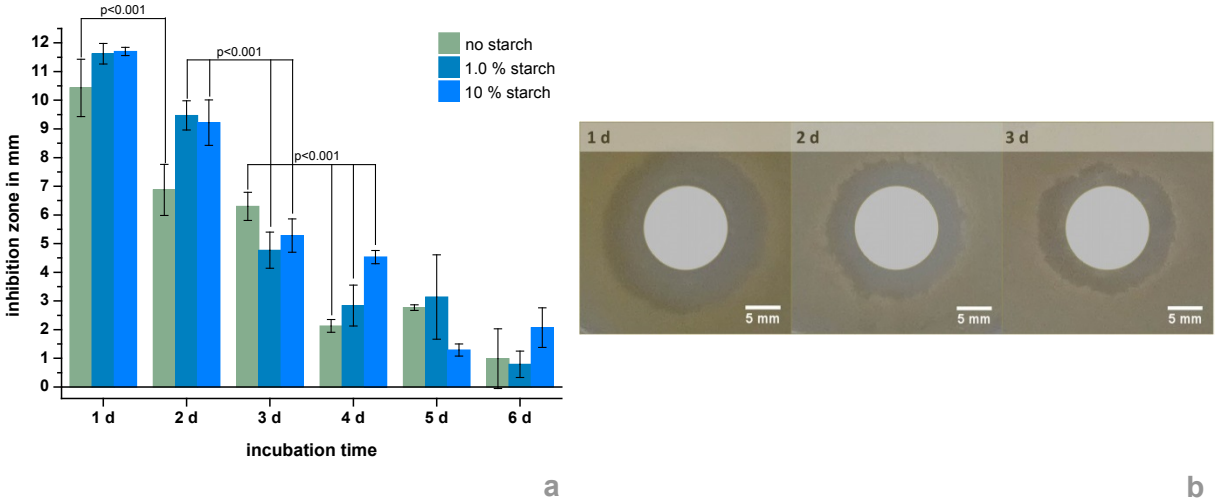

Figure 29: Antibacterial properties. Size of inhibition zones due to vancomycin hydrochloride release from disc-shaped wax samples without starch or with 1.0 or 10 wt.% starch during a deposition on agar plates for 6 d at 37 °C with *S. aureus* (a) and photographs of the time-dependent development of inhibition zones with starch-free samples for 3 d (b). The hatched areas reflect the former position of bone wax discs on the agar. The discs were put on fresh agar plates each after 24 h.

3.1.2.4 Discussion

This work aimed to find alternative bone wax formulations based on mixtures of water soluble PEG and a self-setting HA cement powder. In contrast to common hydrophobic bone waxes, such novel wax formulations are of hydrophilic nature. Following implantation, the PEG phase will dissolve, while the cement powder will simultaneously react with penetrating water to form a structurally stable implant. These features were proved by both XRD analysis showing the conversion to nanocrystalline HA within 2 d (Figure 23 c; Table 18) and FT-IR analysis (Figure 25 a and b) demonstrating the quantitative dissolution of PEG from the wax within a maximum of 6 d. Also, a mass loss of at least 3 % (Figure 23 b) supported this hypothesis.

Key parameters influencing the cohesion of the wax in an aqueous solution were found to be the PEG:CPC ratio, the ratio of different molecular weight PEG and the amount of added sodium phosphate setting accelerator. Above a PEG content of 38 wt.%, wax specimens were not stable in PBS buffer and disintegrated within a couple of minutes. Here, a high amount of PEG increased the distance between cement particles and thus inhibited the formation of a coherent inorganic network. A similar behavior was observed by Han *et al*. [172] for premixed CPC pastes with PEG/glycerol as liquid phase. Further, a PEG 1,500:PEG 400 ratio of ≤3 produced waxes with low cohesiveness (Figure 21 a–d), likely because the lower molecular weight component is liquid at a temperature of 37 °C and therefore dissolves in surrounding water faster than the setting reaction of the cement can occur. However, a certain amount of at least 20 wt.% PEG 400 was necessary to adjust the workability of the waxes since at a lower content it was practically impossible to manually knead and apply the waxes. Regarding the setting accelerator sodium phosphate, it was found to be most effective for cohesiveness and mechanical properties to add pure primary NaH_2PO_4 at a CPC:NaH_2PO_4 weight ratio of 4:1 (Figure 21 e–m; Table 17). The setting accelerating effect of both primary [575] and secondary [61] sodium phosphates in combination with TTCP/DCPA cementitious formulations is well known. Fulmer *et al*. [63] demonstrated that – in an initially neutral aqueous environment (mixture of primary and secondary phosphates) – complete precipitation of HA crystals was delayed by incongruent dissolution of monetite, which resulted in HA overgrowth with subsequent isolation. Under alkaline conditions (only dibasic sodium phosphate), the acidic component dissolved congruently such that a saturated solution with appropriate stoichometry accelerated the whole process. However, the authors also proved that the presence of primary sodium phosphates led to a yet faster reaction. Due to the acidity of the solution, a more soluble brushite phase formed and was immediately consumed in HA formation [63]. In our study, a minimum content of NaH_2PO_4 was necessary to ensure setting acceleration. Also, pure Na_2HPO_4 was not efficient.

Pregelatinized starch was added to the wax, as it is known to be a biocompatible, biodegradable and cost-effective agent to promote liquid sealing ability similar to works performed by Suwanprateeb *et al*. [554]. As a further feature, it also seemed to improve cohesiveness (Figure 21 n–p). Having a look at the field of premixed cement pastes, nature-derived polysaccharides with gelling characteristics as for example HPMC [160], chitosan [170] or alginate [181] were often used supplements for improved washout-resistance.

The compressive strengths of the set wax specimens were in a range of 1.9 to 2.9 MPa (Figure 23 a), which is much lower than the strength of the same cement matrix mixed with water without PEG modification, as compressive strengths between 4.8 and 184 MPa are possible depending on PLR, cement liquid and sample preparation [34]. The underlying reasons could be versatile: Comparing the porosities of these bone waxes to literature [230] after 24 d of setting, they were slightly higher (Figure 26, Table 19), though bone wax specimens were initially compacted by kneading. In both formulations, either TTCP/DCPA with an aqueous solution or TTCP/DCPA with a plastic PEG mixture, pore builders are present in the cement matrix. In the first case, there is no force for the water to diffuse out of the matrix, as it remains inside the pores. In contrast, PEG is soluble in the humid environment of the implantation site and is exchanged with penetrating water. The PEG molecules could even enlarge the pores and pore amount while leaving the matrix. Bohner *et al*. [576] intentionally added non-aqueous liquids to create macroporous CPC based scaffolds with porosities of about 75 %. Another reason for the low mechanical performance could be the crystal structure of the forming HA lattice. We assume that the lattice was strongly disturbed by the presence of PEG and the diffusion and exchange process taking place while setting, as long scan rates were necessary to get XRD patterns with appropriate resolution. Also, atypical partially eroded crystal morphologies (Figure 24) could prove disturbed crystal entanglement and hence, bad mechanical performance. Elongated setting times could explain the mechanical nature of the analyzed bone waxes, as well. Under ordinary conditions, mechanical rigidity is ensured *via* entanglement of HA crystals [10]. Due to PEG diffusion, crystal entanglement could be malfunctioning. Matsuya *et al*. [91] showed that an equimolar ratio of TTCP and DCPA could quantitatively react to form HA within 6 h when pH was kept constant at 8. Here, an approximately complete conversion of the reactants was only seen after 24 d of setting in PBS with TTCP residues (Figure 23 c–d). Simultaneously, the final specific surface areas were slightly larger as exemplarily compared to the report of Barralet *et al*. [107]. We further assume that such a system would not work with formulations that have intrinsically slower setting times (e.g. HA on the basis of α-TCP [577]). As bone waxes shall be applied for mechanical hemostasis in cancellous bone that showed similar compressive strengths between 4 and 40 kp/cm^2 (0.4 to 4 MPa) [578], mechanical performance of our samples can be considered as non-critical. Anyway those waxes withstood a pressure of 140 mm Hg for days (Figure 27). PEG-based bone waxes without cement component showed – at starch contents of 10 wt.% – a liquid sealing duration not exceeding 40 h, as those waxes were entirely resorbable [554].

During setting, a high amount of phosphate was released by bone wax specimens at which the P:Ca ratio amounted approximately 100 until day 4 and constantly 10 afterwards (Figure 25 c and d). The PO_4^{3-} excess was due to the high amount of supplemented setting accelerator being necessary for appropriate cohesiveness. Another side effect of the cement setting was an initial decrease in pH (Figure 25 e) that is normal for alkaline TTCP consumption [34]. However, the pH development took place in a quite neutral range so that we do not expect inflammation reactions.

Modifying the bone waxes with antibiotics showed an initial burst with 60 % being released after only 6 to 8 h (Figure 28). This is quite unusual for pure TTCP/DCPA cements without PEG. According to Schnieders *et al*. [264], the 60 % limit was reached not before 2 to 10 d in

equivalent cement systems. They depicted a correlation between porosity and drug release kinetics. A decrease in PLR led to an increase in porosity and pore sizes and hence accelerated release of vancomycin. The alignment of the release curves with Korsmeyer–Peppas model [87] revealed release exponents of 0.39 and 0.42, which is mainly diffusion controlled [267]. As a value of M_t<0.6·M_∞ was reached already after 8 h at the latest, diffusion of vancomycin took place while plastic and uncured state of bone wax. We assume that the degradation of the waxes as well as swelling of the containing starch and HA formation can further affect the release kinetics instead of solely diffusion at later time points. According to Schnieders *et al*. [264] the release mechanism of encapsulated drugs is irrespective of porosity and pore sizes. A combination of both exposed and encapsulated vancomycin would lead to a release profile with burst release but simultaneously long lasting release. This would offer an optimal clinical situation adapted drug release system. Despite the faster release of vancomycin from our bone waxes, a relatively long antimicrobial activity of at least 5 d was observed (Figure 29). This means that neither the heating nor kneading while fabrication of bone wax specimens did affect the biological activity of vancomycin. The incorporation of encapsulated drugs can also be performed during the kneading step, what would broaden the field of bone waxes for temperature-sensitive drugs, as for example bone morphogenetic proteins [579].

Some starch dependent effects were also monitored. Cohesiveness of the waxes was better with starch supplementation. As gelling agents are able to prevent that water molecules penetrate the cement paste they improve the interaction between single cement particles [580]. Without starch, mass loss of up to 9 % was monitored as a result of diffusing PEG molecules and breaking off cement particles owing to the worse cohesiveness. In the case of starch addition, we assume that the mass loss based on diffused PEG was compensated by the weight gain based on gelling, after an initial mass loss of 2 %. Concerning the liquid sealing ability, the most short duration was observed for the samples with 10 wt.% starch. Certainly, the results of the liquid sealing ability test were not reproducible, so further experiments would be necessary for more reliable statements. Though all bone waxes showed an approximately quantitative drug release, samples with a 10 wt.% starch content had an about 10 % higher release probably also due to gelling. Overall, bone waxes without starch may be less suitable for application, as cohesiveness is a key parameter affecting relevant material properties. However, in contrast to a study from Suwanprateeb *et al*. [554], the maximum starch load was limited for our materials to ~10 %. Higher amounts of starch led to a collapse of the cementitious matrix during the setting reaction due to a strong swelling effect. So, a proper composition has to be found between insufficient cohesiveness and high gelling which has to be additionally adapted to further supplements as for example encapsulated drugs.

3.1.2.5 Conclusion

The present *in vitro* study demonstrated the suitability of a self-setting PEG-CPC mixture as an adequate alternative for conventionally applied bone waxes. It is likewise malleable and, presumably, could be pressed onto osseous wounds to create a physical barrier to bleeding being probably simultaneously hemostatic and osteoconductive. The appropriateness of the novel bone wax as drug carrier system was also shown such that it could be provided with case-specific antimicrobial short as well as long-term features. Clearly, the novel formula-

tions have to be tested *in vivo* to both justify the postulated hemostatic and osteoconductive properties as well as the absence of foreign body reactions related to the release of a large amounts of PEG at the application site. Further improvements of the wax formulations from this study might include the incorporation of a fully degradable cementitious phase, e.g. brushite or struvite [210], to increase the degradation ability and bone regeneration capacity of the materials.

3.1.3 Prefabricated laminates

The subsequent application form describes a method for the treatment of flat cranial bone defects (chapter 2.3.2.3) and takes advantage of the concept of premixed cement systems as presented in chapter 2.2.3. The following section 3.1.3 refers to **Project 1C** *in the experimental section.*

The following section 3.1.3 is likely to be used in a publication manuscript, which is however not submitted or published by the time of the submission of this thesis.

3.1.3.1 Abstract

Polycaprolactone fiber mats with defined pore architecture were shown to provide sufficient support for a premixed CPC to serve as a flat and flexible composite material for the potential application in 2-dimensional, curved cranial defects. Fiber mats were fabricated by either melt electrospinning writing (MEW) or solution electrospinning (SES) with a patterned collector. While MEW processed fiber mats led to a deterioration of the bending strength by approximately 50 % due to a low fiber volume content in conjunction with a weak fiber-matrix interface, fiber mats obtained by SES resulted in a mechanical reinforcement of the ceramic matrix in terms of both bending strength and absorbed fracture energy. This was attributed to a higher fiber volume content and a large contact area between nanosized fibers and cement matrix. Hydrophilization of the PCL scaffolds prior to lamination was demonstrated to further improve composite strength and to preserve the comparably higher fracture energy of 1.5 to 2.0 mJ/mm². The laminate composite approach from this study was successful in demonstrating the limitations and design options of such a novel composite materials, however fiber compatibilization remains an issue to be addressed since a high degree of hydrophilicity must not necessarily provoke a stronger interface.

3.1.3.2 Introduction

As long as CPC still undergo setting from a pasty into the solid state, they need a surrounding supportive structure to maintain pre-modelled implant geometry. Thus, they are preferably used in cavity-like defects, which is additionally emphasized by their classification as “bone void fillers” [15]. So far, flat cranial defects are mostly treated with PMMA or titanium meshes. The former are known for damaging native tissue due to their extreme heat development while the latter suffer from their low malleability [25] and high thermal conductivity [26]. The use of premixed cement paste which is stabilized by layers of degradable polymer mats could be a suitable approach to enable this niche application for mineral bone cements. The composite is built up *via* a layer-by-layer procedure such that the cement paste has a 2-dimensionnally interconnected support structure which keeps it in place as long as the setting reaction proceeds. Until this timepoint, the construct retains its flexibility and adaptability to flat and curvy defects. In the present study, the cement paste consisted of carbonated HA raw powders being stabilized in an oil-based carrier liquid. Among contact with an aqueous environment, the oil phase is exchanged by water diffusion, which initiates the setting process [19, 20]. For the organic part of the laminate, PCL was chosen as a biocompatible and bioresorbable model compound [581]. To ensure a coherent cementitious network and stable

laminate in the uncured status, sufficient penetration of the PCL mats with cement paste is necessary, which is guaranteed by a macroporous structure with defined pore geometry and pore sizes within a large µm-range. For the fabrication of such specific constructs, two common fiber-based electrospinning techniques were chosen: MEW and SES, which both are common in processing PCL [581, 582] and additionally offer technical possibilities to fabricate a macroporous structure [582, 583]. Here, the influence of fiber processing regime, weight/area ratio and post-treatment under alkaline conditions on the handling, mechanical properties and interphase between cementitious matrix and polymer fibers was analyzed. Ideally, the fiber mat(s) can additionally initially reinforce the hardened ceramic and - in case of being biodegradable - leave interconnected cavities for an improved resorption and ingrowth of newly formed tissue.

3.1.3.3 Results and discussion

During MEW, charged polymer melts are extruded through a nozzle onto a grounded, movable platform [582] such that well defined coherent structures from straight fibers can be obtained when jet speed and collector velocity are well coordinated [584]. The technique is a combination of melt extrusion based additive manufacturing approaches with electrospinning [585]. A low melting point and a high thermal stability restrict the application of MEW technique to thermoplastic polymers, whereat PCL with a melting point of 63 °C [582] has been thoroughly analyzed in this context [584, 586-588]. Parameters like the nozzle diameter, flow rate, applied voltage and distance towards the collector influence the diameter of the deposited fibers, wherby the resolution limit of fibers from PCL was found to be around 800 nm [587]. Possible alterations to the fiber surfaces to influence their surface properties and thus biological outcome are typically undertaken during post-processing. This exemplarily includes CaP deposition [585] or NaOH treatment [589].

In the case of SES, a solution of the polymer in an organic solvent (mixture) [581] such as chloroform/methanol [590, 591] or dimethyl formamide/tetrahydrofuran [592] is used for PCL processing [581, 593]. As with MEW, a high voltage is applied such that the polymer solution is continuously ejected onto the grounded collector. Due to fluid bending instabilities, the ejected material is twisted while deposition onto the collector leading to a disordered nonwoven from randomized nano-scaled fibers [583]. Solidification occurs by evaporation of (toxic) solvents [585]. The fiber morphology depends on the solution properties (e.g. viscosity, surface tension), process parameters (e.g. nozzle diameter, flow rate, voltage and distance towards the collector) as well as ambient conditions [581]. With conventional SES technique, the resulting fiber mat would be too dense for being penetrated with cement paste. Macroporous SES fiber mats can be produced either by using porogens [594, 595] or a patterned collector, which allows a disturbance of the electric field such that the deposited fiber mat mimicks this pattern and hence controls SES scaffold porosity [596]. Some surface modifications of SES fibers can be undertaken *in situ* [597, 598], which constitutes a great advantage over MEW. A summary of essential features of MEW and SES for the creation of selected porous fiber mats is given by Table 21.

For this study, four kinds of fiber mats were processed from PCL: MEW lattices with 30 fiber layers each with a fiber diameter of approximately 8 µm and a fiber distance of 200, 500 and

1000 µm, respectively, as well as a perforated SES mat (fiber Ø 800 nm - 2 µm) with round holes (Ø 1 mm) in shifted rows and a hole distance of 2 mm. Corresponding scanning electron micrographs and photographs are depicted in Figure 30.

Table 21: Features of MEW and SES as a method of choice for the fabrication of perforated PCL scaffolds with defined porous structure.

	melt electrospinning writing (MEW)	**solution electrospinning (SES)**
fiber diameter	sub-µm to µm	nm
fiber deposition	straight fibers	twisted fibers
fiber distance	defined fiber distance	dense network
solidification	cooling from melt	evaporation of solvents
incorporation of porous structure	*per se* perforated	needs an own collector pattern for each geometry
surface modification	typically subsequent	subsequent & online

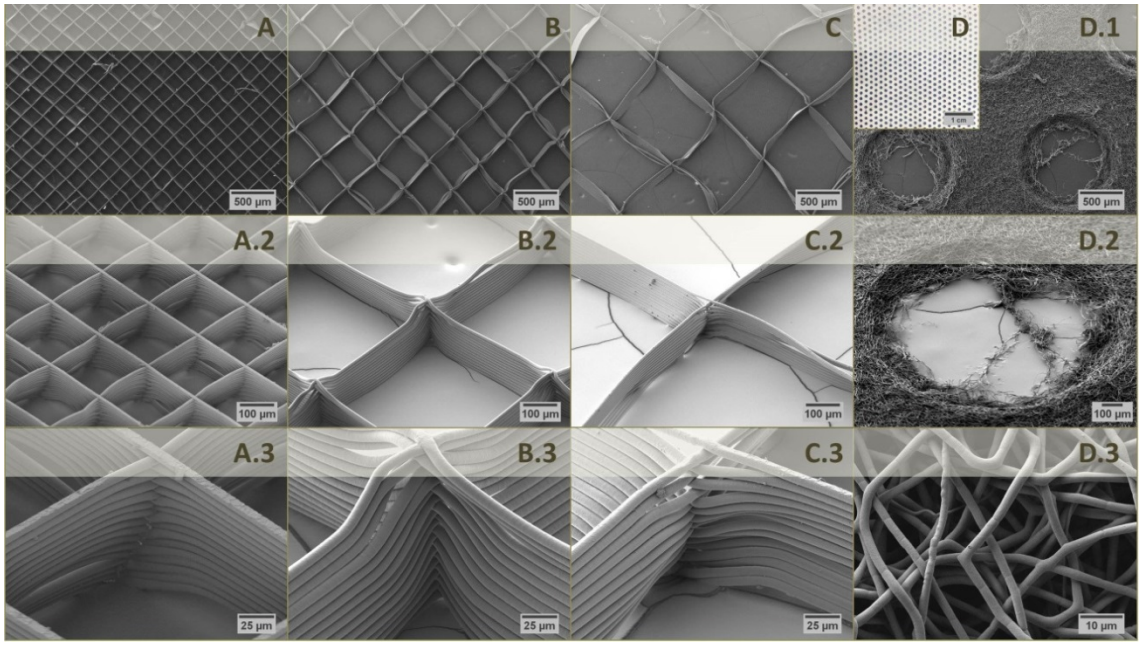

Figure 30: Scanning electron micrographs of MEW fiber mats from PCL with 30 fiber layers and a fiber distance of 200 (A-A.3), 500 (B-B.3) and 1000 µm (C-C.3) and photograph as well as scanning electron micrographs of SES fiber mat from PCL with round holes (Ø 1 mm) in shifted rows and a hole distance of 2 mm (D-D.3).

The as-fabricated scaffolds were used to build up a laminated mat from alternating layers of cement paste and 3 to 7 PCL scaffolds (Figure 31). The use of SES technique for the fabrication of fiber-CPC composite materials has already been reported. Zuo *et al*. [128] produced fiber bundles from PCL and poly(L-lactic acid) *via* SES and cut them into segments of approximately 3 mm length [128]. Bao *et al*. [136] electrospun a PLGA non-woven which was cut into 3x3 mm squares [136]. In both cases, the fibers were manually blended with the as-prepared HA forming cement paste. Besides a mechanical benefit, the high surface area of the fibers should improve the biological outcome [128, 136]. Also, fiber meshes from resorbable poly(glactin) have been used in combination with HA forming CPC. The main concept consisted again of improving the mechanical outcome and leaving an interconnecting porous structure for new tissue ingrowth and ameliorated cement degradation subsequently to fiber

dissolution. Thus single or up to 13 sheets of the fiber mesh were placed into an adequate mold and filled with cement paste [140, 142, 599]. However, none of these composites would enable free flexibility and shaping until application. In contrast, the as-presented laminates from the current study can be cut into arbitrary shape (bending rod, defect-specific etc.) and are flexible until contact with an aqueous solution.

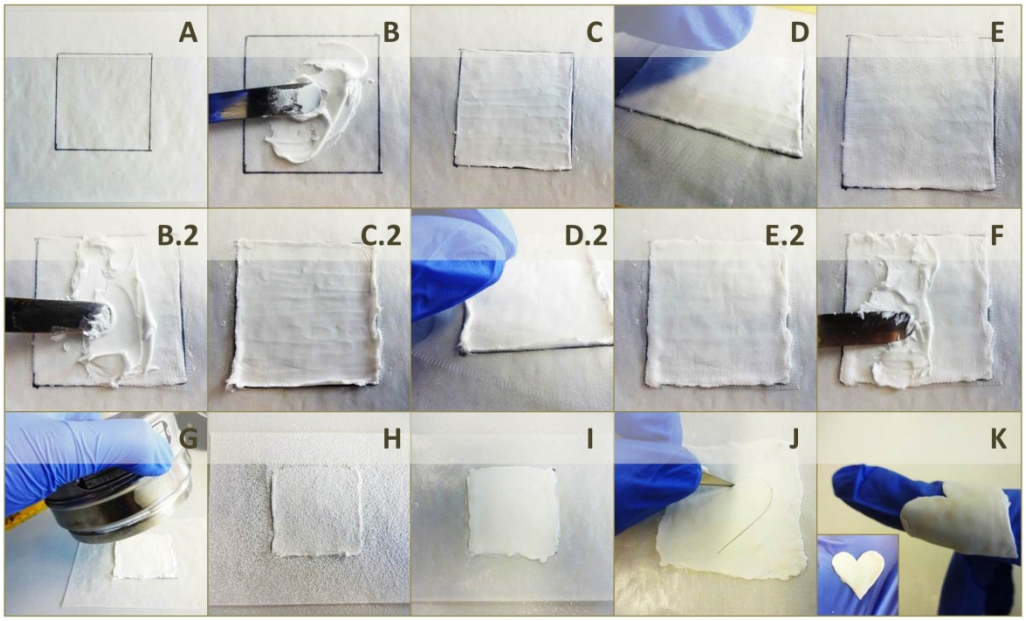

Figure 31: Manufacturing regime of prefabricated laminates using three layers of MEW PCL scaffolds with a fiber distance of 500 µm. 1.5 g of the cement paste is smeared evenly on a 50x50 mm weight paper (A-C) with a PCL scaffold pressed on top (D, E) followed by a second layer of cement paste and PCL scaffold (B.2-E.2). This procedure is repeated thrice with a last cement paste layer on top (F). Lastly, α-TCP is sieved through a 300 µm sieve on the laminate (G, H) and spread to evenly cover all oil residues on top and bottom (I). The fabricated laminate can be cut into arbitrary, flexible form (J, K).

Table 22: Weight/area ratios of MEW and SES fabricated PCL scaffolds with different porous structure. Except for the ♦ marked scaffolds, each scaffold exhibited significantly different ratios with $p<0.001$ to each other.

scaffold type	**weight/area in mg/cm²**
MEW, 200 µm fiber distance	0.91±0.05
MEW, 500 µm fiber distance	0.54±0.04 ♦
MEW, 1000 µm fiber distance	0.20±0.03 ♦
SES	1.57±0.11

The following (subjective) observations were made while processing MEW scaffolds: An increase in fiber space led to an improved cement paste penetration but also resulted in an increase in PCL scaffold deformation through the mechanical stress applied with the spatula. More excessive paste had to be removed while flattening of the surface. This would explain a potential decrease in laminate thickness. At low fiber spaces of 200 µm, the paste was not able to penetrate the scaffolds very well so that a partial separating of single layers within the laminate could be observed. It is supposed that lamination may not work with higher scaffold numbers. Further, the fabrication of PCL scaffolds with this geometry is very time-consuming. An observation similar to MEW lattices with small fiber distance was made using porous SES scaffolds. Though the pore size was only marginally smaller compared to the lattice with cor-

responding fiber distance (0.8 v. 1.0 mm²) those scaffolds exhibited an 8-fold higher weight/area ratio (Table 22) due to the large pore distance of 2 mm. Thus, at least 33 % more cement paste was needed to cover the whole surface. Because of the fast increase in composite thickness, only three SES scaffolds were layered within one composite. In this case, scaffold deformation by manually applied shear stresses did not occur.

The as-fabricated laminates were cut into rod-shape and stored for up to 48 h at 37 °C under moist conditions to initiate hardening of the cement paste followed by mechanical testing within a 4-point bending test setup. The results for the cured prefabricated laminates from cement paste and MEW scaffolds are depicted in Figure 32. As previously indicated, an increase in fiber distance at a constant layer number of 3 resulted in a significant reduction of the laminate thickness from 1.3±0.08 (200 µm fiber distance) to 0.71±0.02 mm (1000 µm fiber distance). This is due to the fact that less cement paste was necessary to cover the whole construct. Simultaneously, composites with a large fiber distance of 1000 µm were extremely thin and thus really fragile. In contrast, increasing the layer number from 3 to 7 layers at a constant fiber distance of 500 µm increased the laminate thickness by 170 % from initially 1.0±0.08 mm (Figure 32 a). As anticipated, the maximum force during 4-point bending test setup behaved proportionally to the laminate thickness such that a decrease in laminate thickness due to fiber distance enlargement reduced the maximal force by 87 % from 1.6±0.45 (200 µm) to 0.21±0.10 MPa (1000 µm). Simultaneously, an increase in laminate thickness from 3 to 7 layers led to a 7-fold increase in bending force to 4.1±0.64 N (Figure 32 a). However, calculation of the corresponding bending strengths revealed, that most formulations exhibited a similar value of approximately 3.5 MPa which was significantly lower compared to the pure cement paste (5.9±0.93 MPa). Only using a small fiber distance of 200 µm at 3 layers or a bigger fiber distance of 500 µm at 5 layers resulted in composites without significant difference of $p<0.001$ towards the control group (Figure 32 c).

Within the research field of FRCPC, it is a common phenomenon that a minimum, so-called critical fiber volume content is needed for a positive reinforcement effect, especially when the interface between fiber and matrix is weak. In contrast, very high fiber amounts might deteriorate the mechanical outcome for aggregation reasons followed by composite inhomogeneities [103]. Xu and Simon [140] continuously observed an increase of both bending strength and work of fracture when increasing the amount of poly(glactin) meshes within their CPC matrix. Even the incorporation of one single sheet led to a mechanical improvement in comparison to the pure CPC control [140]. Contradiction with the present results might be explained with two essential differences towards the study of Xu and Simon: Firstly, the use of an oil-based cement paste introduces additional porosity [232] and secondly, this paste potentially has a higher viscosity such that a higher shear stress is applied for composite fabrication. Consequently, with an increasing number of PCL scaffolds and cement paste layers, the degree of distortion of the regulated lattice structure was higher, which might be the reason for the slight reduction in bending strength at 7 layers.

Though the prefabricated laminates with scaffolds of the smallest fiber distance showed the best results, it has to be mentioned that the generation of such small structures *via* MEW was very time-consuming. Thus, reproducibility of the preparation regime was tested by means of the laminate from 5 layers of the 500 µm-scaffold which exhibited satisfying me-

chanics, either. Even though the bending strengths were comparable in all three attempts considering standard deviations, there were partially significant differences regarding laminate thickness and maximum bending force (Figure 32 d).

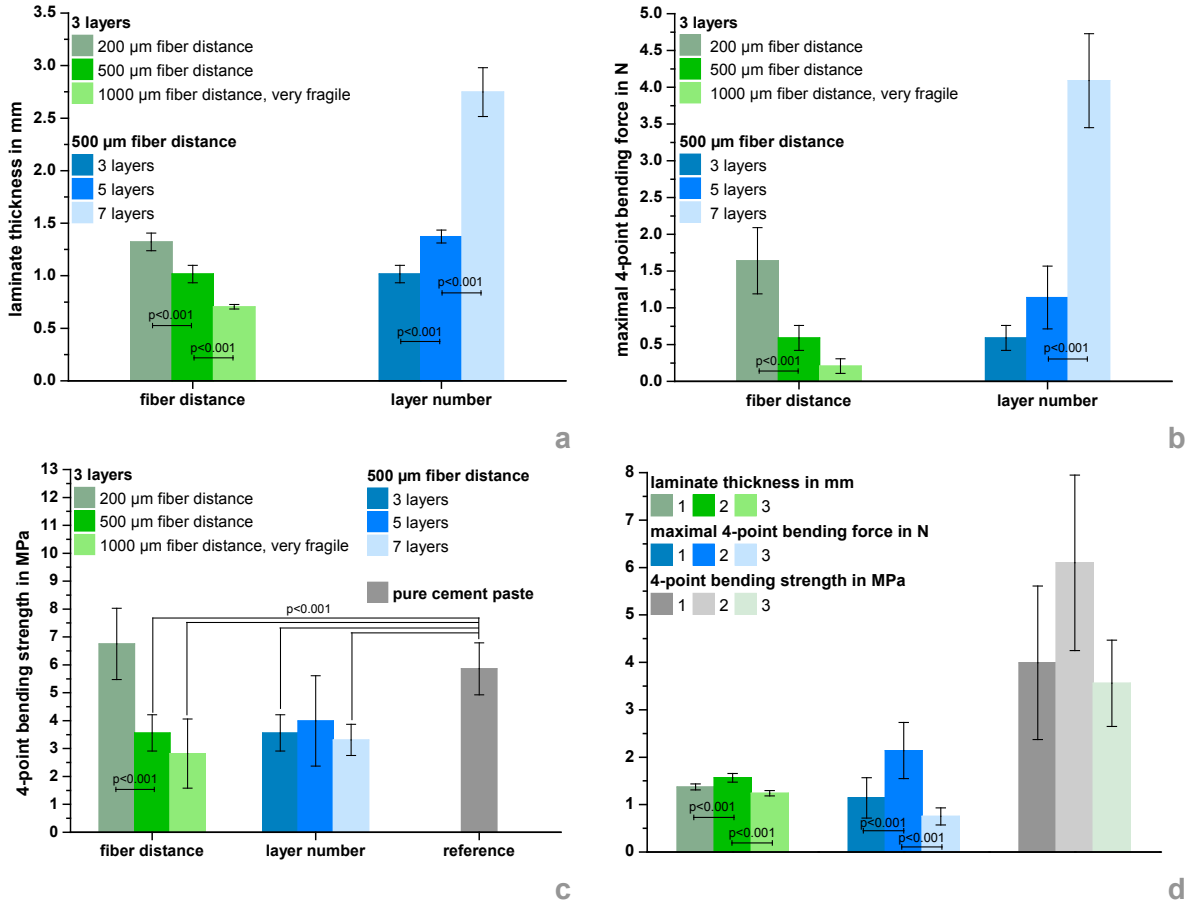

Figure 32: Laminate thickness (a), maximal 4-point bending force (b), 4-point bending strength (c) of prefabricated laminates from oil-based CPC paste and 3, 5 or 7 layers of MEW PCL scaffolds with a fiber distance of 200, 500 and 1000 µm after 48 h of setting under moist conditions at 37 °C. Reproduciblity regarding laminate thickness, maximal bending force and bending strength was analyzed using prefabricated laminates from oil-based CPC paste and 5 layers of MEW PCL scaffolds with a fiber distance of 500 µm as an example (d).

Fracture surfaces of the hardened composite specimens were analyzed *via* SEM (Figure 33). The micrographs revealed that the bending rods tended to break at the lattice junctions (Figure 33 A-E) such that single fibers protruded either from the gaps between imprints of former crossing fiber bundles (Figure 33, 1) or even from the gaps of crossing fiber bundles themselves (Figure 33, 2). Thus, the distance between top-down running (imprints of) fiber bundles might be used to estimate the thickness of single cement layers. As already mentioned, increasing the fiber distance of MEW PCL lattices resulted in a decrease in composite thickness (Figure 33 A-C) due to removal of excess cement paste which further on reduced the thickness of single cement layers between two PCL scaffolds. This amounted to 100-200 µm for a 200 µm fiber distance (Figure 33 A), 70-150 µm for a 500 µm fiber distance (Figure 33 B) while the layer thickness was not evaluable for a 1000 µm fiber distance as the fiber imprints of two PCL scaffolds nearly touched (Figure 33 C). Obviously, the distance between two single PCL lattices varied widely which is owed to the mechanical shear stresses on the scaffolds while preparation. In addition, an increase in fiber distance simultaneously reduced the density of protruding fibers (Figure 33 A-C). The same effect was observed in-

creasing the layer number and the cement layer thickness seemed to be marginally smaller at 7 layers (Figure 33 B, D-E). Having a closer look at the protruding fibers (Figure 33, A.2, D.3), their diameter was ~50 % smaller compared to the pores they left within the cement matrix (Figure 33, A.2) as well as the original sizes (Figure 30, A.3-C.3). This observation is a consequence of the fiber stretching while bending of the rods. A further example of the tapering effect on pulled fibers is given by Figure 33, C.2. Lastly, both Figure 33, C.2 and D.2 illustrate the deficient interface between fiber surface and cement matrix, as only few and small cement fragments were found around PCL fibers. However, it was possible for the cement paste to even penetrate the small gaps between single fibers of a hole bundle (Figure 33, D.3) such that partially equal bending strength compared to the pure hardened cement was observed (Figure 32 c). This is supposably enabled by the fact that PCL has intrincically high hydrophobicity [581] which is also the case for the oil-based cement paste before diffusion of the hydrophobic carrier liquid to the outside.

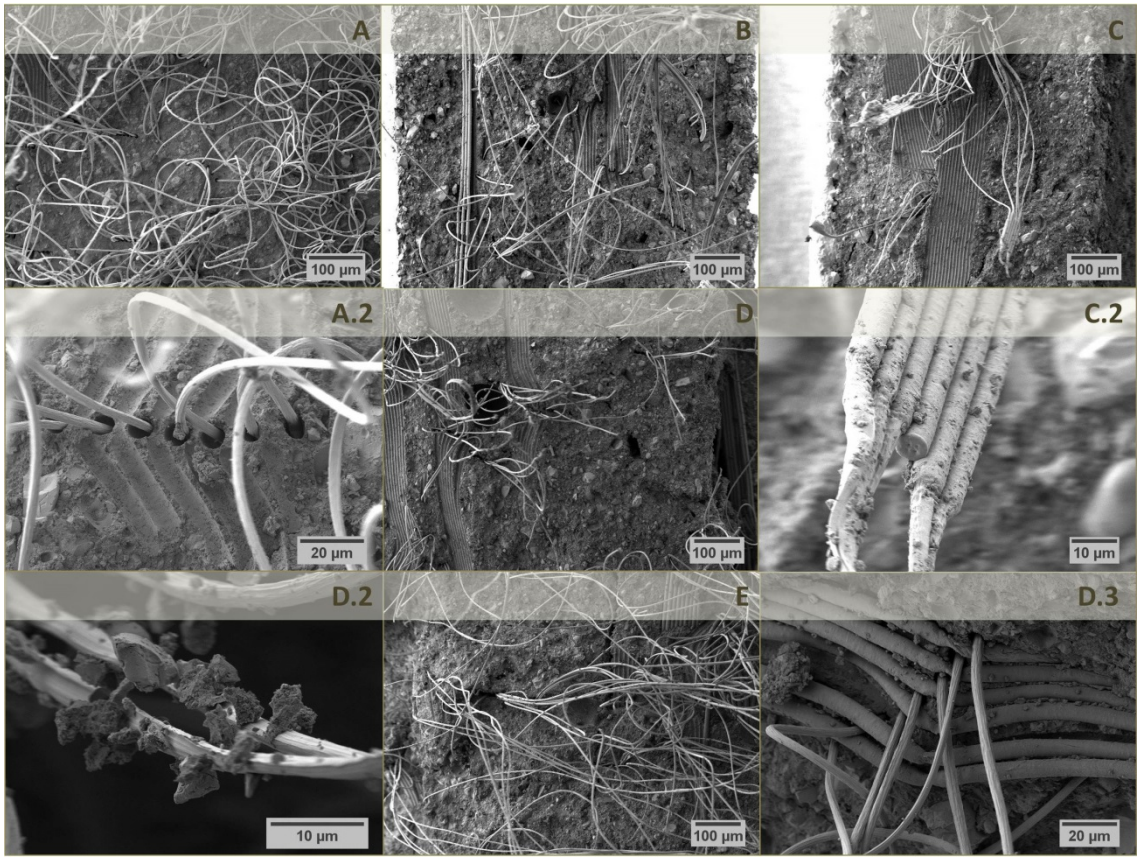

Figure 33: Scanning electron micrographs of total fracture surfaces of prefabricated laminates from oil-based CPC paste and 3 (A-C.2), 5 (D-D.3) or 7 (E) layers of MEW PCL scaffolds with a fiber distance of 200 (A-A.2), 500 (B, D-E) and 1000 µm (C-C.2) after 48 h of setting under moist conditions at 37 °C. Regions of interest (A.2, C.2, D.2-D.3) were recorded at higher magnifications.

Because of the strong distortion of the MEW lattices during laminate preparation, similar experiments were undertaken with SES PCL scaffolds whereby a semi-order was implemented with a perforated collector. Since also a weak interface between the hydrophobic fibers and the hygroscopic cement has been demonstrated, a surface compatibilization by NaOH treatment was tested. In this part of the study, the geometric parameters of the PCL scaffolds as well as the layer number within the laminate were kept constant.

There are different approaches to effectively modify the surfaces of *via* SES fabricated PCL scaffolds [581]. Plasma treatment leads to cleaning and etching of the surface followed by alterations of the surface topography as well as chemical reactions between the plasma and surface molecules. Using oxygen plasma provokes etching of the surface as oxygen reacts with the carbon atoms of the polymer to form volatile products and surface hydroxy (-OH) and carbonyl (-C=O) functionalities. This improves the hydrophilicity of the polymer [581, 600] which has already been reported to enhance adhesion and proliferation of osteoblast, fibroblast and chondrocyte cell lines [601]. Chemical alterations of the PCL fiber surfaces can also be undertaken by means of NaOH to improve wettability [602, 603] and the fiber meshes can be coated retroactively *via* mineral deposition [602, 604] or with biologically relevant substances such as covalently bound gelatin to improve cell adhesion and proliferation [605]. A special benefit of SES technique towards MEW is the possibility to *in situ* incorporate surface functionalities such as isocyanate (-N=C=O) groups which provide an ideal binding partner for -NH_2 or -OH functionalities. This is enabled through the simultaneous spinning of the polymer with a star-shaped statistical copolymer from PEO and PLGA modified with -NCO groups [597, 598].

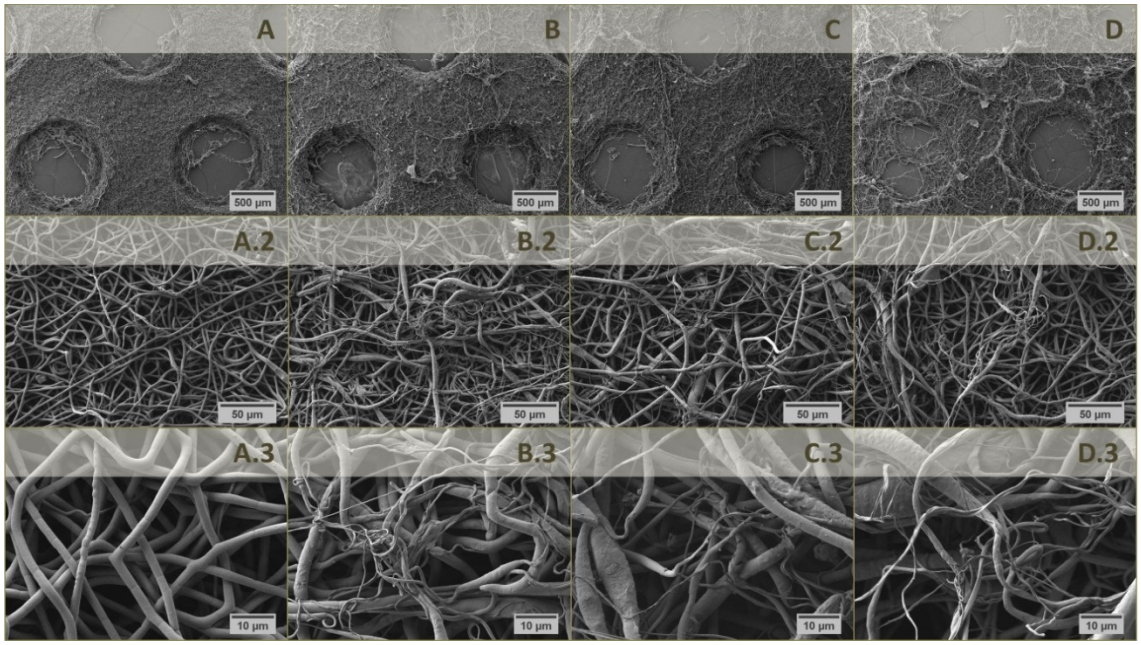

Figure 34: Scanning electron micrographs of SES from PCL with round holes (Ø 1 mm) in shifted rows and a hole distance of 2 mm without treatment (A-A.3) or after deposition for 10 (C-C.3), 30 (B-B.3) and 60 min (D-D.3) in 1.0 (B-B.3) or 2.0 M (C-D.3) NaOH.

In the present study, the SES PCL fiber mats were surface-modified *via* incubation for 10, 30 and 60 min in 1.0 or 2.0 M NaOH (Figure 34). Chemically, hydroxyl and carboxyl (-COOH) functionalities are introduced such that the surface is less hydrobhobic while simultaneously modifying the fiber morphology [581]. Increasing the NaOH concentration and duration of the treatment macroscopically led to a strong devastation of the produced semi-ordered structure (Figure 34 A-D). It seemed that the treatment with 1.0 M NaOH for 30 min had the same effect on the construct appearance as compared to the treatment with 2.0 M NaOH for 10 min (Figure 34 B-C). On a microscopic level, the homogenious distribution of fiber diameters between 800 nm and 2 µm (Figure 34 A.2-A.3) vastly changed. Even, if no differences were seen between the diverse treatments, a lot of really thin fiber strands (~300 nm) were ac-

companied with a lot of thicker fibers (~3.5 µm) whereat the fiber diameters exhibited strong irregularities (Figure 34 A.2-D.3). Besides thinning of the fibers [606-608], other reports describe a variation of the fiber morphology [602], the formation of pits on the fiber surface [606-608] or even a breakup of single filaments [603]. In spite of obvious microscopic differences towards the untreated control, only marginal changes were observed with respect to the corresponding contact angles especially for the lower concentrated NaOH solution. Generally, water contact angles have to be <<90 ° for good wettability and ~0 ° for the liquid to fully spread on the surface [609]. This was only the case for a 60 min treatment with 2.0 M NaOH (Table 23). Thus, chemical treatment with an alkaline solution had a greater impact on the scaffold topography and fiber morphology as compared to the wettability.

Table 23: Contact angles of the surfaces of porous SES scaffolds from PCL without treatment or after deposition for 10, 30 or 60 min in 1.0 or 2.0 M NaOH. In case of ♦ marked scaffolds, the water droplet sunk in within a short time frame such that no contact angle could be measured.

		contact angle	
NaOH concentration	**deposition time**	**above pores**	**between pores**
/	/	157±7 °	156±6 °
1.0 M	10 min	128±5 °	141±5 °
	30 min	136±9 °	136±5 °
	60 min	142±2 °	145±3 °
2.0 M	10 min	♦	155±6 °
	30 min	♦	154±10 °
	60 min	♦	♦

Each three untreated and basically treated SES PCL fiber mats were layerd with oil-based cement paste, as previously described, cut into rod-shaped geometry, stored for 48 h under moist conditions and analyzed *via* 4-point bending test setup. The laminate bending strengths, areas under the stress-displacement curves and selected stress-displacement curves are depicted in Figure 35 a-c. As the layer number was kept constant, expectedly no significant differences in laminate thickness were observed such that it remained ~1.7 mm comparable to prefabricated laminates with 5 layers of MEW scaffolds. This was because more cement paste was necessary to cover the whole surface due to the higher weight/area ratio of SES fiber mats (Table 22). Having a look at corresponding bending strength (Figure 35 a), a higher NaOH concentration seemed to slightly improve this mechanical property while the immersion time had no effect. The laminate with untreated SES PCL scaffolds exhibited a strength of 2.5±0.82 MPa whilst treatment with 1.0 M and 2.0 M NaOH resulted in mechanics of approximately 3.5 MPa and 4.5 MPa, respectively. At first glance, an increase in the hydrophilic character of the scaffolds, as shown *via* water contact angle measurements (Table 23), seemed to steadily improve the bending strength. However, significant differences towards the PCL free control group could solely be realized applying an immersion of the PCL fiber mats for 30 min in 2.0 M NaOH resulting in an almost 3-fold amelioration of the 4-point bending strength. Thus, the corresponding cement receipt was reproduced in terms of laminate thickness, maximum force, bending strength and area under the force displacement-curves, whereat no significant differences were found (Figure 35 d).

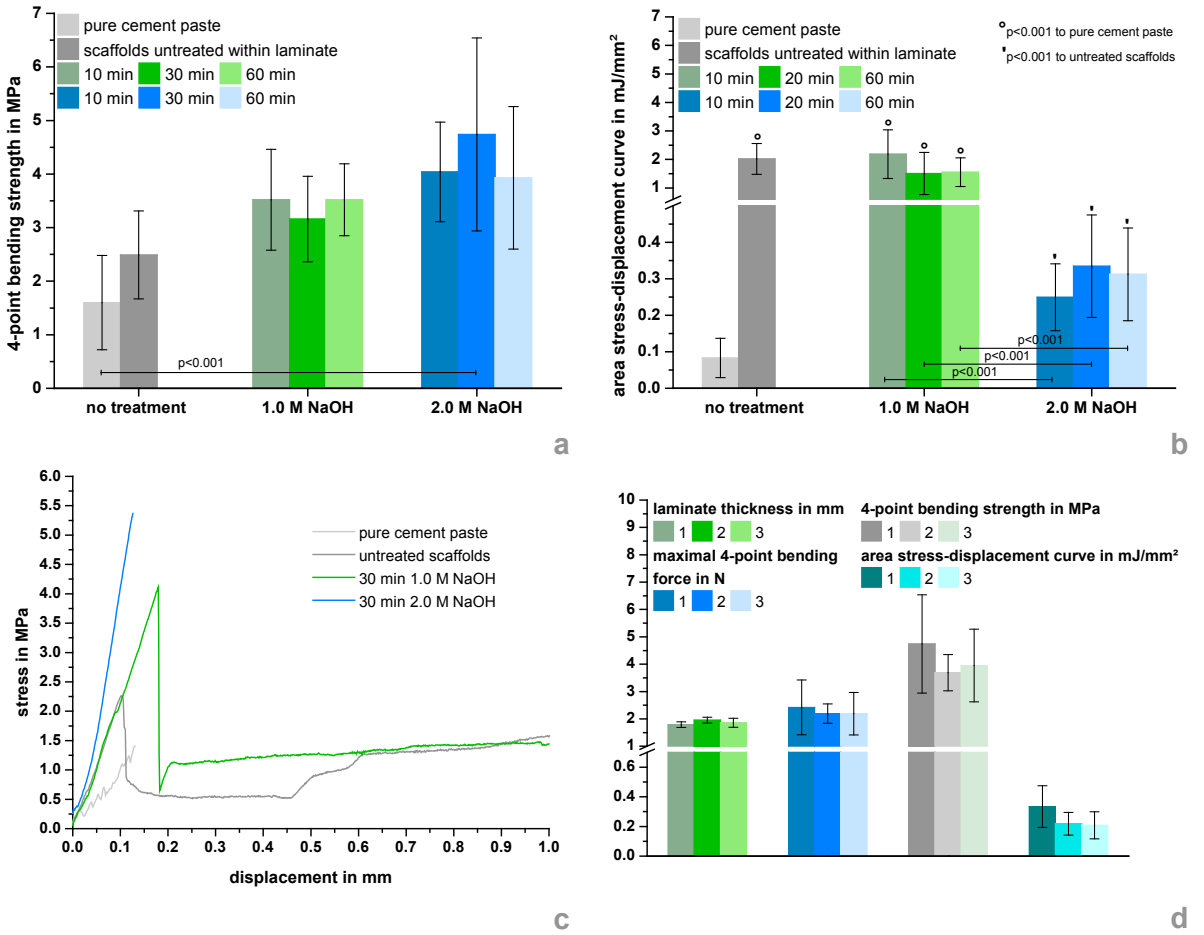

Figure 35: 4-point bending strength (a), area under the stress-displacement curves (b), selected stress-displacement curves (c) of prefabricated laminates from oil-based CPC paste and 3 layers of SES PCL scaffolds with round holes (Ø 1 mm) in shifted rows and a hole distance of 2 mm without treatment or after deposition for 10, 30 and 60 min in 1.0 or 2.0 M NaOH after 48 h of setting under moist conditions at 37 °C. Reproduciblity regarding laminate thickness, maximal bending force, bending strength and area under the force-displacement curves was analyzed using prefabricated laminates from oil-based CPC paste and for 30 min with 2.0 M NaOH treated SES PCL scaffolds as an example (d).

In contrast, evaluation of areas under corresponding stress-displacement curves as a measure for the absorbed fracture energy revealed that only laminates with untreated scaffolds or scaffolds which were immersed in lower concentrated NaOH showed significant amelioration towards cement paste control with values between 1.5±0.74 (30 min 1.0 M NaOH) and 2.2±0.85 mJ/mm² (10 min 1.0 M NaOH) corresponding to a reinforcement by one order of magnitude (Figure 35 b). Those formulations exhibited stress-displacement curves allowing additional force absorption after an initial rupture of the cement matrix. In contrast, the pure cement control as well as formulations with PCL scaffolds that were immersed in 2.0 M NaOH showed a characteristic, ceramic-like, brittle fracture behavior (Figure 35 c). This explains why corresponding areas under stress-displacement curves are ~80-90 % lower with values between 0.25±0.09 (10 min 2.0 M NaOH) to 0.33±0.14 mJ/mm² (30 min 2.0 M NaOH). Again, variation of the immersion time in NaOH seemed to play an inferior role (Figure 35 b). To correctly assess the relation between interface and mechanical output, corresponding scanning electron micrographs (Figure 36) are discussed firstly.

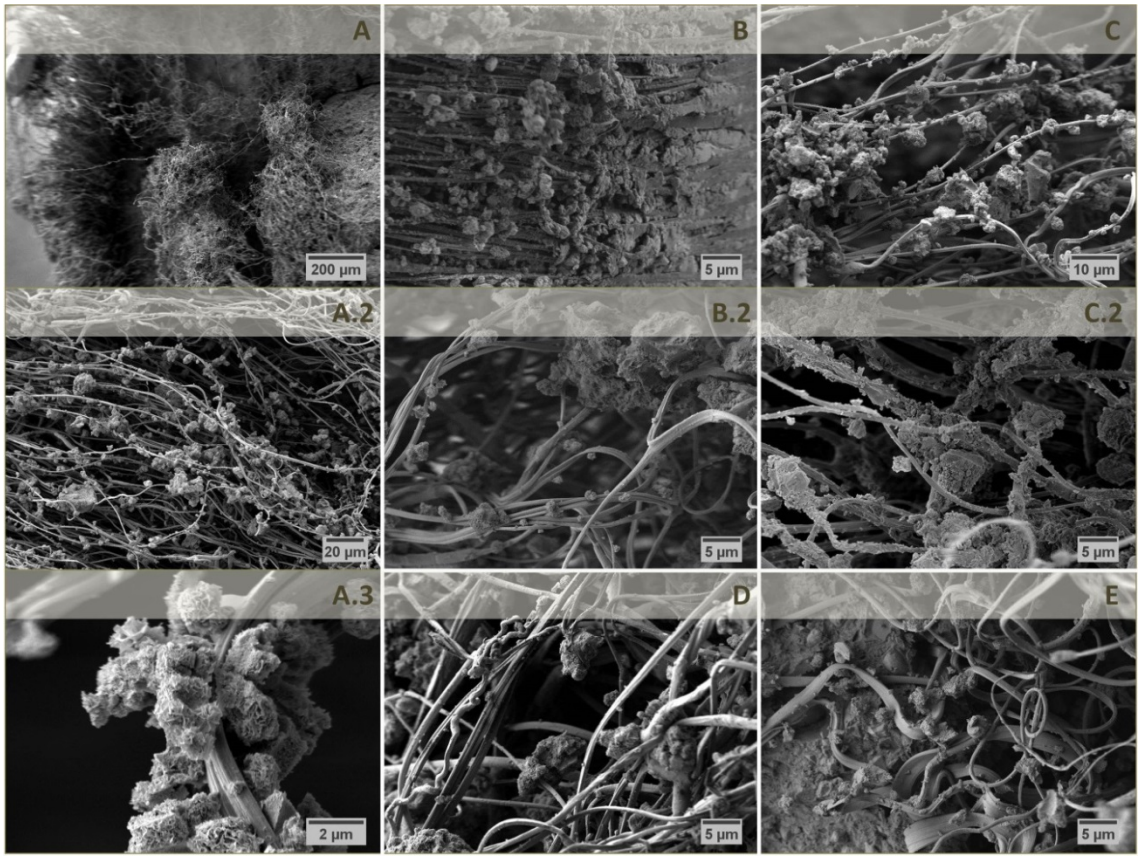

Figure 36: Scanning electron micrographs of total fracture surfaces of prefabricated laminates from oil-based CPC paste and 3 layers of untreated (A-A.3) or for 10 (C-C.2), 30 (B-B.2, D) or 60 min (E) in 1.0 (B-B.2) or 2.0 M NaOH (C-E) immersed MEW PCL scaffolds with round holes (Ø 1 mm) in shifted rows and a hole distance of 2 mm after 48 h of setting under moist conditions at 37 °C.

A macroscopic view of the fracture surface of prefabricated laminates from SES PCL scaffolds and cement paste is given by Figure 36 A and was comparable among all analyzed fracture surfaces. The three layers of PCL fiber mats differed notably, but seemed quite disordered due to the high number of nanosized filaments. Even without any surface treatment, noticeable accumulations of CaP crystals were proven around single PCL filaments. In contrast to the CaP aggregates around MEW fibers (Figure 33 C.2, D.2), those really seemed to have grown along the surface. A gentle immersion in alkaline solution even further improved the interface i.e. interwining of both components though no clear decrease in water contact angle was measurable (Table 23, Figure 36 B-C.2). In case of the treatment in 2.0 M NaOH for 30 min, parts of the PCL construct seemed to be almost completely mineralized and surrounded by a cohesive CaP matrix (Figure 36 C.2). However, longer immersion in 2.0 M NaOH solution strongly weakened the interface, as the surface was too hydrophilic for an initial compatibilization of fiber and oily cement paste (Table 23, Figure 36 D-E). For effective fiber reinforcement, it has to be ensured that the interface is strong enough to enable appropriate load transfer and energy dissipation. This can result in an improved strength as well as work of fracture [103]. The as-presented results have shown that SES PCL fiber mats intrinsically provide a suitable interphase (Figure 36 A.2-A.3), but mild surface modification under alkaline conditions was able to even improve it (Figure 36 B-B.2) and thus further reinforce the cement (Figure 35 a-c). However, a too strong fiber-matrix interaction, which was observed for prefabricated laminates being immersed for 30 min in 2.0 M NaOH (Figure 36 C-C.2), probably avoids potential energy dissipation in form of fiber pull-out or friction, such that

the resulting specimen might have adequate strength supposably due to a reduced cement porosity, but likewise a conventional brittle fracture behavior, as seen in Figure 35 a, c. Due to the initial lipophilic character of the oily cement paste, a high degree of hydrophilicity resulted in a weak interface (Figure 36 D-E) and consecutively ceramic-like fracture behavior (Figure 35 c), as little energy would be consumed during separation of fiber and matrix. Though, it was possible to improve the bending strength in comparison to the pure cement control group (Figure 35 a), as the nanosized fibers might be able to densify the cement matrix which intrinsically contains the oil phase as a leachable porogen [232]. Overall, the critical tranformation of the cement paste from a hydrophobic into a hydrophilic material during setting needs further research in terms of surface compatibilization.

In direct comparison of both appraches, MEW seemed to be the inferior choice. It produces a relative low number of proportionally thick fibers. The resulting contact area between PCL and cement is thus relatively low, such that - in combination with the weak interphase and the overall low fiber volume content - a deterioration of the mechanical properties is not unlikely. Additionnally, scaffolds which were produced with this technique were easy to distort by shear stresses such that the benefit of geometric accuracy is void in this special application. In contrast, the high number of nanofibers within SES PCL scaffolds offers a large contact area towards the cement matrix and - associated with the illustrated stronger interphase and overall higher fiber volume content - a unique opportunity to merge a classic reinforcement strategy for CPC with the novel application form of a flexible, flat bone substitute.

3.1.3.4 Conclusion

In summary, the as-presented layer-by-layer technique was successful in processing flexible laminates from oil-based cement paste and PCL fiber mats with defined pore architecture. It was revealed, that SES with a patterned collector was more suitable for the fabrication of the polymer scaffolds as compared to MEW, as fiber-matrix interface and thus mechanical performance was noteably enhanced. In the long term, PCL filaments would initially support the cement from flowing, provide mechanical reinforcement within the hardened ceramic and among degradation, introduce interconnecting channels for improved resorption and new bone ingrowth.

3.2 Magnesium phosphate cement based approaches

The subsequent chapters refer to **Project 2** *in the experimental section and describe the two novel application forms of drillable mineral bone cements and bone adhesives (chapter 2.3.2). They both are based on the concept of using cation chelating cement additives presented in chapter 2.2.2.*

MPC combine the self-setting ability and osteoconductive character of CPC with the osteogenic influence of Mg^{2+} and additional features such as a better biodegradation potential and higher initial strength (chapter 2.1). Different alternatives compared to classic cement formulations have been discussed in chapter 2.2, however, the need of an ammonium ion source in case of struvite forming cement systems or the acidic setting character of newberyite forming ones might limit the spectrum of alternative formulations.

The basic reason for developing a MPC system with improved mechanics was the clinical need for biodegradable drillable cement formulations [14]. It showed up that the principles and success of the model HA/poly-2-HEMA cement system (3.1.1) could not be transferred without further ado to degradable systems on inorganic as well as on polymeric side. Table 24 depicts examples of failed attempts to obtain a drillable bone cement on a MgP basis.

Table 24: Pretestings and formulations for a biodegradable drillable cement system. The non-biodegradable model CPC system is marked in grey. The idea with the ♦ marked formulation was to use the acidic pH of the struvite reaction for alginate gelling without calcium ion supply.

solid phase	liquid phase	drillability	problems
α-TCP, APS	2-HEMA, TEMED	✔	⃠
farringtonite, MCPA	alginate/pectin	⃠	alginate/pectin reacts too fast with Ca^{2+} from MCPA, and is then destroyed by shear forces
farringtonite, DAHP	alginate	⃠	ammonium phosphates prevent alginate from gelling ♦
farringtonite	DAHP, hyaluronic acid	⃠	interactions between DAHP and low molecular weight hyaluronic acid >0.1 %
farringtonite, APS	2-HEMA, TEMED, DAHP	⃠	reaction kinetics of struvite and poly-2-HEMA (non-biodegradable) can badly be co-coordinated
farringtonite	ethylenediaminetetracetic acid (EDTA)	⃠	no setting observed within an adequate time frame

Therefore, the idea came up to reuse the results of a former study whereat a trimagnesium phosphate (farringtonite) was combined with the chelate forming agent phytic acid. The addition of high contents (30 %) of phytic acid to the aqueous component of the cement system led to the formation of a hydrated cementitious product (newberyite) with low conversion, but

[14] The idea for a degradable, drillable mineral bone cement was proposed by PD Dr. med. Stefanie Hölscher-Doht; University Hospital of Würzburg, Trauma surgery.

high compressive strength. This proof-of-principle study will be described in chapter 3.2.1. It turned out that 1) the chelating process equipped the cement with a quite sticky texture during setting, which 2) glued well on glass slabs and metal spatula. For those reasons, the ascribed cement formulation served as a basic concept for the development of a 1) drillable MPC with 2) additional bone bonding ability which required adjustments of the original formulation. Figure 37 gives an overview about the contents of the following chapters.

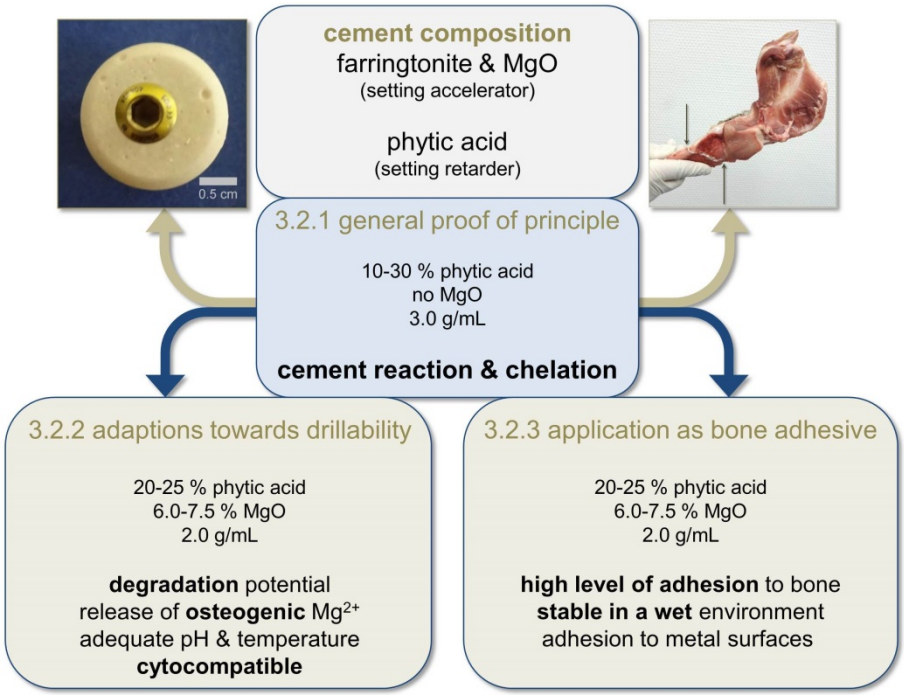

Figure 37: Schematic overview about the development of a farringtonite based cement system which incorporates chelation and enables the fabrication of drillable specimens and bone adhesives.

3.2.1 Chelate bonding mechanism in a novel magnesium phosphate cement

The following section 3.2.1 is reused from the research article: T. Christel, S. Christ, J.E. Barralet, J. Groll, U. Gbureck. Chelate bonding mechanism in a novel magnesium phosphate bone cement. Journal of the American Ceramic Society. 98(3) (2015) 694-697. T. Brückner (née T. Christel) holds first authorship. She designed and executed the whole experimental study. She further wrote the manuscript, whilst S. Christ, J.E. Barralet, J. Groll and U. Gbureck were involved in proof-reading. The latter came up with the idea of the study. Lastly, J.Groll and U. Gbureck were involved in supervision and submission.

3.2.1.1 Abstract

A novel approach to harden magnesium phosphate cements was tested using phytic acid solutions as chelation agent. In addition to complex formation, a cementitious dissolution and precipitation reaction led to the formation of newberyite ($MgHPO_4 \cdot 3H_2O$) as the hydrated form of the farringtonite ($Mg_3(PO_4)_2$) raw powder. The set cements showed good mechanical properties (up to 65 MPa in compression) displaying a doubling of the compressive strength of conventional newberyite forming cements despite of a significantly lower degree of cement conversion. An increasing phytic acid concentration from 10 to 30 % had a retarding effect on the setting time (11 to 16 min), decreased the pH close to acidic conditions (pH=5 to 4) and increased the maximum setting temperature (26 to 31 °C), but none of these factors reached critical values. The presented strategy was successful in fabricating a good workable, novel mineral biocement with promising characteristics for biomedical applications.

3.2.1.2 Introduction

MgP compounds have similar characteristics to CaP bone substitutes, but degrade faster under physiological conditions [301, 376]. Similar to CPC, MgP can undergo a continuous dissolution and precipitation reaction forming a stable ceramic product. Farringtonite ($Mg_3(PO_4)_2$) is known to set with 3.5 M $(NH_4)_2HPO_4$ solution to form struvite ($MgNH_4PO_4 \cdot 6H_2O$) in a neutral reaction [311], at which the product is naturally found in the calcifications of kidney stones [311, 610]. In combination with more acidic components (primary phosphates ($H_2PO_4^-$), for example $Ca(H_2PO_4)_2$), the ammonium free mineral newberyite ($MgHPO_4 \cdot 3H_2O$) can be found as setting product in such cements [81]. In this study, an alternative setting mechanism of MPC was tested, whereas phytic acid ($C_6H_{18}O_{24}P_6$) was used instead of conventional primary (e.g. $Ca(H_2PO_4)_2$) or secondary (HPO_4^{2-}, e.g. $(NH_4)_2HPO_4$) phosphates. Phytic acid is a natural plant antioxidant and acts as a strong chelating agent for polyvalent cations (e.g. Ca^{2+}) [611]. This study hypothesized that phytic acid will also form stable complexes with the magnesium ions from the phosphate cement raw material leading to a hardening process of the cement paste.

Thus, $Mg_3(PO_4)_2$ was mixed with 10, 20 or 30 % diluted phytic acid. Reference cement formulations without chelate setting ability were prepared by mixing the raw powder with either 2.0 M H_3PO_4 and 0.5 M citric acid solution or by combining an equimolar mixture of $Mg_3(PO_4)_2$ and $Ca(H_2PO_4)_2$ with 0.5 M citric acid.

3.2.1.3 Results and discussion

Although MPC are known in civil engineering applications for decades, these compounds were applied quite recently as bone replacement materials, for example, struvite [294] or newberyite forming cements [209], which commonly set by a continuous dissolution/precipitation reaction. More recently, a different setting mechanism was proposed by Takahashi *et al*. [78] for CaP biocements, in which the modification of β-TCP with phytic acid created a cement that set upon mixing with water by chelation between the phosphate groups of phytic acid and released Ca^{2+} ions [78]. This approach was applied in this study on a MgP based cement system by adding differently concentrated (10 to 30 %) phytic acid solutions to farringtonite powder, which resulted in a well working paste that sets according to Equation 21. The release of phosphoric acid (H_3PO_4) during the chelation process leads to a further transformation of farringtonite into the hydrated form newberyite ($MgHPO_4 \cdot 3H_2O$, Equation 22) by continuous dissolution and precipitation reaction:

$$Mg_3(PO_4)_2 + C_6H_{18}O_{24}P_6 \rightarrow C_6H_{12}O_{24}P_6Mg_3 + 2H_3PO_4 \quad \textbf{(21)}$$

$$2H_3PO_4 + 2Mg_3(PO_4)_2 + 18H_2O \rightarrow 6MgHPO_4 \cdot 3H_2O \quad \textbf{(22)}$$

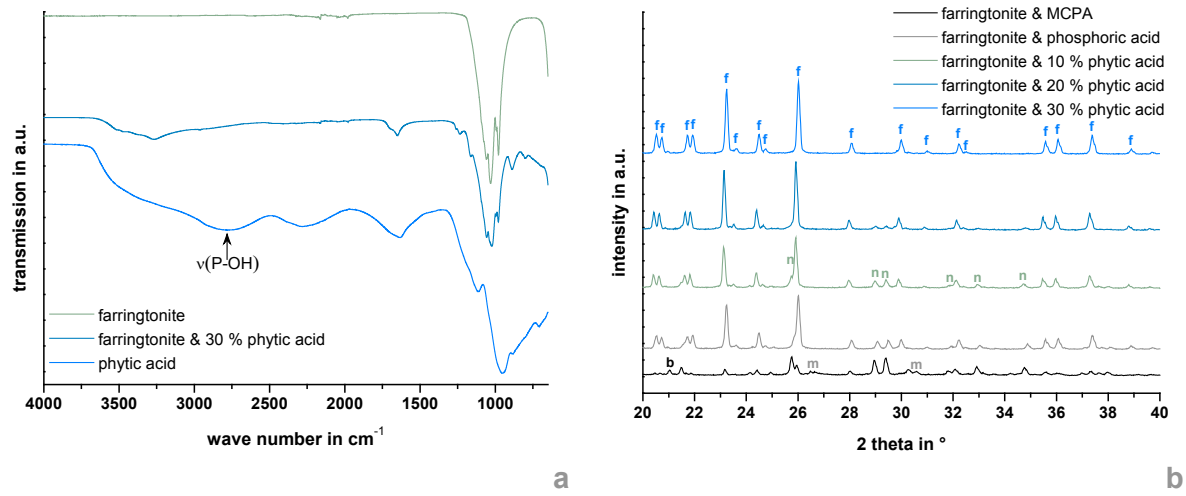

Figure 38: FTIR spectra of phytic acid, $Mg_3(PO_4)_2$ and a cement made from $Mg_3(PO_4)_2$ and 30 % phytic acid. Arrow indicates the position of the ν(P-OH) valence vibration (a). XRD of cements made from $Mg_3(PO_4)_2$ and 10, 20 or 30 % phytic acid, from $Mg_3(PO_4)_2$ and 2.0 M phosphoric and 0.5 M citric acid and of an equimolar mixture of $Mg_3(PO_4)_2$ with $Ca(H_2PO_4)_2$ and 0.5 M citric acid (b). All cement samples were prepared with a PLR of 3.0 g/mL and hardened for 1 h at 37 °C and 100 % humidity (a) or 24 h in water at 37 °C (b). For the XRD measurements, characteristic diffraction reflexes for farringtonite, newberyite, monetite and brushite are labeled with f, n, m and b.

FTIR and XRD measurements were performed to demonstrate that both chelation and conventional cement setting occur simultaneously (Figure 38). The valence vibration ν(P-OH) of pure phytic acid can be found at a wave number of 2770 cm^{-1}. Neither the bonds of the raw powder farringtonite nor those of the setting product interfered at this wave number. As the latter contains a 30 wt.% amount of phytic acid, the extinction of this stretching bond indicates interactions of phytic acid with farringtonite based Mg^{2+} ions and can be considered as

proof for the chelation reaction (Figure 38 a). Using a PLR of 3.0 g/mL, a maximum (calculated) newberyite content of 7 wt.% (10 % phytic acid), 12 wt.% (20 % phytic acid) and 17 wt.% (30 % phytic acid) is possible according to Equations 21 and 22. In contrast, a newberyite content of up to 42 wt.% (farringtonite & phosphoric acid) or 79 wt.% (farringtonite & MCPA) can be realized with conventional cement formulations [81]. This was verified by XRD analysis (Figure 38 b) whereas the set cements mainly consisted of farringtonite and small amounts of newberyite (2θ=29.1 °, 29.5 °, 33.0 ° and 34.8 °). The newberyite content increased with increasing phytic acid concentration and the increase in characteristic newberyite diffraction reflex intensities correlated with a decrease in characteristic farringtonite diffraction reflex intensities. At low phytic acid concentrations (10 %), no newberyite phase could be found. The tendency of these results conforms well with the stoichiometric calculations even though a 7 wt.% content of newberyite could not be reached for the 10 % phytic acid containing cement. As anticipated, the reference sample from farringtonite and MCPA contained most newberyite. Due to the appropriate raw powder composition, some foreign calcium containing phases (monetite $CaHPO_4$ and brushite $CaHPO_4 \cdot 2H_2O$) could be found in the diffraction pattern.

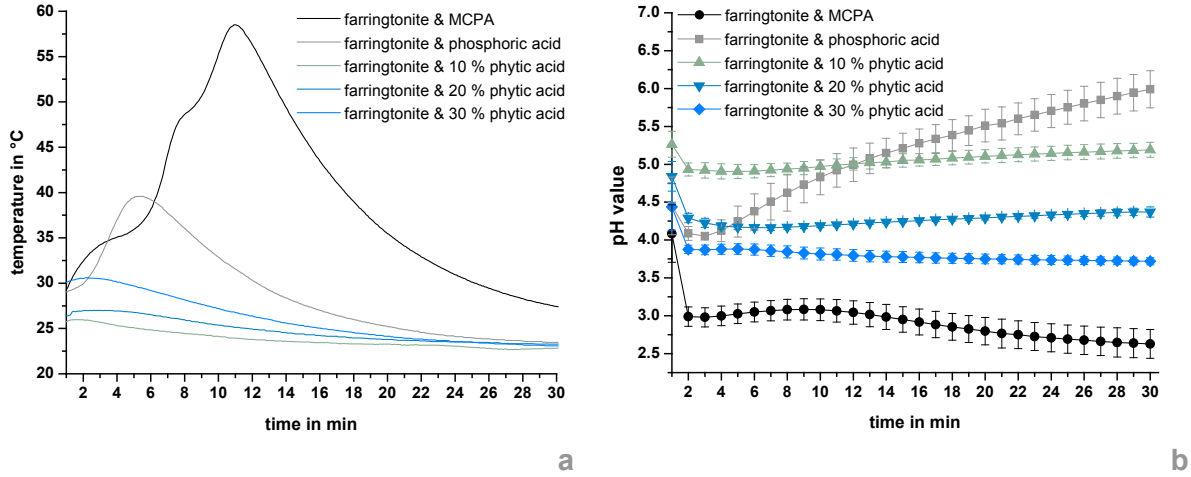

Figure 39: Temperatures (a) and pH profiles (b) of setting cement pastes consisting of $Mg_3(PO_4)_2$ and 2.0 M phosphoric and 0.5 M citric acid, an equimolar mixture of $Mg_3(PO_4)_2$ with $Ca(H_2PO_4)_2$ and 0.5 M citric acid and $Mg_3(PO_4)_2$ and 10, 20, or 30 % phytic acid. All samples were prepared with a PLR of 3.0 g/mL.

While setting, the temperatures of the phytic acid containing cement pastes increased with increasing phytic concentration and reached their maxima after approximately 2 min. The pastes did not exceed physiological temperature of 37 °C (maximum temperature measured: 30.6 °C). In contrast, polymer based bone cements (e.g. PMMA) harden at higher temperatures [27] as it is also the case for the used reference cement, which set with a maximum temperature of 58.5 °C. After 30 min, the setting temperature of all pastes approximated environmental conditions (Figure 39 a). Furthermore, the reaction took place under constant acidic conditions at a pH range from 3.7 to 5.3 in dependence of the phytic acid content. The setting reaction of the control cement with phosphoric acid started at a pH value of 4.1 and almost reached neutral conditions with a pH of 6.0 after 30 min of setting. In contrast, the reference cement with MCPA even hardened with a lower pH value of at least 2.6 (Figure 39 b). The tested cements are therefore comparable to the pH of already commercially available brushite forming cements during setting (pH<4.2) [13, 35].

While the setting time of the reference cements was quite fast (2 to 5 min), the setting time of the phytic acid containing formulations increased with increasing phytic acid content from 11 (10 % phytic acid) to 16 min (30 % phytic acid) (Table 25). Phytic acid seems to have a setting retarding effect comparable to that of citric acid in the case of brushite forming cement systems [71]. Recently, Meininger *et al*. [76] proved the suitability of phytic acid as possible alternative [76]. However, pastes with a high phytic acid content were sticky due to the proceeding chelation. It is assumed that such a paste will not disintegrate in the wet environment of a defect, even if the initial setting time exceeds clinical suggestions [60].

Table 25: Initial setting times of the tested cement formulations with significant differences ($p<0.001$) ● towards farringtonite & MCPA and ♦ towards farringtonite & phosphoric acid, respectively.

sample description	setting time in min
farringtonite & MCPA	5±1
farringtonite & phosphoric acid	2±1
farringtonite & 10 % phytic acid	11±2 ♦
farringtonite & 20 % phytic acid	12±2 ♦
farringtonite & 30 % phytic acid	16±1 ●,♦

Figure 40 shows scanning electron micrographs of the reference cements (Figure 40 a-b) and those cements with a phytic acid content of 10 (Figure 40 c), 20 (Figure 40 d) and 30 % (Figure 40 e) and a storage time of 1 h at 37 °C and 100 % humidity followed by 24 h at 37 °C in water after demolding. Obviously, the microstructure became more dense and homogenous with increasing phytic acid concentration. Without any phytic acid in the cement formulation, the surface was porous and heterogeneous with respect to crystal size and morphology. Also at phytic acid contents of 10 to 20 %, manifold crystal morphologies could be seen as, for example, randomized and layered platelets, clinkers, and unspecific fused geometries. Only at a phytic acid concentration of 30 %, the surface seemed to be dense and consistent.

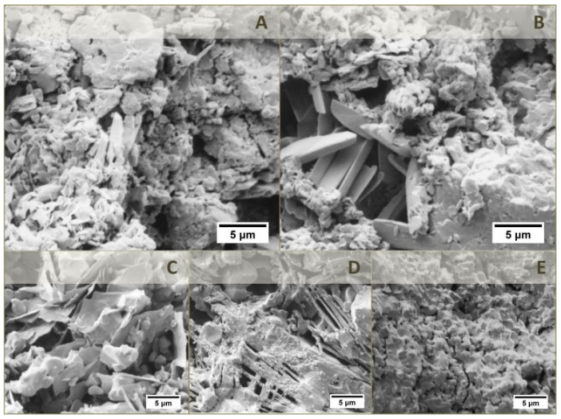

Figure 40: Scanning electron micrographs of surfaces from cement samples consisting of $Mg_3(PO_4)_2$ and 2.0 M phosphoric and 0.5 M citric acid (a), an equimolar mixture of $Mg_3(PO_4)_2$ with $Ca(H_2PO_4)_2$ and 0.5 M citric acid (b) and $Mg_3(PO_4)_2$ and 10 (c), 20 (d) or 30 % (e) phytic acid. The samples were prepared with a PLR of 3.0 g/mL and hardened for 24 h at 37 °C in water.

At low phytic acid contents (10 %), the compressive strength of the samples reached a quarter to a third (~7 MPa) of the compressive strength of the references (17 to 31 MPa). At a phytic acid concentration of 20 %, the compressive strength did not differ significantly from

that of both references after 24 h and 7 d of setting in water. The highest used phytic acid content even led to more than twice stronger cement samples (~65 MPa). In fact, the 30 % phytic acid modified cement took longer to achieve its final strength, but the compressive strength did not deteriorate during a longer deposition in water (Figure 41). The good mechanical properties of the 30 % phytic acid containing sample match well with the dense surface structure seen in Figure 40 e.

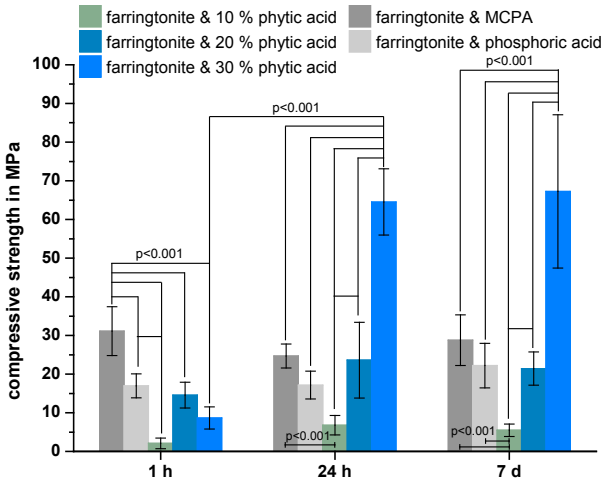

Figure 41: Compressive strength of cement samples consisting of $Mg_3(PO_4)_2$ and 2.0 M phosphoric and 0.5 M citric acid, an equimolar mixture of $Mg_3(PO_4)_2$ with $Ca(H_2PO_4)_2$ and 0.5 M citric acid and $Mg_3(PO_4)_2$ and 10, 20 or 30 % phytic acid. The samples were prepared with a PLR of 3.0 g/mL and hardened for 1 h at 37°C and 100 % humidity, followed by 24 h or 7 d at 37 °C in water.

3.2.1.4 Conclusion

A novel cement material with promising characteristics was obtained by the combination of a chelation mechanism with a cementitious reaction. As the setting product newberyite has already been demonstrated to be a biocompatible and degradable ceramic at *in vivo* conditions [209] and phytic acid used for cement modification in this study is also a bioavailable compound [611], it is assumed that the modified cements would have a clear application as biocements for orthopedic or dental applications. Major advantages of such formulations are their setting at more ambient conditions (temperature and pH) as well as their twice as high compressive strength compared to conventional newberyite forming cements.

3.2.2 *In vitro* study of a degradable & drillable farringtonite based bone cement

The following section 3.2.2 is likely to be used in a publication manuscript, which is however not yet submitted or published by the time of the submission of this thesis.

3.2.2.1 Abstract

Poor bone quality is one of the main indications for the augmentation of screws which can be performed by insertion of a bone cement into the defect followed by drilling after hardening. This facilitates a complete defect filling and adequate screw fit. The main challenge is the brittle mechanical behavior of mineral bone cements. Here, a farringtonite MPC formulation, that hardens by a chelation reaction, is presented. Differently concentrated (20 to 25 %) phytic acid solutions were added and the amounts of the setting accelerator MgO (6.0 to 7.5 %) were adjusted. Actually, three cement formulations were obtained which were drillable and showed screw pull-out forces of up to 148 N. Beside this key criterion, those MPC came along with other promising characteristics including a compressive strength of ~20 MPa, the potential to be degraded in physiological environment (mass loss of 2 wt.%, porosity increase up to 36 %) and the release of leastwise 0.17 mg/g per day of osteogenic Mg^{2+} within a time span of 24 d in PBS. Further, the cement sets under biologically non-critical conditions with respect to pH (slightly acidic) and temperature (30-32 °C) and corresponding eluates were cytocompatible towards human fetal osteoblasts hFOB 1.19.

3.2.2.2 Introduction

This study investigated the development of mineral bone cements with the ability of being drilled and a simultaneous high potential to be degraded *in vivo*, but this requires a material composition with exceptional mechanical properties. A sophisticated approach would exemplarily be to apply the concept of dual setting cement formulations with quasi-ductile fracture behaviour, as it has been shown previously for non-resorbable HA/poly-2-HEMA model systems in chapter 3.1.1.

MPC are considered being an attractive alternative *versus* CPC due to the release of biologically relevant Mg^{2+} ions and a comparably higher degradation potential [210, 288, 299]. In addition to the conventional setting mechanism, as it was proposed by Wagh *et al.* [318] for the formation of chemically bonded phosphate ceramics (e.g. MgO and phosphoric acid) [318], chelation was also shown to be a possible reaction route for MPC: In a proof-of-principle study, diluted phytic acid was used to both form complexes with Mg^{2+} ions and simultaneously enable newberyite formation as seen in chapter 3.2.1.3. This formulation showed a sticky, resinous texture directly after initiating the setting reaction. For the application as drillable cement, the quasi-ductile fracture behaviour must not necessarily be maintained after tapping and drilling, what turns the above mentioned phytic acid/farringtonite system into a suitable formulation for application sites where drilling is needed.

However a modification of the original system has to be performed to fulfil the following requirements: The cement has to be workable for at least 5 min and be drillable after 10 to

15 min which means that it must exhibit sufficient mechanical stability at the same time. An adequate setting time could be achieved while coordinating the phytic acid concentration and the amount of a highly active MgO. The former was shown to have a setting retarding impact on cement hardening [76], so that this effect has to be antagonized. In the following study, the goal was to present a drillable MPC system on the basis of farringtonite and phytic acid solution with concentrations between 20 and 25 % and an adjusted MgO content. Their material characteristics during setting (pH and temperature development, infrared spectrometry) and in a prolonged immersion study under physiological conditions (PBS at pH 7.4, 37 °C) were analyzed. This included composition, morphology, mechanical performance, porosity, mass loss, pH development and ion release. Further, an indirect cell testing towards human fetal osteoblast cell line hFOB 1.19 was performed over a time period of 10 d. The key property drillability was demonstrated in a proof-of-principle experiment. A newberyite forming cement system (farringtonite with phosphoric acid) was considered as control.

3.2.2.3 Results

The previously studied farringtonite/phytic acid system (Chapter 3.2.1) was chosen as a basic material for degradable drillable bone cements, as the chelating process equipped the cement with a sticky, resinous texture during setting. This consistency could be achieved with increasing phytic acid concentration in the liquid phase of the cement paste. Simultaneously, the workability of such cement pastes became worse which could be overcome with an increase in liquid phase content increasing the phytic acid concentration further. An increase in phytic acid concentration was beforehand observed to retard the setting reaction [76]. This effect leads to a discrepancy with the requirements of drillable bone cements: the cement has to have initially appropriate workability but then has to set fast with a resulting non-brittle mechanical behavior to sustain drilling. Thus, highly active MgO was added to counteract the setting retarding effect of phytic acid.

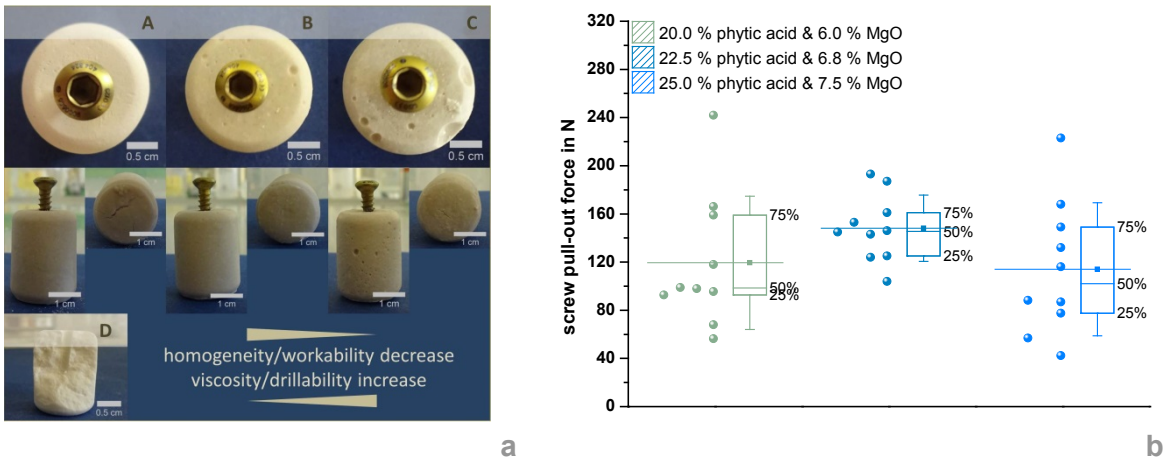

Figure 42: Photographs (a) of screwed cylindrical samples from farringtonite with 6.0 % MgO and 20.0 % phytic acid (A), 6.8 % MgO and 22.5 % phytic acid (B), 7.5 % MgO and 25.0 % phytic acid (C) or 2.0 M phosphoric and 0.5 M citric acid (D) after 15 min of setting and corresponding screw pull-out forces after 2 d storage in PBS at 37 °C (b). All samples were fabricated with a PLR of 2.0 g/mL.

It was shown that a high phytic acid concentration has to be combined with a high MgO concentration to create a balance between fast setting and mechanical resistance towards tapping and drilling. A combination of farringtonite with 6 % MgO as solid phase and 20 % phytic acid as liquid phase in a PLR of 2.0 g/mL finally exhibited appropriate workability and drilla-

bility. To create a certain diversity of cement formulations, other compositions with a constant molar ratio of MgO and phytic acid of 9.83 were tested likewise and were found to behave suitably as well, as seen in Figure 42 a. Although this quotient as well as the PLR were kept constant, the cement formulations behaved slightly different depending on the absolute MgO and phytic acid content, respectively. With increasing amounts of both ingredients, both homogeneity as well as workability became worse, but the drillability increased, as only small cracks originated from screwing. Of course, the crack formation also depends on how much material is extracted by the drill and how deep the screw is placed, which further depends on the chosen sample geometry. To sum up, the MPC formulations shown in Figure 42 are estimated to be drillable. In contrast, the newberyite reference was not drillable as it disrupted in a brittle way when drilling it after 15 min (Figure 42 a). Screw pull-out measures revealed a maximum pull-out force of 148±27 N when a 22.5 % concentrated phytic acid was used (Figure 42 b).

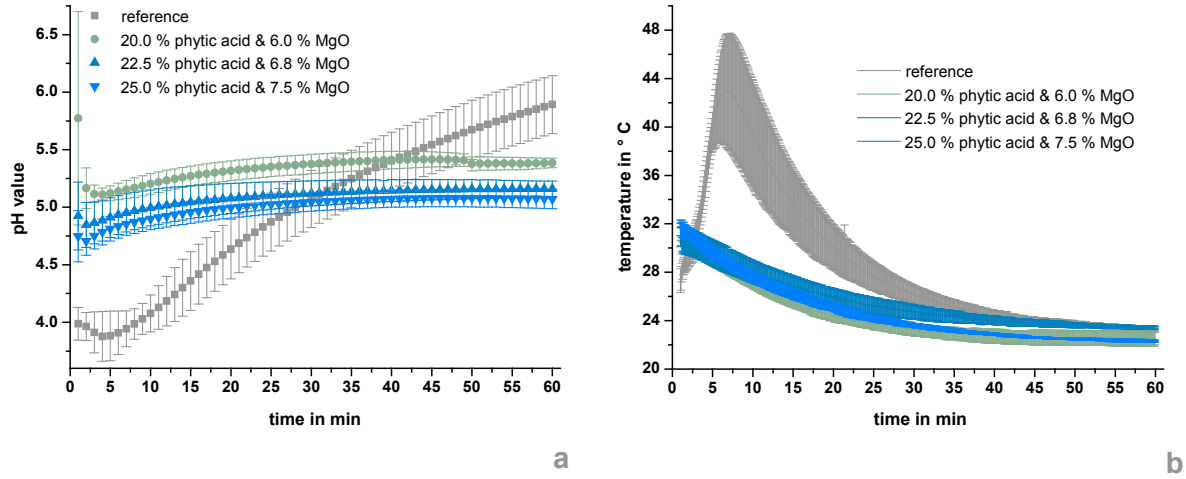

Figure 43: pH (a) and temperature development (b) of different cements from farringtonite with 2.0 M phosphoric and 0.5 M citric acid, 6.0 % MgO and 20.0 % phytic acid, 6.8 % MgO and 22.5 % phytic acid or 7.5 % MgO and 25.0 % phytic acid while setting. All samples were fabricated with a PLR of 2.0 g/mL.

Figure 43 depicts the pH as well as the temperature development of the drillable MPC during the first hour of setting. The phytic acid containing samples showed a very similar pH as well as temperature development at which the pH course remained relatively constant within a range of at least 4.7±0.1 (25.0 % phytic acid) up to 5.4±0.1 (20.0 % phytic acid). A slight tendency of decreased pH with increasing phytic acid and MgO content was visible as well. In contrast, the reference cement setting pH initially dropped in the first 5 min from 4.0±0.1 to 3.9±0.2 and afterwards continuously increased, exceeded the values of the phytic acid containing pastes and reached a pH value of 5.9±0.3 after 60 min (Figure 43 a). Concerning the temperature development, all cements approximated RT within the analyzed time range after having slightly increased to ~30 to 32 °C (phytic acid containing samples) and ~43 °C (reference) whereat the temperature maximum was reached earlier for the phytic acid containing ones. No significant differences could be observed in dependency on phytic acid concentration (Figure 43 b).

The vibrational spectra of the four tested cement pastes within the first hour of setting are shown in Figure 44. Only slight changes could be observed for the phytic acid containing samples, which basically consisted in intensity alterations of the water-linked vibrational

bonds. As the X-Ray patterns of phytic acid containing samples (Figure 45) showed that the samples mainly consisted of farringtonite (which shows no IR peaks at wave numbers beyond the fingerprint range, see chapter 3.2.1.3), the vibrational peaks can only be assigned to water or phytic acid, but the vibrational bonds of water predominate almost the whole wave number range. Hence, possible peak shifts or diminutions that might correlate with a chelation reaction are not visible. However, for the case of the 20 % phytic acid containing cement paste, a peak, which was not visible initially, appeared at ~1480 cm^{-1} and could be a hint for a proceeding reaction.

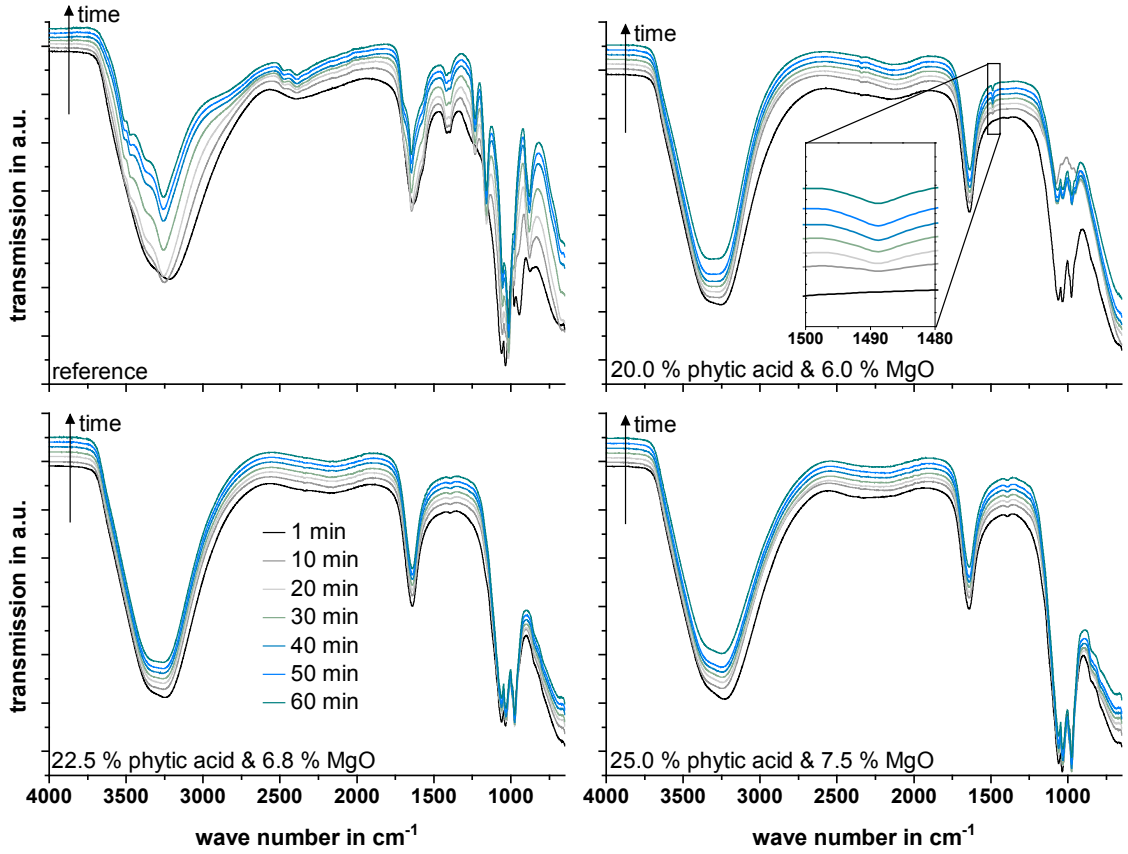

Figure 44: Time-dependent FTIR spectra of different cements from farringtonite with 2.0 M phosphoric and 0.5 M citric acid, 6.0 % MgO and 20.0 % phytic acid, 6.8 % MgO and 22.5 % phytic acid or 7.5 % MgO and 25.0 % phytic acid while setting. All samples were fabricated with a PLR of 2.0 g/mL.

After having proved the ability of phytic acid and MgO containing cements to sustain tapping and drilling already 15 min after initiation of the setting reaction without brittle failure, the cements were systematically analyzed with respect to changes in phase composition, morphology, mechanical performance and pH while being immersed in PBS at 37 °C for 24 d. Further, their ion release behavior (Mg^{2+}, PO_4^{3-}) was examined *via* inductively coupled plasma mass spectrometry.

Figure 45 depicts XRD patterns of the reference as well as phytic acid containing specimens after 24 d (Figure 45 a) and of the cement containing 20 % phytic acid in terms of immersion time (Figure 45 b). Only the reference paste that consisted of farringtonite with phosphoric acid demonstrated the conversion of farringtonite into newberyite. In contrast, this was not visible for the phytic acid containing samples after 24 d in an aqueous environment. The main discrepancy between the different phytic acid containing cements can be determined

with respect to diffraction reflex widths and intensities: The widths/intensities of the XRD pattern of the farringtonite phase, when the phytic acid content was minimal, were broader/lower compared to the other two samples that showed mostly equal patterns (Figure 45 a). However, the broadening and intensity decrease of the diffraction reflexes only occurred in the course of time due to the immersion in an aqueous environment (Figure 45 b) and was not observed being as distinctive for the other samples (data not shown). Small diffraction reflexes at 22.4, 28.2, 33.4 and 36.3 ° are ascribed to contaminations within the raw powder, i.e. sodium magnesium phosphate phase ($NaMg_4(PO_4)_3$).

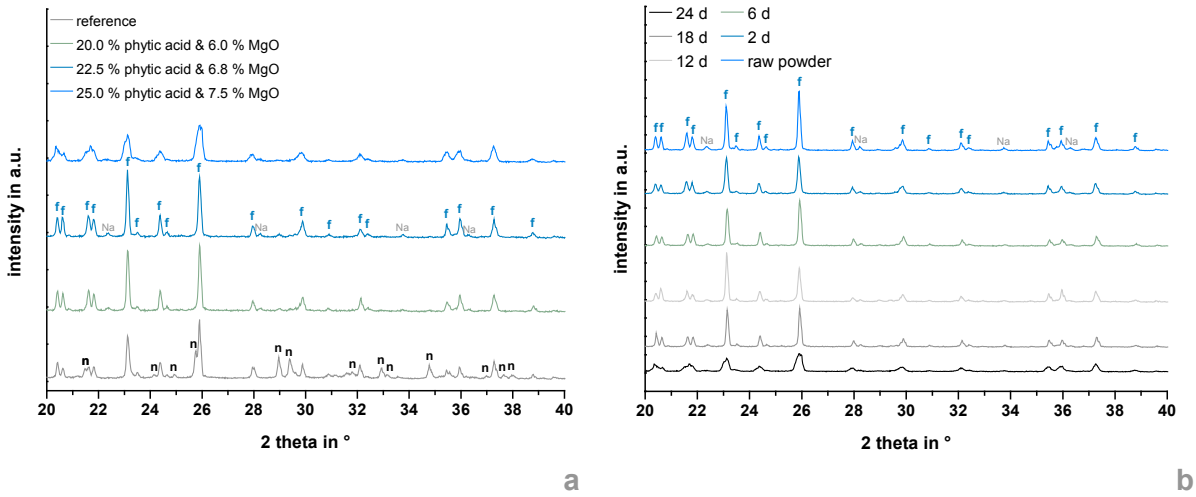

Figure 45: XRD from farringtonite with 2.0 M phosphoric and 0.5 M citric acid, 6.0 % MgO and 20.0 % phytic acid, 6.8 % MgO and 22.5 % phytic acid or 7.5 % MgO and 25.0 % phytic acid after 24 d of setting (a) and diffractograms from farringtonite with 6.0 % MgO and 20.0 % phytic acid after 2, 6, 12, 18 and 24 d of setting (b). All samples were fabricated with a PLR of 2.0 g/mL and stored for in PBS at 37 °C. Relevant reflexes are marked with f (farringtonite), n (newberyite) or Na (sodium magnesium phosphate), respectively.

The microstructure of the different cement systems is reflected in Figure 46. For the reference samples, a surface texture which is characteristic for conventional cement setting could be observed: By the course of time, boulder-like structures in a 10 to 20 µm range that are considered being raw powder residues were gradually predominated by platelet-shaped crystals <2 µm. The microstructure became more finely grained and the amount of entangled crystals increased. In contrast, the phytic acid containing samples showed a quite different surface topography. All samples were lanced with microcracks as well as even, homogeneously distributed pores within a size range of 1 to 10 µm. These pores seemed to decrease in diameter with increasing phytic acid amount. Depending on the phytic acid concentration, different (crystalline) structures could be observed beside vast smooth areas, whereat the amount of those structures seemed to increase with increasing phytic acid concentration as well. For samples with the lowest phytic acid concentration, mainly globular structures of about 2 µm were visible, whereas the other cement compositions predominantly showed platelet-like crystals in the lower µm range that were stacked, entangled or formed rosette-like arrangements.

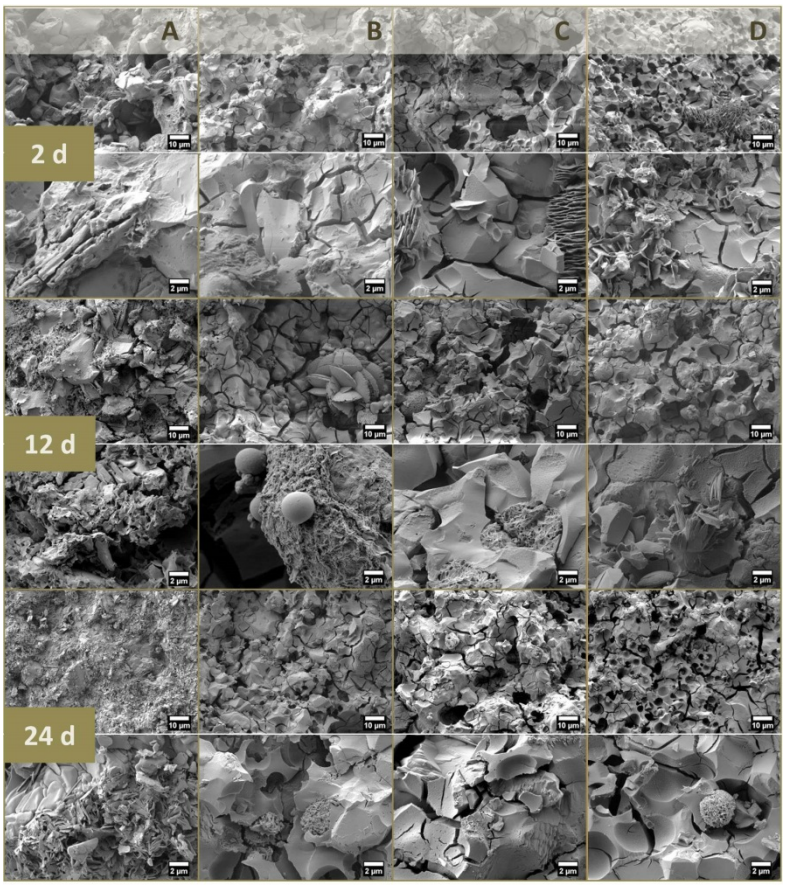

Figure 46: Scanning electron micrographs (2,000- and 10,000-fold) of fracture surfaces from farringtonite with 2.0 M phosphoric and 0.5 M citric acid (A), 6.0 % MgO and 20.0 % phytic acid (B), 6.8 % MgO and 22.5 % phytic acid (C) or 7.5 % MgO and 25.0 % phytic acid (D) after immersion in PBS for 2, 12 and 24 d in PBS at 37 °C. All samples were fabricated with a PLR of 2.0 g/mL.

The compressive strength development during immersion in PBS for 24 d is depicted in Figure 47 a. The reference started with a compressive strength of 8.23±1.27 MPa and increased by time to a final strength of 18.09±4.91 MPa after 24 d. In contrast, the MgO and phytic acid containing samples had comparably high compressive strengths of about 16 to 21 MPa already after 2 d in PBS and remained constant over the whole immersion period with the exception of samples containing 20.0 % phytic acid that gradually experienced a significant decrease in strength from 20.9±4.06 (6 d) to 12.4±1.57 MPa (12 d). All in all, samples with a medium phytic acid content had a significant higher compressive strength compared to the reference up to day 18 as well as compared to samples with a 20 wt.% phytic acid content since day 12 of being immersed in PBS. Concerning the porosity of those cements before and after immersion, all samples showed a significant increase of 12 to 14 % such that a final porosity of 32 (reference) to 36 % (20.0 % phytic acid) at most could be observed (Figure 47 b). The mass loss behavior of the references differed widely from the other samples. When the cuboids were firstly exposed into an aqueous environment, all four formulations showed a similar behavior and gained between 0.3 and 1.4 wt.% of mass, whereat the formulation with 20 % phytic acid gained the least and the reference formulation gained the most. Afterwards the reference weight stayed constant for at least two weeks and even further increased during the last eight days up to 102.1±0.2 wt.% compared to the initial weight. Since day 2 of the immersion study, the phytic acid containing samples constantly lost weight and ended up with around 2 wt.% less compared to their initial masses (Figure 47 c). Regarding the pH development of the supernatant of the immersion study, the reference liquid was

slightly basic (around 8.2 at most) and the phytic acid containing slightly acidic (around 6.9 at least), but fastly approximated physiological conditions (Figure 47 d).

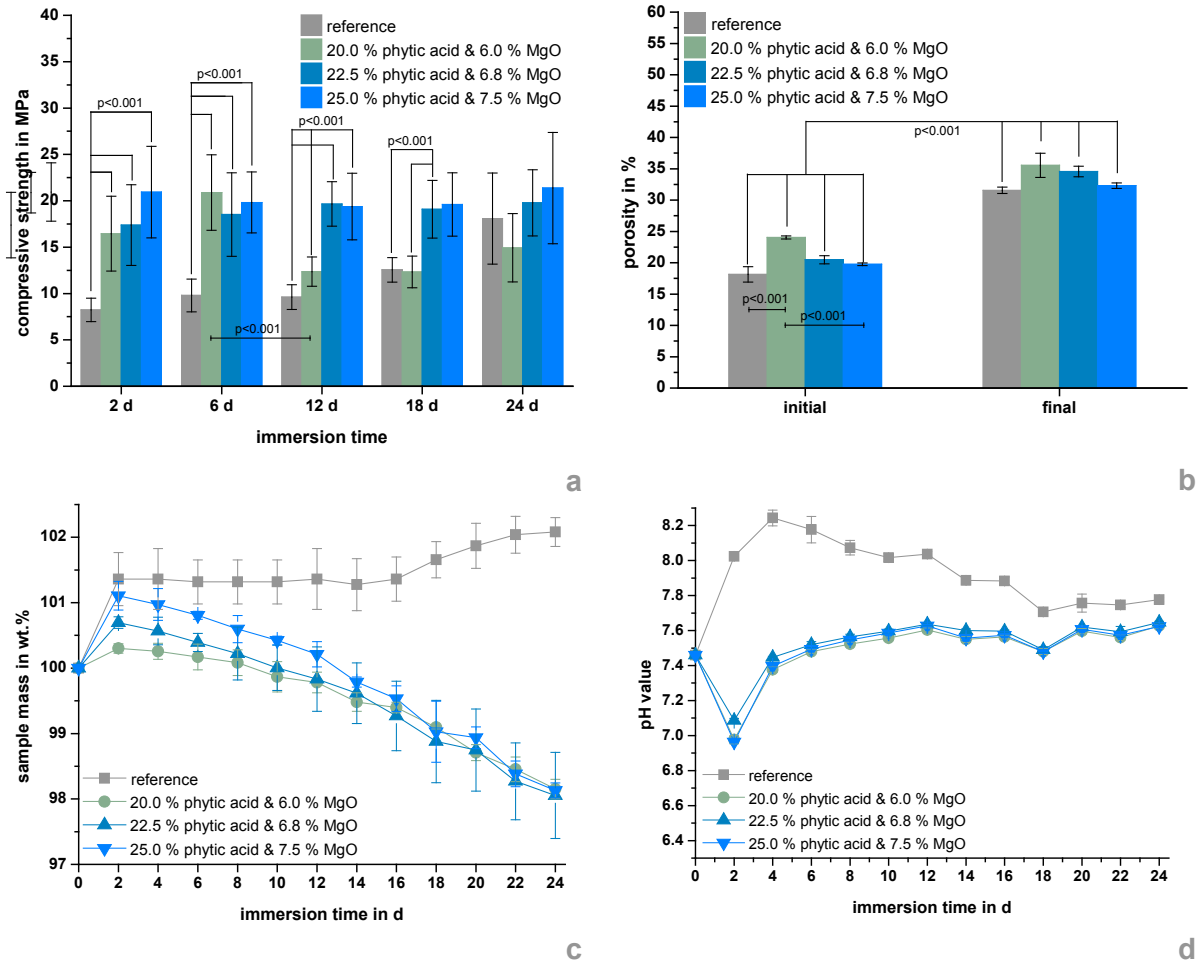

Figure 47: Compressive strengths (a) of cuboidal samples from farringtonite with 2.0 M phosphoric and 0.5 M citric acid, 6.0 % MgO and 20.0 % phytic acid, 6.8 % MgO and 22.5 % phytic acid or 7.5 % MgO and 25.0 % phytic acid and their initial and final porosity (b), respectively. Mass loss (c) of those samples was measured as well as pH development (d) of PBS in which the samples were deposited in. All samples were fabricated with a PLR of 2.0 g/mL and stored for 24 d in PBS at 37 °C.

Figure 48 reveals the results of the mass spectrometry analysis. Except for the first measuring point after 2 d, relatively constant amounts of Mg^{2+} and PO_3^{4-} ions were released over the whole period irrespectively of the sample type. Those were about 0.17 (22.5 % phytic acid) to 0.33 mg/g per day (reference) of Mg^{2+} ions and about 0.29 (20.0 % phytic acid) to 0.37 mg/g per day (reference) of phosphorous in form of PO_4^{3-} ions. Cumulative amounts in the same order of magnitude between 8.96±0.51 (20.0 % phytic acid) and 10.80±0.37 mg/g (reference) of phosphorous could be detected for all four samples, whereas the reference released almost as double as much Mg^{2+} as the phytic acid containing samples (Figure 48). Having a look at the molar Mg-to-P-ratio, the reference release obviously showed mean values of 0.97±0.33, which is in the same range as the theoretical value for the molar Mg-to-P-ratio prior to immersion. In contrast, proportionally less Mg^{2+} ions were released as originally enclosed in the phytic acid containing samples (Table 26).

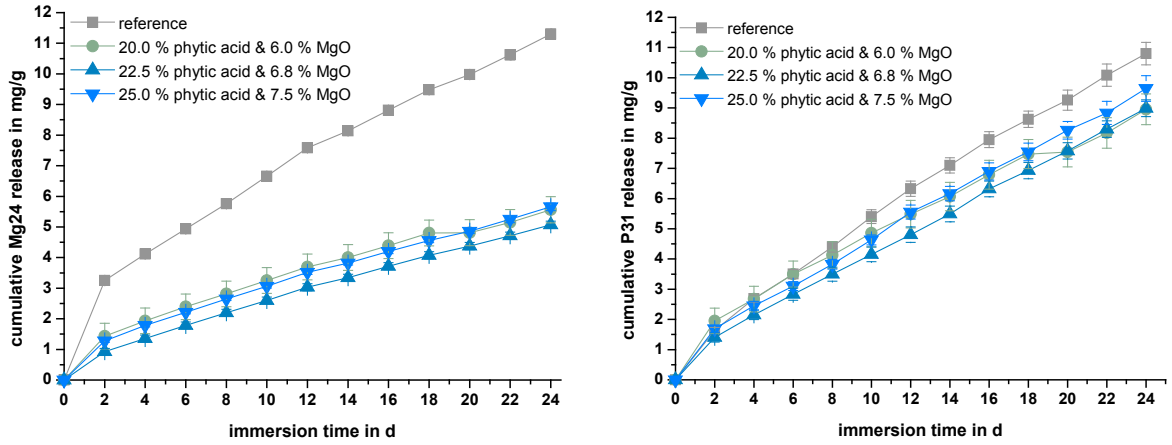

Figure 48: Cumulative Mg^{2+} (a) and PO_4^{3-} (b) release from cuboidal samples from farringtonite with 2.0 M phosphoric and 0.5 M citric acid, 6.0 % MgO and 20.0 % phytic acid, 6.8 % MgO and 22.5 % phytic acid or 7.5 % MgO and 25.0 % phytic acid. All samples were fabricated with a PLR of 2.0 g/mL and stored for 24 d in PBS at 37 °C.

Table 26: Initial and actually released molar Mg-to-P-ratio from cuboidal samples from farringtonite with 2.0 M phosphoric and 0.5 M citric acid, 6.0 % MgO and 20.0 % phytic acid, 6.8 % MgO and 22.5 % phytic acid or 7.5 % MgO and 25.0 % phytic acid. All samples were fabricated with a PLR of 2.0 g/mL and stored for 24 d in PBS at 37 °C.

sample description	Mg:P-ratio	
	initial, theoretical	calculated from release
reference	1.04	0.97±0.33
20.0 % phytic acid & 6.0 % MgO	1.19	0.57±0.14
22.5 % phytic acid & 6.8 % MgO	1.20	0.56±0.08
25.0 % phytic acid & 7.5 % MgO	1.20	0.57±0.10

The results of the cytotoxicity testing are depicted in Figure 49. The cells were not directly seeded on the cement surfaces, but on cell culture plastic (polystyrene, PS) and incubated with cell culture media in which the different cement surfaces have been eluted for 2 d each before medium exchange. The incubation with untreated medium was taken as negative control for cytotoxicity and newberyite (reference) as conventional MPC control. When the eluates were completely given to the cells (100 %, no dilution), cell activities as well as cell numbers were significantly decreased compared to PS. After 4 d of cell culture, the cell activity was decreased by 86 (20.0 % phytic acid) to 92 % (22.5 % phytic acid) depending on the cement composition. However, the cells seemed to recover and showed up to 3-fold higher values after 10 d compared to day 6. Anyway, these activities were at least 79 % less compared to the negative control after the same culture period. In addition the cells showed no activity when they were treated with 100 % eluate derived from reference elution (Figure 49 a). Similar tendencies can be seen concerning the cell numbers with the undiluted eluates. The values were 92 (20.0 % phytic acid) to 98 % (reference) less after 4 d compared to the negative control at the same time point. For phytic acid containing samples, a 3- to 4-fold recovery was possible between day 6 and day 10 so that a final cell concentration of at least 46,000 cells/mL (22.5 % phytic acid) was counted, which nearly conforms to the amount of cells that were seeded on day -1 of cell culture (Figure 49 b). By diluting the eluates in a 1:3

ratio with pure cell culture medium (25 %), this obvious cytotoxic effect could be completely compensated. Partially, even higher values for cell activity could be asserted. After 4 d, activities between 1.9 (20.0 % phytic acid) to 2.8 a.u. (25.0 % phytic acid) resulted which was significantly higher compared to PS as well as the reference. The cell activities constantly increased by time, so that final values between 2.6 (22.5 % phytic acid) to 2.8 a.u. (25.0 % phytic acid) without significant differences towards both of the control groups were reached (Figure 49 a).

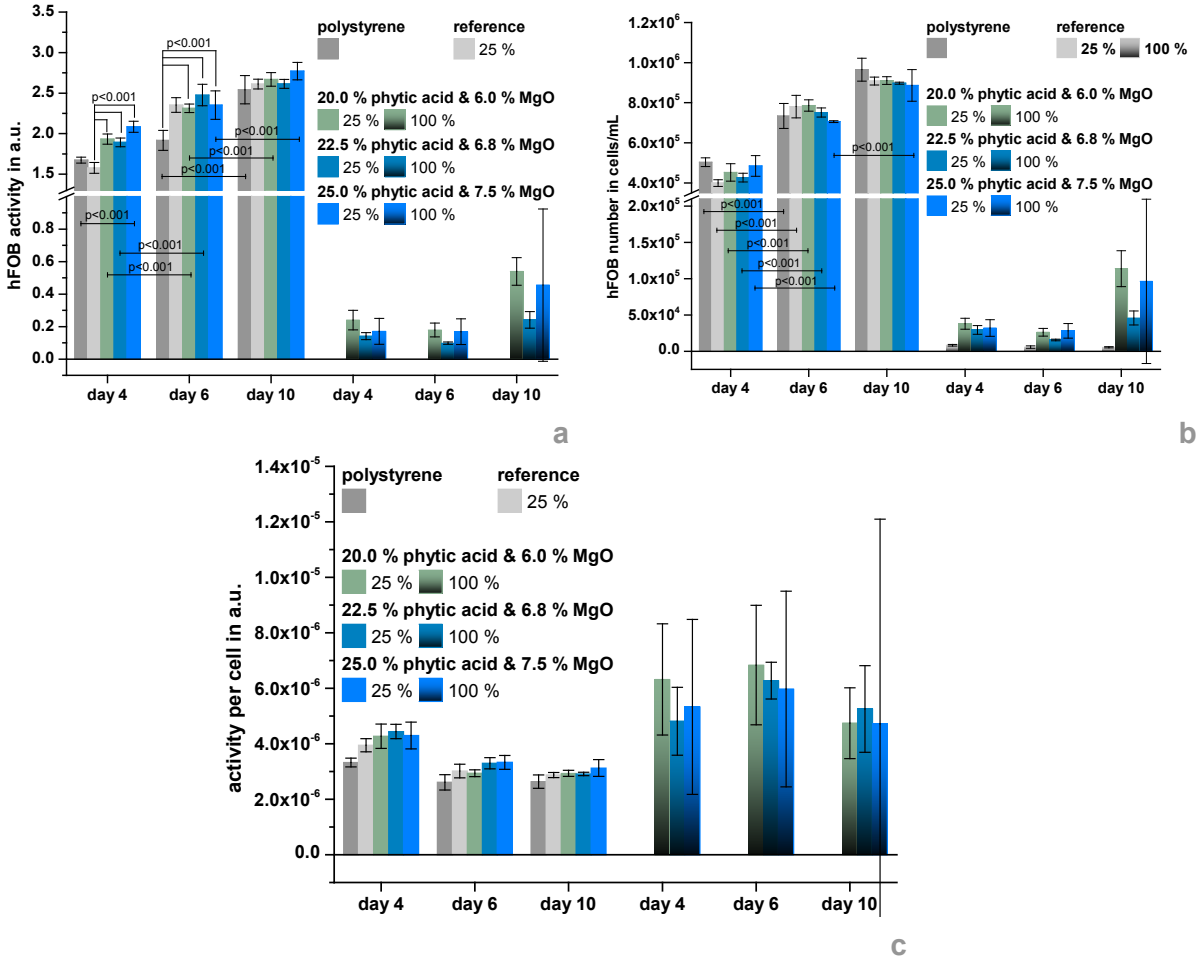

Figure 49: Cell activity (a), number (b) and activity standardized on cell number (c) of human fetal osteoblast cell line hFOB 1.19 that were cultivated with eluates of four different cement systems at 34 °C and 5 % CO_2 for 10 d. PS was taken as a negative control for cytotoxicity. The cements used for elution consisted of farringtonite with 2.0 M phosphoric and 0.5 M citric acid, 6.0 % MgO and 20.0 % phytic acid, 6.8 % MgO and 22.5 % phytic acid or 7.5 % MgO and 25.0 % phytic acid. All cements were fabricated with a PLR of 2.0 g/mL and hardened for 1 h at 37 °C and 100 % humidity.

Concerning cell concentrations with 25 % diluted eluates, the cell numbers constantly increased as well within 10 d of cell culture period but in this case no significant difference towards the control groups was visible. All in all, a maximum cell concentration of about 10^6 cells/mL was reached, which corresponds to a 20-fold growth since seeding of the cells on day -1 (Figure 49 b). Figure 49 c reveals that by normalizing the cell activities on numbers, almost no time or composition dependent effects could be observed and the normalized activities remained quite constant over time.

3.2.2.4 Discussion

The clinical needs for drillable mineral bone cements in general have been vastly discussed in chapter 2.3.2, but there is also a high demand to use MPC for this purpose. In the last years, MPC experienced a shift from their classical application fields (precast construction, road repair, nuclear waste immobilization etc.) [291] towards biomedical applications. The first publication dealing with MPC as a mineral bone cement has already been published in the 1990's [15, 293]. Nevertheless, most of the research has been performed recently [15]. If it would be possible to develop a MPC with drillable characteristics, the formulation would come along with all other advantages that make MPC outstanding compared to conventional HA forming CPC systems including a high initial strength [294], a higher potential to be degraded *in vitro* [218] as well as *in vivo* [209] and the release of Mg^{2+} ions while degradation [218], which exhibit special biological functions such as the increased osteoinductivity of magnesium extracts towards human mesenchymal stem cells [288]. Similar to CPC, conventional MPC undergo a brittle mechanical failure and are thus limited to low- or even non-load-bearing defect sites [15]. There are several approaches to circumvent the brittle mechanical fracture behavior of such cements, as for example *via* fiber reinforcement [103]. The already mentioned commercial cement Norian® Drillable is an example, where fiber reinforcement actually resulted in a cement which is said to be able to sustain tapping and drilling to any time of the setting progress according to manufacturer's instructions [15], but chelation could be a more sophisticated and efficient alternative for MPC as interface compatibilization of fibers and the cementitious matrix is a lasting challenge [103]. Further, fiber reinforcement will not avoid brittle fracture of the cement matrix. The chelating agent that was used in the present study is phytic acid (inositol hexaphosphate, IP6) which is considered as a natural storage for phosphorous and cations in many plant seeds. Because of its six phosphate groups and its high affinity for polyvalent cations, one phytic acid molecule can interact with up to six bivalent cations which could probably bridge leastwise two further phytic acid molecules. The high calcium affinity facilitates the adsorption to hydroxyapatite [611] and the combination of mineral bone cement formulations with phytic acid has already been shown in literature for β-TCP [78] (calcium affinity), alkali substituted calcium orthophosphate [397] (sodium, potassium [612] and calcium affinity) and pure farringtonite (chapter 3.2.1, magnesium affinity) as raw powders. Also, there are some publications with alternative agents (e.g. citric acid [155, 156]), but this is probably the first time that the focus was set on the mechanical output, especial drillability. In a previous work, the efficiency of the phytic acid/farringtonite system was shown in a proof-of-principle manner (chapter 3.2.1) such that the adaption of the existing receipt towards an application-linked direction was the main goal of the present work.

The supplementation of phytic acid into the liquid phase of the cement paste retarded the setting reaction, such that the cement paste would be too soft after 15 min to be taped and drilled without further ado. Here, MgO was added to the solid phase as a reverse-acting, accelerating agent. When the molar ratio of phytic acid to MgO was kept constant at 9.83, the setting accelerator did not detriment the jellylike, sticky texture of the paste which derived from the chelating reaction. Therefore, all three tested cement formulations did fulfill the clini-

[15] Technique guide for the use of Norian® Drillable Inject, DePuy Synthes Biomaterials (2014).

cal requirement to sustain drilling after only 15 min of setting without brittle failure (Figure 42 a) and showed screw-pull-out forces up to ~150 N (Figure 42 b).

It was not possible to directly trace chelate formation in the present cement formulations on the basis of farringtonite, MgO and phytic acid, as differences in vibrational bonds during setting were observable by FTIR (Figure 44). However, combining all other analytical methods, one can presumably reason that the chelation reaction was successful. XRD patterns depicted that no quantitative reaction into newberyite had taken place as only minor amounts of this mineral were found in the setting products depending on the phytic acid content (Figure 45). However, changes in pH (Figure 43 a), temperature (Figure 43 b) and paste viscosity (differences seen during handling) were observed, as well as the formation of a sticky texture that has already been stated before (chapter 3.2.1). However, a solid product with appropriate mechanical performance of approximately 20 MPa for specimens with 22.5 and 25.0 wt.% phytic acid content (Figure 47 a) was formed. SEM micrographs (Figure 46) revealed some crystalline arrangements that were suitably entangled and interlocked promoting the mechanical rigidity of the samples [10]. Lastly, the cements were cohesive under aqueous conditions, as no quantitative disintegration during the prolonged immersion study in PBS was seen. To sum up, a direct detection of the chelation itself was not possible but some of the other analysis methods indicated a successful complexation (as well as little cementitious reaction) and the fabricated cement pastes fulfilled the required criteria towards application as drillable bone cement.

The observed temperature and pH developments during setting can be considered as non-critical for application. For all three phytic acid containing pastes, the temperature courses reached a maximum of about 32 °C which indeed was an increase compared to the surrounding temperature but is still far beyond physiological conditions. In contrast, the reference paste showed much higher maximum temperatures (Figure 43 b) and there are bone cements used in clinics (e.g. PMMA) which have polymerization temperatures of up to 110 °C leading to heat necrosis at the application site [27]. The setting pH of the phytic acid containing cements was non-critical as well (Figure 43 a), as exemplarily brushite forming CPC are currently commercially available for clinical application [40] and initially show even much lower setting pH values [210]. In fact, the phytic acid containing pastes were in an acidic pH range (4.7 to 5.4) (Figure 43 a) but did barely affect the pH of the surrounding PBS solution in which they were immersed (Figure 47 d). For these reasons, it is assumed that the presented cement formulations are able to compete against established cement systems (mineral as well as organic ones or composites) with respect to relevant setting criteria as temperature and pH development.

After an initial mass gain of at least 0.3 wt.%, the phytic acid containing samples lost about 2 wt.% of their initial weight (Figure 47 c). This could be an obvious hint for a possible material degradation, especially, as the cements experienced an increase in porosity by 12 to 14 % (Figure 47 b). In contrast, the reference samples' weight remained constant for about two weeks – contradicting with a possible material degradation – and even further increased afterwards with a total weight gain of 2 % (Figure 47 c). As the material simultaneously registered an increase in porosity (Figure 47 b), it is also probable that a certain degradation process took place anyway leading to an opening and interconnecting of former enclosed pores.

Those could include more water and explain the swelling-like mass change. Macroporosity is an attribute that is oftentimes demanded from a biological point of view. Indeed, a high porosity can impair the mechanical performance of the cement but pores with an appropriate size and interconnectivity can promote bone ingrowth and biodegradability of the cement [21]. In general, MPC have reported porosities starting from only 5 up to 32 % [15]. Therefore, the MPC presented here is – with an initial porosity of already 20 % – located within the upper range of which is possible in the pore-builder-free MPC research.

Table 27: Calculated molar ratio of phytic acid chelating sites to magnesium.

sample description	phytic acid binding sites	Mg from farringtonite	Mg from MgO	molar ratio binding sites to Mg
20.0 % phytic acid & 6.0 % MgO	1.00 mol	11.79 mol	1.64 mol	1:13
22.5 % phytic acid & 6.8 % MgO	1.00 mol	10.41 mol	1.70 mol	1:12
25.0 % phytic acid & 7.5 % MgO	1.00 mol	9.31 mol	1.67 mol	1:11

As mass loss and porosity documented a certain material degradation, it would be interesting to know the underlying degradation mechanism. XRD patterns (Figure 45 a) of the reference cement showed that it mainly consisted of newberyite and some raw powder residues. The degradation mechanism for such biphasic compounds is presumably kinetically controlled by the chemical dissolution of newberyite as this mineral has a higher solubility compared to trimagnesium phosphates. Taylor *et al*. [329] calculated solubility products of $1.5 \cdot 10^{-6}$ for newberyite and $6.3 \cdot 10^{-26}$ for trimagnesium phosphate ($Mg_3(PO_4)_2 \cdot 8H_2O$) at 25 °C [329]. In contrast, the XRD patterns revealed only a minor conversion into newberyite for the phytic acid containing samples (Figure 45 a), for which the main degradation mechanism is probably not based on its solubility but rather on a decreased stability of the complexes between phytic acid and Mg^{2+} ions (= phytates). The inferior solubility of farringtonite compared to newberyite is increased under acidic conditions which is the case in presence of phytic acid. Not only farringtonite, but also MgO as a MPC raw material are known to set within an acid-base-reaction [15] so that free Mg^{2+} ions derive from the raw powder as well as the setting accelerating supplement. If all Mg^{2+} ions would have been released by dissolution of the raw powder in the aqueous environment, there would be an 11 to 13-fold molar excess of Mg compared to possible phytic acid chelating sites (Table 27). Even at a complete occupation of all phytic acid chelating sites, the magnesium-to-phosphate ratio would have been constant and could be compensated by the MgO derived Mg^{2+} which could explain the quantitative occurrence of farringtonite in the XRD pattern after the setting reaction had taken place (Figure 45). Actually, Bieth *et al*. [613] found only minor amounts of 3-fold chelated species at most and at alkaline pH values (0.1 M tetra-n-butyl ammonium bromide at 25 °C) [613]. It is reported that complexes of less-fold chelated phytic acid molecules are very soluble [611]. Also, complexes between phytic acid and Mg^{2+} are said to be less stable as exemplarily compared to Ca^{2+} and that their complexation ability can be affected by alkali-metal cations [613]. The latter were contained in the immersion fluid in form of sodium and potassium ions. Bieth *et al*. [613] further proved that the stability constants for complexes between phytic acid and magnesium (as well as calcium) strongly depend on the presence of potassium in the used medium. Those K^+ ions can compete against Mg^{2+} for the phytic acid chelating sites [613] reducing their complex stability. All those observations found in literature could pre-

sumably provide a possible mechanism of a chemical dissolution of the phytic acid containing MPC system presented here.

Under physiological conditions, the surrounding body fluids have a more complex composition compared to the simple *in vitro* medium PBS and K^+ plays an important role inside of cells [613]. This will alter the purely chemical degradation behavior further. Enzymatic depletion of phytates seems only being related to the intestinal mucosa and bacteria [611], such that this mechanism is not relevant for the presented MPC as bone substitute. However, another active degradation process has to be considered *in vivo*. Bone resorbing osteoclasts locally decrease the pH value of the underlying bone tissue [218], which might further decreases the stability of the phytates as well as increases the solubility of the inorganic component of the cement.

Concerning the compressive strength, the reference cement experienced a continuous increase from 7.4 to 18.1 MPa within 24 d (Figure 47 a). Presumably, this effect is due to a crystal growth and progressing entanglement and advancing conversion from the raw powder into newberyite. Despite of newberyite degradation and progressing conversion that occur simultaneously while immersion for 24 d in PBS, the effect of crystal entanglement seems to predominate the effect of porosity decrease, because a weakening of the mechanical performance was not observed. In contrast, the MgO and phytic acid containing samples reached their maximum compressive strength of 16 to 21 MPa already after two days of post-hardening under aqueous conditions and remained constant over the whole period. Only in the case of a minimum phytic acid content, deterioration by about 41 % was registered. Such a decrease could again be a hint of material degradation and fits well with the results of mass loss and porosity measurements. For the residual phytic acid containing samples, these results imply a quite stable mechanical behavior in spite of mass loss and porosity increase. Comparing the compressive strengths of the phytic acid containing MPC to common literature, a broad range within two orders of magnitude can be seen depending on different parameters as reactant composition or PLR [15]. Kanter *et al*. [210] exemplarily reached a compressive strength of 65.5 MPa for a MPC based on farringtonite and ammonium phosphate solution at a releatively high PLR of 3.0 g/mL [15, 215] but there were also some MPC presented with quite worse mechanical properties of only 6.6 MPa. In the latter case, a low PLR and a 67 % amount of already reacted MgP was chosen with – apart from that – similar composition [313]. Therefore, the as-presented phytic acid containing formulation has – with around 20 MPa – an adequate mechanical performance especially when considering the brittleness of conventional ceramics. As the application of drillable mineral bone cements is indicated with poor bone quality [531] and the natural cancellous bone exhibits compressive strengths between 0.4 to 4 MPa [578], there is no issue with the compressive strength. Further, a stability of mechanical performance for at least 24 d was revealed (Figure 47).

A release of ions into the surrounding aqueous environment is linked to the degradation of the materials. In this special case, the release of Mg^{2+} and PO_4^{3-} was analyzed *via* inductively coupled plasma mass spectrometry. A constant release of phosphate ions from the beginning on was verified according to Figure 48 b. Numerous publications that deal with MPC, magnesium substituted CPC or MgP ceramics do not report ion release of PO_4^{3-} [614] or only show the overall release but not the release kinetics [303]. According to Meininger *et al*. [362]

post-hardening of sintered (strontium doped) farringtonite ceramics in an ammonium phosphate solution resulted in a burst release behavior depending on the degree of Sr^{2+}-doping [362]. In contrast, a constant release of PO_4^{3-} was stated by Sheikh *et al*. [397] who dealed with a similar concept of chelation between phytic acid and alkali substituted CaP. The constant release could be observed for comparable phytic acid concentrations between 20 and 30 % and showed an initial burst at higher amounts [397]. The PO_4^{3-} ion release behavior that was shown here (Figure 48 b) thus fits well with the results of Sheikh *et al*. [397]. As already mentioned above, the mechanism which presumably underlines the progressing material degradation is mainly based on a stability decrease of phytates with farringtonite and MgO derived Mg^{2+} ions. Consequently the main quantity of measured phosphorous probably originates from released phytic acid molecules and rather less from farringtonite. Concerning the Mg^{2+} release, release profiles within the same order of magnitude were observed (Figure 48 a-b). This was not the case for the above mentioned example as an approximately 10-fold amount of phosphorous compared to magnesium was measured [362]. The lack of a distinct initial burst of PO_4^{3-} ions and their comparably low amount could be beneficial for cytocompatible effects of the material (see section below). Concerning the molar Mg-to-P-ratio before and after immersion, obviously proportionally more PO_4^{3-} ions were released as originally contained in the cements (Table 26). This could be a further hint for the instability of the phytates under simple aqueous conditions with competing alkali cations which could predominate the solubility of farringtonite.

Some of the analyzed material characteristics can directly affect the biological response of the body. It has already been argued that temperature and pH of the presented phytic acid containing cement systems during setting (Figure 43) are non-critical for application as bone substitutes, as both parameters approximated physiological conditions and also the immersion fluid was only marginally affected concerning the pH value (Figure 47 d). Some of the performed experiments (mass loss, Figure 47 c; porosity gain, Figure 47 b; ion release, Figure 48) additionally indicated that the novel drillable MPC could be degradable *in vivo* which conforms well to current clinical demands: it is favored to have bone substitutes that are replaced by functioning native bone within an appropriate time range [218]. Simultaneously, porosity is a key factor which provides bone ingrowth and improved biodegradability in case of adequate pore size and interconnectivity [21]. Here, the porosity of the systems was not analyzed in detail but they showed an appropriate porosity compared to other MPC systems already at the beginning (Figure 47 d). The ion release of such cements is particularly interesting for the biological outcome: It is known that a high amount of PO_4^{3-} ions can impair cytocompatibility [615]. According to Meleti *et al*. [615] inorganic phosphates may induce apoptosis in osteoblast-like cells. They found that only dosages underneath 5 mmol/L, which correspond to a phosphorous dosis of approximately 160 mg/L, did not impair cell viability for at least 48 h. After this time, viability of the cells was still 75 % whereat it was solely 40 % after a longer incubation time of 96 h [615]. Figure 48 b revealed a phosphorous occurrence of approximately 120 mg/L also within 2 d that is below this threshold value. Of course, the different cell types (cell line v. primary cells) and concentrations (230 v. 140 cells/mm^2) have to be taken into account as well. However, it is assumed that the actual amount of released PO_4^{3-} ions was about four times as high which is one more order of magnitude. The cytotoxic effect of high PO_4^{3-} amounts was visible in reduced cell viability: the activity was lowered by

92 % at most and similar results were obtained with respect to cell number after 4 d (Figure 49). This observation fits well to the results of Meleti *et al*. [615] who revealed a nearly 100 % cell decease for higher PO_4^{3-} dosages (7 mmol/L) after the same time period [615]. As expected, the cytotoxic effect was completely insubstantial when the cells were incubated with a 4-times diluted eluate (Figure 49) and this dilution effect is also probable under dynamic *in vivo* conditions. In contrast, the release of Mg^{2+} ions can have utile impact on bone biology as they can promote osteogenic proliferation as well as differentiation [288]. In a co-culture study, Wu *et al*. [288] revealed that simultaneously, too high amounts of magnesium (from 14 mmol/L on) might impair osteoclastogenesis. This concentration corresponds to 350 mg/L every second day, which is also far above the values that were measured here for phytic acid containing MPC.

3.2.2.5 Conclusions

The above described study depicted the basic properties of a drillable MPC as its temperature and pH development during setting, its phase composition, morphology, compressive strength, mass loss, porosity change and ion release in a prolonged immersion study in PBS for 24 d at 37 °C as well as its cytocompatibility towards the human fetal osteoblast cell line hFOB 1.19. The presented cement system showed promising *in vitro* properties, but further experiments could exemplarily include the optimization of handling characteristics. The cements presented here could all sustain tapping and drilling 15 min after fabrication, which was considered as clinical demand. The drillability was reached by focusing on chelation as main setting mechanism. Of course, this key property has to be analyzed in more detail exemplarily in a dynamically loaded bone model but the first steps to prove the cements' suitability for screw augmentation have successfully been executed.

3.2.3 A mineral cement for the application as bone and metal adhesive agent

The following section 3.2.3 is likely to be used in a publication manuscript, which is however not submitted or published by the time of the submission of this thesis.

3.2.3.1 Abstract

Mineral bone cements were actually not developed for their application as bone bonding agents, but as bone void fillers. Especially CPC are considered being unsuitable for that application particularly under moist conditions. Here, both the *ex vivo* and *in vitro* ability of special MPC formulations to adhere on bovine cortical bone as well as sandblasted stainless steel with a slight surface roughness of R_a=0.77±0.33 µm were shown. Combining farringtonite ($Mg_3(PO_4)_2$) with 25 % phytic acid ($C_6H_{18}O_{24}P_6$) in a PLR of 2.0 g/mL resulted in shear-off strengths of 0.81±0.12 MPa on bone and 1.71±0.32 MPa on rough steel even after 7 d under aqueous conditions at 37 °C. The presented material demonstrated appropriate bonding characteristics which could enable a broadening of the mineral bone cements' application field.

3.2.3.2 Introduction

MPC are biodegradable but brittle materials. In addition to precipitation, chelation was shown to be a possible reaction route for MPC, where diluted phytic acid formed complexes with Mg^{2+} ions released from farringtonite and simultaneously enabled newberyite formation. In a proof-of-principle study, combinations of farringtonite ($Mg_3(PO_4)_2$) and 10 to 30 % phytic acid ($C_6H_{18}O_{24}P_6$) with a high PLR of 3.0 g/mL were shown to be a combinatory system of cement setting and chelation with adequate mechanical properties (~65 MPa compressive strength). However, phytic acid extended the cement setting and exhibited high cement viscosities which might be detrimental for clinical application (chapter 3.2.1).

Adapting the cement composition for a better compliance with clinical requirements (narrowed phytic acid concentration range of 20 to 25 %, lower PLR of 2.0 g/mL and the addition of reactive magnesia (MgO) to compensate the setting retarding effect of phytic acid), a drillable cement system with screw-pull-out forces of up to 148 MPa was created. Besides drillability, this cement formulation showed a multitude of other positive characteristics for biomedical applications, including a stable compressive strength of ~20 MPa, the potential to be degraded (mass loss of 2 wt.%, porosity increase to up to 36 %) and a release of leastwise 0.17 mg/g per day of osteogenic Mg^{2+} within a time span of 24 d in PBS. Further, the cement set under biologically non-critical conditions with respect to pH (slightly acidic) and temperature (30-32 °C) and corresponding eluates were cytocompatibel towards human fetal osteoblast cell line hFOB 1.19 when suitably diluted (chapter 3.2.2).

These formulations not only showed jellylike haptics directly after initiation of the setting reaction but it was further observed that they were very sticky on glass slabs as well as metal spatula. That is why the idea came up to analyze those cement formulations towards application as bone adhesive or adhesive layer between bone and metal implants. In chapter 2.3.2,

it has already been revealed that mineral bone cements originally were not developed for application as bone adhesives and that especially CPC were shown to have inappropriate bonding properties. Thus, in the present study, the MPC formulation analyzed within chapter 3.2.2 was chosen, whereat farringtonite ($Mg_3(PO_4)_2$) reacted with phytic acid ($C_6H_{18}O_{24}P_6$) *via* chelation mechanism to form a stable complexed MgP. It is assumed that the phytic acid will be the reason for the cement formulation to show a higher bone affinity compared to conventional mineral bone cements, as phytic acid is able to form insoluble complexes with calcium [611, 616] and magnesium cations [566], which appear in the raw powder (magnesium) as well as in the used bone slices [617]. Thus, its adhesiveness was analyzed *ex vivo* on cortical bovine bone and *in vitro* on titanium as well as stainless steel surfaces *via* a shear-off test setup and additionnally *via* energy dispersive X-ray spectroscopy (EDS) and SEM. A newberyite ($MgHPO_4 \cdot 3H_2O$) forming cement from farringtonite and phosphoric acid was chosen as control. As already shown in chapter 3.2.2, this formulation sets under acidic conditions which is evenly the case for phytic acid containing MPC. Thus, it is not clear, if an adequate bone bonding would derive from etching of the bone surface by the acid or the complexation of the chelate forming component with bone deriving calcium and magnesium ions. Therefore, a neutrally setting struvite ($MgNH_4PO_4 \cdot 6H_2O$) forming control was introduced as an additional reference.

3.2.3.3 Results

Before testing the bonding properties of the different materials, their intrinsic strength at corresponding time points was determined *via* a compressive strength test setup (Figure 50 a). Obviously, the phytic acid containing samples had an initially higher and a significant higher compressive strength after 24 h and 7 d compared to the acidic reference (newberyite). Only those samples with the highest phytic acid amount had a quite low initial strength of 2.29±1.76 MPa, which was comparable to the newberyite forming reference strength (2.21±1.76 MPa). In the course of 7 d, the reference compressive strength increased by 305 % to 8.95±1.84 MPa, while the phytic acid containing samples experienced a significant increase of their compressive strength by up to 9.1-fold to 17.4±3.5 (20.0 % phytic acid) and 20.9±3.2 MPa (25.0 % phytic acid) already within the first 24 h. In contrast, the neutral control group (struvite) reached a quite high initial strength of approximately 23 MPa which further increased to approximately 27 MPa within 7 d in an aqueous environment (Figure 50 a).

Corresponding XRD-patterns (Figure 50 b-c) showed no obvious phase transformation independently from the storage time in PBS when differently concentrated phytic acid was added to the raw powder. As anticipated, combining farringtonite with phosphoric acid resulted in the formation of newberyite ($MgHPO_4 \cdot 3H_2O$) and with ammonium phosphate containing solution in the formation of struvite ($NH_4MgPO_4 \cdot 6H_2O$) without clear temporal dependency. Small diffraction reflexes at 22.4, 28.2, 33.4 and 36.3 °, respectively, can be ascribed to a sodium contaminated MgP phase ($NaMg_4(PO_4)_3$) of the raw powder (Figure 50 b-c).

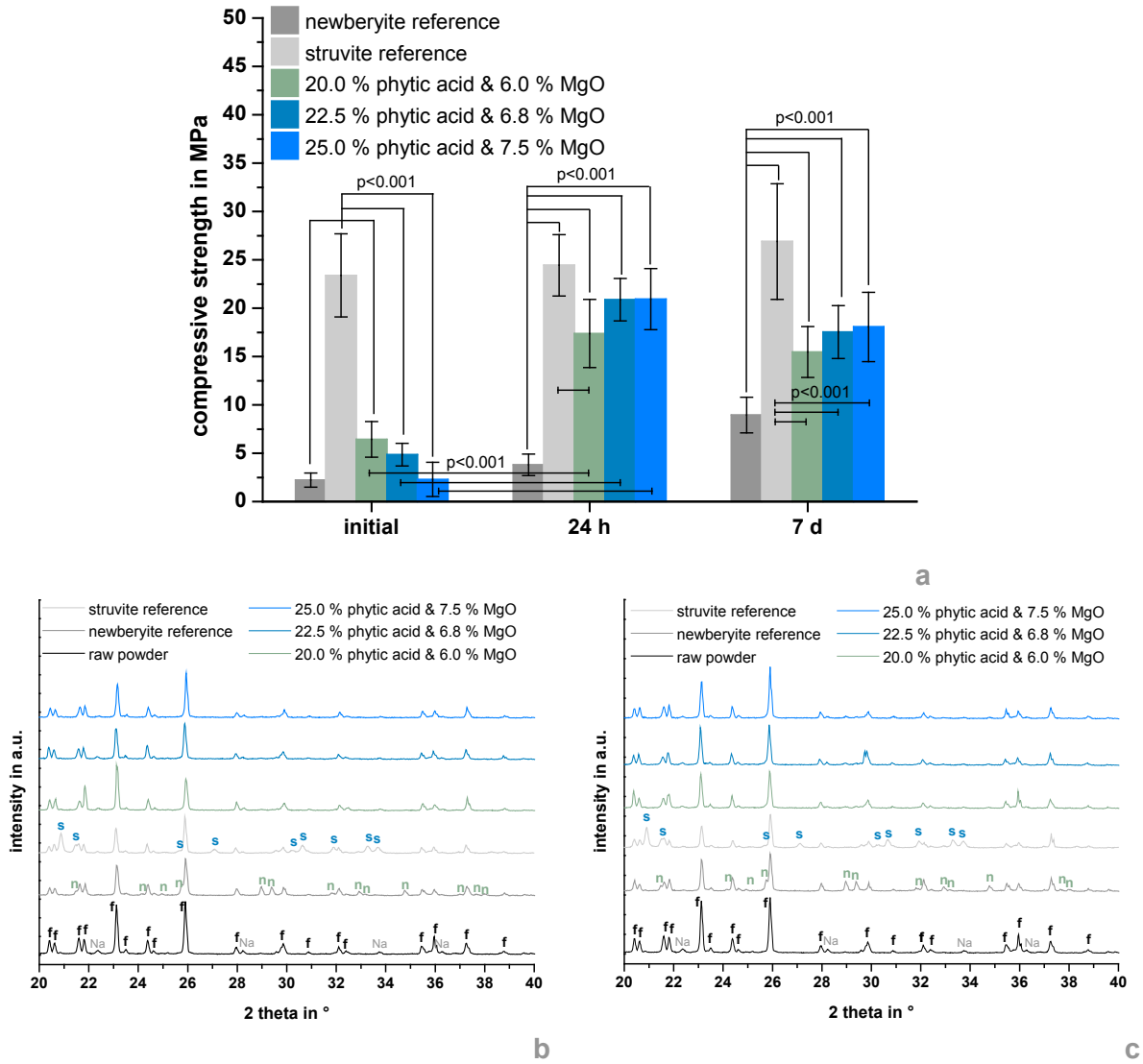

Figure 50: Compressive strength of cement cuboids from farringtonite with 2.0 M phosphoric acid (newberyite reference), farringtonite with 15 % MgO (dead-burnt) and 2.5 M DAHP and 1.5 M ADHP solution (struvite reference), farringtonite with 20.0 % phytic acid and 6.0 % MgO (active), 22.5 % phytic acid and 6.8 % MgO (active) or 25.0 % phytic acid and 7.5 % MgO (active) initially or after 24 h or 7 d hardening in PBS at 37 °C (a) and corresponding XRD patterns initially (b) and after 7 d (c) hardening. All samples were prepared in a PLR of 2.0 g/mL. Characteristic reflexes are marked with f (farringtonite), n (newberyite), s (struvite) or Na (sodium magnesium phosphate).

Before the different surfaces were agglutinated with the five chosen cement formulations, they were characterized with respect to their surface roughness (Table 28). In the case of stainless steel slices, all four surface roughness parameters increased with increase in grain size of the grit between R_a=0.11±0.02 µm / R_q=0.18±0.03 / R_y=2.63 µm / R_z=1.56±0.21 and R_a=2.67±0.12 µm / R_q=3.34±0.17/ R_y=22.11 µm / R_z=12.21±1.36. Sandblasting of titanium slices with 110 µm corundum (Korox 110) resulted in surface roughnesses in the range between stainless steel sandblasted with 110 µm and 250 µm corundum (Korox 250). Bovine bone slices had the highest roughness values in vertical direction (e.g. R_a=3.55±0.66 µm) and were comparable with sandblasted stainless steel slices (110 µm) in parallel direction relative to the scrub marks.

Table 28: Roughness values (arithmetic average of absolute values R_a, root mean squared R_q, maximum height of the profile R_y, average distance between the highest peak and the lowest valley in each sampling length R_z) of the different surfaces used for bone adhesives. ♦ means the direction referring towards grind direction.

surface	used grit	R_a in µm	R_q in µm	R_y in µm	R_z in µm
bone - parallel♦	P80	1.15±0.25	1.48±0.29	13.77	7.59±1.13
bone - orthogonal♦	P80	3.55±0.66	4.41±0.83	33.36	20.49±3.87
stainless steel	/	0.11±0.02	0.18±0.03	2.63	1.56±0.21
	Korox 50	0.77±0.03	0.96±0.02	6.97	5.34±0.26
	Korox 110	1.39±0.06	1.74±0.08	11.83	8.94±0.57
	Korox 250	2.67±0.12	3.34±0.17	22.11	12.21±1.36
titanium	Korox 110	1.81±0.14	2.27±0.18	16.38	11.74±1.19

Figure 51 reveals the corresponding adhesive strengths of various cement formulations on bovine bone and the differently structured metal slices. The white dotted line marks a strength of 0.2 MPa which was determined 1984 by Weber and Chapman [618] to be a threshold value for bone bonding agents. Adherings with a lower strength would not be feasible during surgery [618].

Initially, all samples showed an appropriate adhesiveness on bone between 0.75±0.20 (newberyite control, Figure 51 a) to 1.35±0.68 MPa (struvite control, Figure 51 b). Samples with the lowest phytic acid content represented an exception, as their adhesiveness laid underneath the as-mentioned threshold value (Figure 51 c). Similar tendencies could be seen using rough stainless steel (Korox 50), where initially all formulations showed proper shear strengths between 1.17±0.26 (22.5 % phytic acid, Figure 51 d) to 1.81±0.66 MPa (newberyite control, Figure 51 a) without exception. In contrast, on smooth steel, only the newberyite control showed an appropriate value of 1.50±0.26 MPa, which decreased by immersion in PBS by 70 % (Figure 51 a). The decrease of adhesion while depositing the samples in an aqueous environment was seen on bone as well. Here, only the composition with 25.0 % phytic acid had still an appropriate adhesiveness of 0.81±0.12 MPa after 7 d (Figure 51 e). Interestingly, with a shear strength of 0.79±0.41 MPa, this was also the case for the struvite control after 7 d, even though no adequate strength was observed after 24 h in PBS (Figure 51 b). Using stainless steel surfaces sandblasted with a larger grit than Korox 50, only the struvite control group (Korox 110 & 250, Figure 51 b) as well as the cement formulation with highest phytic acid content of 25.0 % (Korox 110 Figure 51 e) proved proper long-term stability with shear-off strengths between 1.00±0.67 (25.0 % phytic acid, Korox 110) and 1.59±0.62 MPa (struvite, Korox 250) after 7 d. Korox 110 treated titanium interestingly revealed adequate bonding abilities from both control groups and the 25.0 % phytic acid containing formulation at every time point (Figure 51 a-b, e), whereat the worst was observed by the newberyite control with 0.38±0.11 MPa after 24 h and the best by phytic acid containing cement with 1.71±0.61 MPa initially.

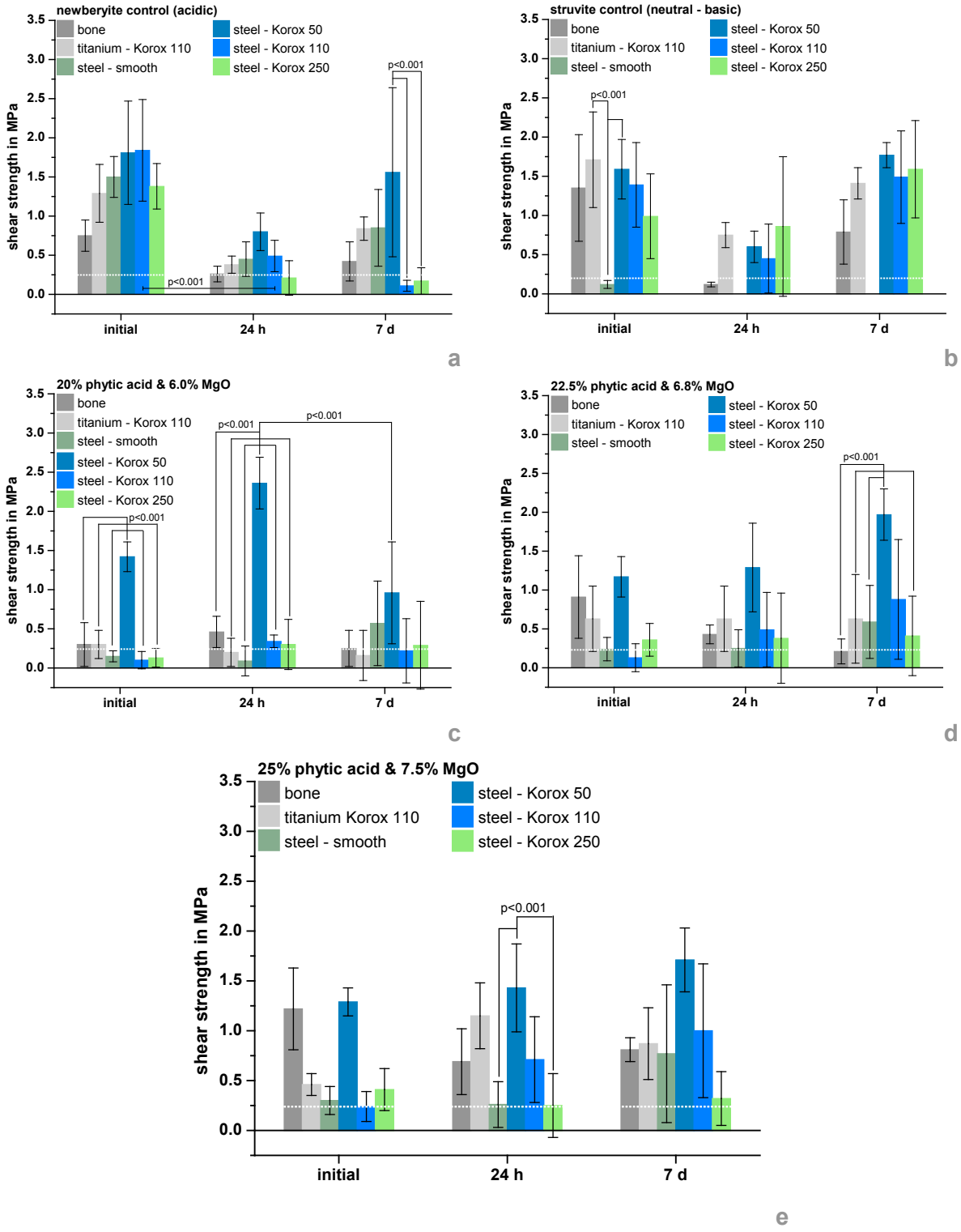

Figure 51: Shear strength of cement adhesives from farringtonite with 2.0 M phosphoric acid (newberyite reference) (a), farringtonite with 15 % MgO (dead-burnt) and 2.5 M DAHP and 1.5 M ADHP solution (struvite reference) (b), farringtonite with 20.0 % phytic acid and 6.0 % MgO (active) (c), 22.5 % phytic acid and 6.8 % MgO (active) (d) or 25.0 % phytic acid and 7.5 % MgO (active) (e) initially or after 24 h or 7 d hardening in PBS at 37 °C on different surfaces. Ground bovine bone slices, smooth stainless steel slices and sandblasted stainless steel as well as titanium slices were chosen as subjacent surfaces. All cements were prepared in a PLR of 2.0 g/mL. The white dotted line marks the threshold value (0.2 MPa) for adhesive materials on bone.

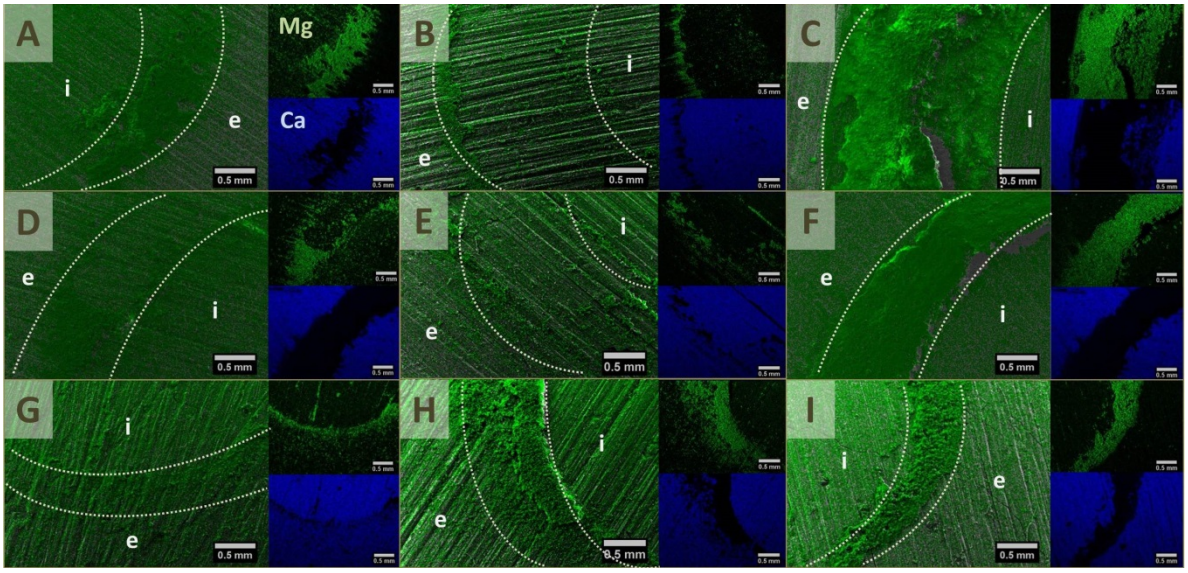

Figure 52: EDS element maps of cement adhesives from farringtonite with 2.0 M phosphoric acid (newberyite reference) (a, d, g), farringtonite with 15 % MgO (dead-burnt) and 2.5 M DAHP and 1.5 M ADHP solution (struvite reference) (b, e, h), and farringtonite with 25.0 % phytic acid and 7.5 % MgO (active) (c, f, i) initially (a-c) or after 24 h (d-f) or 7 d (g-i) hardening in PBS at 37 °C on bovine bone slices. All cements were prepared in a PLR of 2.0 g/mL. Large pictures show an overlay of magnesium dispersion with corresponding scanning electron micrographs and small pictures show the magnesium and calcium map dispersion solely. The interior (i) as well as the exterior (e) of the adhesive surfaces are shown whereat the white dotted lines mark the border area.

Possible adhesive residues on bone were verified *via* EDS measurements and exemplarily shown for both references as well as the 25.0 % phytic acid containing cement formulation (Figure 52). For the newberyite forming reference, initially more magnesium was visible on the adhesive surfaces compared to untreated bone. Also, whole cement fragments were found in this area. This attribution is obvious as no calcium was found at this site (Figure 52 a). In the course of time, the magnesium content on the adhesive surfaces approximated the appearance of untreated bone but some magnesium accumulations were visible inside the scrub marks which derived from bone slice preparation (Figure 52 d, g). A quantitative analysis documented this assumption as the initial Ca-to-Mg-ratio on bone and former adhesive surface exhibited a difference of 89 % and decreased by time (Table 29). For the 25.0 % phytic acid containing adhesives on bone, the overall magnesium content on the adhesive surfaces seemed to be comparable to the content of untreated bone at any time point but some magnesium accumulations were still visible inside the scrub marks (Figure 52 c, f, i). Additionally, the quantitative Ca-to-Mg-ratio was ever greater on pure bone compared to former adhesive surfaces (Table 29). This was similar for all phytic acid containing formulations (other data not shown). The struvite forming reference showed a behavior which laid in between both the newberyite control and the phytic acid containing formulations: No obvious differences between native bone and ancient adhesive residues were visible initially and after 7 d, whereas large portions of magnesium were apparent inside the scrub marks after 24 h (Figure 52 b, e, h). A semi-quantitative evaluation of the corresponding EDS element maps revealed the highest difference of 65 % in Ca-to-Mg-ratio which was at least 25 % greater compared to initial and 7 d ratios (Table 29).

Table 29: Ca-to-Mg-ratio on bone and adhesive surface of the different bone adhesive samples. Concentrations of Ca and Mg were calculated on the basis of corresponding EDS element maps. The ratios of one row derive each from the same EDS element map (Figure 52). The difference between adhesive and bone is negative in case of decrease and positive in case of increase in Ca-to-Mg-ratio in comparison to native bone.

		Ca-to-Mg-ratio (wt.%/wt.%)		difference between
sample description	**time**	**bone**	**adhesive**	**adhesive and native bone**
newberyite control	initial	28±6	3.0±0.2	- 89±29 %
	24 h	9.6±1.3	2.7±0.2	- 72±17 %
	7 d	4.9±0.3	5.6±0.5	+ 14±12 %
struvite control	initial	31±8.8	25±5.8	- 19±34 %
	24 h	28±5.3	9.7±1.3	- 65±23 %
	7 d	7.1±0.6	4.9±0.4	- 39±10 %
20.0 % phytic acid & 6.0 % MgO	initial	55±17	4.9±0.5	- 91±42 %
	24 h	7.4±0.7	4.7±0.2	- 36±10 %
	7 d	14±2	8.8±0.7	- 37±16 %
22.5 % phytic acid & 6.8 % MgO	initial	37±10	6.2±0.5	- 83±35 %
	24 h	17±2	8.8±0.9	- 48±14 %
	7 d	14±2	8.3±0.6	- 41±16 %
25.0 % phytic acid & 7.5 % MgO	initial	∞	7.3±0.8	n.a.
	24 h	9.5±1.1	3.9±0.3	- 60±14 %
	7 d	15±2	9.9±0.8	- 34±15 %

Additionally, the surface of native bone (Figure 53) and ancient adhesive (Figure 54) was analyzed *via* SEM. At a small magnification, spherical (A-B) and elongated (A, C) cellular structures of a µm-range were visible on untreated bone. Some of the spherical cells seemed to be very active in mitosis (B), some of them exhibited distinctive cytoplasmic pseudopods (A). At higher magnifications of 75,000, the nanocrystalline structure of biological apatite was visible (D), but the single crystals were too small to be resolved at a higher quality.

Figure 54 shows the influence of various adherents on the bone structure. Concerning the nanostructure, no obvious differences were observed in comparison to the untreated bone surface independently from the used cement formulation (Figure 54, A-E). Organic structures, as they were visible on untreated bone, could not be found on both acidic newberyite as well as neutral struvite control. In contrast, spherical cellular structures (partially with cytoplasmic pseudopods) in a µm-range were visible on bone surfaces with all phytic acid containing formulations (Figure 54, b-d). Additionally, larger spherical granules with a broad particle size distribution (approximately 2 to 10 µm) could be found in the cases of 20.0 (b) and 22.5 % phytic acid (not shown). Those seemed to be of non-living nature because of the perfectly smooth surface. Similar structures have already been found analyzing the crystal morphology of the pure 20.0 % phytic acid containing cement formulation after a longer immersion in PBS for 12 d (Figure 46, chapter 3.2.2.3) and can thus be regarded as bone adhesive residues.

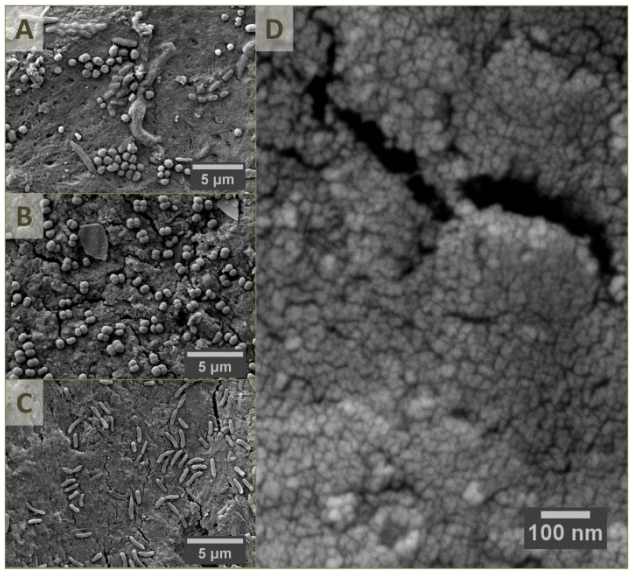

Figure 53: SEM micrographs of bovine bone surfaces at a magnification of 5,000 (A-C) to reveal cell colonization and 75,000 (D) to reveal the characteristics of a normal nanocrystalline mineral bone matrix.

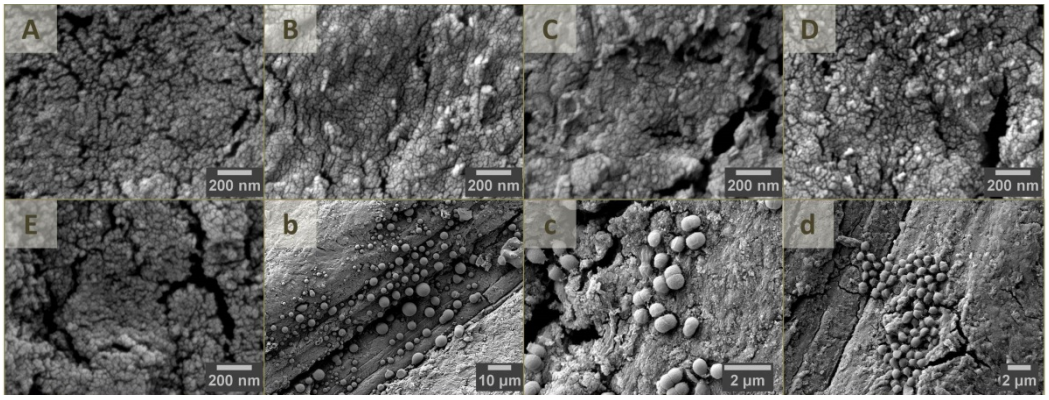

Figure 54: SEM micrographs of bovine bone surfaces after having performed shear-strength tests of different bone adhesives after 24 h storage in PBS at 37 °C. The adhesive formulations consisted of farringtonite with 2.0 M phosphoric acid (newberyite reference) (A), farringtonite with 15 % MgO (dead-burnt) and 2.5 M DAHP and 1.5 M ADHP solution (struvite reference) (E), farringtonite with 20.0 % phytic acid and 6.0 % MgO (active) (B, b), 22.5 % phytic acid and 6.8 % MgO (active) (C, c) or 25.0 % phytic acid and 7.5 % MgO (active) (D, d). Magnifications of 75,000 (A-E) or 1,000 (b), 10,000 (c) and 5,000 (d) were used to analyze alterations to the nanocrystalline mineral bone matrix or alterations to possible cell colonization and cement residue anomalies.

The shear-off tests revealed that only the cement formulation with a phytic acid concentration of 25.0 % was able to sustain shearing forces on bone even after 24 h and 7 d under moist conditions (Figure 51 e). Thus, it was tested *in vitro* to bond “real” bone fragments using the example of a sawn porcine jawbone. Approximately 1 h after having attended to the bone fragments, the jawbone could be hung onto the smaller fragment without any indication of failure (Figure 55).

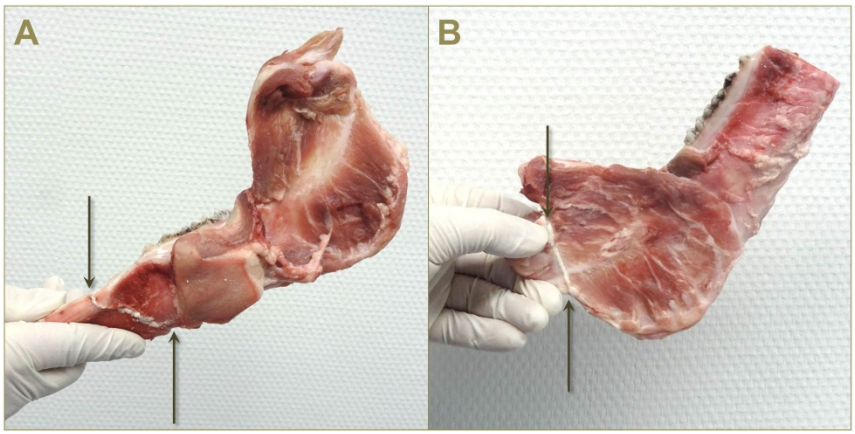

Figure 55: Visualization of adhesive sealing between two sawn porcine jawbone fragments *via* a cement formulation on the basis of farringtonite with 7.5 % MgO, 25.0 % phytic acid and a PLR of 2.0 g/mL. The arrows each indicate the beginning and ending of the sealing interface.

3.2.3.4 Discussion

In the present study, diluted phytic acid was used as the liquid component of a MPC system to improve its adhesiveness on bone. The naturally deriving phytic acid is known to insolubly bind polyvalent cations such as Ca^{2+} [611, 616] and Mg^{2+} [616], which are both constituents of bone [617]. Additionally, the raw powder farringtonite ($Mg_3(PO_4)_2$) contained magnesium as well. For this reason it was assumed that a strong bonding between the cement and the bone surface would be generated.

Farrar [1] recapped the most crucial demands for bone adhesives which comprises an adequate setting time. This is obvious from a clinical perspective, as the surgeon has to have enough time to unify the bone fragments. Afterwards, the adhesive must harden quickly [1]. This setting time is also relevant for the as-shown *in vitro* study, as the presented system does not work with an external setting initiator (e.g. UV light) that would provide a “setting on demand” system. To control the setting time of the presented MPC system, MgO was supplemented as a component counteracting the setting retarding effect that has been observed for phytic acid in combination with mineral bone cements before (chapter 3.2.1). The addition of 6.0, 6.8 or 7.5 wt.% MgO in combination with 20.0, 22.5 and 25.0 % phytic acid were used to facilitate the demolding of adhesive-surface constructs already after 10 min.

According to Farrar [1] it is also important that a certain mechanical stability of the cement itself is ensured [1]. Here the intrinsic material strength under compression (Figure 50 a) was determined. As seen, the newberyite control experienced a gradual increase in compressive strength to approximately 9 MPa at a maximum (Figure 50 a). It is assumed that the immersion in an aqueous environment can promote post-curing of the crystal water containing mineral which explains the increase in mechanical performance probably due to an incremental crystal entanglement [10]. Concerning the phytic acid containing formulations, a maximum mechanical performance of ~17 (20.0 %) to ~21 MPa (25.0 %) was already reached after 24 h under aqueous conditions. Furthermore, an increase in phytic acid amount seemed to impair the mechanical performance initially but behaved *vice versa* during deposition in an aqueous environment. However, post-curing in water did not lead to a distinct conversion from farringtonite into newberyite as shown by corresponding XRD patterns (Figure 50 b-c), but the differences in mechanical performance compared to the dry storage (initial values)

were significant (Figure 50 a). All in all, the best intrinsic mechanical performance of the phytic acid containing cement formulations was observed for samples with the highest phytic acid amount after 24 h (Figure 50 a). Only the struvite forming reference showed superior values (Figure 50 a), but such formulations are typically known for their high initial strength [294]. Basically, all formulations exhibited an adequate intrinsic strength under compression which was initially in the range and after longer immersion superior to the compressive strength of human cancellous bone [578]. Klammert *et al*. [81] obtained similar values for the reaction of farringtonite with the acidic reactant monocalcium phosphate [81].

The preparation of different surfaces was performed as follows: The metal slices were either used as received ("smooth") or sandblasted with corundum and then agglutinated in the dry state. In contrast, the bone slices were sawn, ground smooth and pasted in the moist state. Because of this preparation method, the bone topography was anisotropic with unidirectional scrub marks. Regarding the surface roughness, the following sequence could be asserted with respect to all roughness parameters R_a, R_q, R_y and R_z (Table 28):

stainless steel, smooth < stainless steel, Korox 50 < bone, parallel< stainless steel, Korox 110 < titanium, Korox 110 < stainless steel, Korox 250 < bone, orthogonal

Table 30: Qualitative evaluation of the results depicted in Figure 51 showing the shear strength of cement adhesives newberyite, struvite or farringtonite with 20.0 (6.0 % MgO), 22.5 (6.8 % MgO) or 25.0 % (7.5 % MgO) phytic acid initially or after 24 h or 7 d hardening in PBS at 37 °C on different surfaces.

	initial shear strength	**prolonged immersion**	**best overall result**	**suitable on bone?**
newberyite control	proper on all surfaces with best on steel (Korox 50 & 110) & worst on bone	proper on titanium & steel (smooth & Korox 50)	steel (Korox 50)	no
struvite control	proper on all surfaces with best on titanium & worst on steel (Korox 250)	proper on titanium & steel (smooth & Korox 50)	titanium & steel (Korox 50)	no
20.0 % phytic acid (6.0 % MgO)	proper on steel (Korox 50)	proper on steel (Korox 50)	steel (Korox 50)	no
22.5 % phytic acid (6.8 % MgO)	proper on steel (Korox 50)	proper on steel (Korox 50)	steel (Korox 50)	no
25.0 % phytic acid (7.5 % MgO)	proper on bone, titanium and steel (Korox 50) with best on bone & steel	proper on bone, titanium and steel (Korox 50)	steel (Korox 50)	yes

Concerning strength of adhesiveness as well as stability in an aqueous environment, it is obvious that among all cements with phytic acid, only cements with a content of 25.0 % seemed to be a suitable adhesive for bone as well as ground titanium (Korox 110) and stainless steel (Korox 50). A similar outcome was visible for the acidic as well as the neutral control group, but adequate bonding on bone could not be realized using these classic cement

formulations. Using 25.0 % phytic acid solution as liquid phase of the cement paste even resulted in a shear strength which was four times higher as compared to the threshold value of 0.2 MPa proposed by Weber and Chapman [618] even after 7 d of deposition in an aqueous environment (Figure 51). An overall qualitative evaluation of the mechanical results is given by Table 30.

The strong difference in adhesive strength between smooth and sandblasted metal slices (Figure 51) reveals that a certain surface roughness is indispensable for adequate adhesion to surgical alloys. Some research indicates that slightly increasing metal surface roughness can improve adhesive bond strengths as a consequence of increased surface area and ameliorated interlocking. However, a highly increased surface roughness showed opposite effects because of insufficient wettability [619, 620]. Beside sand-blasting, alternative methods of metal implant surface treatments include etching, heat treatment [621] or ceramic coatings e.g. *via* plasma spraying or immersion in SBF [622]. The bone surfaces presented here had the highest surface roughness as a result of bone slice preparation and the average shear strength was partially significantly higher on sandblasted Korox 50 treated stainless steel (Figure 51, Table 28), which could be attributed to the presumably worse wettability of the bone specimens. Further, a crucial factor is supposably the difference in surface humidity which has already been mentioned before. The bone slices were stored at 4 °C in PBS and were not older than 2 d when used. Thus, the bonding was prepared on moist bone surfaces compared to dry metal slices. The problem with adhesives under moist conditions has already been described in literature [623]. Additionally, the bone seemed to get leached by time with respect to calcium ions (Table 29) which indicates a decrease in bone quality. However, the cement with a 25.0 % phytic acid amount showed adequate adhesive strengths on bone at every time point, which exceeded the required threshold value up to six times (Figure 51).

Comparing both intrinsic mechanical properties and bone bonding ability, the newberyite forming control as well as the 22.5 and 25.0 % phytic acid containing formulation initially exhibited values in the same order of magnitude. For all other cement systems and time points, the intrinsic strength was at least one order of magnitude greater compared to the bone bonding strength (Figure 50 a, Figure 51). For both mechanical parameters being in the same order of magnitude, one would assume that cement residues could be visible on the ancient bonding surface. However this was only the case for the newberyite control (Figure 52). Also, a correlation between possible cement residues and mechanical performance seems not to exist, which might be an issue of cement paste viscosity and thus wettability of the bone surface.

Using a mineral bone cement, Grover *et al*. [304] observed an initial adhesive strength of 1.3±0.8 MPa on ovine cortical bone which is comparable to what has been reached with 25 % phytic acid containing samples [304]. Here, the bone-bonding properties were tested on ground bone slices but natural impurities as fats and proteins were not removed. In contrast, Grover *at al*. [304] defatted the bone samples prior to bond fabrication [304]. Further, our longer-term experiments were performed in a wet and not just humid environment which also can impair the actual bonding strength but better reflects *in vivo* conditions. The upper limit of described adhesion to bone is 14 MPa using a 4-methacryloyloxyethyl trimellitic an-

hydride / methyl methacrylate as an interface between human cortical femur and PMMA [1, 624] but the lack of biodegradability is crucial [1].

Lastly, the question arose if acidic etching or chelation was the main reason for the good bone bonding ability of the 25.0 % phytic acid containing cement system. Figure 51 indicated that none of the used control MPC showed adequate long-term stability on bovine bone slices, which permits the conclusion that a possible etching effect on the bone surfaces by an acidic cement formulation would not be sufficient to enable appropriate bone bonding. This argument might be supported by SEM pictures of corresponding bone/cement interfaces (Figure 54). The acid character of the newberyite control or potentially also the phytic acid containing samples were considered to have a slight edging effect on the nano-topography, but this could not be proven *via* SEM as no obvious differences and thus etching effects could be verified between native bone (Figure 53 d), bone with ancient acidic or bone with ancient neutral cement formulations (Figure 54 a, e). On a macroscopic level, slight differences were seen between the newberyite and the struvite forming reference: more cement residues of acid origin seemed to remain on bone within the scrub marks which was analyzed *via* EDS measurements (Figure 52 a, d, g). It has to be mentioned, that the newberyite forming MPC had a much lower intrinsic strength compared to the struvite control. This could additionally explain why the bonding strength was comparably higher in contrast to the intrinsic strength and left more material on the ancient bonding areas. To sum up, only the addition of the chelating agent phytic acid elevated the bone bonding to adequate values, even if the “pure” acid possibly had a slight impact. This was especially observed on metal slices, where neutral setting prevented (long-term) stability on surfaces with low roughness (Figure 51 b). However, an analytical proof of chelation was not possible. In contrast to the used control groups, the bone surface underneath ancient adhesives from 25.0 % phytic acid containing cements seemed to be still active (Figure 54, c), which renders this cement formulation also interesting from a biological point of view.

3.2.3.5 Conclusion

Mineral bone cements are barely tested *in vitro* for their application as bone bonding agents and are mostly considered being non-suitable. In the present study, it was shown that a MPC with unconventional setting mechanism could yet be used as an adhesive on bone as well as metal alloys, since adhesive strengths of partially >2.0 MPa were obtained. Presumably, this is the first time that such high values were reported for mineral bone cements under aqueous conditions. Although just tested in a proof-of-principle manner with a selected number of surfaces and experiments, the results indicate that moisture and surface roughness play a crucial role for the *in vitro* bonding character. Further, the experiments revealed that conventional magnesium phosphate cements might also be bonding-able on selected surfaces whereat the setting pH as well as the roughness of the metal substrate have a (slight) impact.

4. Current issues and future directions

4.1 Limitations and options of mineral bone cements

As an outcome of the experimental phase of the present thesis and results from literature known studies, it turned out that only HA-CPC ($Ca_{10-x}(HPO_4)_x(PO_4)_{6-x}(OH)_{2-x}$, $0 \leq x \leq 1$) are implementable to diverse paste systems with minor challenges, as raw powders are storage stable, setting is neutral and water is sufficient for setting [12, 21]. One major requirement to mineral bone cements is their cohesive nature in an aqueous environment to avoid blood clotting [10, 12, 21, 174, 182], but the slow reaction velocity of HA might be detrimental to paste cohesiveness. In the past as well as in the present thesis, this issue could successfully be solved by using gelation agents (e.g. HPMC [160]; starch, chapter 3.1.2), surfactant molecules (e.g. castor oil ethoxylate 35, hexadecyl phosphate, chapter 3.1.3 [19, 20]) and high amounts of an adequate setting accelerator (e.g. NaH_2PO_4, chapter 3.1.3; seed crystals [19, 20]). There is a multitude of publications about dual setting [16, 17, 149, 150, 389, 390], prefabricated [19, 20, 160, 170, 173, 175, 404, 405] and calcium binding systems [18, 77, 78, 143-147, 388, 394, 397] mostly on HA-basis. In the case of dual setting systems, the slow reaction kinetic of HA is yet beneficial, as it does not interact with the polymerization reaction. This could exemplarily lead to a reduced mobility of monomer chains. Here, the cohesion is promoted by the fast curing of the polymer which encases unreacted raw powder particulates (chapter 3.1.1). Last but not least, HA-based formulations are preferred, as they are intensively studied since decades and as they form the majority of commercially available paste systems for bone substitution. [13]. For the mentioned reasons, it was possible to introduce different paste systems and application forms on HA-basis in the present work. In this context, the apatite premixed paste of which the company InnoTERE (Dresden, Germany) holds clinical accreditation in the EU since 2015 is especially emphasized [16].

Besides all advantages, a major drawback of HA-CPC is their restricted biodegradability [188-191, 199, 200, 210]. Under physiological conditions, HA is not chemically soluble as demonstrated by Klammert *et al*. [209] who implanted HA cylinders in a heterotopic implantation site without seeing any dissolution for 15 months [209]. This clearly showed that acid producing osteoclasts are necessary for HA resorption which might take for years [10]. The presented systems are thus considered being rather model formulations for further developments. Though, suitable biodegradability of HA was described due to a smart pore design (porosity and pore size) [111, 199, 222]. An increase in pore sizes from 230 to 540 µm at a minimal increase in porosity of 73 to 75 % doubled the mass loss of HA to approximately 10 % within 24 weeks in PBS under dynamic conditions [111]. *In vivo*, residual cement material of only 35 % was observed after 12 weeks of implantation in the femur of New Zealand white rabbits when using a 75 % macroporous cement [199]. In addition, a recently published research report of Bohner *et al*. [625] overhauled the outdated opinion that bone ingrowth only occurs for pores with sizes >100 µm. Although sintered β-TCP scaffolds were tested for up to 24 weeks in ovine studies, the results were quite imposing: Mineralized tissue from CaP, collagen and associated cells was observed in micropores >1 µm especially in early states after implantation. Even though this phenomenon did only appear in case of pore in-

[16] www.innotere.de/velox (11.10.2017).

terconnections of at least 1 to 10 µm and did not involve degradation processes, this knowledge is a big step for a deeper understanding of the role of pores as regards biodegradation of ceramic implants [625].

The secondary CaP brushite ($CaHPO_4 \cdot 2H_2O$) and monetite ($CaHPO_4$) as possible alternatives to HA should show a clearly improved degradation behavior *in vivo* [10, 204], but it was observed many a time that brushite tends to re-precipitate into less soluble CaP compounds such as OCP ($Ca_8H_2(PO_4)_6 \cdot 5H_2O$) [206, 209, 210] which was not the case for monetite [217]. A common approach to avoid recrystallization is the addition of magnesium containing salts [208, 212] as firstly suggested by Bohner and Matter [626] in 2004. Further issues when using secondary CaP in distinct paste formulations are difficulties with the limited shelf-life of multi-component systems (e.g. β-TCP/MCPA) [408] in prefabricated pastes as well as the acidic setting reaction [210] which prevents the polymerization of acid-susceptible educts in dual setting systems. The pH of the reaction is also critical, when acid-labile active ingredients are embedded.

As the formation of brushite is generally thermodynamically favored towards monetite, focused modifications of the paste, just like a particularly low pH or a high ionic strength, have to be undertaken [39-42]. It is questionable, if such alterations would be compatible with dual setting or prefabricated paste systems. Last but not least, the fast setting especially of brushite [10, 21] might lead to problems with the compatibilization of the kinetics of both cement setting and polymerization. There are few examples displaying that the compatibilization of a system setting at acidic pH exemplarily in the dual setting regime actually works. In such cases, the changes in pH even promoted the polymerization of the second compound (e.g. silica gel, silk fibroin) mostly by forming the preferred monetite instead of brushite as a by-product. The cause for this effect is the low water availability for brushite as the gel constituent might compete for it [215, 391]. According to Geffers *et al*. [215], pH changes while the setting of β-TCP/MCPA to form brushite initiated the condensation of pre-hydrolyzed tetraethyl orthosilicate. This resulted in a purely inorganic composite with dual pore sizes, increased density and compressive strength and controllable brushite-to-monetite ratio. The latter could be regulated by the amount of the orthosilicate which in turn competed for the water contained in the composite [215]. In a further study, the pH and ionic force dependent gelation of *Bombyx mori* derived silk fibroin from its random coil into the more stable β-sheet structure could likewise be tailored to the acid setting reaction of a β-TCP/MCPA derived brushite cement which led to an extreme reinforcement of the inorganic matrix and showed self-densifying properties. Again, the additional occurrence of monetite was detected [391]. The use of secondary CaP in prefabricated cement pastes is described rather seldom exemplarily in form of frozen [403] or non-aqueous, but water-miscible [171, 172, 406, 407, 627] formulations. Such systems require a storage under frigid and absolutely water-free conditions. This might takes an aimed dehydration of the paste after its fabrication such that all components of the paste should be compatible with the drying regime. For instance, Cox *et al*. [627] reported that they had produced a premixed, monetite-forming cement paste from β-TCP, MCPM and glycerol. The cohesiveness was assured by the addition of alginate, the monetite formation was initiated by the usage of the water-miscible glycerol instead of water, but as expected, the paste was only stable for 2 weeks. This was demonstrated by a significant decrease in compressive strength after a longer storage duration [627]. Calcium binding

systems with brushite and/or monetite are conceivable, as well [18, 148]. Chen *et al*. [18] demonstrated that brushite and monetite can actually occur as the main setting products of intrinsically HA forming raw powders (TTCP/DCPA) in combination with PAA [18] and Kashaba *et al*. [148] showed that the secondary CaP developed at least in addition to HA [148]. Alternative calcium binding systems (e.g. by using citrates or phytic acid) were previously only applied in low concentrations for their setting decelerating effects and/or an improved injectability rather than using them as stoichiometric brushite/monetite cement reactants [66, 71, 76, 108].

As described earlier, creating biodegradable HA formulations is possible as well as the development of different systems based on secondary CaP, which might be a challenge. However, the current trend goes more and more towards MPC, whereby the most common systems form either (K-)struvite ($K/NH_4MgPO_4 \cdot 6H_2O$) or newberyite ($MgHPO_4 \cdot 3H_2O$) [15]. While the former needs a potassium or ammonium ion source, newberyite cements are challenging similar to brushite: multi-constituent educts are probably not storage stable and the acid pH while setting might affect acid-labile paste components such as monomers or biologically active substances with respect to their reactivity and efficiency. In addition, both struvite and newberyite forming systems are of fast setting nature, which includes challenges when the kinetics of all reactions within one formulation have to be coordinated.

Dual setting systems based on MPC are not known from current literature. In the present work, it failed to develop a dual setting MPC as drillable and degradable bone substitute material exemplarily on the basis of farringtonite and 2-HEMA. In this case, the solid phase additionally contained the initiator APS and the liquid phase the setting regulator DAHP as well as the polymerization initiator TEMED. However, matching of the reaction kinetics seemed impossible and no reinforcement effects by the incorporation of the organic phase into the ceramic matrix were observed (chapter 3.2). Combining the chelating agent phytic acid with farringtonite as a common MPC raw mineral turned out being a promising problem-solving strategy. It was not only feasible to prove the drillability of this system by terms of a screw pull-out test setup (chapter 3.2.2), but it was likewise shown that this material is further suitable for application as bone and metal implant adhesive (chapter 3.2.3). The field of bone adhesives based on mineral bone cements is *hitherto* strongly limited [1, 304, 306, 567] and most research in this topic focused on the incorporation of ceramic fillers in an organic matrix [564-566]. As the chelate complexes within this system maintain the raw mineral farringtonite and simultaneously form glassy structures which could not be proven *via* XRD, *in vivo* studies should be attached to the presented research results. This would enable concrete statements on the degradation and regeneration behavior in an adequate defect model to test both the drillability as well as the actual suitability of this cement formulation as bone adhesive. The pure biomechanical testing of screw-cement combinations is often performed on artificial [535] or corpse bone [23, 537] including dynamic mechanical loading conditions, but those do not allow any statement about the long-term and biological behavior. Doht *et al*. [23] described a technique whereby human cadaver tibiae were insulated and tibial depression fractures were simulated *via* axial force on five circular (Ø 12 mm) arranged drilling holes. The depth was reproducibly kept at 15 mm under the plateau. The tibial depression fractures were then reduced and stabilized *via* augmentation with cement paste followed by jail technique (four crossing screws) [23]. As biomechanical and biological properties might be diffi-

cult to evaluate in one single model, independent models should be performed. For the assessment of the biocompatibility, biodegradation and bone regeneration, simple burr hole defects filled with cement paste in a small animal model (e.g. New Zealand white rabbit) should be sufficient. Among all existing animal models to test bone substitutes, the distal femur of rabbits is the most prominent [628]. The biomechanical test setup could be based on the above described technique [23]. As concerns the bone bonding ability, an *in vivo* test setup comparable to that applied by Schendel and Peauroi [382] can be used to approximate the later application as bone adhesives. In their study, New Zealand white rabbits received cranial burr holes (Ø 10 mm) which were then refixed in place *via* mineral bone cement paste [382]. It would also be interesting to take advantage of the exceptionally good measured shear strengths of the as-presented cement system by either applying the paste only selectively or by incorporating a sacrificial mesh e.g. from soluble collagen. Both approaches would lead to the *in situ* formation of channels providing a fast and facilitated vascularization and thus regeneration of the bone fragments. Indeed, there already exist some animal studies to characterize MPC in general, but those are numerically limited and mostly focused on the crystalline MgP struvite and newberyite [195, 301, 361, 382-384]. Regarding premixed paste systems, the company InnoTERE (Radebeul, Germany) vehemently works on the development of such receipts based on struvite within a joint project.

Table 31: List of possible wet-chemical reaction receipts for the precipitation of alternative MgP and magnesium ammonium phosphates bobierrite, catiite, dittmarite and schertelite.

MgP compound	wet-chemical reaction receipt, example	literature
bobierrite $Mg_3(PO_4)_2 \cdot 8H_2O$	4.1 g $MgSO_4 \cdot 7H_2O$ and 4.0 g $Na_2HPO_4 \cdot 12H_2O$ in 1.5 L water, pH adjusted with HCl to 6.6-7.0, addition of $Ca(NO_3)_2 \cdot 4H_2O$ in a molar ratio to $MgSO_4$ of 1:100, heated at 90 °C for 2 h	Kanazawa, 1979 [629]
cattiite $Mg_3(PO_4)_2 \cdot 22H_2O$	20.0 g $MgSO_4 \cdot 7H_2O$ in 2.0 L water and 19.4 g $Na_2HPO_4 \cdot 12H_2O$ in 1.0 L water mixed at 5 °C	Catti, 1980 [630]
dittmarite $NH_4MgPO_4 \cdot H_2O$	0.12 g $MgSO_4$ and 0.14 g Na_2HPO_4 in 50 mL water, addition of 0.05 mol/L urea, pH adjusted to 7.5, heated at 90 °C for 60 min	Chen, 2010 [631]
schertelite $(NH_4)_2Mg(HPO_4)_2 \cdot 4H_2O$	32.2 g $NH_4H_2PO_4$ and 3.1 g $NH_4C_2H_3O_2$ in 100 mL water, addition of 8.6 g $Mg(CH_3COO)_2$	Frazier, 1963 [327]

An essential difference between CPC and MPC is that the products of CPC can always be ascribed to brushite or HA [39]. It appears, that even in the case of MPC, either (K-)struvite or newberyite would consistently be formed [15]. However, a deeper research on MgP revealed that there is a variety of alternative MgP (e.g. bobierrite, $Mg_3(PO_4)_2 \cdot 8H_2O$; cattiite, $Mg_3(PO_4)_2 \cdot 22H_2O$ [327]) and magnesium ammonium phosphates (e.g. dittmarite, $NH_4MgPO_4 \cdot H_2O$ [291, 322]; schertelite, $(NH_4)_2Mg(HPO_4)_2 \cdot 4H_2O$ [327]). Those minerals are normally not thermodynamically favored within cementitious reactions, but it is possible to shift the reaction equilibrium by triggering the reaction conditions such that those minerals

are presumably formed as intermediates or by-products [291, 294, 303, 308, 315, 321, 322, 327]. For instance, dittmarite is described as an intermediate product of struvite formation, if the reaction runs very fast [291, 322]. Apart from their occasional occurrence as by-products, there are no scientific reports about those alternative MgP within cement systems. However, it is possible to gain these compounds as precipitates of wet-chemical processes (Table 31). It would be interesting if the knowledge from such precipitation reactions could be transferred on cements which potentially would have a higher compatibility towards non-classic paste systems.

It was revealed in a - at present - non-published study [17] that farringtonite can actually be hydrolyzed *via* high energy ball milling. The resulting partial amorphization of the raw powder leads to the formation of the MgP hydrate cattiite which is intrinsically described as the metastable MgP while ageing of struvite to bobierrite in water [327]. The setting kinetics, the product content and the mechanical stability of the hydrated MgP can be controlled by the grinding time. After 24 h high energy milling, the farringtonite raw powder contained more than 70 % amorphous phase leading to a conversion to 40 % cattiite with appropriate wet compressive strength of approximately 11 MPa [17]. As MPC generally react *via* an acid-base reaction [315] and not *via* hydrolysis, this is the first time that a MgP based mineral system is described which - similar to α-TCP based HA [12] - simply needs water for setting. This allows for the likewise use of this novel cement formulation exemplarily in dual setting cements which represented the greatest threshold while realizing different paste systems based on MPC, so far. A second idea would be the usage of mechanically activated farringtonite for 3D-powder printing applications such that water or phosphoric acid would be sufficient for a fast reaction during printing. Experts in 3D-powder printing reported on difficulties while printing with alternative binder liquids such as ammonium phosphate solution with concentrations >1.0 M [18]. Lastly, mechanically activated farringtonite could (partially) substitute basic setting MgO [319] in directly applicable cement formulations for pH adjustment. The control of the setting time by the milling procedure simultaneously enables the renunciation of other commonly used setting regulators such as ammonium phosphates [210, 218, 310-313] or borax [294], respectively. This is also valuable from a biological point of view: While the former might release noxious ammonia while setting or degradation [294], the latter was shown to be eventually toxic [359, 360].

Evaluation of the biocompatibility, biodegradation and bone regeneration in relevant animal studies provides a further research approach with respect to alternative MgP and magnesium ammonium phosphates. So far, this was not examined but embodies an essential aspect with the development of osteoconductive, degradable bone substitution materials.

[17] T. Brückner *et al.*, Mechanical activation and Cement Formation of Trimagnesium Phosphate, submitted to J. Amer. Ceram. Soc. (2017).

[18] Personal communication from Prof. Dr. Uwe Gbureck.

4.2 Further applications of non-classic cement pastes

The paste systems used in the present work (drillable cements, chapter 3.1.1 & 3.2.2; bone wax, chapter 3.1.2; prefabricated laminates, chapter 3.1.3; bone adhesives, chapter 3.2.3), offer a vast leeway to generate further applications. Thus and besides their drillability, dual setting systems might be cut arbitrarily into shape, as illustrated by Schamel *et al*. [391] or can be used as a starting material for 3D-plotted structures, whereat a whole construct is built up from single paste strands extruded from movable nozzles in a computer-aided manner. In this way, the special mechanical characteristics of such systems would be extended by further advantageous parameters such as the generation of customized implants and the incorporation of defined macroporous structures [453, 483, 484, 507-509]. The controlled deposition of cement strands to form distinct geometries might additionally set the stiffness and flexibility. In the past, such systems consisting of an elastic polymer matrix were mostly equipped with inactive fillers [453, 483, 484, 507-509, 514, 515, 517-524, 526-529]. In 2016, Jakus *et al*. [632] reported of a so-called “hyperelastic bone”. Their 3D-printable bioink consisted of PCL and PLGA diluted in adequate solvent and filled with inactive HA powder. The solidification of printed constructs was enabled *via* solvent evaporation. The resulting composite displayed high elasticity (up to 67 % strain) at 50 % porosity though the solid phase initially consisted of 90 wt.% HA. Besides, they used organic solvents for adequate ink viscosity [632], which might be critical from a biological point of view and another aspect also has to be taken into account: Schamel *et al*. [390] revealed in a comparative study with active and inactive fillers that the mechanical reinforcement only takes place when the cementitious reaction occurs parallel to the gelation. The inorganic phase of the cement contained either α-TCP, β-TCP or HA nanoparticles, the organic component was a star-shaped polymer with statistical ethylene and propylene oxide backbone and reactive terminal isocyanate groups. When in contact with water, the isocyanate groups were hydrolyzed to amines, while α-TCP was hydrolyzed to form nanocrystalline HA. In the case of a cementitious reaction, a 30-fold strength improvement was observed in contrast to systems with comparable amounts of unreactive filler. Moreover, the workability was improved in dual setting systems [390] and they generally allow a higher polymer amount [102] which enables ideal coordination of the strength of the ceramic and the elasticity of the organic component. In current literature, there are only few reports being based on the concept of using composite bioinks with *in situ* hardening ceramic constituents [510-513, 516].

As the dual setting system from α-TCP and 2-HEMA (chapter 3.1.1) hardens *in situ*, modifications of the current formulation have to be undertaken for a well working printing process. Initiation of the setting reaction is controlled both by the water content as well as by the chemical initiator system (TEMED, APS). While the former is required for the cementitious reaction of α-TCP to form CDHA and can additionally be bound physically within the poly-2-HEMA network, the latter activates the polymerization of the as-mentioned hydrogel. Renunciation of the water would delay the dissolution/precipitation of the inorganic constituent until the paste strands are exemplarily deposited on a platform which is situated underwater. Alternatively, when the water should be retained within the paste formulation, the conversion to HA might be retarded by the use of $MgCl_2$, as it was described by Bohner *et al*. [400] for the stabilization of purely inorganic pastes. They achieved to keep their suspension inactive for at least 1 year, when the incorporated α-TCP has been calcined for 25 h at 500 °C [400].

Anyway, the deposition of the dual setting bioink would have to take place in an aqueous environment delivering the activator (e.g. $CaCl_2$ at the same concentration as $MgCl_2$ [400]) of the setting reaction. Alternatively, post-hardening of the freshly printed scaffold in an adequate medium could be performed, which is a common approach for constructs based on premixed cement paste [510-512]. The chemical initiator couple of the α-TCP/2-HEMA system could be substituted with a photo-initiator (e.g. Irgacure and UV-light [633]). To activate the polymerization reaction, the printed construct would have to be exposed in regular intervals, for instance after each completed strand layer. However, the maximum strand thickness would be limited due to the restricted irradiation depth of light into non-transparent materials. Additionnally, the incorporation of gelating agents or surfactant molecules might be necessary to improve the cohesiveness while direct printing in an aqueous solution. A Similar concept by Maazouz *et al*. [516] depicted the combination of reactive α-TCP and inert β-TCP with 10 % aqueous gelatin solution, but they pointed out one major issue. As expected, the reactive CaP started setting some time (~100 min) after mixing which significantly increased the force needed for paste extrusion such that mixing actually has to take place immediately before plotting. For the inert CaP filler, this was not observed. The mechanical and biological outcome could be taylored by additional chemical crosslinking [516].

In contrast to *in situ* hardening dual setting systems, prefabricated cement pastes are ideal for the application in a 3D-plotter. Due to the fact, that the whole process including post-treatment can be undertaken at RT, physiological pH and without the need for volatile organic solvents, it is especially valuable for the incorporation of biologically relevant, but sensitive agents (e.g. VEGF) [510]. As illustrated by Akkineni *et al*. [510], the paste strands stay dimensionally stable within the finished construct, such that this has not to be printed underwater. Instead, the construct can be post-hardened in a suitable aqueous environment or at least humid atmosphere [510]. This concept is rarely popular in common literature. Indeed, there are numerous publications that deal with developing storage stable pastes [19, 20, 160, 170-172, 398-400, 404-407], but more seldom with their application in the 3D-printing sector. All of them could be attributed to the same paste composition [510-513], probably similar to that one which has been brought to market by InnoTERE (Radebeul, Germany).

When the premixed paste is rigid (i.e. already polymerized and highly viscous) at RT, the printing process has to take place at elevated temperatures corresponding to the melting temperature of the organic phase or, at least, allow suitable processing. For instance, this would enable printing of the introduced bone wax formulations from TTCP/DCPA and PEG mixtures (chapter 3.1.2). Actually, FDM technique has already been applied on the reinforcement of thermoplastic materials such as polypropylene [634], PCL [635-637] or PLGA [638] with inactive ceramic CaP particles such as β-TCP [634, 638] and HA [635, 637, 638]. In the field of drug release, Perissutti *et al*. [639] unveiled that homogenous strands from PEG 4,000 could likewise be extruded slightly below its melting temperature [639]. Usually, commercial FDM machines work with readied polymer filaments to feed a liquefying compartment followed by melt extrusion [637], but buckling of the filaments represents a major problem [640] such that a directly connected melt extrusion system prior to FDM could be reasonable for bone wax processing. In this case, the intention of plotting is not based on the generation of customized constructs with defined macroporosity, but 1) on a standardization of the bone wax dosage form with respect to the later operator and 2) on an improvement of

the kneadability. Combining big pores with thin single strands will substantially reduce the physical effort due to the reduced bulk density. Quenching of the molten wax on a cooled platform additionally could prevent the formation of semi-crystalline PEG [641]. According to Li *et al*. [642] who systematically analyzed the crystallization behavior of PLA, the crystallinity was confined at high cooling rates and low processing temperatures [642]. This again would facilitate and simplify the preparation of the wax prior to application.

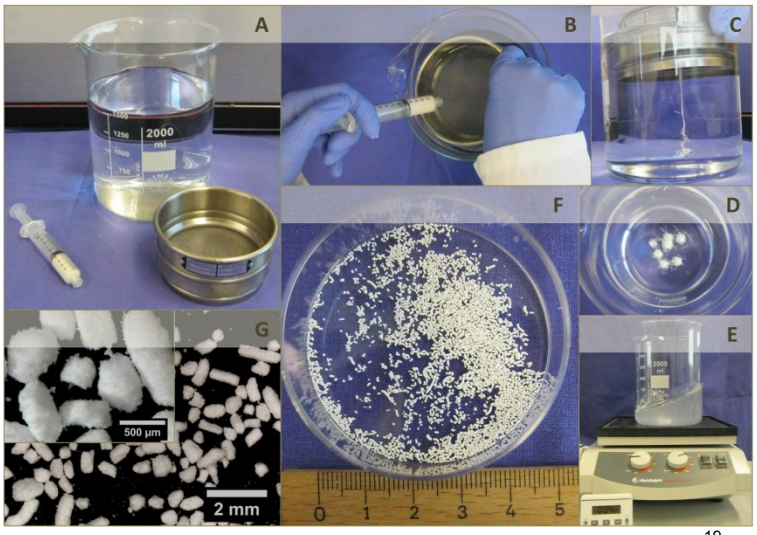

Figure 56: Procedure of sieve-shaking with calcium substituted, oil-based MPC paste [19] as an example. 5 mL of the cement paste delivered in a 10 mL syringe, 1.5 L of an ammonium phosphate containing solution and a 300 µm sieve were used (a). The paste was extruded through the sieve (b) and directly transferred into the setting accelerator solution (c, d). Radial motion of the aqueous phase (e) led to the formation of strand segments resulting in ellipsoid µm- to mm-sized granules (f, g).

The fabrication of granules *via* sieve-shaking represents a further possible application of oil-based pastes. As described by Bohner *et al*. [410] a viscous paste is thereby pressed through the pores of a sieve by means of a pestle [410]. Tas [239] used this technique for the fabrication of porous HA granules within a size range of approximately 1 to 3 mm. The cement raw powder was mixed with a porogen, wetted with an adequate mixture of ethanol and water and immediately pushed through the pores of a sieve-shaking tower. After ethanol evaporation on air, setting and porogen leaching were undertaken in water for 48 h [239]. Using a premixed cement paste with water-immiscible binder, this technique had to be slightly altered. Here, the paste was initially delivered by syringe, extruded through the sieve and directly transferred in an aqueous phase which contained setting regulators to accelerate the reaction. While hardening, radial motions of the aqueous phase led to a disintegration of the formed strands into smaller segments with a length of few mm. Those segments were stored in the aqueous phase until solidification was completed. The example of a calcium substituted, oil-based MPC paste revealed the functioning of this concept (Figure 56). Experimentally, the granule diameter can be controlled by the pore diameter of the used sieve. As the cement paste might clog small sieve openings, the diameter in turn is restricted to sizes >100 µm [410]. The resulting ellipsoid granules could be used for particular bone graft in dental and orthopedic applications [410] where enhanced resorption and new bone formation are required. This is ensured *via* a promoted diffusion of ions and nutrients through the intergranular space [414].

[19] The premixed cement paste was kindly provided by InnoTERE, Radebeul, Germany.

The present work has already disclosed the diversity of chelate forming cement pastes based on MgP with respect to application (chapter 3.2). Both drillability (chapter 3.2.2) and adhesion to bone and typical implant materials (chapter 3.2.3) are properties which are hardly represented in the sector of mineral bone cements. This emphasizes the novelty of this formulation because the clinical need for drillable cement systems as well as approximately working bone adhesives provides a topical subject. That has been discussed with experienced clinicians from the fields of trauma and maxillofacial surgery [20]. The efficacy of both properties takes primarily effect in the initial states of setting such that transfer of this paste system on 3D-plotting is not intended. In view of later application, the special properties of this cement enable adhesive bonding of smaller fragments and the simultaneous stabilization of larger fragments *via* augmented screw or plate osteosynthesis without the need of a second product.

Conclusion

The presented work demonstrated the diversity of possible receipts, but also current limitations and challenges for the generation of mineral bone cements on both CaP and MgP basis. The cement formulations can be used for the fabrication of multifaceted common application forms such as 3D-printed scaffolds or granules, but also for the development of application fields which currently constitute niche sectors, such as drillable cements, bone waxes, prefabricated laminates and bone adhesives. Together with the research on unknown minerals for their potential use in biocements, this strongly expands the current market for those cement systems as bone graft substitutes in dental and orthopedic surgery.

[20] Personal communication from PD Dr. med. Stefanie Hölscher-Doht; University Hospital Würzburg, Trauma surgery and Prof. Dr. Dr. Alexander C. Kübler; University Hospital Würzburg, Maxillofacial surgery.

5. Summary

Mineral bone cements based on calcium phosphate chemistry represent valuable synthetic bone graft substitutes, as they are self-setting, biocompatible, osteoconductive and in their composition similar to the inorganic phase of human bone. Due to their long shelf-life, neutral setting and since water is sufficient for initiating the setting reaction, hydroxyapatite ($Ca_{10-x}(HPO_4)_x(PO_4)_{6-x}(OH)_{2-x}$; $0 \leq x \leq 1$) forming cement systems are processed in different paste formulations, which not necessarily need to be purely aqueous and inorganic. Those comprise 1) dual setting, 2) calcium binding and 3) premixed cement systems. With dual setting formulations, both dissolution and precipitation of the cement raw powder occur simultaneously to the polymerization of water-soluble monomers to form a hydrogel leading to composites with a pseudoplastic mechanical behavior though the ceramic is intrinsically brittle. The use of chelating agents, which are able to form complexes with calcium ions released from the raw powder, can in addition lead to an improvement of the fracture mechanics. Premixed systems mostly contain the raw powder of the cement reaction and a non-aqueous binder liquid which delays the setting reaction until an application into the moist physiological environment. In the present work, two of those reaction mechanisms allowed the development of hydroxyapatite based cement formulations whose application forms (drillable cements, bone waxes, prefabricated laminates) each represent a niche in the field of mineral bone cements (chapter 3.1; *Calcium phosphate cement based approaches*).

Drillable cements are of high clinical interest, as the quality of screw and plate osteosynthesis techniques can be improved by cement augmentation. In chapter 3.1.1 (*A systematic study of a drillable, injectable and fast-setting cement system*), a drillable, dual setting composite from hydroxyapatite and a poly(2-hydroxyethyl methacrylate) based hydrogel was systematically analyzed with respect to the influence of monomer content, hardening time and powder-to-liquid ratio on setting kinetics and mechanical outcome. While the conversion to hydroxyapatite and crystal growth were constantly confined with increased monomer amount, a minimum concentration of 50 % monomer was required to see impressive ameliorations of the fracture behavior within a 4-point bending test setup. This included a low bending modulus of 5.5 GPa and high fracture energy of 13.3 mJ/mm² at improved bending strength. Increasing the liquid amount enabled injection of the paste with 75 N injection force as well as drilling after only 10 min of pre-setting. The corresponding screw pull-out force was 260 N.

The clinical purpose of calcium phosphate cement based bone waxes is depicted in chapter 3.1.2 (*Bone wax from poly(ethylene glycol)-calcium phosphate cement mixtures*). While classic bone wax formulations have drawbacks such as infection, inflammation, hindered osteogenesis and a lack of biodegradability, the as-presented premixed formulation is believed to exhibit outmatching properties. It consisted of hydroxyapatite raw powders, intrinsically hemostatic supplements and a non-aqueous, but water-miscible carrier liquid from solid and liquid poly(ethylene glycol). The bone wax was proved to be cohesive and malleable, it withstood systolic blood pressure conditions and among deposition in an aqueous environment, poly(ethylene glycol) was exchanged such that highly porous, nanocrystalline hydroxyapatite with a compressive strength comparable to that of cancellous bone was formed. Incorpora-

tion of a model antibiotic proved the suitability of the novel bone wax formulation for drug release purposes.

Prefabricated laminates from premixed carbonated apatite forming cement paste and poly(ε-caprolactone) fiber mats with defined pore architecture were presented as a potential approach for the treatment of 2-dimensional, curved cranial defects (chapter 3.1.3; *prefabricated laminates*). They are flexible until application and were produced in a layer-by-layer approach from both components such that the polymer scaffold prevents the cement from flowing during hardening. It was demonstrated that solution electrospinning with a patterned collector for the fabrication of perforated fiber mats was suitable in relation to this application, as high fiber volume contents in combination with an appropriate interface enabled the successfull fabrication of the laminates including a 25-fold mechanical reinforcement at most in terms of fracture energy. Mild immersion of the scaffolds under alkaline conditions additionally improved the interphase followed by an increase in bending-strength from 2.5±0.82 to approximately 3.5 MPa.

Since few years, magnesium phosphate cements have attracted increasing attention for bone replacement. Compared to calcium phosphate based formulations, magnesium phosphate cements exhibit a higher degradation potential and high early strength and they release biologically valuable magnesium ions. However, common systems offer some challenges while using them in non-classic cement formulations such as the need for foreign ion supply (ammonium ions for struvite, $NH_4MgPO_4 \cdot 6H_2O$), the potential acidity of the setting reaction (newberyite, $MgHPO_4 \cdot 3H_2O$) or the fast setting kinetics. Here, it was possible to develop a chelate-setting magnesium phosphate based cement paste, which offered a broad spectrum of potential applications (chapter 3.2; *Magnesium phosphate cement based approaches*).

In chapter 3.2.1 (*Chelate bonding mechanism in a novel magnesium phosphate cement*), the general mechanism of the novel setting principle was tested in a proof-of-principle manner. The cement paste consisted of farringtonite ($Mg_3(PO_4)_2$) with differently concentrated phytic acid ($C_6H_{18}O_{24}P_6$) solution for chelate formation with magnesium ions released from the cement raw powder. In addition to chelation, high phytic acid amounts of up to 30 % fostered a simultaneous dissolution and precipitation reaction to form small quantities of newberyite with a mechanical strength of up to 65 MPa in compression. Altering the recipe by adjusting the phytic acid content (20 to 25 % aqueous solution at a powder-to-liquid ratio of 2.0 g/mL) and adding a magnesium oxide (MgO) as setting regulator to compensate its retarding effect (6 to 7.5 % MgO) resulted in drillable formulations with screw pull-out forces of up to 148 N (chapter 3.2.2; *In vitro study of a degradable & drillable farringtonite based bone cement).* Besides missing drillable cement formulations, there is a strong clinical demand for well working bone adhesives especially in a moist environment. Mostly the existing formulations are non-biodegradable. In the subsequent chapter 3.2.3 (*A mineral cement for the application as bone and metal adhesive agent*) both *ex vivo* and *in vitro* adhesion of the above presented magnesium phosphate under wet conditions on bone just as sandblasted stainless steel was demonstrated over a course of 7 d within a shear test setup which delivered strengths of 0.8 and 1.7 MPa, respectively. According to literature, the lower limit must score to 0.2 MPa. Further, the hardened cement specimens showed a mass loss of 2 wt.% within 24 d in an aque-

ous environment and released about 0.17 mg/g of osteogenic magnesium ions per day. Together with the demonstrated cytocompatibility towards human fetal osteoblasts at appropriate dilution of corresponding eluates (chapter 3.2.2), this cement system showed promising characteristics in terms of degradable biocements with special application purposes. It should be noted that both application forms, drillable cements as well as bone adhesives, exhibit a high degree of novelty within the field of mineral bone cements, as the currently available literature is strongly limited in this context.

6. Zusammenfassung

Mineralische Knochenzemente auf Calciumphosphat-Basis stellen ein klinisch bedeutsames Knochenersatzmaterial dar, denn sie sind selbst-abbindend, biokompatibel, osteokonduktiv und in ihrer Zusammensetzung der anorganischen Komponente menschlichen Knochens ähnlich. Auf Grund ihrer langen Lagerstabilität, neutralen Abbindereaktion und da Wasser zum Abbinden ausreicht, werden Hydroxylapatit ($Ca_{10-x}(HPO_4)_x(PO_4)_{6-x}(OH)_{2-x}$; $0 \leq x \leq 1$) bildende Zementsysteme bevorzugt in verschiedenen Pastensystemen verarbeitet. Diese müssen nicht zwingend rein wässrig und anorganisch sein. Hierzu gehören 1) dual abbindende, 2) Calcium chelatisierende und 3) vorgefertigte Zementsysteme. Bei dual abbindenden Formulierungen findet die Lösungs-Fällungs-Reaktion des Zementrohpulvers zeitgleich mit der Polymerisation wasserlöslicher Monomere zu einem Hydrogel statt. Dieses verleiht dem Komposit - trotz des spröden Charakters des reinen Zements - pseudoplastische mechanische Eigenschaften. Die Verwendung von Chelatbildnern, welche mit freigesetzten Calciumionen Komplexe bilden können, kann ebenfalls zu einer Verbesserung der Bruchmechanik führen. Vorgefertigte Zementsysteme bestehen zumeist aus dem Rohpulver der Abbindereaktion und einer nicht-wässrigen Trägerflüssigkeit, welche die Abbindereaktion bis zur Anwendung des Zements im feuchten Milieu verhindert. In der vorliegenden Arbeit war es möglich, zwei dieser Reaktionsmechanismen zur Entwicklung Hydroxylapatit basierter Zementformulierungen einzusetzen. Die jeweiligen Anwendungsformen (bohrbare Zemente, Knochenwachse, präfabrizierte Laminate) stellen eine Nische auf dem Gebiet mineralischer Knochenzemente dar (Kapitel 3.1; *Calcium phosphate cement based approaches*).

Bohrbare Zemente sind dabei von hohem klinischen Interesse, da die Qualität einer Schrauben- oder Plattenosteosynthese durch Augmentation mit dem Zement verbessert werden kann. In Kapitel 3.1.1 (*A systematic study of a drillable, injectable and fast-setting cement system*) wurde ein bohrbarer, dual abbindender Komposit aus Hydroxylapatit und einem Poly-2-Hydroxyethylmethacrylat Hydrogel systematisch analysiert. Dabei wurde der Einfluss des Monomergehalts, der Aushärtezeit und des Pulver-zu-Flüssigkeits-Verhältnisses auf die Abbindekinetik und mechanischen Eigenschaften untersucht. Während die Umwandlung zu Hydroxylapatit und das Kristallwachstum mit zunehmendem Monomergehalt stetig reduziert wurden, zeigte sich, dass eine minimale Konzentration von 50 % nötig war, um signifikante Verbesserungen des Bruchverhaltens innerhalb eines 4-Punkt-Biegeversuchs zu erfassen. Dies bedeutete einen niedrigen Biegemodul von 5.5 GPa und eine hohe Bruchenergie von 13.3 mJ/mm² bei gesteigerter Biegefestigkeit. Wurde der Flüssigkeitsgehalt erhöht, so konnte die Paste mit einer Kraft von 75 N injiziert und bereits nach 10 min des Abbindens ohne Bildung von Anrissen gebohrt werden. Die entsprechende Schraubenausrisskraft lag bei 260 N.

Der klinische Zweck für Calciumphosphatzement basierte Knochenwachse wurde in Kapitel 3.1.2 (*Bone wax from poly(ethylene glycol)-calcium phosphate cement mixtures*) veranschaulicht. Während klassische Knochenwachsformulierungen Infektionen, Entzündungen, gehinderte Knochenneubildung und mangelhafte Bioabbaubarkeit vorweisen, so zeigen die hier dargestellten Formulierungen überlegene Eigenschaften. Das Knochenwachs bestand aus Hydroxylapatit-Rohpulvern, blutstillenden Zusätzen und einer nicht-wässrigen, aber mit Wasser mischbaren Trägermasse bestehend aus festem und flüssigem Polyethylenglycol.

Es wurde gezeigt, dass das Knochenwachs kohäsiv und knetbar ist und systolischen Blutdruckbedingungen standhält. Bei Kontakt mit einer wässrigen Phase wurde das Polyethylenglycol mit Wasser diffusiv ausgetauscht, so dass ein stark poröser, nanokristalliner Hydroxylapatit mit einer dem spongiösen Knochen vergleichbaren Druchfestigkeit präzipitieren konnte. Die Einbettung eines Modell-Antibiotikums bestätigte zudem die Eignung des neuartigen Wachses als Wirkstoffdepot.

Als eine mögliche Behandlung von 2-dimensionalen, gekrümmten Defekten der Schädeldecke wurden präfabrizierte Laminate aus lagerstabiler, Carbonatapatit bildender Zementpaste und Polycaprolakton-Fasermatten mit definierter Porenarchitektur vorgestellt (Kapitel 3.1.3; *prefabricated laminates*). Diese sind bis zu ihrer Anwendung flexibel und wurden durch einen schichtweisen Aufbau aus beiden Komponenten erzeugt, so dass der Polymerscaffold den Zement während der Abbindereaktion daran hindert, zu zerfließen. Es wurde gezeigt, dass die Herstellung makroporöser Fasermatten durch Elektrospinnen aus der Lösung mittels eines perforierten Kollektors bezüglich der genannten Anwendung besonders geeignet war. Trotz des hohen Faservolumengehalts wurden die Laminate erfolgreich hergestellt und wiesen auf Grund einer angemessenen Faser-Zement-Grenzfläche um das 25-fach verbesserte mechanische Eigenschaften im Sinne der Bruchenergie auf. Bei milder Behandlung der Scaffolds mit alkalischer Lösung wurden die Grenzflächeneigenschaften weiter verbessert, was zu einer zusätzlichen Steigerung der Biegefestigkeit von 2.5±0.82 auf ca. 3.5 MPa führte.

Seit einigen Jahren geht der Trend der Knochenzementforschung immer stärker in Richtung von Magnesiumphosphatzementen, da diese - verglichen mit Calciumphosphat basierten Formulierungen - ein erhöhtes Degradationspotential, eine hohe initiale Festigkeit, sowie die Freisetzung biologisch wertvoller Magnesiumionen aufweisen. Jedoch stellen gängige Systeme hohe Anforderungen bei der Verwendung in nicht-klassischen Zementformulierungen wie unter anderem der Bedarf an Fremdionen (Ammoniumionen bei Struvit, $NH_4MgPO_4 \cdot 6H_2O$) und die saure (Newberyit) sowie schnelle Abbindereaktion. Dennoch war es möglich, eine chelatisierende, Magnesiumphosphatzement basierte Paste zu entwickeln, welche ein breites Spektrum an möglichen Anwendungsformen bot (Kapitel 3.2; *Magnesium phosphate cement based approaches*).

In Kapitel 3.2.1 (*Chelate bonding mechanism in a novel magnesium phosphate cement*) wurde dabei in einer Machbarkeitsstudie untersucht, ob das neue Abbindeprinzip grundsätzlich funktioniert. Die entsprechende Zementpaste bestand aus Farringtonit ($Mg_3(PO_4)_2$) und unterschiedlich konzentrierter Phytinsäurelösung ($C_6H_{18}O_{24}P_6$). Diese sollte mit durch das Rohpulver freigesetzten Magnesiumionen komplexieren. Zusätzlich zur Chelatisierung führten hohe Phytinsäurekonzentrationen von maximal 30 % zu einer gleichzeitigen Lösungs-Fällungs-Reaktion von geringen Mengen an Newberyit. Das Produkt wies eine Druckfestigkeit von bis zu 65 MPa auf. Durch Anpassung der Phytinsäurekonzentration (20 bis 25 %ige wässrige Lösung bei einem Pulver-zu-Flüssigkeits-Verhältnis von 2.0 g/mL) und Zugabe von Magnesiumoxid (MgO) als Abbindemodulator (6 bis 7.5 % MgO) wurden bohrbare Formulierungen mit einer Schraubenausrisskraft von bis zu 148 N erhalten (Kapitel 3.2.2; *In vitro study of a degradable & drillable farringtonite based bone cement)*. Neben der Bohrbarkeit sind auch adhäsive Eigenschaften der Zemente im feuchten Milieu klinisch von hohem Interesse,

wobei kommerziell erhältliche Formulierungen zumeist nicht bioabbaubar sind. Im anschließenden Kapitel 3.2.3 (*A mineral cement for the application as bone and metal adhesive agent*) wurde daher sowohl die *ex vivo* als auch *in vitro* Langzeit-Klebehaftung (7 d) des vorab vorgestellten Magnesiumphosphatzements unter nassen Bedingungen auf Knochen und sandgestrahlten Edelstahloberflächen analysiert. Es ergaben sich Abscherfestigkeiten von 0.8 beziehungsweise 1.7 MPa, der minimale, durch die Fachliteratur geforderte Wert der Abscherfestigkeit liegt bei 0.2 MPa. Des Weiteren zeigten die ausgehärteten Zementproben einen Masseverlust von 2 Gew.% innerhalb von 24 d in wässriger Umgebung, sowie die Freisetzung von 0.17 mg/g an osteogenen Magnesiumionen pro Tag. Zusammen mit der bestätigten Zytokompatibilität bezüglich humaner fetaler Osteoblasten bei angemessener Verdünnung des Eluats (Kapitel 3.2.2), scheint dieses Zementsystem vielversprechende Eigenschaften für die Anwendung als abbaubarer Biozement für unterschiedliche klinische Zwecke zu besitzen. Beide Anwendungsformen als bohrbare Zemente sowie als Knochenkleber verfügen über einen hohen Neuheitsgrad auf dem Gebiet mineralischer Knochenzemente.

7. Experimental section

The following Table 32 gives an overview about the performed experiments which will be described in detail in the subsequent sections.

Table 32: Summary of the different projects and applied characterization methods which form the basis of the present thesis. The ♦ marked project was a collaboration with the Department of Mineralogy, Erlangen.

No.	cement type		application form	composition
Project 1A	CPC	dual setting	1) setting kinetics ♦ 2) drillable cement	solid phase: α-TCP & APS liquid phase: 2-HEMA, Na_2HPO_4 & water
characterization methods: 1) 4-point bending test & SEM of fractured samples ♦ 2) injectability & initial setting time, 4-point bending test & screw pull-out test, XRD & SEM of fractured surfaces, BET surface area				
Project 1B	CPC	premixed	bone wax	solid phase: TTCP, DCPA, Na_2HPO_4, NaH_2PO_4, (pregelatinized starch & vancomycin hydrochloride) liquid phase: PEG 1,500 & PEG 400
characterization methods: cohesiveness & sealing ability, compressive strength, porosity & BET surface area, mass loss; FTIR, ICP-MS & pH development of PBS supernatant; FTIR, XRD & SEM of fractured surfaces, antibiotics release & agar diffusion test				
Project 1C	CPC	premixed	prefabricated laminates (proof-of-principle)	solid phase: electrospun PCL scaffolds & α-TCP liquid phase: cement paste from bio-cement D, synthetic triglyceride & surfactants (provided by InnoTERE)
characterization methods: contact angle & SEM of PCL scaffolds, 4-point bending test, SEM of fractured surfaces				
Project 2	MPC	magnesium binding	1) proof-of-principle 2) drillable cement 3) bone adhesive	solid phase: $Mg_3(PO_4)_2$ (& MgO) liquid phase: phytic acid solution
characterization methods: 1) temperature & pH while setting, initial setting time, compressive strength; FTIR; XRD & SEM of fractured samples 2) temperature, pH & FTIR while setting; compressive strength & screw pull-out test; porosity, mass loss, ICP-MS & pH development of PBS supernatant, XRD & SEM of fractured samples, cytocompatibility 3) surface roughness of diverse bonding surfaces, compressive & shear strength, XRD of fractured samples, SEM & EDS of ancient bonding surfaces from bovine bone				

7.1 Raw powder synthesis

Project 1A/C

α-$Ca_3(PO_4)_2$ (α-TCP) was synthesized *via* sintering a 2.15:1 molar ratio of $CaHPO_4$ (monetite, DCPA, J.T.Baker, Griesheim, Germany) and $CaCO_3$ (calcium carbonate, Merck, Darmstadt, Germany) for 5 h at 1400 °C in a sintering furnace (Oyten Thermotechnic, Oyten, Germany). The sintering cake was crushed, sieved <355 µm and milled for 4 h in a planetary ball mill (Retsch, Haan, Germany) at 200 rpm.

Project 1B

1.05 mol monetite was heated with 1 mol $CaCO_3$ for 5 h at 1500 °C in a sintering furnace to form $Ca_4(PO_4)_2O$ (TTCP) in a solid state reaction. The sintering product was crushed, sieved <125 µm and milled for 10 min at 200 rpm in a planetary ball mill. Monetite was milled wetly in ethanol for 24 h at 250 rpm and dried under vacuum whereat 30.0 g of it were blended with 74.2 g of the above synthesized and conditioned TTCP for 20 min at 100 rpm (TTCP/DCPA raw powder).

Starch from corn (food grade, Frießinger Mühle, Bad Wimpfen, Germany) was gelatinized in ultrapure hot water with a PLR of 1/6 g/mL. Afterwards, the same amount of ethanol was added and the mixture was filtered and dried at RT. The so-called pregelatinized starch was crushed and sieved <125 µm.

Project 1C

The raw powder mixture for biocement D (60 % α-TCP, 26 % DCPA, 10 % $CaCO_3$, 4 % precipitated $Ca_5(PO_4)_3OH$ (HA)) was prepared by InnoTERE, Radebeul, Germany.

Project 2

A 2:1 molar mixture of $MgHPO_4 \cdot 3H_2O$ (newberyite, Sigma Aldrich, Steinheim, Germany) and $Mg(OH)_2$ (brucite, Sigma Aldrich, Steinheim, Germany) was sintered for 5 h at 1050 °C in a sintering furnace to gain $Mg_3(PO_4)_2$ (farringtonite) in a solid state reaction. The product was crushed with a pestle and mortar, sieved <355 µm and milled in a planetary ball mill for 1 h at 200 rpm.

MgO (Magnesia 291, Magnesia, Lüneburg, Germany) was tempered at 1500 °C for 6 h in a sintering furnace to reduce its reactivity. The sintering cake was crushed and sieved <355 µm and milled in a planetary ball mill for 2 h at 200 rpm.

7.2 Further preliminaries and characterization techniques

7.2.1 Melt electrospinning writing (MEW)

Project 1C

Melt electrospinning written PCL-scaffolds (50x50 mm) from Purac PCL (PURASORB PC12, Corbion, Amsterdam, Netherlands) with box-shaped structure (fiber space: 200, 500 or 1000 µm; fiber diameter: 8 µm; layer number: 30) were kindly provided by Gernot Hochleitner.

7.2.2 Perforated solution electrospinning (SES)

Project 1C

306 mg Purac PCL (20 %, PURASORB PC12, Corbion, Amsterdam, Netherlands) was dissolved in 800 µL dichlormethane, 200 µL ethanol was added to this solution and stirred for at least 5 min. The polymer solution was transferred into a 1 mL syringe which was placed on a syringe pump (11Plus, Harvard Apparatus, Holliston, Massachusetts, USA). Solution electrospinning was performed with a blunt 27 G stainless steel cannula and a pumping speed of 0.5 mL/h. A high voltage of 12 kV (PS 2403D power supply, Voltcraft, Conrad, Hirschau, Germany) was applied at the spinneret tip and charged threads of the polymer solution were deposited on a rotating, grounded collector (Ø 80 mm) with the following perforation characteristics: round holes in shifted rows with a hole diameter of 1 mm, a hole distance of 2 mm and a hole depth of 1 mm. The perforated plate was purchased from Dillinger Fabrik gelochter Bleche (Dillingen, Germany). After the spinning process, the scaffolds were relieved from the collector with water, dried in air, and cut into 50x50 mm square pieces.

7.2.3 Surface treatment & contact angle measurement

Project 1C

The SES scaffolds were each incubated in 1.0 or 2.0 M NaOH for 10, 30 or 60 min under shaking (50 rpm) at RT. The NaOH-to-area ratio was 1 mL/cm². Afterwards, the scaffolds were washed thrice in the same amount of water at 50 rpm and RT for 5 min, (dried with compressed air) and additionally dried overnight at RT. Contact angle of the scaffolds was measured with the system OCA20 (Dataphysics, Filderstadt, Germany) using a dispense dosage of 3 µL and a dosing rate of 1.0 µL/s. Each measurement was performed thrice on the smooth surface (drop above pore and between pores).

7.2.4 Sandblasting & surface roughness

Project 2

Bovine bone (cortical, femur) slices (3x10x20 mm) were ground with SiC-paper (grit P80, Schmitz-Metallographie, Herzogenrath, Germany). Stainless steel (XCrNi18, no. 1.4301) and titanium slices (grade 2, no. 3.7035) of 1x10x20 mm dimensions were sandblasted [21] for 20 s with Korox 50, Korox 110 or Korox 250 at 3 bar with a distance of 20 mm (Basic Quattro, Renfert, Hilzingen, Germany). The surface roughness was measured using the roughness tester SJ-201 (Mitutoya, Oberndorf, Germany) with a cutoff length of 0.8 mm, a total length of 40 mm, a scan speed of 0.25 mm/s and a resolution of 0.01-0.04 µm. The scanning tip was a 5 µm diamond and each sample of bone, smooth as well as rough stainless steel (n=3) was scanned thrice. The output parameters were the arithmetic average of absolute values R_a, the root mean squared R_q, the maximum height of the profile R_y and the average distance between the highest peak and the lowest valley in each sampling length R_z.

[21] Sandblasting was performed by Markus Meininger.

7.3 Cement preparation

Project 1A

For the solid phase of the cement paste, α-TCP was mixed with 0.5 % APS (Sigma Aldrich, Steinheim, Germany). For the liquid phase; 10, 25 or 50 % 2-HEMA (Sigma Aldrich, Steinheim, Germany), 2.5 % Na_2HPO_4 (Merck, Darmstadt, Germany) and 0.25 % TEMED were dissolved in water. The solid and the liquid phase were mixed in a PLR of 1.6, 1.8, 2.0 and 3.0 g/mL for 30 s on a glass slab. For reference samples, pure α-TCP was mixed with 2.5 % Na_2HPO_4 aqueous solution in a PLR of 2.0 or 3.0 g/mL, respectively.

For the fabrication of phase pure CDHA (reference for quantitative XRD evaluation), 100 g α-TCP was stirred for 7 d in 1.03 L of 0.07 % Na_2HPO_4, filtered and dried at 60 °C.

Project 1B

The TTCP/DCPA powder mixture was supplemented with 20 % NaH_2PO_4 and 0, 1.0 or 10 wt.% of previously pregelatinized starch and blended with a PEG melt in a PLR of 5 g per 3 g. The PEG itself was a 4:1 weight blend from PEG 1,500 and PEG 400 (Sigma Aldrich, Steinheim, Germany). The cooled wax formulations were homogenized by softening and kneading.

Project 1C

A premixed cement paste was kindly provided by InnoTERE, Radebeul, Germany. It consisted of the biocement D raw powder mixture and contained quantitative amounts of a water-immiscible synthetic triglyceride (Mygliol 812, Caesar&Loretz, Hilden, Germany) and a mixture of two surface reactants (castor oil ethoxylate 35, BASF, Ludwigshafen, Germany and haxadecyl phosphate, Brenntag AG, Mülheim, Germany).

1.5 g of the cement paste was evenly smeared with a spatula on a weight paper (50x50 mm). A PCL scaffold was pressed onto the cement layer and a second layer was smeared evenly on top. This procedure was repeated until 3 to 7 layers of PCL scaffolds have been laminated with a last cement paste layer on top. In the case of melt electrospinning written scaffolds, excess cement of each layer was removed by exfoliation with a sheet of aluminum foil. Each additional cement layer had a weight of about 1.5 (melt electrospinning written scaffolds) or 2.0 g (perforated solution electrospun scaffolds), respectively. Finally, α-TCP was sieved through a 300 µm sieve on top of the laminate and spread, so that all oil residues on top were covered evenly. The laminate was separated from the weight paper and the backside was treated with raw powder as previously described. Excess of raw powder was removed *via* compressed air.

Project 2

Farringtonite was manually blended with 0, 6.0, 6.8 or 7.5 wt.% highly active MgO (Magnesia 2933, Magnesia, Lüneburg, Germany) and mixed with 10, 20, 22.5, 25 or 30 % phytic acid solution (Sigma Aldrich, Steinheim, Germany) in a PLR of 2.0 or 3.0 g/mL, respectively. The mixture was homogenized for 30 s on a glass slab. The following reference pastes were prepared accordingly: $Mg_3(PO_4)_2$ with 2.0 M phosphoric (Merck, Darmstadt, Germany) and 0.5 M citric ($C_6H_8O_7 \cdot H_2O$, Sigma Aldrich, Steinheim, Germany) acid in a PLR of 2.0 or 3.0 g/mL, respectively; an equimolar mixture of $Mg_3(PO_4)_2$ and $Ca(H_2PO_4)_2$ (MCPA, Buden-

heim, Budenheim, Germany) with 0.5 M citric acid in a PLR of 3.0 g/mL and a blend of $Mg_3(PO_4)_2$ with 15 wt.% dead-burnt MgO 291 with 2.5 M DAHP/1.0 M ADHP ($(NH_4)_2HPO_4/NH_4H_2PO_4$, Merck, Darmstadt, Germany) solution in a PLR of 2.0 g/mL.

7.4 Setting behavior of the cement pastes

7.4.1 Temperature and pH development

Project 2

The temperature and pH profiles of the first 30 to 60 min of the setting reaction were measured every 5 s *via* a K202 Datalogger thermometer (Voltcraft, Conrad, Hirschau, Germany) and every 60 s *via* a surface electrode (inoLab® pH Level 2, WTW, Weilheim, Germany), respectively (n=3).

7.4.2 Injectability

Project 1A

The cement paste was manually injected trough a syringe without needle from 60 s after mixing on and its injectability was monitored every 30 s to determine the time it was injectable for. On the other hand, the required injection force was automatically monitored *via* compressive test setup. For the automatic setup, a 5 mL syringe both with and without a 14 G needle filled with cement paste from 5 g raw powder was fixed in a universal testing machine Z010 (Zwick, Ulm, Germany), loaded with a 2.5 kN cell, and the paste was extruded with a crosshead speed of 30 mm/min. Extrusion started 150 s after mixing of the cement paste. The percentaged mass of extruded cement paste was calculated (n=3).

7.4.3 Setting time

Project 1A/2

According to ASTM standard, the initial setting times of the cement pastes were analyzed *via* Gilmore needle test setup in a humidity chamber at >90 % humidity and 37 °C with a needle of 113.98 g and a 2.117 mm diameter (n=3).

7.4.4 Cohesiveness

Project 1B

Cuboidal samples with 6x6x12 mm dimensions were kneaded, deposited in petri dishes with 5 mL ultrapure water and their cohesiveness was evaluated subjectively. Additionally, their wet compressive strength was measured after 24 h setting in water with a universal testing machine, a crosshead speed of 1 mm/min and a 2.5 kN load cell.

7.4.5 Sealing ability

Project 1B

Suwanprateeb *et al*. [554] proposed a simple test setup for the quantification of the liquid sealing ability of bone waxes [554], which was reproduced in the present work. Acrylic glass tubes (length: 2.00 m, inner diameter: 3 mm; KUSKunststofftechnik, Recklinghausen, Germany) were filled with 1.91 m (systolic blood pressure conditions; 18.68 kPa, 140 mm Hg) of

dyed ultrapure water. The undermost openings were sealed each with 0.3 g of cone-shaped bone wax (n=3). The locked tubes were kept at RT and monitored until leakage.

7.4.6 Fourier-transform infrared spectrometer (FTIR)

Project 2

For further observation of the setting reaction, the cement pastes were directly transferred onto the attenuated total reflexion (ATR) unit of the Fourier-transform infrared spectrometer (FTIR, Nicolet is10, Thermo Fisher Scientific, Waltham, Massachusetts, USA) and measured with a scan number of 16 and a resolution of 4 from 4000 to 650 cm^{-1}. An FTIR spectrum was recorded in the 1st minute and every 10 min afterwards (n=1).

7.5 Mechanical testing

7.5.1 Compression test setup

Project 1B/2

In the case of a waxy consistency of the cement formulation, testing cuboids (6x6x12 mm) were kneaded (n=6). In the case of a paste-like consistency, the cements were directly transferred into silicone rubber molds with the as-mentioned dimensions and stored for 1 h at 37 °C and >90 % humidity (n=12). After demolding, they were covered with ultrapure water and stored at 37 °C for 24 h or 7 d or they were all immersed in 5 mL PBS (8.0 g/L NaCl, 1.1 g/L Na_2HPO_4; Sigma Aldrich, Steinheim, Germany; 0.2 g/L KCl, 0.2 g/L KH_2PO_4; Merck, Darmstadt, Germany) per sample and kept there for 24 d at 37 °C. The solution was changed every second day and set aside.

Wet mechanical behavior of the samples in a compression test setup was measured using a universal testing machine with a crosshead speed of 1 mm/min and a 2.5 kN load cell initially and after 24 h, 2 d, 6 d, 7 d, 12 d, 18 d and 24 d of setting in PBS or water, respectively. Before, the cuboids were ground with SiC sand paper (grit P500, Schmitz-Metallographie, Herzogenrath, Germany) if needed. For initial mechanical testing, the samples were directly analyzed after demolding. For the 7 d deposition in PBS, the buffer was changed twice. The compressive strength σ_C (MPa) was calculated according to Equation (23).

$$\sigma_C = \frac{F_{max}}{A}; \quad A = a \cdot b \tag{23}$$

F_{max} (N) is the maximum occurring force and A (mm²) is the cross-sectional area orthogonally to the force, calculated from the sample height a (mm) and the sample width b (mm).

7.5.2 4-point-bending test setup

Project 1A/C

In case of dual setting systems and premixed reference, the paste was transferred into silicone rubber molds (3x4x45 mm), demolded after 1 h at 37 °C and >90 % humidity and stored in water at 37 °C for 2 h, 4 h, 6 h, 12 h, 24 h, 2 d and 7 d since paste preparation. In case of prefabricated laminates, they were cut into rods with 4x45 mm dimensions *via* two parallel cutter blades (n=10), stored for 24 h at 37 °C and >90 % humidity and finally retained underwater for another 24 h at 37 °C. Force-displacement curves were recorded in a 4-point-bending test setup on a universal testing machine with a crosshead speed of 1 mm/min and a 2.5 kN load cell and used to calculate bending strength σ_b (MPa) and bending modulus E (MPa) as follows (Equation 24-25):

$$\sigma_b = \frac{3 \cdot l_A \cdot F_{max}}{b \cdot a^2} \quad \textbf{(24)}$$

$$E = \frac{3 \cdot l_A \cdot l_B^2 \cdot (F_H - F_L)}{4 \cdot X \cdot b \cdot a^3} \quad \textbf{(25)}$$

where l_A=10 mm is the span length, l_B=20 mm the length of the reference bar, F_{max} (N) is the maximum occurring force, F_H (N) is the end and F_L (N) the beginning force of the bending modulus calculation, X (mm) is the bar bending, b (mm) is the bar width and a (mm) is the bar height. The areas under stress-displacement-curves were calculated as a measure for material toughness.

7.5.3 Screw pull-out test setup

Project 1A/2

For evaluation of the drillability, surgical screws (Ø3.5 mm titanium cortex screws, length: 24 mm, self-tapping, Synthes, Umkirch, Germany) were either embedded into a cylindrical cement matrix (16x20 mm) or the cement cylinders were tapped and drilled 10-15 min after mixing. After 24 h or 2 d of storage in water or PBS at 37 °C, the screws were pulled out of the cement matrix *via* axial force by universal testing machine, a crosshead-speed of 1 mm/min and a 10 kN load cell (n=10).

7.5.4 Shear test setup

Project 2

A disc-shaped silicone rubber mold (2x5 mm) was fastened onto a bovine bone slice (3x10x20 mm) and filled with the as-prepared cement paste. After 10 min, the disc was demolded and directly stuck on the bone surface. The same preparation method was used on smooth stainless steel slices as well as ground stainless steel and titanium slices (1x10x20 mm). The shear force as a measure for adhesiveness (n=5) was tested *via* universal testing machine with a crosshead speed of 1 mm/min and a 2.5 kN load cell in the dry state in air after fabrication (initial adhesiveness) and after further deposition for 24 h or 7 d in PBS at 37 °C. For the 7 d deposition in PBS, the buffer was changed twice. When the samples dropped off before measurement, the shear strength was set 0, when the samples dropped off because of the net weight (66.23 g) of the stamp, this weight was taken into account for further shear strength calculations. For all other samples, the net force F_0 (N) of the

stamp was added to the maximum force F_{max} (N) and consequently included in shear strength σ_s (MPa) calculations (Equation 26).

$$\sigma_s = \frac{F_{max} + F_0}{A}; \quad A = \frac{1}{4} \cdot \pi \cdot d^2 \tag{26}$$

A (mm²) is the circular contact area between the cement and the different surfaces and is calculated on the basis of the circle diameter d (mm).

7.6 Prolonged immersion study

In case of wax-like cements, cuboidal samples with a 6x6x12 mm geometry were kneaded and in the case of cement pastes, the pastes were directly transferred into cuboidal silicone rubber molds of the above dimensions and allowed to harden for 1 h at 37 °C and >90 % humidity. All cuboids were demolded, if needed, transferred into 5 mL PBS each and stored for up to 24 d at 37 °C with a PBS change every second day.

7.6.1 Porosity

Project 1B/2

The final porosity Φ (%) of the cement cuboids (n=3) was calculated referring to literature [643] (Equation 27):

$$\Phi = \frac{m_w - m_d}{\rho \cdot V} \cdot 100\% \tag{27}$$

whereat m_w (g) is the wet and m_d (g) the dry mass after 24 d of immersion in PBS, ρ (g/cm³) is the density of PBS at 37 °C and V (cm³) the volume of the analyzed cuboid.

Project 1B

Further, mercury porosimetry (PASCAL 140/440, Porotec GmbH, Hofheim, Germany) was performed to compare initial and final porosity, pore size distribution and pore volume of freeze-dried samples (n=1) [22].

7.6.2 Specific surface area

Project 1A/B

Specific surface area of the dried and crushed samples was measured with the TriStar surface area and porosity analyzer (Micromeritics, Norcross, Georgia, USA) *via* Brunauer-Emmet-Teller (BET) method (n=1).

[22] Mercury porosimetry was performed by Martha Schamel.

7.6.3 Mass loss

Project 1B/2

Every second day, the current mass of the samples (n=3) was analyzed with an analytical balance (Explorer, OHAUS Corporation, Parsippany, New Jersey, USA). The residual mass $m_{\%}$ (%) is described as follows (Equation 28):

$$m_{\%} = \frac{m_c}{m_i} \cdot 100\% \quad \textbf{(28)}$$

whereat m_c (mg) is the current and m_i (mg) the initial mass. Due to the different setting mechanisms of the waxy and pasty cement formulations, the initial mass for waxy systems was set at day 2 and the initial mass for pasty systems was set at day 0.

7.6.4 FTIR

Project 1B

Each 10 µL of PBS supernatant was analyzed with the FT-IR spectrometer *via* ATR mode. Adjusted parameters were a wave number range of 4000 to 650 cm^{-1}, a scan number of 16 and a resolution of 4 (n=1). FTIR analysis was further performed on dry hardened and crushed specimens under the same conditions (n=1).

7.6.5 Inductively coupled plasma mass spectrometry (ICP-MS)

Project 1B/2

The PBS supernatants were analyzed with respect to released calcium (Ca 44 isotope), magnesium (Mg 24 isotope) and phosphate (P 31 isotope) ions (n=3). The occurring concentrations were measured with a mass spectrometer with inductively coupled plasma (ICP-MS, Varian, Darmstadt, Germany) by means of standard solutions (5 mg/L, 10 mg/L, ICP standard solutions).

7.6.6 pH development

Project 1B/2

The pH values of PBS supernatants (n=3) were followed with the pH meter (inoLab® pH Level 2, WTW, Weilheim, Germany).

7.7 X-ray diffractometry

Project 1A/B/2

X-ray diffraction (XRD) patterns of the dry hardened and crushed cement samples were recorded on a diffractometer (D5005, Siemens, Karlsruhe, Germany) with Cu-K_α radiation and the following parameters: a voltage of 40 kV, a current of 40 mA, a 2 theta range from 20 to 40 °, a step size of 0.02 ° and a scan rate of 1.5 or 12 s/step (n=1). The patterns were compared with JCPDS (The Joint Committee on Powder Diffraction Standards) references. Table 33 gives an overview about the reference diffractograms used for comparison.

Table 33: PDF (powder diffraction file)-numbers of reference spectra used for XRD pattern evaluation.

mineral compound	chemical formula	PDF-number
α-TCP	α-$Ca_3(PO_4)_2$	29-0359
CDHA	$Ca_9(PO_4)_5(HPO_4)(OH)$	46-0905
DCPA	$CaHPO_4$	09-0080
DCPD	$CaHPO_4 \cdot 2H_2O$	09-0077
farringtonite	$Mg_3(PO_4)_2$	33-0876
HA	$Ca_{10}(PO_4)_6(OH)_2$	09-0432
newberyite	$MgHPO_4 \cdot 3H_2O$	35-0780
struvite	$NH_4MgPO_4 \cdot 6H_2O$	15-0762
TTCP	$Ca_4(PO_4)_2O$	25-1137
sodium magnesium phosphate	$NaMg_4(PO_4)_3$ [23]	/

Project 1A/B

The Scherrer Equation (Equation 29) was used to estimate the length l (nm) of the crystals [644]:

$$l = \frac{k \cdot \lambda}{FWHM(2\theta) \cdot \cos\theta} \quad \textbf{(29)}$$

whereat k (0.9) is the shape factor, λ is the wave length of Cu-K_α radiation (0.154 nm) and $FWHM$ (radian) the full width at half maximum at a diffraction angle 2θ of 26 °.

Project 1A

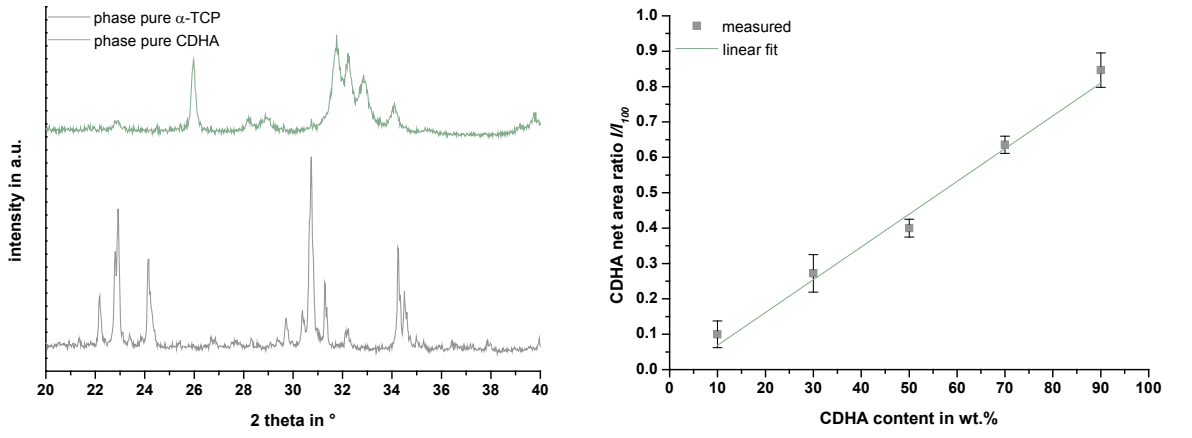

Figure 57: XRD of phase pure CDHA and α-TCP (a) and calibration curve i.e. correlation of the ratio of diffraction reflex net areas at a diffraction angle of 26.0 ° with corresponding composition (CDHA weight fraction) (b).

As a measure for the conversion from the educt to the product, the ratio of diffraction reflex net areas at a diffraction angle 2 theta of 26.0 ° of CDHA in the 2-component mixture of unknown composition I and of a 100 % pure CDHA powder I_{100}, i.e. I/I_{100}, was calculated and compared with a linear calibration slope (Figure 57 b). Thus, mixtures of known composition from phase pure (Figure 57 a) α-TCP and CDHA (10/90, 30/70, 50/50, 70/30, 90/10; in wt.%) were recorded on the diffractometer with the as-mentioned parameters (n=3) and the ratios

[23] This compound was revealed by Katrin Hurle, Department for Mineralogy, Erlangen.

I/I_{100} were calculated and correlated with the corresponding composition in accordance to Alexander and Klug [645]. Linear alignment of the measured data revealed the following Equation 30:

$$I/I_0 = 0.009 \cdot f_{CDHA} - 0.024 \quad \textbf{(30)}$$

f_{CDHA} is the CDHA weight fraction and R^2 was calculated to be 0.976.

7.8 Scanning electron microscopy & energy dispersive X-ray spectroscopy

Beside bovine bone slices and pure fiber meshes, small fragments (n=1) from mechanical tests were used for scanning electron microscopy (SEM). Samples without special pre-treatment were dried at 40 °C for at least 24 h.

7.8.1 Critical point drying & freeze drying

Project 2

The bone slices were put into corresponding acetone dilution with ultrapure water (30, 50, 70, 90 and 6x100 %) and the vessels were shaken each for 1 h at 50 rpm. They were stored in 100 % acetone until super-critical drying. For this purpose, the device CPD 030 (Bal-Tec, Balzers, Liechtenstein) was used. Firstly, the acetone was exchanged by liquid CO_2 at a temperature of 6 to 11 °C. The exchange cycle was repeated 10 times. Afterwards, the CO_2 sublimated at 41 to 42 °C.

Project 1A

Fragments of hydrogel containing cement formulations were freeze-dried before coating. Lyophylization was performed using the freeze-dryer Alpha 1-2 LD (Martin Christ Gefriertrocknungsanlagen, Osterode, Germany).

7.8.2 Sputter coating

all

Coarse samples were stuck on special SEM specimen holders *via* conductive paste Leit-C (Plano, Wetzlar, Germany) and light samples *via* conductive stickers. The samples were then coated with a 4 nm (8 min) thick layer of (gold or) platinum, respectively. Therefore, the sputter device (Emitech K550, Quorum Technologies, Guelph, Ontario, Canada or) Leica EM ACE600 (Leica Microsystems, Wetzlar, Germany) was used.

7.8.3 Scanning electron microscopy

all

The morphology of the samples was analyzed by SEM DSM 940 (Zeiss, Oberkochen, Germany) or crossbeam SEM CB 340 (Zeiss, Oberkochen, Germany) with an acceleration voltage of 2.0 to 5.0 kV *via* detection of secondary electrons.

7.8.4 Energy dispersive X-ray spectroscopy

Project 2

Energy dispersive X-ray spectroscopy (EDS) was performed with an INCA Energy 350 Az-Tec Advanced system using a silicon drift detector (Oxford Instruments, Abingdon, UK) for element mapping with a resolution of 512, 10 frames, a process time of 4, a pixel retention time of 10 µs, a 60 µm slit, a high voltage of 20 kV, a work distance of 5 mm and a 64-fold magnification. For semi-quantitative evaluations of corresponding Ca-to-Mg-ratios, the percentaged amount of Ca and Mg was calculated on the basis of the border EDS element maps. For each region (bone, adherend), three ellipsoid sectors were analyzed each.

7.9 Biological properties

7.9.1 Antibiotics release

Project 1B

Bone wax samples (6x6x12 mm) were prepared as described above, but supplemented with 1.24 wt.% vancomycin hydrochloride (Hikma Pharma, Gräfelfing, Germany) referred to the powder phase. Each 3 cuboids were immersed for 24 d in 5 mL PBS at 37 °C. The solution was renewed after 2 h, 4 h, 6 h, 8 h, 24 h, 2 d, 3 d, 4 d and later on every second day. By means of UV-Vis spectroscopy (GENESYSTM 10S, Thermo Scientific, Waltham, Massachusetts, USA) the released vancomycin amount was evaluated from the absorption at 281 nm. The cumulative release was fitted with the aid of the Korsmeyer–Peppas model [87] (Equation 31):

$$M_t/M_\infty = K \cdot t^n; \quad M_t < 0.6 \cdot M_\infty \tag{31}$$

M_t is the amount of released drug after time t, M_∞ is the amount of released drug after an infinite time, K is a geometric factor and n the release exponent.

7.9.2 Agar diffusion test

Project 1B

20 µL of a glycerin culture from gram positive bacterium *S. aureus* (strain RN 4220) was dispersed in 10 mL LB (lysogeny broth)-medium (0.5 % yeast extract, Becton, Dickinson and Company, Sparks, Maryland, USA; 1.0 % Trypton, AppliChem, Darmstadt, Germany; 0.5 % NaCl, Sigma Aldrich, Steinheim, Germany), shaked overnight at 250 rpm and 37 °C and each 100 µL were plated onto agar plates (diameter: 100 mm, height: 3 mm; LB-medium with 1.5 % agar, AppliChem, Darmstadt, Germany). To test the antibacterial activity of the vancomycin laden waxes, discs (n=3) à 2x12 mm were kneaded and put onto those agar plates which were consecutively stored at 37 °C. After each 24 h and up to day 6, the discs were changed over new agar plates with fresh overnight culture. The forming inhibition zones (bacteria free diameter minus sample diameter) were measured daily.

7.9.3 Cytocompatibility

Project 2

The cement pastes were transferred into disc-shaped (2x15 mm) silicone rubber molds, stored at 37 °C and >90 % humidity for 1 h, demolded and dried for at least 24 h. Afterwards, the samples were disinfected each for 1 h in 70 % ethanol. The samples were immersed in 1 mL/disc Dulbeccos's Modified Eagle's Medium (DMEM) with 1 % penicillin/streptomycin, 0.3 mg/mL geneticin (G-418) sulfate and 10 % fetal calf serum at 34 °C and 5 % CO_2. The liquid-to-sample volume ratio was four times lower compared to the prolonged immersion study. The medium was renewed every second day and centrifuged for 5 min at 4,700 rpm (Mega Star 1.6 R, VWR, Radnor, Pennsylvania, USA). Human fetal osteoblast cell line hFOB 1.19 (LGC Standards, Wesel, Germany) was cultivated in the above mentioned medium at 34 °C and 5 % CO_2. 50,000 cells/mL (23,000 cells/cm²) were seeded onto cell culture plastic surfaces of 24-well-plates and cultivated at 34 °C and 5 % CO_2 (n=3). After 24 h of pre-culture, the medium was exchanged and substituted with 100 % or 25 % diluted and centrifuged eluate. The eluate on the cell layer also was exchanged every second day with freshly eluted medium in the same manner. After 4, 6 and 10 d of cultivating the cells with eluted medium, cytotoxicity tests were performed and cells which were cultivated in untreated cell culture medium (polystyrene, PS) were taken as a negative control for cytotoxicity. Cell numbers and cell activities were chosen as a measure to evaluate the cytocompatibility of the different cement surfaces. For cell counting, the cells were detached from the surfaces by means of accutase (Sigma Aldrich, Steinheim, Germany), diluted in Coulter Isoton III Diluent buffer (Beckman Coulter, Krefeld, Germany) and counted automatically via Casy® Cell Counter (Model TT, Roche Diagnostics, Mannheim, Germany). For measurement of the cell activities, the cells were incubated with a 1:10 dilution of the cell proliferation agent WST-1 (Roche Diagnostics, Mannheim, Germany) for 30 min at 34 °C and 5 % CO_2, and the absorption of the supernatant at 450 nm was measured with the photometer SpectraFluor Plus (Tecan, Crailsheim, Germany). The cell culture medium as well as its supplements – if not else described – derived from Gibco® (Fisher Scientific, Schwerte, Germany).

7.10 Statistics

Significant differences ($p<0.001$) were investigated performing a one way analysis of variance (1-way ANOVA) with an all pairwise multiple comparison procedure (Tukey Test) using the software SigmaPlot (Systat Software, Erkrath, Germany), version 12.

Literature

[1] D.F. Farrar, Bone adhesives for trauma surgery: A review of challenges and developments, Int. J. Adhes. Adhes. 33 (2012) 89-97.
[2] C. Schonauer, E. Tessitore, G. Barbagallo, V. Albanese, A. Moraci, The use of local agents: bone wax, gelatin, collagen, oxidized cellulose, Eur. Spine. J. 13(1) (2004) S89-S96.
[3] P.V. Giannoudis, H. Dinopoulos, E. Tsiridis, Bone substitutes: An update, Injury 36(3, Supplement) (2005) S20-S27.
[4] R.Z. LeGeros, Calcium phosphate-based osteoinductive materials, Chem. Rev. 108(11) (2008) 4742-4753.
[5] W.R. Moore, S.E. Graves, G.I. Bain, Synthetic bone graft substitutes, ANZ J. Surg. 71(6) (2001) 354-361.
[6] M. Bohner, Resorbable biomaterials as bone graft substitutes, Mater. Today 13(1–2) (2010) 24-30.
[7] C.J. Damien, J.R. Parsons, Bone graft and bone graft substitutes: A review of current technology and applications, J. Appl. Biomater. 2(3) (1991) 187-208.
[8] J.M. Rueger, J. Hägele, W. Lehmann, A. Rücker, C. Schlickewei, Knochenaufbau – Knochenersatzmaterialien, Z. Orthop. Unfall. 5(05) (2010) 295-314.
[9] C.A.C. Zavaglia, M.H. Prado da Silva, Feature Article: Biomaterials, Reference Module in Materials Science and Materials Engineering, Elsevier2016.
[10] M. Bohner, Calcium orthophosphates in medicine: from ceramics to calcium phosphate cements, Injury 31, Supplement 4(0) (2000) D37-D47.
[11] L.C. Chow, Next generation calcium phosphate-based biomaterials, Dent. Mater. J. 28(1) (2009) 1-10.
[12] S. Dorozhkin, Calcium orthophosphate cements for biomedical application, J. Mater. Sci. 43(9) (2008) 3028-3057.
[13] M. Bohner, U. Gbureck, J.E. Barralet, Technological issues for the development of more efficient calcium phosphate bone cements: A critical assessment, Biomaterials 26(33) (2005) 6423-6429.
[14] B. Wopenka, J.D. Pasteris, A mineralogical perspective on the apatite in bone, Mater. Sci. Eng.: C 25(2) (2005) 131-143.
[15] N. Ostrowski, A. Roy, P.N. Kumta, Magnesium phosphate cement systems for hard tissue applications: A review, ACS Biomater. Sci. Eng. 2(7) (2016) 1067–1083.
[16] J. Wang, C. Liu, Y. Liu, S. Zhang, Double-network interpenetrating bone cement via in situ hybridization Protocol, Adv. Funct. Mater. 20(22) (2010) 3997-4011.
[17] T. Christel, M. Kuhlmann, E. Vorndran, J. Groll, U. Gbureck, Dual setting α-tricalcium phosphate cements, J. Mater. Sci. - Mater. Med. 24(3) (2013) 573-581.
[18] W.-C. Chen, C.-P. Ju, J.-C. Wang, C.-C. Hung, J.-H. Chern Lin, Brittle and ductile adjustable cement derived from calcium phosphate cement/polyacrylic acid composites, Dent. Mater. 24(12) (2008) 1616-1622.
[19] S. Heinemann, S. Rössler, M. Lemm, M. Ruhnow, B. Nies, Properties of injectable ready-to-use calcium phosphate cement based on water-immiscible liquid, Acta Biomater. 9(4) (2013) 6199-6207.
[20] E. Vorndran, M. Geffers, A. Ewald, M. Lemm, B. Nies, U. Gbureck, Ready-to-use injectable calcium phosphate bone cement paste as drug carrier, Acta Biomater. 9(12) (2013) 9558-9567.
[21] S.V. Dorozhkin, Self-setting calcium orthophosphate formulations: Cements, concretes, pastes and putties, Int. J. Mater, Chem. 1(1) (2011) 1-48.
[22] K. Reese, A. Litsky, C. Kaeding, A. Pedroza, N. Shah, Cannulated screw fixation of jones fractures: A clinical and biomechanical study, Am. J. Sports Med. 32(7) (2004) 1736-1742.
[23] S. Doht, T. Lehnert, S. Frey, K. Fehske, H. Jansen, T. Blunk, R. Meffert, Effective combination of bone substitute and screws in the jail technique: a biomechanical study of tibial depression fractures, Int. Orthop. 36(10) (2012) 2121-2125.
[24] G.D. Angelini, F.A. El-Ghamari, E.G. Butchart, Poststernotomy pseudo-arthrosis due to foreign body reaction to bone wax, Eur. J. Cardiothorac. Surg. 1(2) (1987) 129-130.
[25] B.A. Khader, M.R. Towler, Materials and techniques used in cranioplasty fixation: A review, Mater. Sci. Eng.: C 66 (2016) 315-322.
[26] U. Klammert, U. Gbureck, E. Vorndran, J. Rödiger, P. Meyer-Marcotty, A.C. Kübler, 3D powder printed calcium phosphate implants for reconstruction of cranial and maxillofacial defects, J. Craniomaxillofac. Surg. 38(8) (2010) 565-570.
[27] G. Lewis, Alternative acrylic bone cement formulations for cemented arthroplasties: Present status, key issues, and future prospects, J. Biomed. Mater. Res. B: Appl. Biomat. 84B(2) (2008) 301-319.
[28] J.C.J. Webb, R.F. Spencer, The role of polymethylmethacrylate bone cement in modern orthopaedic surgery, J. Bone Joint Surg, Br. 89-B(7) (2007) 851-857.
[29] J.T. Scales, W. Herschell, Perspex in orthopaedics, Br. Med. J. 2(4421) (1945) 423-424.
[30] T. Kindt-Larsen, D.B. Smith, J.S. Jensen, Innovations in acrylic bone cement and application equipment, J. Appl. Biomater. 6(1) (1995) 75-83.
[31] J.A. Dipisa, G.S. Sih, A.T. Berman, The temperature problem at the bone-acrylic cement interface of the total hip replacement, Clin. Orthop. Rel. Res. 121 (1976) 95-98.
[32] I. Khairoun, M.G. Boltong, F.C.M. Driessens, J.A. Planell, Effect of calcium carbonate on clinical compliance of apatitic calcium phosphate bone cement, J. Biomed. Mater. Res. 38(4) (1997) 356-360.
[33] W.E. Brown, L.C. Chow, Dental restorative cement pastes, American Dental Association Health Foundation, 1985.

[34] C. Moseke, U. Gbureck, Tetracalcium phosphate: Synthesis, properties and biomedical applications, Acta Biomater. 6(10) (2010) 3815-3823.
[35] M.P. Ginebra, M. Espanol, E.B. Montufar, R.A. Perez, G. Mestres, New processing approaches in calcium phosphate cements and their applications in regenerative medicine, Acta Biomater. 6(8) (2010) 2863-2873.
[36] S.V. Dorozhkin, Bioceramics of calcium orthophosphates, Biomaterials 31(7) (2010) 1465-1485.
[37] J. Zhang, W. Liu, V. Schnitzler, F. Tancret, J.-M. Bouler, Calcium phosphate cements for bone substitution: Chemistry, handling and mechanical properties, Acta Biomater. 10(3) (2014) 1035-1049.
[38] K. Kuroda, M. Okido, Hydroxyapatite coating of titanium implants using hydroprocessing and evaluation of their osteoconductivity, Bioinorg. Chem. Appl. 2012 (2012) 1-7.
[39] M. Bohner, U. Gbureck, Thermal reactions of brushite cements, J. Biomed. Mater. Res. B: Appl. Biomat. 84B(2) (2008) 375-385.
[40] F. Tamimi, Z. Sheikh, J. Barralet, Dicalcium phosphate cements: Brushite and monetite, Acta Biomater. 8(2) (2012) 474-487.
[41] E. Sahin, M. Ciftcioglu, Monetite promoting effect of NaCl on brushite cement setting kinetics, J. Mater. Chem. B 1(23) (2013) 2943-2950.
[42] G. Cama, B. Gharibi, M.S. Sait, J.C. Knowles, A. Lagazzo, S. Romeed, L. Di Silvio, S. Deb, A novel method of forming micro- and macroporous monetite cements, J. Mater. Chem. B 1(7) (2013) 958-969.
[43] F. Tamimi, J. Torres, C. Kathan, R. Baca, C. Clemente, L. Blanco, E.L. Cabarcos, Bone regeneration in rabbit calvaria with novel monetite granules, J. Biomed. Mater. Res. A 87A(4) (2008) 980-985.
[44] F. Tamimi, D.L. Nihouannen, H. Eimar, Z. Sheikh, S. Komarova, J. Barralet, The effect of autoclaving on the physical and biological properties of dicalcium phosphate dihydrate bioceramics: Brushite vs. monetite, Acta Biomater. 8(8) (2012) 3161-3169.
[45] W.E. Brown, J.P. Smith, J.R. Lehr, A.W. Frazier, Octacalcium phosphate and hydroxyapatite: Crystallographic and chemical relations between octacalcium phosphate and hydroxyapatite, Nature 196(4859) (1962) 1050-1055.
[46] O. Suzuki, Octacalcium phosphate (OCP)-based bone substitute materials, Jpn. Dent. Sci. Rev. 49(2) (2013) 58-71.
[47] Y. Fukase, E.D. Eanes, S. Takagp, L.C. Chow, W.E. Brown, Setting reactions and compressive strengths of calcium phosphate cements, J. Dent. Res. 69(12) (1990) 1852-1856.
[48] M. Zoulgami, A. Lucas, P. Briard, J. Gaudé, A self-setting single-component calcium phosphate cement, Biomaterials 22(13) (2001) 1933-1937.
[49] J. Lemaître, A. Mirtchi, A. Mortier, Calcium phosphate cements for medical use: state of the art and perspectives of development, Silic. Indus. 9-10 (1987) 141-146.
[50] M. Bohner , P. van Landuyt , H.P. Merkle , J. Lemaître Composition effects on the pH of a hydraulic calcium phosphate cement, J. Mater. Sci. - Mater. Med. 8(11) (1997) 675-681.
[51] F. Tamimi, J. Torres, E. Lopez-Cabarcos, D.C. Bassett, P. Habibovic, E. Luceron, J.E. Barralet, Minimally invasive maxillofacial vertical bone augmentation using brushite based cements, Biomaterials 30(2) (2009) 208-216.
[52] R.G. Carrodeguas, S. De Aza, α-Tricalcium phosphate: Synthesis, properties and biomedical applications, Acta Biomater. 7(10) (2011) 3536-3546.
[53] E. Fernández, F.J. Gil, M.P. Ginebra, F.C.M. Driessens, J.A. Planell, S.M. Best, Calcium phosphate bone cements for clinical applications. Part I: Solution chemistry, J. Mater. Sci. - Mater. Med. 10(3) (1999) 169-176.
[54] M. Bohner, G. Baroud, Injectability of calcium phosphate pastes, Biomaterials 26(13) (2005) 1553-1563.
[55] U. Gbureck, O. Grolms, J.E. Barralet, L.M. Grover, R. Thull, Mechanical activation and cement formation of β-tricalcium phosphate, Biomaterials 24(23) (2003) 4123-4131.
[56] U. Gbureck, J.E. Barralet, L. Radu, H.G. Klinger, R. Thull, Amorphous α-tricalcium phosphate: Preparation and aqueous setting Reaction, J. Am. Ceram. Soc. 87(6) (2004) 1126-1132.
[57] M. Bohner, Reactivity of calcium phosphate cements, J. Mater. Chem. 17(38) (2007) 3980-3986.
[58] J. Bae, Y. Ida, K. Sekine, F. Kawano, K. Hamada, Effects of high-energy ball-milling on injectability and strength of β-tricalcium-phosphate cement, J. Mech. Behav. Biomed. Mater. 47 (2015) 77-86.
[59] U. Gbureck, J.E. Barralet, M. Hofmann, R. Thull, Mechanical activation of tetracalcium phosphate, J. Am. Ceram. Soc. 87(2) (2004) 311-313.
[60] M.P. Ginebra, E. Fernández, M.G. Boltong, O. Bermúdez, J.A. Planell, F.C.M. Driessens, Compliance of an apatitic calcium phosphate cement with the short-term clinical requirements in bone surgery, orthopaedics and dentistry, Clin. Mater. 17(2) (1994) 99-104.
[61] M. Komath, H.K. Varma, R. Sivakumar, On the development of an apatitic calcium phosphate bone cement, Bull. Mater. Sci. 23(2) (2000) 135-140.
[62] M.P. Ginebra, M.G. Boltong, E. Fernández, J.A. Planell, F.C.M. Driessens, Effect of various additives and temperature on some properties of an apatitic calcium phosphate cement, J. Mater. Sci. - Mater. Med. 6(10) (1995) 612-616.
[63] M.T. Fulmer, P.W. Brown, Effects of Na2HPO4 and NaH2PO4 on hydroxyapatite formation, J. Biomed. Mater. Res. 27(8) (1993) 1095-1102.
[64] C. Liu, W. Shen, Effect of crystal seeding on the hydration of calcium phosphate cement, J. Mater. Sci. - Mater. Med. 8(12) (1997) 803-807.

[65] M.P. Ginebra, E. Fernández, F.C.M. Driessens, M.G. Boltong, J. Muntasell, J. Font, J.A. Planell, The effects of temperature on the behaviour of an apatitic calcium phosphate cement, J. Mater. Sci. - Mater. Med. 6(12) (1995) 857-860.
[66] M. Bohner, J. Lemaitre, T.A. Ring, Effects of sulfate, pyrophosphate, and citrate ions on the physicochemical properties of cements made of β-tricalcium phosphate-phosphoric acid-water mixtures, J. Am. Ceram. Soc. 79(6) (1996) 1427-1434.
[67] A.A. Mirtchi, J. Lemaître, E. Hunting, Calcium phosphate cements: action of setting regulators on the properties of the β-tricalcium phosphate-monocalcium phosphate cements, Biomaterials 10(9) (1989) 634-638.
[68] F. Tamimi-Mariño, J. Mastio, C. Rueda, L. Blanco, E. López-Cabarcos, Increase of the final setting time of brushite cements by using chondroitin 4-sulfate and silica gel, J. Mater. Sci. - Mater. Med. 18(6) (2007) 1195-1201.
[69] M. Bohner, J. Lemaître, P.V. Landuyt, P.-Y. Zambelli, H.P. Merkle, B. Gander, Gentamicin-loaded hydraulic calcium phosphate bone cement as antibiotic delivery system, J. Pharm. Sci. 86(5) (1997) 565-572.
[70] L.M. Grover, U. Gbureck, A.M. Young, A.J. Wright, J.E. Barralet, Temperature dependent setting kinetics and mechanical properties of β-TCP-pyrophosphoric acid bone cement, J. Mater. Chem. 15(46) (2005) 4955-4962.
[71] J.E. Barralet, L.M. Grover, U. Gbureck, Ionic modification of calcium phosphate cement viscosity. Part II: hypodermic injection and strength improvement of brushite cement, Biomaterials 25(11) (2004) 2197-2203.
[72] F.T. Mariño, J. Torres, M. Hamdan, C.R. Rodríguez, E.L. Cabarcos, Advantages of using glycolic acid as a retardant in a brushite forming cement, J. Biomed. Mater. Res. B: Appl. Biomat. 83B(2) (2007) 571-579.
[73] J.E. Barralet, M. Tremayne, K.J. Lilley, U. Gbureck, Modification of Calcium Phosphate Cement with α-Hydroxy Acids and Their Salts, Chem. Mat. 17(6) (2005) 1313-1319.
[74] K.J. Lilley, U. Gbureck, A.J. Wright, D. Farrar, J.E. Barralet, Investigation into carboxylic acids as cement reactants, Key Eng. Mater. 309-311 (2006) 853-856.
[75] S. Chauhan, M.P. Hofmann, R.M. Shelton, Effect of protein addition on the setting behaviour of a calcium phosphate Cement Key Eng. Mater. 309-311 (2006) 841-844.
[76] S. Meininger, C. Blum, M. Schamel, J.E. Barralet, A. Ignatius, U. Gbureck, Phytic acid as alternative setting retarder enhanced biological performance of dicalcium phosphate cement in vitro, Sci. Rep. 7(1) (2017) 558.
[77] T. Konishi, M. Mizumoto, M. Honda, Z. Zhuang, M. Aizawa, Fabrication of chelate-setting cements from hydroxyapatite powders surface-modified with various sodium inositol hexaphosphate concentrations and their mechanical properties, Procedia Eng. 36 (2012) 137-143.
[78] S. Takahashi, T. Konishi, K. Nishiyama, M. Mizumoto, M. Honda, Y. Horiguchi, K. Oribe, M. Aizawa, Fabrication of novel bioresorbable β-tricalcium phosphate cement on the basis of chelate-setting mechanism of inositol phosphate and its evaluation, J. Ceram. Soc. Jpn. 119(1385) (2011) 35-42.
[79] F. Grases, M. Ramis, A. Costa-Bauzá, Effects of phytate and pyrophosphate on brushite and hydroxyapatite crystallization, Urol. Res. 28(2) (2000) 136-140.
[80] S. Pina, P.M. Torres, F. Goetz-Neunhoeffer, J. Neubauer, J.M.F. Ferreira, Newly developed Sr-substituted α-TCP bone cements, Acta Biomater. 6(3) (2010) 928-935.
[81] U. Klammert, T. Reuther, M. Blank, I. Reske, J.E. Barralet, L.M. Grover, A.C. Kübler, U. Gbureck, Phase composition, mechanical performance and in vitro biocompatibility of hydraulic setting calcium magnesium phosphate cement, Acta Biomater. 6(4) (2010) 1529-1535.
[82] Z. Huan, J. Chang, Novel bioactive composite bone cements based on the β-tricalcium phosphate–monocalcium phosphate monohydrate composite cement system, Acta Biomater. 5(4) (2009) 1253-1264.
[83] P.W. Brown, N. Hocker, S. Hoyle, Variations in solution chemistry during the low-temperature formation of hydroxyapatite, J. Am. Ceram. Soc. 74(8) (1991) 1848-1854.
[84] K.S. TenHuisen, P.W. Brown, Effects of magnesium on the formation of calcium-deficient hydroxyapatite from CaHPO4 · 2H2O and Ca4(PO4)2O, J. Biomed. Mater. Res. 36(3) (1997) 306-314.
[85] S. Sarda, E. Fernández, M. Nilsson, M. Balcells, J.A. Planell, Kinetic study of citric acid influence on calcium phosphate bone cements as water-reducing agent, J. Biomed. Mater. Res. 61(4) (2002) 653-659.
[86] K.S. Tenhuisen, P.W. Brown, The effects of citric and acetic acids on the formation of calcium-deficient hydroxyapatite at 38 °C, J. Mater. Sci. - Mater. Med. 5(5) (1994) 291-298.
[87] M.-P. Ginebra, C. Canal, M. Espanol, D. Pastorino, E.B. Montufar, Calcium phosphate cements as drug delivery materials, Adv. Drug Deliv. Rev. 64(12) (2012) 1090-1110.
[88] A. Ferreira, C. Oliveira, F. Rocha, The different phases in the precipitation of dicalcium phosphate dihydrate, J. Crys. Growth 252(4) (2003) 599-611.
[89] C. Oliveira, P. Georgieva, F. Rocha, A. Ferreira, S. Feyo de Azevedo, Dynamical model of brushite precipitation, J. Crys. Growth 305(1) (2007) 201-210.
[90] A.P. Legrand, H. Sfihi, N. Lequeux, J. Lemaître, 31P Solid-State NMR study of the chemical setting process of a dual-paste injectable brushite cements, J. Biomed. Mater. Res. B: Appl. Biomat. 91B(1) (2009) 46-54.
[91] S. Matsuya, S. Takagi, L.C. Chow, Effect of mixing ratio and pH on the reaction between Ca4(PO4)2O and CaHPO4, J. Mater. Sci. - Mater. Med. 11(5) (2000) 305-311.
[92] K. Hurle, J. Neubauer, M. Bohner, N. Doebelin, F. Goetz-Neunhoeffer, Effect of amorphous phases during the hydraulic conversion of α-TCP into calcium-deficient hydroxyapatite, Acta Biomater. 10(9) (2014) 3931-3941.

[93] T.A. Fuierer, M. LoRe, S.A. Puckett, G.H. Nancollas, A mineralization adsorption and mobility study of hydroxyapatite surfaces in the presence of zinc and magnesium ions, Langmuir 10 (1994) 4721-4725.
[94] E. Boanini, M. Gazzano, A. Bigi, Ionic substitutions in calcium phosphates synthesized at low temperature, Acta Biomater. 6(6) (2010) 1882-1894.
[95] A. Bigi, E. Foresti, M. Gandolfi, M. Gazzano, N. Roveri, Inhibiting effect of zinc on hydroxylapatite crystallization, J. Inorg. Biochem. 58(1) (1995) 49-58.
[96] A. Bigi, G. Falini, E. Foresti, A. Ripamonti, M. Gazzano, N. Roveri, Magnesium influence on hydroxyapatite crystallization, J. Inorg. Biochem. 49(1) (1993) 69-78.
[97] F. Barrere, C.A. van Blitterswijk, K. de Groot, P. Layrolle, Nucleation of biomimetic Ca–P coatings on Ti6Al4V from a SBF×5 solution: influence of magnesium, Biomaterials 23(10) (2002) 2211-2220.
[98] Z.Y. Li, W.M. Lam, C. Yang, B. Xu, G.X. Ni, S.A. Abbah, K.M.C. Cheung, K.D.K. Luk, W.W. Lu, Chemical composition, crystal size and lattice structural changes after incorporation of strontium into biomimetic apatite, Biomaterials 28(7) (2007) 1452-1460.
[99] F. Barrere, C.A. van Blitterswijk, K. de Groot, P. Layrolle, Influence of ionic strength and carbonate on the Ca-P coating formation from SBF×5 solution, Biomaterials 23(9) (2002) 1921-1930.
[100] S. Hesaraki, F. Moztarzadeh, N. Nezafati, Evaluation of a bioceramic-based nanocomposite material for controlled delivery of a non-steroidal anti-inflammatory drug, Med. Eng. Phys. 31(10) (2009) 1205-1213.
[101] U. Gbureck, K. Spatz, R. Thull, J.E. Barralet, Rheological enhancement of mechanically activated α-tricalcium phosphate cements, J. Biomed. Mater. Res. B: Appl. Biomat. 73B(1) (2005) 1-6.
[102] M. Geffers, J. Groll, U. Gbureck, Reinforcement strategies for load-bearing calcium phosphate biocements, Materials 8(5) (2015) 2700-2717.
[103] R. Krüger, J. Groll, Fiber reinforced calcium phosphate cements – On the way to degradable load bearing bone substitutes?, Biomaterials 33(25) (2012) 5887-5900.
[104] J.T. Zhang, F. Tancret, J.M. Bouler, Fabrication and mechanical properties of calcium phosphate cements (CPC) for bone substitution, Mater. Sci. Eng.: C 31(4) (2011) 740-747.
[105] M.P. Hofmann, A.R. Mohammed, Y. Perrie, U. Gbureck, J.E. Barralet, High-strength resorbable brushite bone cement with controlled drug-releasing capabilities, Acta Biomater. 5(1) (2009) 43-49.
[106] C. Pittet, J. Lemaître, Mechanical characterization of brushite cements: A Mohr circles' approach, J. Biomed. Mater. Res. 53(6) (2000) 769-780.
[107] J.E. Barralet, L. Grover, T. Gaunt, A.J. Wright, I.R. Gibson, Preparation of macroporous calcium phosphate cement tissue engineering scaffold, Biomaterials 23(15) (2002) 3063-3072.
[108] U. Gbureck, J.E. Barralet, K. Spatz, L.M. Grover, R. Thull, Ionic modification of calcium phosphate cement viscosity. Part I: hypodermic injection and strength improvement of apatite cement, Biomaterials 25(11) (2004) 2187-2195.
[109] J.E. Barralet, M. Hofmann, L.M. Grover, U. Gbureck, High-strength apatitic cement by modification with α-hydroxy acid salts, Adv. Mater. 15(24) (2003) 2091-2094.
[110] A.J. Wagoner Johnson, B.A. Herschler, A review of the mechanical behavior of CaP and CaP/polymer composites for applications in bone replacement and repair, Acta Biomater. 7(1) (2011) 16-30.
[111] B. Feng, M. Guolin, Y. Yuan, L. Changshen, W. Zhen, L. Jian, Role of macropore size in the mechanical properties and in vitro degradation of porous calcium phosphate cements, Mater. Lett. 64(18) (2010) 2028-2031.
[112] T. Gu, H. Shi, J. Ye, Reinforcement of calcium phosphate cement by incorporating with high-strength β-tricalcium phosphate aggregates, J. Biomed. Mater. Res. B: Appl. Biomat. 100B(2) (2012) 350-359.
[113] C. Liu, H. Shao, F. Chen, H. Zheng, Effects of the granularity of raw materials on the hydration and hardening process of calcium phosphate cement, Biomaterials 24(23) (2003) 4103-4113.
[114] M. Otsuka, Y. Matsuda, Y. Suwa, J.L. Fox, W.I. Higuchi, Effect of particle size of metastable calcium phosphates on mechanical strength of a novel self-setting bioactive calcium phosphate cement, J. Biomed. Mater. Res. 29(1) (1995) 25-32.
[115] Q. Yang, T. Troczynski, D.-M. Liu, Influence of apatite seeds on the synthesis of calcium phosphate cement, Biomaterials 23(13) (2002) 2751-2760.
[116] C. Durucan, P.W. Brown, Reactivity of α-tricalcium phosphate, J. Mater. Sci. 37(5) (2002) 963-969.
[117] M. Bohner, H.P. Merkle, P.V. Landuyt, G. Trophardy, J. Lemaitre, Effect of several additives and their admixtures on the physico-chemical properties of a calcium phosphate cement, J. Mater. Sci. - Mater. Med. 11(2) (2000) 111-116.
[118] F.A. Müller, U. Gbureck, T. Kasuga, Y. Mizutani, J.E. Barralet, U. Lohbauer, Whisker-reinforced calcium phosphate cements, J. Am. Ceram. Soc. 90(11) (2007) 3694-3697.
[119] I.S. Neira, Y.V. Kolen'ko, K.P. Kommareddy, I. Manjubala, M. Yoshimura, F. Guitián, Reinforcing of a calcium phosphate cement with hydroxyapatite crystals of various morphologies, ACS Appl. Mater. Interfaces 2(11) (2010) 3276-3284.
[120] H.H.K. Xu, D.T. Smith, C.G. Simon, Strong and bioactive composites containing nano-silica-fused whiskers for bone repair, Biomaterials 25(19) (2004) 4615-4626.
[121] Y.E. Greish, P.W. Brown, Characterization of wollastonite-reinforced HAp–Ca polycarboxylate composites, J. Biomed. Mater. Res. 55(4) (2001) 618-628.
[122] M. Kon, L.M. Hirakata, Y. Miyamoto, H. Kasahara, K. Asaoka, Strengthening of calcium phosphate cement by compounding calcium carbonate whiskers, Dent. Mater. J. 24(1) (2005) 104-110.

[123] H.H.K. Xu, F.C. Eichmiller, A.A. Giuseppetti, Reinforcement of a self-setting calcium phosphate cement with different fibers, J. Biomed. Mater. Res. 52(1) (2000) 107-114.
[124] L.A. dos Santos, R.G. Carrodéguas, A.O. Boschi, A.C. Fonseca de Arruda, Fiber-enriched double-setting calcium phosphate bone cement, J. Biomed. Mater. Res. A 65A(2) (2003) 244-250.
[125] L.A. Dos Santos, L.C. De Oliveira, E.C. Da Silva Rigo, R.G. Carrodéguas, A.O. Boschi, A.C. Fonseca de Arruda, Fiber reinforced calcium phosphate cement, Artif. Organs 24(3) (2000) 212-216.
[126] Z. Pan, P. Jiang, Q. Fan, B. Ma, H. Cai, Mechanical and biocompatible influences of chitosan fiber and gelatin on calcium phosphate cement, J. Biomed. Mater. Res. B: Appl. Biomat. 82B(1) (2007) 246-252.
[127] Z.H. Pan, H.P. Cai, P.P. Jiang, Q.Y. Fan, Properties of a calcium phosphate cement synergistically reinforced by chitosan fiber and gelatin, J. Polym. Res. 13(4) (2006) 323.
[128] Y. Zuo, F. Yang, J.G.C. Wolke, Y. Li, J.A. Jansen, Incorporation of biodegradable electrospun fibers into calcium phosphate cement for bone regeneration, Acta Biomater. 6(4) (2010) 1238-1247.
[129] N.J.S. Gorst, Y. Perrie, U. Gbureck, A.L. Hutton, M.P. Hofmann, L.M. Grover, J.E. Barralet, Effects of fibre reinforcement on the mechanical properties of brushite cement, Acta Biomater. 2(1) (2006) 95-102.
[130] W.D. Losquadro, S.A. Tatum, M.J. Allen, K.A. Mann, Polylactide-co-glycolide fiber–reinforced calcium phosphate bone cement, Arch. Facial Plast. Surg. 11(2) (2009) 104-109.
[131] H.H.K. Xu, M.D. Weir, E.F. Burguera, A.M. Fraser, Injectable and macroporous calcium phosphate cement scaffold, Biomaterials 27(24) (2006) 4279-4287.
[132] H.H.K. Xu, J.B. Quinn, Calcium phosphate cement containing resorbable fibers for short-term reinforcement and macroporosity, Biomaterials 23(1) (2002) 193-202.
[133] Y. Zhang, H.H.K. Xu, Effects of synergistic reinforcement and absorbable fiber strength on hydroxyapatite bone cement, J. Biomed. Mater. Res. A 75A(4) (2005) 832-840.
[134] L. Zhao, E.F. Burguera, H.H.K. Xu, N. Amin, H. Ryou, D.D. Arola, Fatigue and human umbilical cord stem cell seeding characteristics of calcium phosphate–chitosan–biodegradable fiber scaffolds, Biomaterials 31(5) (2010) 840-847.
[135] H.H.K. Xu, C.G. Simon, Self-hardening calcium phosphate composite scaffold for bone tissue engineering, J. Orthop. Res. 22(3) (2004) 535-543.
[136] C. Bao, W. Chen, M.D. Weir, W. Thein-Han, H.H.K. Xu, Effects of electrospun submicron fibers in calcium phosphate cement scaffold on mechanical properties and osteogenic differentiation of umbilical cord stem cells, Acta Biomater. 7(11) (2011) 4037-4044.
[137] E.F. Burguera, H.H.K. Xu, S. Takagi, L.C. Chow, High early strength calcium phosphate bone cement: Effects of dicalcium phosphate dihydrate and absorbable fibers, J. Biomed. Mater. Res. A 75A(4) (2005) 966-975.
[138] Q. Lian, D.-C. Li, J.-K. He, Z. Wang, Mechanical properties and in-vivo performance of calcium phosphate cement—chitosan fibre composite, Proc. Inst. Mech. Eng. H 222(3) (2008) 347-353.
[139] Q. Lian, D. Li, Z. Jin, J. Wang, A. Li, Z. Wang, Z. Jin, Fabrication and in vitro evaluation of calcium phosphate combined with chitosan fibers for scaffold structures, J. Bioact. Compat. Polym. 24(1_suppl) (2009) 113-124.
[140] H.H.K. Xu, C.G. Simon, Self-hardening calcium phosphate cement–mesh composite: Reinforcement, macropores, and cell response, J. Biomed. Mater. Res. A 69A(2) (2004) 267-278.
[141] H.H.K. Xu, J.B. Quinn, S. Takagi, L.C. Chow, Synergistic reinforcement of in situ hardening calcium phosphate composite scaffold for bone tissue engineering, Biomaterials 25(6) (2004) 1029-1037.
[142] A.S. Von Gonten, J.R. Kelly, J.M. Antonucci, Load-bearing behavior of a simulated craniofacial structure fabricated from a hydroxyapatite cement and bioresorbable fiber-mesh, J. Mater. Sci. - Mater. Med. 11(2) (2000) 95-100.
[143] S. Hesaraki, D. Sharifi, R. Nemati, N. Nezafati, Preparation and characterisation of calcium phosphate cement made by poly(acrylic/itaconic) acid, Adv. Appl. Ceram. 108(2) (2009) 106-110.
[144] A.O. Majekodunmi, S. Deb, Poly(acrylic acid) modified calcium phosphate cements: the effect of the composition of the cement powder and of the molecular weight and concentration of the polymeric acid, J. Mater. Sci. - Mater. Med. 18(9) (2007) 1883-1888.
[145] A.O. Majekodunmi, S. Deb, J.W. Nicholson, Effect of molecular weight and concentration of poly(acrylic acid) on the formation of a polymeric calcium phosphate cement, J. Mater. Sci. - Mater. Med. 14(9) (2003) 747-752.
[146] K.S. TenHuisen, P.W. Brown, The formation of hydroxyapatite-ionomer cements at 38°C, J. Dent. Res. 73(3) (1994) 598-606.
[147] K.E. Watson, K.S. Tenhuisen, P.W. Brown, The formation of hydroxyapatite–calcium polyacrylate composites, J. Mater. Sci. - Mater. Med. 10(4) (1999) 205-213.
[148] R.M. Khashaba, M. Moussa, C. Koch, A.R. Jurgensen, D.M. Missimer, R.L. Rutherford, N.B. Chutkan, J.L. Borke, Preparation, physical-chemical characterization, and cytocompatibility of polymeric calcium phosphate cements, Int. J. Biomater. 2011 (2011) 13.
[149] L.A. Dos Santos, L.C. De Oliveira, E.C.S. Rigo, R.G. Carrodeguas, A.O. Boschi, A.C.F. De Arruda, Influence of polymeric additives on the mechanical properties of α-tricalcium phosphate cement, Bone 25(2, Supplement 1) (1999) 99S-102S.
[150] L.A. Dos Santos, R.G. Carrodeguas, A.O. Boschi, A.C. De Arruda, Dual-setting calcium phosphate cement modified with ammonium polyacrylate, Artif. Organs 27(5) (2003) 412-418.

[151] J.L. Moreau, M.D. Weir, H.H.K. Xu, Self-setting collagen-calcium phosphate bone cement: Mechanical and cellular properties, J. Biomed. Mater. Res. A 91A(2) (2009) 605-613.
[152] W. Schneiders, A. Reinstorf, A. Biewener, A. Serra, R. Grass, M. Kinscher, J. Heineck, S. Rehberg, H. Zwipp, S. Rammelt, In vivo effects of modification of hydroxyapatite/collagen composites with and without chondroitin sulphate on bone remodeling in the sheep tibia, J. Orthop. Res. 27(1) (2009) 15-21.
[153] F. Tamimi, B. Kumarasami, C. Doillon, U. Gbureck, D.L. Nihouannen, E.L. Cabarcos, J.E. Barralet, Brushite–collagen composites for bone regeneration, Acta Biomater. 4(5) (2008) 1315-1321.
[154] L. Leroux, Z. Hatim, M. Frèche, J.L. Lacout, Effects of various adjuvants (lactic acid, glycerol, and chitosan) on the injectability of a calcium phosphate cement, Bone 25(2, Supplement 1) (1999) 31S-34S.
[155] H. Liu, H. Li, W. Cheng, Y. Yang, M. Zhu, C. Zhou, Novel injectable calcium phosphate/chitosan composites for bone substitute materials, Acta Biomater. 2(5) (2006) 557-565.
[156] A. Yokoyama, S. Yamamoto, T. Kawasaki, T. Kohgo, M. Nakasu, Development of calcium phosphate cement using chitosan and citric acid for bone substitute materials, Biomaterials 23(4) (2002) 1091-1101.
[157] M.H. Alkhraisat, C. Rueda, F.T. Mariño, J. Torres, L.B. Jerez, U. Gbureck, E.L. Cabarcos, The effect of hyaluronic acid on brushite cement cohesion, Acta Biomater. 5(8) (2009) 3150-3156.
[158] I. Khairoun, F.C.M. Driessens, M.G. Boltong, J.A. Planell, R. Wenz, Addition of cohesion promotors to calcium phosphate cements, Biomaterials 20(4) (1999) 393-398.
[159] A. Cherng, S. Takagi, L.C. Chow, Effects of hydroxypropyl methylcellulose and other gelling agents on the handling properties of calcium phosphate cement, J. Biomed. Mater. Res. 35(3) (1997) 273-277.
[160] S. Takagi, L.C. Chow, S. Hirayama, A. Sugawara, Premixed calcium–phosphate cement pastes, J. Biomed. Mater. Res. B: Appl. Biomat. 67B(2) (2003) 689-696.
[161] K. Ishikawa, Effects of spherical tetracalcium phosphate on injectability and basic properties of apatitic cement, Key Eng. Mater. 240-242 (2003) 369-372.
[162] K. Ishikawa, S. Matsuya, M. Nakagawa, K. Udoh, K. Suzuki, Basic properties of apatite cement containing spherical tetracalcium phosphate made with plasma melting method, J. Mater. Sci. - Mater. Med. 15(1) (2004) 13-17.
[163] E.F. Burguera, H.H.K. Xu, L. Sun, Injectable calcium phosphate cement: Effects of powder-to-liquid ratio and needle size, J. Biomed. Mater. Res. B: Appl. Biomat. 84B(2) (2008) 493-502.
[164] D. Kai, D. Li, X. Zhu, L. Zhang, H. Fan, X. Zhang, Addition of sodium hyaluronate and the effect on performance of the injectable calcium phosphate cement, J. Mater. Sci. - Mater. Med. 20(8) (2009) 1595-1602.
[165] E.F. Burguera, H.H.K. Xu, M.D. Weir, Injectable and rapid-setting calcium phosphate bone cement with dicalcium phosphate dihydrate, J. Biomed. Mater. Res. B: Appl. Biomat. 77B(1) (2006) 126-134.
[166] H.L.R. Alves, L.A. dos Santos, C.P. Bergmann, Injectability evaluation of tricalcium phosphate bone cement, J. Mater. Sci. - Mater. Med. 19(5) (2008) 2241-2246.
[167] G.C. Anselmetti, Osteoplasty: Percutaneous bone cement injection beyond the spine, Semin. Intervent. Radiol. 27(2) (2010) 199-208.
[168] M. Habib, G. Baroud, L. Galea, M. Bohner, Evaluation of the ultrasonication process for injectability of hydraulic calcium phosphate pastes, Acta Biomater. 8(3) (2012) 1164-1168.
[169] G. Baroud, C. Matsushita, M. Samara, L. Beckman, T. Steffen, Influence of oscillatory mixing on the injectability of three acrylic and two calcium-phosphate bone cements for vertebroplasty, J. Biomed. Mater. Res. B: Appl. Biomat. 68B(1) (2004) 105-111.
[170] L.E. Carey, H.H.K. Xu, C.G. Simon Jr, S. Takagi, L.C. Chow, Premixed rapid-setting calcium phosphate composites for bone repair, Biomaterials 26(24) (2005) 5002-5014.
[171] J. Engstrand, J. Aberg, H. Engqvist, Influence of water content on hardening and handling of a premixed calcium phosphate cement, Mater. Sci. Eng.: C 33(1) (2013) 527-531.
[172] B. Han, P.-W. Ma, L.-L. Zhang, Y.-J. Yin, K.-D. Yao, F.-J. Zhang, Y.-D. Zhang, X.-L. Li, W. Nie, β-TCP/MCPM-based premixed calcium phosphate cements, Acta Biomater. 5(8) (2009) 3165-3177.
[173] H.H.K. Xu, L.E. Carey, C.G. Simon Jr, S. Takagi, L.C. Chow, Premixed calcium phosphate cements: Synthesis, physical properties, and cell cytotoxicity, Dent. Mater. 23(4) (2007) 433-441.
[174] K.L. Low, S.H. Tan, S.H.S. Zein, J.A. Roether, V. Mouriño, A.R. Boccaccini, Calcium phosphate-based composites as injectable bone substitute materials, J. Biomed. Mater. Res. B: Appl. Biomat. 94B(1) (2010) 273-286.
[175] F. Wu, Y. Ngothai, J. Wei, C. Liu, B. O'Neill, Y. Wu, Premixed, injectable PLA-modified calcium deficient apatite biocement (cd-AB) with washout resistance, Colloids Surf. B: Biointerfaces 92(0) (2012) 113-120.
[176] A. Aryaei, J. Liu, A.H. Jayatissa, A. Champa Jayasuriya, Cross-linked chitosan improves the mechanical properties of calcium phosphate–chitosan cement, Mater. Sci. Eng.: C 54 (2015) 14-19.
[177] M. Takechi, Y. Miyamoto, K. Ishikawa, T. Toh, T. Yuasa, M. Nagayama, K. Suzuki, Initial histological evaluation of anti-washout type fast-setting calcium phosphate cement following subcutaneous implantation, Biomaterials 19(22) (1998) 2057-2063.
[178] Y. Miyamoto, K. Ishikawa, M. Takechi, T. Toh, T. Yuasa, M. Nagayama, K. Suzuki, Histological and compositional evaluations of three types of calcium phosphate cements when implanted in subcutaneous tissue immediately after mixing, J. Biomed. Mater. Res. 48(1) (1999) 36-42.

[179] B.T. Smith, M. Santoro, E.C. Grosfeld, S.R. Shah, J.J.J.P. van den Beucken, J.A. Jansen, A.G. Mikos, Incorporation of fast dissolving glucose porogens into an injectable calcium phosphate cement for bone tissue engineering, Acta Biomater. 15 (2017) 68-77.
[180] K. Ishikawa, Y. Miyamoto, M. Kon, M. Nagayama, K. Asaoka, Non-decay type fast-setting calcium phosphate cement: composite with sodium alginate, Biomaterials 16(7) (1995) 527-532.
[181] K. Ishikawa, Y. Miyamoto, M. Takechi, T. Toh, M. Kon, M. Nagayama, K. Asaoka, Non-decay type fast-setting calcium phosphate cement: Hydroxyapatite putty containing an increased amount of sodium alginate, J. Biomed. Mater. Res. 36(3) (1997) 393-399.
[182] J. Krebs, N. Aebli, B.G. Goss, S. Sugiyama, T. Bardyn, I. Boecken, P.J. Leamy, S.J. Ferguson, Cardiovascular changes after pulmonary embolism from injecting calcium phosphate cement, J. Biomed. Mater. Res. B: Appl. Biomat. 82B(2) (2007) 526-532.
[183] M. Bohner, N. Doebelin, G. Baroud, Theoretical and experimental approach to test the cohesion of calcium phosphate pastes, Eur. Cell. Mater. 12 (2006) 26-35.
[184] M. Bohner, Physical and chemical aspects of calcium phosphates used in spinal surgery, Eur. Spine. J. 10(2) (2001) S114-S121.
[185] P.D. Costantino, C.D. Friedman, K. Jones, L.C. Chow, H.J. Pelzer, G.A. Sisson, Sr, Hydroxyapatite cement: I. basic chemistry and histologic properties, Arch. Otolaryngol. Head Neck Surg. 117(4) (1991) 379-384.
[186] C.D. Friedman, P.D. Costantino, K. Jones, L.C. Chow, H.J. Pelzer, G.A. Sisson, Sr, Hydroxyapatite cement: Ii. obliteration and reconstruction of the cat frontal sinus, Arch. Otolaryngol. Head Neck Surg. 117(4) (1991) 385-389.
[187] B.R. Constantz, B.M. Barr, I.C. Ison, M.T. Fulmer, J. Baker, L. McKinney, S.B. Goodman, S. Gunasekaren, D.C. Delaney, J. Ross, R.D. Poser, Histological, chemical, and crystallographic analysis of four calcium phosphate cements in different rabbit osseous sites, J. Biomed. Mater. Res. 43(4) (1998) 451-461.
[188] E.P. Frankenburg, S.A. Goldstein, T.W. Bauer, S.A. Harris, R.D. Poser, Biomechanical and histological evaluation of a calcium phosphate cement, J. Bone Joint Surg. Am. 80(8) (1998) 1112-1124.
[189] H. Yuan, Y. Li, J.D. de Bruijn, K. de Groot, X. Zhang, Tissue responses of calcium phosphate cement: a study in dogs, Biomaterials 21(12) (2000) 1283-1290.
[190] E.M. Ooms, J.G.C. Wolke, M.T. van de Heuvel, B. Jeschke, J.A. Jansen, Histological evaluation of the bone response to calcium phosphate cement implanted in cortical bone, Biomaterials 24(6) (2003) 989-1000.
[191] E.M. Ooms, J.G.C. Wolke, J.P.C.M. van der Waerden, J.A. Jansen, Trabecular bone response to injectable calcium phosphate (Ca-P) cement, J. Biomed. Mater. Res. 61(1) (2002) 9-18.
[192] F. Theiss, D. Apelt, B. Brand, A. Kutter, K. Zlinszky, M. Bohner, S. Matter, C. Frei, J.A. Auer, B. von Rechenberg, Biocompatibility and resorption of a brushite calcium phosphate cement, Biomaterials 26(21) (2005) 4383-4394.
[193] P. Frayssinet, L. Gineste, P. Conte, J. Fages, N. Rouquet, Short-term implantation effects of a DCPD-based calcium phosphate cement, Biomaterials 19(11) (1998) 971-977.
[194] B. Flautre, C. Delecourt, M.C. Blary, P. Van Landuyt, J. Lemaître, P. Hardouin, Volume effect on biological properties of a calcium phosphate hydraulic cement: experimental study in sheep, Bone 25(2, Supplement 1) (1999) 35S-39S.
[195] B. Flautre, J. Lemaître, C. Maynou, P. Van Landuyt, P. Hardouin, Influence of polymeric additives on the biological properties of brushite cements: An experimental study in rabbit, J. Biomed. Mater. Res. A 66A(2) (2003) 214-223.
[196] J.M. Kuemmerle, A. Oberle, C. Oechslin, M. Bohner, C. Frei, I. Boecken, B.v. Rechenberg, Assessment of the suitability of a new brushite calcium phosphate cement for cranioplasty – an experimental study in sheep, J. Craniomaxillofac. Surg. 33(1) (2005) 37-44.
[197] G. Penel, N. Leroy, P. Van Landuyt, B. Flautre, P. Hardouin, J. Lemaître, G. Leroy, Raman microspectrometry studies of brushite cement: in vivo evolution in a sheep model, Bone 25(2, Supplement 1) (1999) 81S-84S.
[198] A.M.C. Barradas, H. Yuan, C.A.v. Blitterswijk, P. Habibovic, Osteoinductive biomaterials: current knowledge of properties, experimental models and biological mechanisms, Eur. Cell. Mater. 21 (2011) 407-429.
[199] S.d. Valle, N. Miño, F. Muñoz, A. González, J.A. Planell, M.-P. Ginebra, In vivo evaluation of an injectable macroporous calcium phosphate cement, J. Mater. Sci. - Mater. Med. 18(2) (2007) 353-361.
[200] Y. Miyamoto, K. Ishikawa, M. Takechi, T. Toh, Y. Yoshida, M. Nagayama, M. Kon, K. Asaoka, Tissue response to fast-setting calcium phosphate cement in bone, J. Biomed. Mater. Res. 37(4) (1997) 457-464.
[201] A.K. Gosain, L. Song, P. Riordan, M.T. Amarante, P.G. Nagy, C.R. Wilson, J.M. Toth, J.L. Ricci, A 1-year study of osteoinduction in hydroxyapatite-derived biomaterials in an adult sheep model: part I, Plast. Reconstr. Surg. 109 (2002).
[202] B.M. Holzapfel, J.C. Reichert, J.-T. Schantz, U. Gbureck, L. Rackwitz, U. Nöth, F. Jakob, M. Rudert, J. Groll, D.W. Hutmacher, How smart do biomaterials need to be? A translational science and clinical point of view, Adv. Drug Deliv. Rev. 65(4) (2013) 581-603.
[203] D.P. Pioletti, H. Takei, T. Lin, P. Van Landuyt, Q. Jun Ma, S. Yong Kwon, K.L. Paul Sung, The effects of calcium phosphate cement particles on osteoblast functions, Biomaterials 21(11) (2000) 1103-1114.
[204] K. Ohura, M. Bohner, P. Hardouin, J. Lemaître, G. Pasquier, B. Flautre, Resorption of, and bone formation from, new β-tricalcium phosphate-monocalcium phosphate cements: An in vivo study, J. Biomed. Mater. Res. 30(2) (1996) 193-200.
[205] L.M. Grover, J.C. Knowles, G.J.P. Fleming, J.E. Barralet, In vitro ageing of brushite calcium phosphate cement, Biomaterials 24(23) (2003) 4133-4141.

[206] Z. Sheikh, Y.L. Zhang, L. Grover, G.E. Merle, F. Tamimi, J. Barralet, In vitro degradation and in vivo resorption of dicalcium phosphate cement based grafts, Acta Biomater. 26 (2015) 338-346.
[207] C. de Oliveira Renó, N. Pereta, C. Bertran, M. Motisuke, E. de Sousa, Study of in vitro degradation of brushite cements scaffolds, J. Mater. Sci. - Mater. Med. 25(10) (2014) 2297-2303.
[208] M. Bohner, F. Theiss, D. Apelt, W. Hirsiger, R. Houriet, G. Rizzoli, E. Gnos, C. Frei, J.A. Auer, B. von Rechenberg, Compositional changes of a dicalcium phosphate dihydrate cement after implantation in sheep, Biomaterials 24(20) (2003) 3463-3474.
[209] U. Klammert, A. Ignatius, U. Wolfram, T. Reuther, U. Gbureck, In vivo degradation of low temperature calcium and magnesium phosphate ceramics in a heterotopic model, Acta Biomater. 7(9) (2011) 3469-3475.
[210] B. Kanter, M. Geffers, A. Ignatius, U. Gbureck, Control of in vivo mineral bone cement degradation, Acta Biomater. 10(7) (2014) 3279-3287.
[211] L.M. Grover, U. Gbureck, A.J. Wright, M. Tremayne, J.E. Barralet, Biologically mediated resorption of brushite cement in vitro, Biomaterials 27(10) (2006) 2178-2185.
[212] K.J. Lilley, U. Gbureck, J.C. Knowles, D.F. Farrar, J.E. Barralet, Cement from magnesium substituted hydroxyapatite, J. Mater. Sci. - Mater. Med. 16(5) (2005) 455-460.
[213] J. Xie, C. Riley, K. Chittur, Effect of albumin on brushite transformation to hydroxyapatite, J. Biomed. Mater. Res. 57(3) (2001) 357-365.
[214] A.L. Boskey, Matrix proteins and mineralization: An overview, Connect. Tissue Res. 35(1-4) (1996) 357-363.
[215] M. Geffers, J.E. Barralet, J. Groll, U. Gbureck, Dual-setting brushite–silica gel cements, Acta Biomater. 11(0) (2015) 467-476.
[216] M. Montazerolghaem, M. Karlsson Ott, H. Engqvist, H. Melhus, A.J. Rasmusson, Resorption of monetite calcium phosphate cement by mouse bone marrow derived osteoclasts, Mater. Sci. Eng.: C 52 (2015) 212-218.
[217] U. Gbureck, T. Hölzel, U. Klammert, K. Würzler, F.A. Müller, J.E. Barralet, Resorbable dicalcium phosphate bone substitutes prepared by 3D powder printing, Adv. Funct. Mater. 17(18) (2007) 3940-3945.
[218] C. Großardt, A. Ewald, L.M. Grover, J.E. Barralet, U. Gbureck, Passive and active in vitro resorption of calcium and magnesium phosphate cements by osteoclastic cells, Tissue Eng. Part A 16(12) (2010) 3687-3695.
[219] Z. Xia, L.M. Grover, Y. Huang, I.E. Adamopoulos, U. Gbureck, J.T. Triffitt, R.M. Shelton, J.E. Barralet, In vitro biodegradation of three brushite calcium phosphate cements by a macrophage cell-line, Biomaterials 27(26) (2006) 4557-4565.
[220] P. Jamshidi, R.H. Bridson, A.J. Wright, L.M. Grover, Brushite cement additives inhibit attachment to cell culture beads, Biotechnol. Bioeng. 110(5) (2013) 1487-1494.
[221] B. Flautre, C. Maynou, J. Lemaitre, P. Van Landuyt, P. Hardouin, Bone colonization of β–TCP granules incorporated in brushite cements, J. Biomed. Mater. Res. 63(4) (2002) 413-417.
[222] H.C. Kroese-Deutman, J.G.C. Wolke, P.H.M. Spauwen, J.A. Jansen, Closing capacity of cranial bone defects using porous calcium phosphate cement implants in a rabbit animal model, J. Biomed. Mater. Res. A 79A(3) (2006) 503-511.
[223] M.-C. von Doernberg, B. von Rechenberg, M. Bohner, S. Grünenfelder, G.H. van Lenthe, R. Müller, B. Gasser, R. Mathys, G. Baroud, J. Auer, In vivo behavior of calcium phosphate scaffolds with four different pore sizes, Biomaterials 27(30) (2006) 5186-5198.
[224] S.V. Dorozhkin, Calcium orthophosphates, J. Mater. Sci. 42(4) (2007) 1061-1095.
[225] G. Carotenuto, G. Spagnuolo, L. Ambrosio, L. Nicolais, Macroporous hydroxyapatite as alloplastic material for dental applications, J. Mater. Sci. - Mater. Med. 10(10) (1999) 671-676.
[226] K.A. Hing, S.M. Best, W. Bonfield, Characterization of porous hydroxyapatite, J. Mater. Sci. - Mater. Med. 10(3) (1999) 135-145.
[227] J.J. Klawitter, S.F. Hulbert, Application of porous ceramics for the attachment of load bearing internal orthopedic applications, J. Biomed. Mater. Res. 5(6) (1971) 161-229.
[228] N. Tamai, A. Myoui, M. Hirao, T. Kaito, T. Ochi, J. Tanaka, K. Takaoka, H. Yoshikawa, A new biotechnology for articular cartilage repair: subchondral implantation of a composite of interconnected porous hydroxyapatite, synthetic polymer (PLA-PEG), and bone morphogenetic protein-2 (rhBMP-2), Osteoarthritis Cartilage 13(5) (2005) 405-417.
[229] X. Qi, J. Ye, Mechanical and rheological properties and injectability of calcium phosphate cement containing poly (lactic-co-glycolic acid) microspheres, Mater. Sci. Eng.: C 29(6) (2009) 1901-1906.
[230] S. Hesaraki, F. Moztarzadeh, D. Sharifi, Formation of interconnected macropores in apatitic calcium phosphate bone cement with the use of an effervescent additive, J. Biomed. Mater. Res. A 83A(1) (2007) 80-87.
[231] R.Q. Ruhé, E.L. Hedberg-Dirk, N.T. Padron, P.H.M. Spauwen, J.A. Jansen, A.G. Mikos, Porous poly(DL-lactic-co-glycolic acid)/calcium phosphate cement composite for reconstruction of bone defects, Tissue Eng. 12(4) (2006) 789-800.
[232] M. Bohner, Calcium phosphate emulsions: possible applications, Key Eng. Mater. 192-195 (2001) 765-768.
[233] H.H.K. Xu, J.B. Quinn, S. Takagi, L.C. Chow, F.C. Eichmiller, Strong and macroporous calcium phosphate cement: Effects of porosity and fiber reinforcement on mechanical properties, J. Biomed. Mater. Res. 57(3) (2001) 457-466.
[234] M. Markovic, S. Takagi, L.C. Chow, Formation of macropores in calcium phosphate cements through the use of mannitol crystals, Key Eng. Mater. 192-195 (2000) 773-776.
[235] M. Tang, M.D. Weir, H.H.K. Xu, Mannitol-containing macroporous calcium phosphate cement encapsulating human umbilical cord stem cells, J. Tissue Eng. Regen. M. 6(3) (2012) 214-224.

[236] S. Tajima, Y. Kishi, M. Oda, M. Maruta, S. Matsuya, K. Ishikawa, Fabrication of biporous low-crystalline apatite based on mannitol dissolution from apatite cement, Dent. Mater. J. 25(3) (2006) 616-620.
[237] S. Takagi, L.C. Chow, Formation of macropores in calcium phosphate cement implants, J. Mater. Sci. - Mater. Med. 12(2) (2001) 135-139.
[238] H. Guo, J. Su, J. Wei, H. Kong, C. Liu, Biocompatibility and osteogenicity of degradable Ca-deficient hydroxyapatite scaffolds from calcium phosphate cement for bone tissue engineering, Acta Biomater. 5(1) (2009) 268-278.
[239] A.C. Tas, Preparation of porous apatite granules from calcium phosphate cement, J. Mater. Sci. - Mater. Med. 19(5) (2008) 2231-2239.
[240] D.P. Link, J. van den Dolder, W.J.F.M. Jurgens, J.G.C. Wolke, J.A. Jansen, Mechanical evaluation of implanted calcium phosphate cement incorporated with PLGA microparticles, Biomaterials 27(28) (2006) 4941-4947.
[241] Z. Fei, Y. Hu, D. Wu, H. Wu, R. Lu, J. Bai, H. Song, Preparation and property of a novel bone graft composite consisting of rhBMP-2 loaded PLGA microspheres and calcium phosphate cement, J. Mater. Sci. - Mater. Med. 19(3) (2008) 1109-1116.
[242] P.Q. Ruhé, O.C. Boerman, F.G.M. Russel, P.H.M. Spauwen, A.G. Mikos, J.A. Jansen, Controlled release of rhBMP-2 loaded poly(dl-lactic-co-glycolic acid)/calcium phosphate cement composites in vivo, J. Control. Release 106(1–2) (2005) 162-171.
[243] D.P. Link, J. van den Dolder, J.J.J.P. van den Beucken, V.M. Cuijpers, J.G.C. Wolke, A.G. Mikos, J.A. Jansen, Evaluation of the biocompatibility of calcium phosphate cement/PLGA microparticle composites, J. Biomed. Mater. Res. A 87A(3) (2008) 760-769.
[244] R.J. Klijn, J.J.J.P. van den Beucken, R.P. Félix Lanao, G. Veldhuis, S.C. Leeuwenburgh, J.G.C. Wolke, G.J. Meijer, J.A. Jansen, Three different strategies to obtain porous calcium phosphate cements: comparison of performance in a rat skull bone augmentation model, Tissue Eng. Part A 18(11-12) (2012) 1171-1182.
[245] M. Li, X. Liu, X. Liu, B. Ge, K. Chen, Creation of macroporous calcium phosphate cements as bone substitutes by using genipin-crosslinked gelatin microspheres, J. Mater. Sci. - Mater. Med. 20(4) (2009) 925-934.
[246] W.J.E.M. Habraken, L.T. de Jonge, J.G.C. Wolke, L. Yubao, A.G. Mikos, J.A. Jansen, Introduction of gelatin microspheres into an injectable calcium phosphate cement, J. Biomed. Mater. Res. A 87A(3) (2008) 643-655.
[247] W. Chen, H. Zhou, M. Tang, M.D. Weir, C. Bao, H.H.K. Xu, Gas-foaming calcium phosphate cement scaffold encapsulating human umbilical cord stem cells, Tissue Eng. Part A 18(7-8) (2011) 816-827.
[248] A. Almirall, G. Larrecq, J.A. Delgado, S. Martínez, J.A. Planell, M.P. Ginebra, Fabrication of low temperature macroporous hydroxyapatite scaffolds by foaming and hydrolysis of an α-TCP paste, Biomaterials 25(17) (2004) 3671-3680.
[249] R.P. del Real, J.G.C. Wolke, M. Vallet-Regí, J.A. Jansen, A new method to produce macropores in calcium phosphate cements, Biomaterials 23(17) (2002) 3673-3680.
[250] E.B. Montufar, T. Traykova, J.A. Planell, M.-P. Ginebra, Comparison of a low molecular weight and a macromolecular surfactant as foaming agents for injectable self setting hydroxyapatite foams: Polysorbate 80 versus gelatine, Mater. Sci. Eng.: C 31(7) (2011) 1498-1504.
[251] M.-P. Ginebra, J.-A. Delgado, I. Harr, A. Almirall, S. Del Valle, J.A. Planell, Factors affecting the structure and properties of an injectable self-setting calcium phosphate foam, J. Biomed. Mater. Res. A 80A(2) (2007) 351-361.
[252] F. Perut, E.B. Montufar, G. Ciapetti, M. Santin, J. Salvage, T. Traykova, J.A. Planell, M.P. Ginebra, N. Baldini, Novel soybean/gelatine-based bioactive and injectable hydroxyapatite foam: Material properties and cell response, Acta Biomater. 7(4) (2011) 1780-1787.
[253] A. Kovtun, M.J. Goeckelmann, A.A. Niclas, E.B. Montufar, M.-P. Ginebra, J.A. Planell, M. Santin, A. Ignatius, In vivo performance of novel soybean/gelatin-based bioactive and injectable hydroxyapatite foams, Acta Biomater. 12(0) (2015) 242-249.
[254] U. Joosten, A. Joist, T. Frebel, B. Brandt, S. Diederichs, C. von Eiff, Evaluation of an in situ setting injectable calcium phosphate as a new carrier material for gentamicin in the treatment of chronic osteomyelitis: Studies in vitro and in vivo, Biomaterials 25(18) (2004) 4287-4295.
[255] H.P. Stallmann, C. Faber, A.L.J.J. Bronckers, A.V. Nieuw Amerongen, P.I.J.M. Wuisman, In vitro gentamicin release from commercially available calcium-phosphate bone substitutes influence of carrier type on duration of the release profile, BMC Musculoskelet. Disord. 7 (2006) 18-18.
[256] C. Hamanishi, K. Kitamoto, S. Tanaka, M. Otsuka, Y. Doi, T. Kitahashi, A self-setting TTCP-DCPD apatite cement for release of vancomycin, J. Biomed. Mater. Res. 33(3) (1996) 139-143.
[257] P.-J. Jiang, S. Patel, U. Gbureck, R. Caley, L.M. Grover, Comparing the efficacy of three bioceramic matrices for the release of vancomycin hydrochloride, J. Biomed. Mater. Res. B: Appl. Biomat. 93B(1) (2010) 51-58.
[258] T. Sasaki, Y. Ishibashi, H. Katano, A. Nagumo, S. Toh, In vitro elution of vancomycin from calcium phosphate cement, J. Arthroplasty 20(8) (2005) 1055-1059.
[259] C.-H. David Chen, C.-C. Chen, M.-Y. Shie, C.-H. Huang, S.-J. Ding, Controlled release of gentamicin from calcium phosphate/alginate bone cement, Mater. Sci. Eng.: C 31(2) (2011) 334-341.
[260] S. Sasaki, Y. Ishii, Apatite cement containing antibiotics: efficacy in treating experimental osteomyelitis, J. Orthop. Sci. 4(5) (1999) 361-369.
[261] T. Tani, K. Okada, S. Takahashi, N. Suzuki, Y. Shimada, E. Itoi, Doxorubicin-loaded calcium phosphate cement in the management of bone and soft tissue tumors, In Vivo 20(1) (2006) 55-60.

[262] Z. Jindong, T. Hai, G. Junchao, W. Bo, B. Li, W.B. Qiang, Evaluation of a novel osteoporotic drug delivery system in vitro: Alendronate-loaded calcium phosphate cement, Orthopedics 33(8) (2010).
[263] V. Schnitzler, F. Fayon, C. Despas, I. Khairoun, C. Mellier, T. Rouillon, D. Massiot, A. Walcarius, P. Janvier, O. Gauthier, G. Montavon, J.-M. Bouler, B. Bujoli, Investigation of alendronate-doped apatitic cements as a potential technology for the prevention of osteoporotic hip fractures: Critical influence of the drug introduction mode on the in vitro cement properties, Acta Biomater. 7(2) (2011) 759-770.
[264] J. Schnieders, U. Gbureck, E. Vorndran, M. Schossig, T. Kissel, The effect of porosity on drug release kinetics from vancomycin microsphere/calcium phosphate cement composites, J. Biomed. Mater. Res. B: Appl. Biomat. 99B(2) (2011) 391-398.
[265] J. Schnieders, U. Gbureck, R. Thull, T. Kissel, Controlled release of gentamicin from calcium phosphate—poly(lactic acid-co-glycolic acid) composite bone cement, Biomaterials 27(23) (2006) 4239-4249.
[266] S. Girod Fullana, H. Ternet, M. Freche, J.L. Lacout, F. Rodriguez, Controlled release properties and final macroporosity of a pectin microspheres–calcium phosphate composite bone cement, Acta Biomater. 6(6) (2010) 2294-2300.
[267] J. Siepmann, N.A. Peppas, Modeling of drug release from delivery systems based on hydroxypropyl methylcellulose (HPMC), Adv. Drug Deliv. Rev. 48(2–3) (2001) 139-157.
[268] T. Higuchi, Mechanism of sustained-action medication. Theoretical analysis of rate of release of solid drugs dispersed in solid matrices, J. Pharm. Sci. 52(12) (1963) 1145-1149.
[269] M. Li, X. Liu, X. Liu, B. Ge, Calcium phosphate cement with BMP-2-loaded gelatin microspheres enhances bone healing in osteoporosis: A pilot study, Clin. Orthop. Relat. Res. 468(7) (2010) 1978-1985.
[270] W. Pan, Y. Wei, L. Zhou, D. Li, Comparative in vivo study of injectable biomaterials combined with BMP for enhancing tendon graft osteointegration for anterior cruciate ligament reconstruction, J. Orthop. Res. 29(7) (2011) 1015-1021.
[271] R.G. Sorensen, U.M.E. Wikesjö, A. Kinoshita, J.M. Wozney, Periodontal repair in dogs: evaluation of a bioresorbable calcium phosphate cement (Ceredex) as a carrier for rhBMP-2, J. Clin. Periodontol. 31(9) (2004) 796-804.
[272] K. Ohura, C. Hamanishi, S. Tanaka, N. Matsuda, Healing of segmental bone defects in rats induced by a β-TCP-MCPM cement combined with rhBMP-2, J. Biomed. Mater. Res. 44(2) (1999) 168-175.
[273] S.J. Saint-Jean, C.L. Camiré, P. Nevsten, S. Hansen, M.P. Ginebra, Study of the reactivity and in vitro bioactivity of Sr-substituted α-TCP cements, J. Mater. Sci. - Mater. Med. 16(11) (2005) 993.
[274] D. Guo, K. Xu, X. Zhao, Y. Han, Development of a strontium-containing hydroxyapatite bone cement, Biomaterials 26(19) (2005) 4073-4083.
[275] M. Baier, P. Staudt, R. Klein, U. Sommer, R. Wenz, I. Grafe, P.J. Meeder, P.P. Nawroth, C. Kasperk, Strontium enhances osseointegration of calcium phosphate cement: a histomorphometric pilot study in ovariectomized rats, J. Orthop. Surg. Res. 8(1) (2013) 16.
[276] G. Dagang, X. Kewei, H. Yong, The influence of Sr doses on the in vitro biocompatibility and in vivo degradability of single-phase Sr-incorporated HAP cement, J. Biomed. Mater. Res. A 86A(4) (2008) 947-958.
[277] M. Hamdan Alkhraisat, C. Moseke, L. Blanco, J.E. Barralet, E. Lopez-Carbacos, U. Gbureck, Strontium modified biocements with zero order release kinetics, Biomaterials 29(35) (2008) 4691-4697.
[278] G. Mestres, C. Le Van, M.-P. Ginebra, Silicon-stabilized α-tricalcium phosphate and its use in a calcium phosphate cement: Characterization and cell response, Acta Biomater. 8(3) (2012) 1169-1179.
[279] C.L. Camiré, S. Jegou Saint-Jean, C. Mochales, P. Nevsten, J.-S. Wang, L. Lidgren, I. McCarthy, M.-P. Ginebra, Material characterization and in vivo behavior of silicon substituted α-tricalcium phosphate cement, J. Biomed. Mater. Res. B: Appl. Biomat. 76B(2) (2006) 424-431.
[280] X. Li, Y. Sogo, A. Ito, H. Mutsuzaki, N. Ochiai, T. Kobayashi, S. Nakamura, K. Yamashita, R.Z. LeGeros, The optimum zinc content in set calcium phosphate cement for promoting bone formation in vivo, Mater. Sci. Eng. C Mater. Biol. Appl. 29(3) (2009) 969-975.
[281] S. Pina, S.I. Vieira, P. Rego, P.M.C. Torres, O.A.P.d.C.e. Silva, E.F.d.C.e. Silva, J.M.F. Ferreira, Biological responses of brushite-forming Zn- and ZnSr- substituted beta-tricalcium phosphate bone cements, Eur. Cell. Mater. 20 (2010) 162-177.
[282] J. Lu, J. Wei, Y. Yan, H. Li, J. Jia, S. Wei, H. Guo, T. Xiao, C. Liu, Preparation and preliminary cytocompatibility of magnesium doped apatite cement with degradability for bone regeneration, J. Mater. Sci. - Mater. Med. 22(3) (2011) 607-615.
[283] A. Ewald, D. Hösel, S. Patel, L.M. Grover, J.E. Barralet, U. Gbureck, Silver-doped calcium phosphate cements with antimicrobial activity, Acta Biomater. 7(11) (2011) 4064-4070.
[284] U. Gbureck, O. Knappe, L.M. Grover, J.E. Barralet, Antimicrobial potency of alkali ion substituted calcium phosphate cements, Biomaterials 26(34) (2005) 6880-6886.
[285] E. Bonnelye, A. Chabadel, F. Saltel, P. Jurdic, Dual effect of strontium ranelate: Stimulation of osteoblast differentiation and inhibition of osteoclast formation and resorption in vitro, Bone 42(1) (2008) 129-138.
[286] E.M. Carlisle, Silicon: A possible factor in bone calcification, Science 167(3916) (1970) 279-280.
[287] M. Yamaguchi, Role of nutritional zinc in the prevention of osteoporosis, Mol. Cell. Biochem. 338(1) (2010) 241-254.
[288] L. Wu, F. Feyerabend, A.F. Schilling, R. Willumeit-Römer, B.J.C. Luthringer, Effects of extracellular magnesium extract on the proliferation and differentiation of human osteoblasts and osteoclasts in coculture, Acta Biomater. 27 (2015) 294-304.
[289] L. Wang, G.H. Nancollas, Calcium orthophosphates: Crystallization and dissolution, Chem. Rev. 108(11) (2008) 4628-4669.

[290] J.L. Clement, P.S. Jarrett, Antibacterial silver, Met. Based Drugs 1(5-6) (1994) 467-482.
[291] S.A. Walling, J.L. Provis, Magnesia-based cements: A journey of 150 years, and cements for the future?, Chem. Rev. 116(7) (2016) 4170-4204.
[292] P. David, R.W. Limes, Basic refractory compositions for intermediate temperature zones, Republic Steel Corp, 1966.
[293] F.C.M. Driessens, M.G. Boltong, M.I. Zapatero, R.M.H. Verbeeck, W. Bonfield, O. Bérmúdez, E. Fernández, M.P. Ginebra, J.A. Planell, In vivo behaviour of three calcium phosphate cements and a magnesium phosphate cement, J. Mater. Sci. - Mater. Med. 6(5) (1995) 272-278.
[294] G. Mestres, M.-P. Ginebra, Novel magnesium phosphate cements with high early strength and antibacterial properties, Acta Biomater. 7(4) (2011) 1853-1861.
[295] K.D. Cashman, A. Flynn, Optimal nutrition: calcium, magnesium and phosphorus, Proc. Nutr. Soc. 58(2) (1999) 477-487.
[296] M.P. Staiger, A.M. Pietak, J. Huadmai, G. Dias, Magnesium and its alloys as orthopedic biomaterials: A review, Biomaterials 27(9) (2006) 1728-1734.
[297] F. Witte, V. Kaese, H. Haferkamp, E. Switzer, A. Meyer-Lindenberg, C.J. Wirth, H. Windhagen, In vivo corrosion of four magnesium alloys and the associated bone response, Biomaterials 26(17) (2005) 3557-3563.
[298] F. Witte, H. Ulrich, C. Palm, E. Willbold, Biodegradable magnesium scaffolds: Part II: Peri-implant bone remodeling, J. Biomed. Mater. Res. A 81A(3) (2007) 757-765.
[299] S. Yoshizawa, A. Brown, A. Barchowsky, C. Sfeir, Magnesium ion stimulation of bone marrow stromal cells enhances osteogenic activity, simulating the effect of magnesium alloy degradation, Acta Biomater. 10(6) (2014) 2834-2842.
[300] L. Wu, B.J.C. Luthringer, F. Feyerabend, A.F. Schilling, R. Willumeit, Effects of extracellular magnesium on the differentiation and function of human osteoclasts, Acta Biomater. 10(6) (2014) 2843-2854.
[301] F. Wu, J. Wei, H. Guo, F. Chen, H. Hong, C. Liu, Self-setting bioactive calcium–magnesium phosphate cement with high strength and degradability for bone regeneration, Acta Biomater. 4(6) (2008) 1873-1884.
[302] W. Fan, S. Jiacan, W. Jie, G. Han, L. Changsheng, Injectable bioactive calcium–magnesium phosphate cement for bone regeneration, Biomed. Mater. 3(4) (2008) 044105.
[303] G. Mestres, M. Abdolhosseini, W. Bowles, S.H. Huang, C. Aparicio, S.U. Gorr, M.P. Ginebra, Antimicrobial properties and dentin bonding strength of magnesium phosphate cements, Acta Biomater. 9(9) (2013) 8384-8393.
[304] L.M. Grover, U. Gbureck, D. Farrar, J.E. Barralet, Adhesion of a novel calcium phosphate cement to cortical bone and several common biomaterials, Key Eng. Mater. 309-311 (2006) 859-852.
[305] L.J.M. Hirvinen, A.S. Litsky, V.F. Samii, S.E. Weisbrode, A.L. Bertone, Influence of bone cements on bone-screw interfaces in the third metacarpal and third metatarsal bones of horses, Am. J. Vet. Res, 70(8) (2009) 964-972.
[306] L.V. Gulotta, D. Kovacevic, L. Ying, J.R. Ehteshami, S. Montgomery, S.A. Rodeo, Augmentation of tendon-to-bone healing with a magnesium-based bone adhesive, Am. J. Sports Med. 36(7) (2008) 1290-1297.
[307] A.-J. Wang, J. Zhang, J.-M. Li, A.-B. Ma, L.-T. Liu, Effect of liquid-to-solid ratios on the properties of magnesium phosphate chemically bonded ceramics, Mater. Sci. Eng. C Mater. Biol. Appl. 33(5) (2013) 2508-2512.
[308] G. Mestres, F.S. Aguilera, N. Manzanares, S. Sauro, R. Osorio, M. Toledano, M.P. Ginebra, Magnesium phosphate cements for endodontic applications with improved long-term sealing ability, Int. Endod. J. 47(2) (2014) 127-139.
[309] G. Yang, J. Liu, F. Li, Z. Pan, X. Ni, Y. Shen, H. Xu, Q. Huang, Bioactive calcium sulfate/magnesium phosphate cement for bone substitute applications, Mater. Sci. Eng.: C 35 (2014) 70-76.
[310] C. Moseke, V. Saratsis, U. Gbureck, Injectability and mechanical properties of magnesium phosphate cements, J. Mater. Sci. - Mater. Med. 22(12) (2011) 2591-2598.
[311] E. Vorndran, A. Ewald, F. Müller, K. Zorn, A. Kufner, U. Gbureck, Formation and properties of magnesium–ammonium–phosphate hexahydrate biocements in the Ca–Mg–PO4 system, J. Mater. Sci. - Mater. Med. 22(3) (2011) 429-436.
[312] V.S. Nicole Ostrowski, Abhijit Roy, Prashant N. Kumta, Systematic assessment of synthesized tri-magnesium phosphate powders (amorphous, semi-crystalline and crystalline) and cements for ceramic bone cement applications, J. Mater. Sci. Technol. 31(5) (2015) 437-444.
[313] A. Ewald, K. Helmschrott, G. Knebl, N. Mehrban, L.M. Grover, U. Gbureck, Effect of cold-setting calcium- and magnesium phosphate matrices on protein expression in osteoblastic cells, J. Biomed. Mater. Res. B: Appl. Biomat. 96B(2) (2011) 326-332.
[314] H. Zhou, A.K. Agarwal, V.K. Goel, S.B. Bhaduri, Microwave assisted preparation of magnesium phosphate cement (MPC) for orthopedic applications: A novel solution to the exothermicity problem, Mater. Sci. Eng.: C 33(7) (2013) 4288-4294.
[315] N. Yang, C. Shi, Y. Chang, Research progresses in magnesium phosphate cement based materials, J. Mater. Civil Eng. 26(10) (2014).
[316] J. Yang, C. Qian, Effect of borax on hydration and hardening properties of magnesium and potassium phosphate cement pastes, J. Wuhan Univ. Technol. Mater. Sci. Ed. 25 (2010) 613-618.
[317] Z. Ding, B. Dong, F. Xing, N. Han, Z. Li, Cementing mechanism of potassium phosphate based magnesium phosphate cement, Ceram. Int. 38(8) (2012) 6281-6288.
[318] A.S. Wagh, S.Y. Jeong, Chemically bonded phosphate ceramics: I, A dissolution model of formation, J. Am. Ceram. Soc. 86(11) (2003) 1838-1844.
[319] E. Soudée, J. Péra, Mechanism of setting reaction in magnesia-phosphate cements, Cem. Concr. Res. 30(2) (2000) 315-321.
[320] R. Neiman, A.C. Sarma, Setting and thermal reactions of phosphate investments, J. Dental Res. 59 (1980) 1478.

[321] Q. Yang, X. Wu, Factors influencing properties of phosphate cement-based binder for rapid repair of concrete, Cem. Concr. Res. 29(3) (1999) 389-396.
[322] D.V. Ribeiro, M.R. Morelli, Performance analysis of magnesium phosphate cement mortar containing grinding dust, Mat. Res. 12 (2009) 51-56.
[323] U. Klammert, E. Vorndran, T. Reuther, F.A. Müller, K. Zorn, U. Gbureck, Low temperature fabrication of magnesium phosphate cement scaffolds by 3D powder printing, J. Mater. Sci. - Mater. Med. 21(11) (2010) 2947-2953.
[324] A.-J. Wang, Z.-L. Yuan, J. Zhang, L.-T. Liu, J.-M. Li, Z. Liu, Effect of raw material ratios on the compressive strength of magnesium potassium phosphate chemically bonded ceramics, Mater. Sci. Eng.: C 33(8) (2013) 5058-5063.
[325] A.K. Sarkar, Hydration/dehydration characteristics of struvite and dittmarite pertaining to magnesium ammonium phosphate cement systems, J. Mater. Sci. 26(9) (1991) 2514-2518.
[326] D.A. Hall, R. Stevens, B.E. Jazairi, Effect of water content on the structure and mechanical properties of magnesia-phosphate cement mortar, J. Am. Ceram. Soc. 81(6) (1998) 1550-1556.
[327] A.W. Frazier, J.R. Lehr, J.P. Smith, The magnesium phosphates hannayite, schertelite and bobierrite, Am. Mineral. 48 (1963) 635-641.
[328] T. Finch, J.H. Sharp, Chemical reactions between magnesia and aluminium orthophosphate to form magnesia-phosphate cements, J. Mater. Sci. 24(12) (1989) 4379-4386.
[329] A.W. Taylor, A.W. Frazier, E.L. Gurney, J.P. Smith, Solubility products of di- and trimagnesium phosphates and the dissociation of magnesium phosphate solutions, T. Faraday Soc. 59(0) (1963) 1585-1589.
[330] M.I.H. Bhuiyan, D.S. Mavinic, F.A. Koch, Thermal decomposition of struvite and its phase transition, Chemosphere 70(8) (2008) 1347-1356.
[331] S.V. Golubev, O.S. Pokrovsky, V.S. Savenko, Homogeneous precipitation of magnesium phosphates from seawater solutions, J. Crys. Growth 223(4) (2001) 550-556.
[332] A.W. Taylor, A.W. Frazier, E.L. Gurney, Solubility products of magnesium ammonium and magnesium potassium phosphates, T. Faraday Soc. 59(0) (1963) 1580-1584.
[333] C.K. Chau, Z. Li, Accelerated reactivity assessment of light burnt magnesium oxide, J. Am. Ceram. Soc. 91(5) (2008) 1640-1645.
[334] F. Abbona, H.E. Lundager Madsen, R. Boistelle, Crystallization of two magnesium phosphates, struvite and newberyite: Effect of pH and concentration, J. Crys. Growth 57(1) (1982) 6-14.
[335] R.E. Dinnebier, D. Freyer, S. Bette, M. Oestreich, 9Mg(OH)2·MgCl2·4H2O, a high temperature phase of the magnesia binder system, Inorg. Chem. 49(21) (2010) 9770-9776.
[336] Y. Tan, Y. Liu, L. Grover, Effect of phosphoric acid on the properties of magnesium oxychloride cement as a biomaterial, Cem. Concr. Res. 56 (2014) 69-74.
[337] Y. Tan, Y. Liu, Z. Zhao, J.Z. Paxton, L.M. Grover, Synthesis and in vitro degradation of a novel magnesium oxychloride cement, J. Biomed. Mater. Res. A 103(1) (2015) 194-202.
[338] J.B. Shaw, G.A. Bole, New developments in oxychloride stucco and flooring, J. Am. Ceram. Soc. 5(6) (1922) 311-321.
[339] H. Bilinski, B. Matković, C. Mažuranić, T.B. Žunić, The formation of magnesium oxychloride phases in the systems MgO-MgCl2-H2O and NaOH-MgCl2-H2O, J. Am. Ceram. Soc. 67(4) (1984) 266-269.
[340] P.H. Bates, R.K. Young, Plastic magnesia cements, J. Am. Ceram. Soc. 4(7) (1921) 570-596.
[341] Z. Li, C.K. Chau, Influence of molar ratios on properties of magnesium oxychloride cement, Cem. Concr. Res. 37(6) (2007) 866-870.
[342] H. Ba, H. Guan, Influence of MgO/MgCl2 molar ratio on phase stability of magnesium oxychloride cement, J. Wuhan Univ. Technol. Mater. Sci. Ed. 24(3) (2009) 476-481.
[343] F.C. Harper, Effect of calcination temperature on the properties of magnesium oxides for use in magnesium oxychloride cements, J. Appl. Chem. 17(1) (1967) 5-10.
[344] S. Alegret, M. Blanco, R. Subirats, Potentiometric study of the reactivity of calcined magnesites for use in magnesium oxychloride cements, J. Am. Ceram. Soc. 67(9) (1984) 579-582.
[345] D. Dehua, Z. Chuanmei, The formation mechanism of the hydrate phases in magnesium oxychloride cement, Cem. Concr. Res. 29 (1999) 1365-1371.
[346] H.S. Lukens, The composition of magnesium oxychloride, J. Am. Chem. Soc. 54(6) (1932) 2372-2380.
[347] D. Deng, The mechanism for soluble phosphates to improve the water resistance of magnesium oxychloride cement, Cem. Concr. Res. 33(9) (2003) 1311-1317.
[348] J.H. Canterford, Magnesia—an important industrial mineral: A review of processing options and uses, Min. Proc. Ext. Met. Rev. 2(1-2) (1985) 57-104.
[349] M. Krähenbühl, B. Etter, K.M. Udert, Pretreated magnesite as a source of low-cost magnesium for producing struvite from urine in Nepal, Sci. Total Environ. 542, Part B (2016) 1155-1161.
[350] Y. Kotera, T. Saito, M. Terada, Crystal growth of magnesium oxide prepared by the thermal decomposition of magnesium hydroxide, Bull. Chem. Soc. Jpn. 36(2) (1963) 195-199.
[351] C.A. Strydom, E.M. van der Merwe, M.E. Aphane, The effect of calcining conditions on the rehydration of dead burnt magnesium oxide using magnesium acetate as a hydrating agent, J. Therm. Anal. Calorim. 80(3) (2005) 659-662.
[352] W.R. Eubank, Calcination studies of magnesium oxides, J. Am. Ceram. Soc. 34(8) (1951) 225-229.

[353] X. Zhang, Y. Zheng, X. Feng, X. Han, Z. Bai, Z. Zhang, Calcination temperature-dependent surface structure and physicochemical properties of magnesium oxide, RSC Adv. 5(105) (2015) 86102-86112.
[354] E. Soudée, J. Péra, Influence of magnesia surface on the setting time of magnesia–phosphate cement, Cem. Concr. Res. 32(1) (2002) 153-157.
[355] E. Vorndran, C. Moseke, U. Gbureck, 3D printing of ceramic implants, MRS Bull. 40(2) (2015) 127-136.
[356] T. Sugama, L. Kukacka, Characteristics of magnesium polyphosphate cements derived from ammonium polyphosphate solutions, Cem. Concr. Res. 13 (1983) 499.
[357] Q. Yang, B. Zhu, S. Zhang, X. Wu, Properties and applications of magnesia–phosphate cement mortar for rapid repair of concrete, Cem. Concr. Res. 30(11) (2000) 1807-1813.
[358] D.A. Hall, R. Stevens, B. El-Jazairi, The effect of retarders on the microstructure and mechanical properties of magnesia–phosphate cement mortar, Cem. Concr. Res. 31 (2001) 455.
[359] M. Kabu, M. Tosun, B. Elitok, M.S. Akosman, Histological evaluation of the effects of borax obtained from various sources in different rat organs, Int. J. Morphol. 33 (2015) 255-261.
[360] N. Gülsoy, C. Yavas, Ö. Mutlu, Genotoxic effects of boric acid and borax in zebrafish, Danio rerio using alkaline comet assay, EXCLI J. 14 (2015) 890-899.
[361] Y. Yu, J. Wang, C. Liu, B. Zhang, H. Chen, H. Guo, G. Zhong, W. Qu, S. Jiang, H. Huang, Evaluation of inherent toxicology and biocompatibility of magnesium phosphate bone cement, Colloids Surf. B: Biointerfaces 76(2) (2010) 496-504.
[362] S. Meininger, S. Mandal, A. Kumar, J. Groll, B. Basu, U. Gbureck, Strength reliability and in vitro degradation of three-dimensional powder printed strontium-substituted magnesium phosphate scaffolds, Acta Biomater. 31 (2016) 401-411.
[363] M. Le Rouzic, T. Chaussadent, L. Stefan, M. Saillio, On the influence of Mg/P ratio on the properties and durability of magnesium potassium phosphate cement pastes, Cem. Concr. Res. 96 (2017) 27-41.
[364] C.A. Sorre, C.R. Armstrong, Reactions and equilibria in magnesium oxychloride cements, J. Am. Ceram. Soc. 59(1-2) (1976) 51-54.
[365] L. Urwongse, C.A. Sorrell, The System MgO-MgCl2-H2O at 23°C, J. Am. Ceram. Soc. 63(9-10) (1980) 501-504.
[366] K. Sugimoto, R.E. Dinnebier, T. Schlecht, Chlorartinite, a volcanic exhalation product also found in industrial magnesia screed, J. Appl. Crystallogr. 39(5) (2006) 739-744.
[367] J. Péra, J. Ambroise, Fiber-reinforced magnesia-phosphate cement composites for rapid repair, Cem. Concr. Comp. 20(1) (1998) 31-39.
[368] P. Frantzis, R. Baggott, Bond between reinforcing steel fibres and magnesium phosphate/calcium aluminate binders, Cem. Concr. Comp. 22(3) (2000) 187-192.
[369] A. Robisson, S. Maheshwari, S. Musso, J.J. Thomas, F.M. Auzerais, D. Han, M. Qu, F.-J. Ulm, Reactive elastomeric composites: When rubber meets cement, Compos. Sci. Technol. 75 (2013) 77-83.
[370] R. Krüger, J.-M. Seitz, A. Ewald, F.-W. Bach, J. Groll, Strong and tough magnesium wire reinforced phosphate cement composites for load-bearing bone replacement, J. Mech. Behav. Biomed. Mater. 20 (2013) 36-44.
[371] M.P. Ginebra, M.G. Boltong, F.C.M. Driessens, O. Bermúdez, E. Fernández, J.A. Planell, Preparation and properties of some magnesium-containing calcium phosphate cements, J. Mater. Sci. - Mater. Med. 5(2) (1994) 103-107.
[372] I. Khairoun, M.G. Boltong, F.C.M. Driessens, J.A. Planell, Limited compliance of some apatitic calcium phosphate bone cements with clinical requirements, J. Mater. Sci. - Mater. Med. 9(11) (1998) 667-671.
[373] F.C.M. Driessens, M.G. Boltong, O. Bermúdez, J.A. Planell, M.P. Ginebra, E. Fernández, Effective formulations for the preparation of calcium phosphate bone cements, J. Mater. Sci. - Mater. Med. 5(3) (1994) 164-170.
[374] J. Jia, H. Zhou, J. Wei, X. Jiang, H. Hua, F. Chen, S. Wei, J.-W. Shin, C. Liu, Development of magnesium calcium phosphate biocement for bone regeneration, J. R. Soc. Interface 7(49) (2010) 1171-1180.
[375] D. Pijocha, G. Lói, W. Nocun-Wczelik, A. Slósarczyk, Effect of retardants on the heat release during setting of bone cement-type composites, J. Achiev. Mater. Manuf. Eng. 49(2) (2011) 204-209.
[376] J. Wei, J. Jia, F. Wu, S. Wei, H. Zhou, H. Zhang, J.-W. Shin, C. Liu, Hierarchically microporous/macroporous scaffold of magnesium–calcium phosphate for bone tissue regeneration, Biomaterials 31(6) (2010) 1260-1269.
[377] R.J. Elin, Assessment of magnesium status, Clin. Chem. 33(11) (1987) 1965-1970.
[378] R.K. Rude, Magnesium deficiency: A cause of heterogenous disease in humans, J. Bone Miner. Res. 13(4) (1998) 749-758.
[379] M.A. Kenney, H. McCoy, L. Williams, Effects of magnesium deficiency on strength, mass, and composition of rat femur, Calcif. Tissue Int. 54(1) (1994) 44-49.
[380] R.K. Rude, M.E. Kirchen, H.E. Gruber, A.A. Stasky, M.H. Meyer, Magnesium deficiency induces bone loss in the rat, Miner. Electrolyte Metab. 24(5) (1998) 314-320.
[381] A. Burmester, R. Willumeit-Römer, F. Feyerabend, Behavior of bone cells in contact with magnesium implant material, J. Biomed. Mater. Res. B: Appl. Biomat. 105(1) (2015) 165-179.
[382] S.A. Schendel, J. Peauroi, Magnesium-based bone cement and bone void filler: preliminary experimental studies, J. Craniofac. Surg. 20(2) (2009) 461-464.
[383] D. Zeng, L. Xia, W. Zhang, H. Huang, B. Wei, Q. Huang, J. Wei, C. Liu, X. Jiang, Maxillary sinus floor elevation using a tissue-engineered bone with calcium-magnesium phosphate cement and bone marrow stromal cells in rabbits, Tissue Eng. Part A 18(7-8) (2011) 870-881.

[384] J.-A. Kim, J. Lim, R. Naren, H.-S. Yun, E.K. Park, Effect of the biodegradation rate controlled by pore structures in magnesium phosphate ceramic scaffolds on bone tissue regeneration in vivo, Acta Biomater. 44 (2016) 155-167.
[385] C. Blum, T. Brückner, A. Ewald, A. Ignatius, U. Gbureck, Mg:Ca ratio as regulating factor for osteoclastic in vitro resorption of struvite biocements, Mater. Sci. Eng.: C 73 (2017) 111-119.
[386] M. Meininger, C. Wolf-Brandstetter, J. Zerweck, F. Wenninger, U. Gbureck, J. Groll, C. Moseke, Electrochemically assisted deposition of strontium modified magnesium phosphate on titanium surfaces, Mater. Sci. Eng.: C 67 (2016) 65-71.
[387] J. Lee, M.M. Farag, E.K. Park, J. Lim, H.-S. Yun, A simultaneous process of 3D magnesium phosphate scaffold fabrication and bioactive substance loading for hard tissue regeneration, Mater. Sci. Eng.: C 36(0) (2014) 252-260.
[388] A. Sugawara, J.M. Antonucci, S. Takagi, L.C. Chow, M. Ohashi, Formation of hydroxyapatite in hydrogels from tetracalcium phosphate/dicalcium phosphate mixtures, J. Nihon Univ. Sch. Dent. 31(1) (1989) 372-381.
[389] E.C.S. Rigo, L.A.d. Santos, L.C.O. Vercik, R.G. Carrodeduas, A.O. Boschi, Alpha-tricalcium phosphate- and tetracalcium phosphate/dicalcium phosphate-based dual setting, Lat. am. appl. res. 37(4) (2007) 267-274.
[390] M. Schamel, J. Groll, U. Gbureck, Simultaneous formation and mineralization of star-P(EO-stat-PO) hydrogels, Mater. Sci. Eng.: C 75 (2017) 471-477.
[391] M. Schamel, J.E. Barralet, M. Gelinsky, J. Groll, U. Gbureck, Intrinsic 3D prestressing: A new route for increasing strength and improving toughness of hybrid inorganic biocements, Adv. Mater. 29(35) (2017) 1701035.
[392] A.W.G. Walls, Glass polyalkenoate (glass-ionomer) cements: a review, J. Dent. 14(6) (1986) 231-246.
[393] A.D. Wilson, S. Crisp, A.J. Ferner, Reactions in glass-ionomer Cements: IV. Effect of chelating comonomers on setting behavior, J. Dent. Res. 55(3) (1976) 489-495.
[394] Y. Matsuya, J.M. Antonucci, S. Matsuya, S. Takagi, L.C. Chow, Polymeric calcium phosphate cements derived from poly(methyl vinyl ether-maleic acid), Dent. Mater. 12(1) (1996) 2-7.
[395] Y.E. Greish, P.W. Brown, Chemically formed HAp-Ca poly(vinyl phosphonate) composites, Biomaterials 22(8) (2001) 807-816.
[396] Y.E. Greish, P.W. Brown, J.D. Bender, H.R. Allcock, S. Lakshmi, C.T. Laurencin, Hydroxyapatite–polyphosphazane composites prepared at low temperatures, J. Am. Ceram. Soc. 90(9) (2007) 2728-2734.
[397] Z. Sheikh, M. Geffers, T. Christel, J.E. Barralet, U. Gbureck, Chelate setting of alkali ion substituted calcium phosphates, Ceram. Int. 41(8) (2015) 10010-10017.
[398] J. LeMaitre, C. Pittet, D. Brendlen, Pasty or liquid multiple constituent compositions for injectable calcium phosphate cements, Ecole Polytechnique Federale de Lausanne (EPFL), 2008.
[399] L. Chow, S. Takagi, Dual-Phase Cement Precursor Systems for Bone Repair, American Dental Association Health Foundation, 2007.
[400] M. Bohner, H. Tiainen, P. Michel, N. Döbelin, Design of an inorganic dual-paste apatite cement using cation exchange, J. Mater. Sci. - Mater. Med. 26(2) (2015) 63.
[401] M. Bohner, R. Luginbühl, C. Reber, N. Doebelin, G. Baroud, E. Conforto, A physical approach to modify the hydraulic reactivity of α-tricalcium phosphate powder, Acta Biomater. 5(9) (2009) 3524-3535.
[402] T. Aoba, E.C. Moreno, S. Shimoda, Competitive adsorption of magnesium and calcium ions onto synthetic and biological apatites, Calcif. Tissue Int. 51(2) (1992) 143-150.
[403] L.M. Grover, M.P. Hofmann, U. Gbureck, B. Kumarasami, J.E. Barralet, Frozen delivery of brushite calcium phosphate cements, Acta Biomater. 4(6) (2008) 1916-1923.
[404] H.H.K. Xu, L.E. Carey, C.G. Simon, Premixed macroporous calcium phosphate cement scaffold, J. Mater. Sci. - Mater. Med. 18(7) (2007) 1345-1353.
[405] A. Sugawara, L.C. Chow, S. Takagi, H. Chohayeb, In vitro evaluation of the sealing ability of a calcium phosphate cement when used as a root canal sealer-filler, J. Endod. 16(4) (1990) 162-165.
[406] J. Aberg, H. Brisby, H.B. Henriksson, A. Lindahl, P. Thomsen, H. Engqvist, Premixed acidic calcium phosphate cement: Characterization of strength and microstructure, J. Biomed. Mater. Res. B: Appl. Biomat. 93B(2) (2010) 436-441.
[407] J. Åberg, E. Pankotai, G. Hulsart Billström, M. Weszl, S. Larsson, C. Forster-Horváth, Z. Lacza, H. Engqvist, In vivo evaluation of an injectable premixed radiopaque calcium phosphate cement, Int. J. Biomater. 2011 (2011) 7.
[408] U. Gbureck, S. Dembski, R. Thull, J.E. Barralet, Factors influencing calcium phosphate cement shelf-life, Biomaterials 26(17) (2005) 3691-3697.
[409] S.R. Paital, N.B. Dahotre, Calcium phosphate coatings for bio-implant applications: Materials, performance factors, and methodologies, Mater. Sci. Eng. R Rep. 66(1–3) (2009) 1-70.
[410] M. Bohner, S. Tadier, N. van Garderen, A. de Gasparo, N. Döbelin, G. Baroud, Synthesis of spherical calcium phosphate particles for dental and orthopedic applications, Biomatter 3(2) (2013) e25103.
[411] M. Bohner, F. Baumgart, Theoretical model to determine the effects of geometrical factors on the resorption of calcium phosphate bone substitutes, Biomaterials 25(17) (2004) 3569-3582.
[412] O. Gauthier, J.-M. Bouler, P. Weiss, J. Bosco, G. Daculsi, E. Aguado, Kinetic study of bone ingrowth and ceramic resorption associated with the implantation of different injectable calcium-phosphate bone substitutes, J. Biomed. Mater. Res. 47(1) (1999) 28-35.

[413] O. Malard, J.M. Bouler, J. Guicheux, D. Heymann, P. Pilet, C. Coquard, G. Daculsi, Influence of biphasic calcium phosphate granulometry on bone ingrowth, ceramic resorption, and inflammatory reactions: Preliminary in vitro and in vivo study, J. Biomed. Mater. Res. 46(1) (1999) 103-111.
[414] F.M. Tamimi, J. Torres, I. Tresguerres, C. Clemente, E. López-Cabarcos, L.J. Blanco, Bone augmentation in rabbit calvariae: comparative study between Bio-Oss® and a novel β-TCP/DCPD granulate, J. Clin. Periodontol. 33(12) (2006) 922-928.
[415] F. Tamimi, J. Torres, D. Bassett, J. Barralet, E.L. Cabarcos, Resorption of monetite granules in alveolar bone defects in human patients, Biomaterials 31(10) (2010) 2762-2769.
[416] C. Moseke, C. Bayer, E. Vorndran, J. Barralet, J. Groll, U. Gbureck, Low temperature fabrication of spherical brushite granules by cement paste emulsion, J. Mater. Sci. - Mater. Med. 23(11) (2012) 2631-2637.
[417] D.J. Misiek, J.N. Kent, R.F. Carr, Soft tissue responses to hydroxylapatite particles of different shapes, J. Oral Maxillofac. Surg. 42(3) (1984) 150-160.
[418] W. Paul, C.P. Sharma, Development of porous spherical hydroxyapatite granules: application towards protein delivery, J. Mater. Sci. - Mater. Med. 10(7) (1999) 383-388.
[419] V.S. Komlev, S.M. Barinov, E.V. Koplik, A method to fabricate porous spherical hydroxyapatite granules intended for time-controlled drug release, Biomaterials 23(16) (2002) 3449-3454.
[420] V.S. Komlev, S.M. Barinov, E. Girardin, S. Oscarsson, Å. Rosengren, F. Rustichelli, V.P. Orlovskii, Porous spherical hydroxyapatite and fluorhydroxyapatite granules: processing and characterization, Sci. Technol. Adv. Mater. 4(6) (2003) 503-508.
[421] R.A. Perez, S. Del Valle, G. Altankov, M.-P. Ginebra, Porous hydroxyapatite and gelatin/hydroxyapatite microspheres obtained by calcium phosphate cement emulsion, J. Biomed. Mater. Res. B: Appl. Biomat. 97B(1) (2011) 156-166.
[422] T. Christel, M. Geffers, U. Klammert, B. Nies, A. Höß, J. Groll, A.C. Kübler, U. Gbureck, Fabrication and cytocompatibility of spherical magnesium ammonium phosphate granules, Mater. Sci. Eng.: C 42(0) (2014) 130-136.
[423] S. Nomura, K. Tsuru, S. Matsuya, I. Takahashi, K. Ishikawa, Fabrication of spherical carbonate apatite using calcium sulfate as a precursor by W/O emulsion method Key Eng. Mater. 529-530 (2013) 78-81.
[424] C.W. Kim, Y.-P. Yun, H.J. Lee, Y.-S. Hwang, I.K. Kwon, S.C. Lee, In situ fabrication of alendronate-loaded calcium phosphate microspheres: Controlled release for inhibition of osteoclastogenesis, J. Control. Release 147(1) (2010) 45-53.
[425] T.S. Pradeesh, M.C. Sunny, H.K. Varma, P. Ramesh, Preparation of microstructured hydroxyapatite microspheres using oil in water emulsions, Bull. Mater. Sci. 28(5) (2005) 383-390.
[426] J.-H. Yang, K.-H. Kim, C.-K. You, T.R. Rautray, T.-Y. Kwon, Synthesis of spherical hydroxyapatite granules with interconnected pore channels using camphene emulsion, J. Biomed. Mater. Res. B: Appl. Biomat. 99B(1) (2011) 150-157.
[427] H.-H. Lee, S.-J. Hong, C.-H. Kim, E.-C. Kim, J.-H. Jang, H.-I. Shin, H.-W. Kim, Preparation of hydroxyapatite spheres with an internal cavity as a scaffold for hard tissue regeneration, J. Mater. Sci. - Mater. Med. 19(9) (2008) 3029-3034.
[428] Y. Gonda, K. Ioku, Y. Shibata, T. Okuda, G. Kawachi, M. Kamitakahara, H. Murayama, K. Hideshima, S. Kamihira, I. Yonezawa, H. Kurosawa, T. Ikeda, Stimulatory effect of hydrothermally synthesized biodegradable hydroxyapatite granules on osteogenesis and direct association with osteoclasts, Biomaterials 30(26) (2009) 4390-4400.
[429] J.-S. Park, S.-J. Hong, H.-Y. Kim, H.-S. Yu, Y.I. Lee, C.-H. Kim, S.-J. Kwak, J.-H. Jang, J.K. Hyun, H.-W. Kim, Evacuated calcium phosphate spherical microcarriers for bone regeneration, Tissue Eng. Part A 16(5) (2009) 1681-1691.
[430] S.M. Oliveira, C.C. Barrias, I.F. Almeida, P.C. Costa, M.R.P. Ferreira, M.F. Bahia, M.A. Barbosa, Injectability of a bone filler system based on hydroxyapatite microspheres and a vehicle with in situ gel-forming ability, J. Biomed. Mater. Res. B: Appl. Biomat. 87B(1) (2008) 49-58.
[431] P.P. Cortez, L.M. Atayde, M.A. Silva, P. Armada-da-Silva, M.H. Fernandes, A. Afonso, M.A. Lopes, A.C. Maurício, J.D. Santos, Characterization and preliminary in vivo evaluation of a novel modified hydroxyapatite produced by extrusion and spheronization techniques, J. Biomed. Mater. Res. B: Appl. Biomat. 99B(1) (2011) 170-179.
[432] M. Fabbri, G.C. Celotti, A. Ravaglioli, Granulates based on calcium phosphate with controlled morphology and porosity for medical applications: physico-chemical parameters and production technique, Biomaterials 15(6) (1994) 474-477.
[433] A.Y.P. Mateus, C.C. Barrias, C. Ribeiro, M.P. Ferraz, F.J. Monteiro, Comparative study of nanohydroxyapatite microspheres for medical applications, J. Biomed. Mater. Res. A 86A(2) (2008) 483-493.
[434] M. Descamps, J.C. Hornez, A. Leriche, Manufacture of hydroxyapatite beads for medical applications, J. Eur. Ceram. Soc. 29(3) (2009) 369-375.
[435] E. Meurice, A. Leriche, J.-C. Hornez, F. Bouchart, E. Rguiti, L. Boilet, M. Descamps, F. Cambier, Functionalisation of porous hydroxyapatite for bone substitutes, J. Eur. Ceram. Soc. 32(11) (2012) 2673-2678.
[436] J.S. Cho, Y.N. Ko, H.Y. Koo, Y.C. Kang, Synthesis of nano-sized biphasic calcium phosphate ceramics with spherical shape by flame spray pyrolysis, J. Mater. Sci. - Mater. Med. 21(4) (2010) 1143-1149.
[437] D. Mohn, N. Doebelin, S. Tadier, R.E. Bernabei, N.A. Luechinger, W.J. Stark, M. Bohner, Reactivity of calcium phosphate nanoparticles prepared by flame spray synthesis as precursors for calcium phosphate cements, J. Mater. Chem. 21(36) (2011) 13963-13972.
[438] M. Aizawa, T. Terado, F.S. Howell, K. Itatani, Preparation of spherical apatite particles by the homogeneous precipitation method in the presence of magnesium ions and their ion-exchange properties, Mater. Res. Bull. 34(8) (1999) 1215-1225.

[439] K. Kandori, A. Yasukawa, T. Ishikawa, Preparation and characterization of spherical calcium hydroxyapatite, Chem. Mat. 7(1) (1995) 26-32.
[440] A. Cuneyt Tas, Submicron spheres of amorphous calcium phosphate forming in a stirred SBF solution at 55 °C, J. Non-Cryst. Solids 400 (2014) 27-32.
[441] W.Y. Zhou, M. Wang, W.L. Cheung, B.C. Guo, D.M. Jia, Synthesis of carbonated hydroxyapatite nanospheres through nanoemulsion, J. Mater. Sci. - Mater. Med. 19(1) (2008) 103-110.
[442] K. Tomoda, H. Ariizumi, T. Nakaji, K. Makino, Hydroxyapatite particles as drug carriers for proteins, Colloids Surf. B: Biointerfaces 76(1) (2010) 226-235.
[443] G. Bhakta, S. Mitra, A. Maitra, DNA encapsulated magnesium and manganous phosphate nanoparticles: potential non-viral vectors for gene delivery, Biomaterials 26(14) (2005) 2157-2163.
[444] G. Bhakta, A. Shrivastava, A. Maitra, Magnesium phosphate nanoparticles can be efficiently used in vitro and in vivo as non-viral vectors for targeted gene delivery, J. Biomed. Nanotechnol. 5(1) (2009) 106-114.
[445] E.H. Chowdhury, M. Kunou, M. Nagaoka, A.K. Kundu, T. Hoshiba, T. Akaike, High-efficiency gene delivery for expression in mammalian cells by nanoprecipitates of Ca–Mg phosphate, Gene 341 (2004) 77-82.
[446] M. Laurenti, A. Al Subaie, M.-N. Abdallah, A.R.G. Cortes, J.L. Ackerman, H. Vali, K. Basu, Y.L. Zhang, M. Murshed, S. Strandman, J. Zhu, N. Makhoul, J.E. Barralet, F. Tamimi, Two-dimensional magnesium phosphate nanosheets form highly thixotropic gels that up-regulate bone formation, Nano Lett. 16(8) (2016) 4779-4787.
[447] T. Brückner, U. Gbureck, Nano-magnesium phosphate hydrogels: efficiency of an injectable and biodegradable gel formulation towards bone regeneration, AME Med. J. 2(5) (2017).
[448] X. Li, Y. Niu, H. Guo, H. Chen, F. Li, J. Zhang, W. Chen, Z. Wu, Y. Deng, J. Wei, C. Liu, Preparation and osteogenic properties of magnesium calcium phosphate biocement scaffolds for bone regeneration, J. Instrum. 8(07) (2013) C07010.
[449] J. Zhang, W. Liu, O. Gauthier, S. Sourice, P. Pilet, G. Rethore, K. Khairoun, J.-M. Bouler, F. Tancret, P. Weiss, A simple and effective approach to prepare injectable macroporous calcium phosphate cement for bone repair: Syringe-foaming using a viscous hydrophilic polymeric solution, Acta Biomater. 31 (2016) 326-338.
[450] Y.H. Hsu, I.G. Turner, A.W. Miles, Mechanical characterization of dense calcium phosphate bioceramics with interconnected porosity, J. Mater. Sci. - Mater. Med. 18(12) (2007) 2319-2329.
[451] Y.H. Hsu, I.G. Turner, A.W. Miles, Fabrication of porous bioceramics with porosity gradients similar to the bimodal structure of cortical and cancellous bone, J. Mater. Sci. - Mater. Med. 18(12) (2007) 2251-2256.
[452] Y.H. Hsu, I.G. Turner, A.W. Miles, The effect of slip loading on the properties of porous calcium phosphate bioceramics, Key Eng. Mater. 361-363 (2008) 19-22.
[453] R. Detsch, F. Uhl, U. Deisinger, G. Ziegler, In vitro studies of cell growth on three differently fabricated hydroxyapatite ceramic scaffolds for bone tissue engineering, Key Eng. Mater. 361-363 (2008) 1181-1184.
[454] A. Ewald, B. Lochner, U. Gbureck, J. Groll, R. Krüger, Structural optimization of macroporous magnesium phosphate scaffolds and their cytocompatibility, Key Eng. Mater. 493-494 (2012) 813-819.
[455] S. Deville, E. Saiz, A.P. Tomsia, Freeze casting of hydroxyapatite scaffolds for bone tissue engineering, Biomaterials 27(32) (2006) 5480-5489.
[456] E. Landi, F. Valentini, A. Tampieri, Porous hydroxyapatite/gelatine scaffolds with ice-designed channel-like porosity for biomedical applications, Acta Biomater. 4(6) (2008) 1620-1626.
[457] S. Deville, Freeze-casting of porous ceramics: A review of current achievements and issues, Adv. Eng. Mater. 10(3) (2008) 155-169.
[458] S. Yunoki, T. Ikoma, A. Monkawa, K. Ohta, M. Kikuchi, S. Sotome, K. Shinomiya, J. Tanaka, Control of pore structure and mechanical property in hydroxyapatite/collagen composite using unidirectional ice growth, Mater. Lett. 60(8) (2006) 999-1002.
[459] G. Turco, E. Marsich, F. Bellomo, S. Semeraro, I. Donati, F. Brun, M. Grandolfo, A. Accardo, S. Paoletti, Alginate/hydroxyapatite biocomposite for bone ingrowth: A trabecular structure with high and isotropic connectivity, Biomacromolecules 10(6) (2009) 1575-1583.
[460] F. Ghorbani, H. Nojehdehian, A. Zamanian, Physicochemical and mechanical properties of freeze cast hydroxyapatite-gelatin scaffolds with dexamethasone loaded PLGA microspheres for hard tissue engineering applications, Mater. Sci. Eng.: C 69 (2016) 208-220.
[461] Y. Suetsugu, Y. Hotta, M. Iwasashi, M. Sakane, M. Kikuchi, T. Ikoma, T. Higaki, N. Ochiai, M. Tanaka, Structural and tissue reaction properties of novel hydroxyapatite ceramics with unidirectional pores, Key Eng. Mater. 330-332 (2007) 1003-1006.
[462] Q. Fu, M.N. Rahaman, B.S. Bal, R.F. Brown, Proliferation and function of MC3T3-E1 cells on freeze-cast hydroxyapatite scaffolds with oriented pore architectures, J. Mater. Sci. - Mater. Med. 20(5) (2009) 1159-1165.
[463] Q. Fu, M.N. Rahaman, B.S. Bal, R.F. Brown, In vitro cellular response to hydroxyapatite scaffolds with oriented pore architectures, Mater. Sci. Eng.: C 29(7) (2009) 2147-2153.
[464] Q. Fu, M.N. Rahaman, F. Dogan, B.S. Bal, Freeze casting of porous hydroxyapatite scaffolds. I. Processing and general microstructure, J. Biomed. Mater. Res. B: Appl. Biomat. 86B(1) (2008) 125-135.
[465] Q. Fu, M.N. Rahaman, F. Dogan, B.S. Bal, Freeze casting of porous hydroxyapatite scaffolds. II. Sintering, microstructure, and mechanical behavior, J. Biomed. Mater. Res. B: Appl. Biomat. 86B(2) (2008) 514-522.

[466] K.H. Zuo, Y.-P. Zeng, D. Jiang, Effect of polyvinyl alcohol additive on the pore structure and morphology of the freeze-cast hydroxyapatite ceramics, Mater. Sci. Eng.: C 30(2) (2010) 283-287.
[467] Y. Yang, F. He, J. Ye, Preparation, mechanical property and cytocompatibility of freeze-cast porous calcium phosphate ceramics reinforced by phosphate-based glass, Mater. Sci. Eng.: C 69 (2016) 1004-1009.
[468] Z.A. Shazni, M. Mariatti, A. Nurazreena, K.A. Razak, Properties of calcium phosphate scaffolds produced by freeze-casting, Procedia Chem. 19 (2016) 174-180.
[469] H. Lee, T.-S. Jang, J. Song, H.-E. Kim, H.-D. Jung, The production of porous hydroxyapatite scaffolds with graded porosity by sequential freeze-casting, Materials 10(4) (2017) 367.
[470] A. Zamanian, S. Farhangdoust, M. Yasaei, M. Khorami, M. Hafezi, The effect of particle size on the mechanical and microstructural properties of freeze-casted macroporous hydroxyapatite scaffolds, Int. J. Appl. Ceram. Tec. 11(1) (2014) 12-21.
[471] B.-H. Yoon, C.-S. Park, H.-E. Kim, Y.-H. Koh, In-situ fabrication of porous hydroxyapatite (HA) scaffolds with dense shells by freezing HA/camphene slurry, Mater. Lett. 62(10) (2008) 1700-1703.
[472] E.-J. Lee, Y.-H. Koh, B.-H. Yoon, H.-E. Kim, H.-W. Kim, Highly porous hydroxyapatite bioceramics with interconnected pore channels using camphene-based freeze casting, Mater. Lett. 61(11) (2007) 2270-2273.
[473] B.-H. Yoon, Y.-H. Koh, C.-S. Park, H.-E. Kim, Generation of large pore channels for bone tissue engineering using camphene-based freeze casting, J. Am. Ceram. Soc. 90(6) (2007) 1744-1752.
[474] Y.-M. Soon, K.-H. Shin, Y.-H. Koh, J.-H. Lee, H.-E. Kim, Compressive strength and processing of camphene-based freeze cast calcium phosphate scaffolds with aligned pores, Mater. Lett. 63(17) (2009) 1548-1550.
[475] S.-W. Yook, H.-E. Kim, B.-H. Yoon, Y.-M. Soon, Y.-H. Koh, Improvement of compressive strength of porous hydroxyapatite scaffolds by adding polystyrene to camphene-based slurries, Mater. Lett. 63(11) (2009) 955-958.
[476] K.K. Mallick, Freeze casting of porous bioactive glass and bioceramics, J. Am. Ceram. Soc. 92 (2009) S85-S94.
[477] M. Jafarkhani, A. Fazlali, F. Moztarzadeh, Z. Moztarzadeh, M. Mozafari, Fabrication and characterization of PLLA/chitosan/nano calcium phosphate scaffolds by freeze-casting technique, Ind. Eng. Chem. Res. 51(27) (2012) 9241-9249.
[478] S. Hesaraki, Freeze-casted nanostructured apatite scaffold obtained from low temperature biomineralization of reactive calcium phosphates, Key Eng. Mater. 587 (2014) 21-26.
[479] X. Qi, J. Ye, Y. Wang, Alginate/poly (lactic-co-glycolic acid)/calcium phosphate cement scaffold with oriented pore structure for bone tissue engineering, J. Biomed. Mater. Res. A 89A(4) (2009) 980-987.
[480] F. He, J. Li, J. Ye, Improvement of cell response of the poly(lactic-co-glycolic acid)/calcium phosphate cement composite scaffold with unidirectional pore structure by the surface immobilization of collagen via plasma treatment, Colloids Surf. B: Biointerfaces 103 (2013) 209-216.
[481] M. Schumacher, U. Deisinger, R. Detsch, G. Ziegler, Indirect rapid prototyping of biphasic calcium phosphate scaffolds as bone substitutes: influence of phase composition, macroporosity and pore geometry on mechanical properties, J. Mater. Sci. - Mater. Med. 21(12) (2010) 3119-3127.
[482] M. Schumacher, F. Uhl, R. Detsch, U. Deisinger, G. Ziegler, Static and dynamic cultivation of bone marrow stromal cells on biphasic calcium phosphate scaffolds derived from an indirect rapid prototyping technique, J. Mater. Sci. - Mater. Med. 21(11) (2010) 3039-3048.
[483] R. Detsch, F. Uhl, U. Deisinger, G. Ziegler, 3D-cultivation of bone marrow stromal cells on hydroxyapatite scaffolds fabricated by dispense-plotting and negative mould technique, J. Mater. Sci. - Mater. Med. 19(4) (2008) 1491-1496.
[484] U. Deisinger, S. Hamisch, M. Schumacher, F. Uhl, R. Detsch, G. Ziegler, Fabrication of tailored hydroxyapatite scaffolds: Comparison between a direct and an indirect rapid prototyping technique, Key Eng. Mater. 361-363 (2008) 915-918.
[485] T.-M.G. Chu, J.W. Halloran, S.J. Hollister, S.E. Feinberg, Hydroxyapatite implants with designed internal architecture, J. Mater. Sci. - Mater. Med. 12(6) (2001) 471-478.
[486] C.E. Wilson, C.A. van Blitterswijk, A.J. Verbout, W.J.A. Dhert, J.D. de Bruijn, Scaffolds with a standardized macro-architecture fabricated from several calcium phosphate ceramics using an indirect rapid prototyping technique, J. Mater. Sci. - Mater. Med. 22(1) (2011) 97-105.
[487] C.E. Wilson, J.D. de Bruijn, C.A. van Blitterswijk, A.J. Verbout, W.J.A. Dhert, Design and fabrication of standardized hydroxyapatite scaffolds with a defined macro-architecture by rapid prototyping for bone-tissue-engineering research, J. Biomed. Mater. Res. A 68A(1) (2004) 123-132.
[488] A. Butscher, M. Bohner, C. Roth, A. Ernstberger, R. Heuberger, N. Doebelin, P. Rudolf von Rohr, R. Müller, Printability of calcium phosphate powders for three-dimensional printing of tissue engineering scaffolds, Acta Biomater. 8(1) (2012) 373-385.
[489] A. Butscher, M. Bohner, N. Doebelin, S. Hofmann, R. Müller, New depowdering-friendly designs for three-dimensional printing of calcium phosphate bone substitutes, Acta Biomater. 9(11) (2013) 9149-9158.
[490] A. Butscher, M. Bohner, N. Doebelin, L. Galea, O. Loeffel, R. Müller, Moisture based three-dimensional printing of calcium phosphate structures for scaffold engineering, Acta Biomater. 9(2) (2013) 5369-5378.
[491] F. Tamimi, J. Torres, U. Gbureck, E. Lopez-Cabarcos, D.C. Bassett, M.H. Alkhraisat, J.E. Barralet, Craniofacial vertical bone augmentation: A comparison between 3D printed monolithic monetite blocks and autologous onlay grafts in the rabbit, Biomaterials 30(31) (2009) 6318-6326.
[492] U. Gbureck, T. Hölzel, I. Biermann, J.E. Barralet, L.M. Grover, Preparation of tricalcium phosphate/calcium pyrophosphate structures via rapid prototyping, J. Mater. Sci. - Mater. Med. 19(4) (2008) 1559-1563.

[493] M. Castilho, C. Moseke, A. Ewald, U. Gbureck, J. Groll, I. Pires, J. Teßmar, E. Vorndran, Direct 3D powder printing of biphasic calcium phosphate scaffolds for substitution of complex bone defects, Biofabrication 6(1) (2014) 015006.
[494] F. Tamimi, J. Torres, K. Al-Abedalla, E. Lopez-Cabarcos, M.H. Alkhraisat, D.C. Bassett, U. Gbureck, J.E. Barralet, Osseointegration of dental implants in 3D-printed synthetic onlay grafts customized according to bone metabolic activity in recipient site, Biomaterials 35(21) (2014) 5436-5445.
[495] M. Castilho, M. Dias, U. Gbureck, J. Groll, P. Fernandes, I. Pires, B. Gouveia, J. Rodrigues, E. Vorndran, Fabrication of computationally designed scaffolds by low temperature 3D printing, Biofabrication 5(3) (2013) 035012.
[496] E. Vorndran, M. Klarner, U. Klammert, L.M. Grover, S. Patel, J.E. Barralet, U. Gbureck, 3D powder printing of β-tricalcium phosphate ceramics using different strategies, Adv. Eng. Mater. 10(12) (2008) B67-B71.
[497] U. Gbureck, T. Hölzel, C.J. Doillon, F.A. Müller, J.E. Barralet, Direct printing of bioceramic implants with spatially localized angiogenic factors, Adv. Mater. 19(6) (2007) 795-800.
[498] U. Gbureck, E. Vorndran, F.A. Müller, J.E. Barralet, Low temperature direct 3D printed bioceramics and biocomposites as drug release matrices, J. Control. Release 122(2) (2007) 173-180.
[499] E. Vorndran, U. Klammert, A. Ewald, J.E. Barralet, U. Gbureck, Simultaneous immobilization of bioactives during 3D powder printing of bioceramic drug-release matrices, Adv. Funct. Mater. 20(10) (2010) 1585-1591.
[500] J.A. Inzana, D. Olvera, S.M. Fuller, J.P. Kelly, O.A. Graeve, E.M. Schwarz, S.L. Kates, H.A. Awad, 3D printing of composite calcium phosphate and collagen scaffolds for bone regeneration, Biomaterials 35(13) (2014) 4026-4034.
[501] M. Castilho, J. Rodrigues, I. Pires, B. Gouveia, M. Pereira, C. Moseke, J. Groll, A. Ewald, E. Vorndran, Fabrication of individual alginate-TCP scaffolds for bone tissue engineering by means of powder printing, Biofabrication 7(1) (2015) 015004.
[502] J. Suwanprateeb, W. Suvannapruk, K. Wasoontararat, Low temperature preparation of calcium phosphate structure via phosphorization of 3D-printed calcium sulfate hemihydrate based material, J. Mater. Sci. - Mater. Med. 21(2) (2010) 419-429.
[503] A. Khalyfa, S. Vogt, J. Weisser, G. Grimm, A. Rechtenbach, W. Meyer, M. Schnabelrauch, Development of a new calcium phosphate powder-binder system for the 3D printing of patient specific implants, J. Mater. Sci. - Mater. Med. 18(5) (2007) 909-916.
[504] E. Vorndran, K. Wunder, C. Moseke, I. Biermann, F.A. Müller, K. Zorn, U. Gbureck, Hydraulic setting Mg3(PO4)2 powders for 3D printing technology, Adv. Appl. Ceram. 110(8) (2011) 476-481.
[505] J. Will, R. Melcher, C. Treul, N. Travitzky, U. Kneser, E. Polykandriotis, R. Horch, P. Greil, Porous ceramic bone scaffolds for vascularized bone tissue regeneration, J. Mater. Sci. - Mater. Med. 19(8) (2008) 2781-2790.
[506] H. Seitz, U. Deisinger, B. Leukers, R. Detsch, G. Ziegler, Different calcium phosphate granules for 3-D printing of bone tissue engineering scaffolds, Adv. Eng. Mater. 11(5) (2009) B41-B46.
[507] R. Detsch, I. Dieser, U. Deisinger, F. Uhl, S. Hamisch, G. Ziegler, G. Lipps, Biofunctionalization of dispense-plotted hydroxyapatite scaffolds with peptides: Quantification and cellular response, J. Biomed. Mater. Res. A 92A(2) (2010) 493-503.
[508] B. Barboni, C. Mangano, L. Valbonetti, G. Marruchella, P. Berardinelli, A. Martelli, A. Muttini, A. Mauro, R. Bedini, M. Turriani, R. Pecci, D. Nardinocchi, V.L. Zizzari, S. Tetè, A. Piattelli, M. Mattioli, Synthetic bone substitute engineered with amniotic epithelial cells enhances bone regeneration after maxillary sinus augmentation, PLOS ONE 8(5) (2013) e63256.
[509] C. Mangano, B. Sinjari, J.A. Shibli, F. Mangano, S. Hamisch, A. Piattelli, V. Perrotti, G. Iezzi, A human clinical, histological, histomorphometrical, and radiographical study on biphasic HA-beta-TCP 30/70 in maxillary sinus augmentation, Clin. Implant Dent. Relat. Res. 17(3) (2015) 610-618.
[510] A.R. Akkineni, Y. Luo, M. Schumacher, B. Nies, A. Lode, M. Gelinsky, 3D plotting of growth factor loaded calcium phosphate cement scaffolds, Acta Biomater. 27 (2015) 264-274.
[511] A. Lode, K. Meissner, Y. Luo, F. Sonntag, S. Glorius, B. Nies, C. Vater, F. Despang, T. Hanke, M. Gelinsky, Fabrication of porous scaffolds by three-dimensional plotting of a pasty calcium phosphate bone cement under mild conditions, J. Tissue Eng. Regen. M. 8(9) (2014) 682-693.
[512] Y. Luo, A. Lode, F. Sonntag, B. Nies, M. Gelinsky, Well-ordered biphasic calcium phosphate-alginate scaffolds fabricated by multi-channel 3D plotting under mild conditions, J. Mater. Chem. B 1(33) (2013) 4088-4098.
[513] T. Ahlfeld, A.R. Akkineni, Y. Förster, T. Köhler, S. Knaack, M. Gelinsky, A. Lode, Design and fabrication of complex scaffolds for bone defect healing: combined 3D plotting of a calcium phosphate cement and a growth factor-loaded hydrogel, Ann. Biomed. Eng. 45(1) (2017) 224-236.
[514] A. Kumar, A.R. Akkineni, B. Basu, M. Gelinsky, Three-dimensional plotted hydroxyapatite scaffolds with predefined architecture: comparison of stabilization by alginate cross-linking versus sintering, J. Biomater. Appl. 30(8) (2016) 1168-1181.
[515] Y. Luo, A. Lode, C. Wu, J. Chang, M. Gelinsky, Alginate/nanohydroxyapatite scaffolds with designed core/shell structures fabricated by 3D plotting and in situ mineralization for bone tissue engineering, ACS Appl. Mater. Interfaces 7(12) (2015) 6541-6549.
[516] Y. Maazouz, E.B. Montufar, J. Guillem-Marti, I. Fleps, C. Ohman, C. Persson, M.P. Ginebra, Robocasting of biomimetic hydroxyapatite scaffolds using self-setting inks, J. Mater. Chem. B 2(33) (2014) 5378-5386.
[517] P. Miranda, A. Pajares, E. Saiz, A.P. Tomsia, F. Guiberteau, Mechanical properties of calcium phosphate scaffolds fabricated by robocasting, J. Biomed. Mater. Res. A 85A(1) (2008) 218-227.
[518] J. Cesarano, J.G. Dellinger, M.P. Saavedra, D.D. Gill, R.D. Jamison, B.A. Grosser, J.M. Sinn-Hanlon, M.S. Goldwasser, Customization of load-bearing hydroxyapatite lattice scaffolds, Int. J. Appl. Ceram. Tec. 2(3) (2005) 212-220.

[519] P. Miranda, E. Saiz, K. Gryn, A.P. Tomsia, Sintering and robocasting of β-tricalcium phosphate scaffolds for orthopaedic applications, Acta Biomater. 2(4) (2006) 457-466.
[520] P. Miranda, A. Pajares, E. Saiz, A.P. Tomsia, F. Guiberteau, Fracture modes under uniaxial compression in hydroxyapatite scaffolds fabricated by robocasting, J. Biomed. Mater. Res. A 83A(3) (2007) 646-655.
[521] J. Franco, P. Hunger, M.E. Launey, A.P. Tomsia, E. Saiz, Direct-write assembly of calcium phosphate scaffolds using a water-based hydrogel, Acta Biomater. 6(1) (2010) 218-228.
[522] J.G. Dellinger, J. Cesarano, R.D. Jamison, Robotic deposition of model hydroxyapatite scaffolds with multiple architectures and multiscale porosity for bone tissue engineering, J. Biomed. Mater. Res. A 82A(2) (2007) 383-394.
[523] M. Houmard, Q. Fu, M. Genet, E. Saiz, A.P. Tomsia, On the structural, mechanical, and biodegradation properties of HA/β-TCP robocast scaffolds, J. Biomed. Mater. Res. B: Appl. Biomat. 101(7) (2013) 1233-1242.
[524] R.C. Richard, M.S. Sader, J. Dai, R.M.S.M. Thiré, G.D.A. Soares, Beta-type calcium phosphates with and without magnesium: From hydrolysis of brushite powder to robocasting of periodic scaffolds, J. Biomed. Mater. Res. A 102(10) (2014) 3685-3692.
[525] U. Deisinger, Generating porous ceramic scaffolds: Processing and properties, Key Eng. Mater. 441 (2010) 155-179.
[526] T.H. Ang, F.S.A. Sultana, D.W. Hutmacher, Y.S. Wong, J.Y.H. Fuh, X.M. Mo, H.T. Loh, E. Burdet, S.H. Teoh, Fabrication of 3D chitosan–hydroxyapatite scaffolds using a robotic dispensing system, Mater. Sci. Eng.: C 20(1–2) (2002) 35-42.
[527] F.C.G.d. Sousa, J.R.G. Evans, Tubular hydroxyapatite scaffolds, Adv. Appl. Ceram. 104(1) (2005) 30-34.
[528] S. Michna, W. Wu, J.A. Lewis, Concentrated hydroxyapatite inks for direct-write assembly of 3-D periodic scaffolds, Biomaterials 26(28) (2005) 5632-5639.
[529] J.L. Simon, S. Michna, J.A. Lewis, E.D. Rekow, V.P. Thompson, J.E. Smay, A. Yampolsky, J.R. Parsons, J.L. Ricci, In vivo bone response to 3D periodic hydroxyapatite scaffolds assembled by direct ink writing, J. Biomed. Mater. Res. A 83A(3) (2007) 747-758.
[530] M. Casas-Luna, S. Tkachenko, M. Horynová, L. Klakurková, P. Gejdos, S. Diaz-de-la-Torre, L. Celko, J. Kaiser, E.B. Montufar, Interpenetrated magnesium–tricalcium phosphate composite: Manufacture, characterization and in vitro degradation test, Acta Metall. Sin.-Engl. 30(4) (2017) 319-325.
[531] J.M. Lane, J.E. Mait, A. Unnanuntana, B.P. Hirsch, A.D. Shaffer, O.A. Shonuga, 6.616 - Materials in fracture fixation, in: P. Ducheyne (Ed.), Comprehensive biomaterials, Elsevier, Oxford, 2011, pp. 219-235.
[532] V.A. Stadelmann, E. Bretton, A. Terrier, P. Procter, D.P. Pioletti, Calcium phosphate cement augmentation of cancellous bone screws can compensate for the absence of cortical fixation, J. Biomech. 43(15) (2010) 2869-2874.
[533] M. Gao, W. Lei, Z. Wu, D. Liu, L. Shi, Biomechanical evaluation of fixation strength of conventional and expansive pedicle screws with or without calcium based cement augmentation, Clin. Biomech. 26(3) (2011) 238-244.
[534] W.G. Horstmann, C.C.P.M. Verheyen, R. Leemans, An injectable calcium phosphate cement as a bone-graft substitute in the treatment of displaced lateral tibial plateau fractures, Injury 34(2) (2003) 141-144.
[535] S. Hoelscher-Doht, M. Jordan, C. Bonhoff, S. Frey, T. Blunk, R. Meffert, Bone substitute first or screws first? A biomechanical comparison of two operative techniques for tibial-head depression fractures, J. Orthop. Sci. 19(6) (2014) 978-983.
[536] Y.P. Charles, H. Pelletier, P. Hydier, S. Schuller, J. Garnon, E.A. Sauleau, J.P. Steib, P. Clavert, Pullout characteristics of percutaneous pedicle screws with different cement augmentation methods in elderly spines: An in vitro biomechanical study, Orthop. Traumatol. Surg. Res. 101(3) (2015) 369-374.
[537] B.J. Ahern, R.D. Harten, E.A. Gruskin, T.P. Schaer, Evaluation of a fiber reinforced drillable bone cement for screw augmentation in a sheep model—mechanical testing, Clin. Tansl. Sci. 3(3) (2010) 112-115.
[538] H.E. Achneck, B. Sileshi, R.M. Jamiolkowski, D.M. Albala, M.L. Shapiro, J.H. Lawson, A comprehensive review of topical hemostatic agents: Efficacy and recommendations for use, Ann. Surg. 251(2) (2010) 217-228.
[539] N. Howe, B. Cherpelis, Obtaining rapid and effective hemostasis: Part I. Update and review of topical hemostatic agents, J. Am. Acad. Dermatol. 69(5) (2013) 659.e1-659.e17.
[540] E.B. Wolvius, K.G.H. van der Wal, Bone wax as a cause of a foreign body granuloma in a cranial defect: a case report, Int. J. Oral. Maxillofac. Surg. 32(6) (2003) 656-658.
[541] W.K. Low, C.S. Sim, Bone wax foreign body granuloma in the mastoid, J. Otorhinolaryngol. Head Neck Surg. 64(1) (2002) 38-40.
[542] G. Ozerdem, M. Hidiroglu, A. Kucuker, A. Kunt, L. Cetin, Bone wax as a cause of a foreign body granuloma in a resternotomy : a case report, J. Cardiothorac. Surg. 8(Suppl 1) (2013) 121.
[543] A. Qayum, A.H. Koka, Foreign body reaction to bone wax an unusual cause of persistent serous discharge from iliac crest graft donor site and the possible means to avoid such complication - a case report, J. Med. Case Rep. 2(9097) (2009).
[544] F. Bhatti, J. Dunning, Does liberal use of bone wax increase the risk of mediastinitis?, Interact. Cardiovasc. Thorac. Surg. 2(4) (2003) 410-412.
[545] C. Katre, A. Triantafyllou, R.J. Shaw, J.S. Brown, Inferior alveolar nerve damage caused by bone wax in third molar surgery, Int. J. Oral. Maxillofac. Surg. 39(5) (2010) 511-513.
[546] J.M. Stein, C.J. Eskey, A.C. Mamourian, Mass effect in the thoracic spine from remnant bone wax: An MR imaging pitfall, Am. J. Neuroradiol. 31(5) (2010) 844-846.

[547] M.D. Finn, S.R. Schow, E.D. Schneiderman, Osseous regeneration in the presence of four common hemostatic agents, J. Oral Maxillofac. Surg. 50(6) (1992) 608-612.
[548] J.L. Ibarrola, J.E. Bjorenson, B. Peter Austin, H. Gerstein, Osseous reactions to three hemostatic agents, J. Endod. 11(2) (1985) 75-83.
[549] R.F. Vestergaard, A. Brüel, J.S. Thomsen, E.M. Hauge, K. Søballe, J.M. Hasenkam, The influence of hemostatic agents on bone healing after sternotomy in a porcine model, Ann. Thorac. Surg. 99(3) (2015) 1005-1011.
[550] T. Wellisz, J.K. Armstrong, J. Cambridge, Y.H. An, X. Wen, C.M. Hill, T.C. Fisher, The effects of a soluble polymer and bone wax on sternal healing in an animal model, Ann. Thorac. Surg. 85(5) (2008) 1776-1780.
[551] T. Wellisz, J. Armstrong, J. Cambridge, T. Fisher, Ostene, a new water-soluble bone hemostasis agent, J. Craniofac. Surg. 17(3) (2006) 420-425.
[552] J.R. Geary, V.K. Frantz, New absorbable hemostatic bone wax: experimental and clinical studies, Ann. Surg. 132(6) (1950) 1128-1137.
[553] D.P. Orgill, F.W. Ehret, J.F. Regan, J. Glowacki, J.B. Mulliken, Polyethylene glycol/microfibrillar collagen composite as a new resorbable hemostatic bone wax, J. Biomed. Mater. Res. 39(3) (1998) 358-363.
[554] J. Suwanprateeb, W. Suvannapruk, F. Thammarakcharoen, W. Chokevivat, P. Rukskul, Preparation and characterization of PEG–PPG–PEG copolymer/pregelatinized starch blends for use as resorbable bone hemostatic wax, J. Mater. Sci. - Mater. Med. 24(12) (2013) 2881-2888.
[555] J. Suwanprateeb, S. Kiertkrittikhoon, J. Kintarak, W. Suvannapruk, F. Thammarakcharoen, P. Rukskul, In vivo assessment of new resorbable PEG–PPG–PEG copolymer/starch bone wax in bone healing and tissue reaction of bone defect in rabbit model, J. Mater. Sci. - Mater. Med. 25(9) (2014) 2131-2139.
[556] B. Hoffmann, E. Volkmer, A. Kokott, M. Weber, S. Hamisch, M. Schieker, W. Mutschler, G. Ziegler, A new biodegradable bone wax substitute with the potential to be used as a bone filling material, J. Mater. Chem. 17(38) (2007) 4028-4033.
[557] K. Björses, L. Faxälv, C. Montan, K. Wildt-Persson, P. Fyhr, J. Holst, T.L. Lindahl, In vitro and in vivo evaluation of chemically modified degradable starch microspheres for topical haemostasis, Acta Biomater. 7(6) (2011) 2558-2565.
[558] G.H.P. Te Wierik, A.C. Eissens, J. Bergsma, A.W. Arends-Scholte, C.F. Lerk, A new generation of starch products as excipient in pharmaceutical tablets. II. High surface area retrograded pregelatinized potato starch products in sustained-release tablets, J. Control. Release 45(1) (1997) 25-33.
[559] V. Michailova, S. Titeva, R. Kotsilkova, E. Krusteva, E. Minkov, Influence of hydrogel structure on the processes of water penetration and drug release from mixed hydroxypropylmethyl cellulose/thermally pregelatinized waxy maize starch hydrophilic matrices, Int. J. Pharm. 222(1) (2001) 7-17.
[560] P.B. Malafaya, G.A. Silva, R.L. Reis, Natural–origin polymers as carriers and scaffolds for biomolecules and cell delivery in tissue engineering applications, Adv. Drug Deliv. Rev. 59(4–5) (2007) 207-233.
[561] J. Nakamatsu, F.G. Torres, O.P. Troncoso, Y. Min-Lin, A.R. Boccaccini, Processing and characterization of porous structures from chitosan and starch for tissue engineering scaffolds, Biomacromolecules 7(12) (2006) 3345-3355.
[562] F.G. Torres, A.R. Boccaccini, O.P. Troncoso, Microwave processing of starch-based porous structures for tissue engineering scaffolds, J. Appl. Polym. Sci. 103(2) (2007) 1332-1339.
[563] C. Chen, H. Li, J. Pan, Z. Yan, Z. Yao, W. Fan, C. Guo, Biodegradable composite scaffolds of bioactive glass/chitosan/carboxymethyl cellulose for hemostatic and bone regeneration, Biotechnol. Lett. 37(2) (2015) 457-465.
[564] A.M. Young, S. Man Ho, E.A. Abou Neel, I. Ahmed, J.E. Barralet, J.C. Knowles, S.N. Nazhat, Chemical characterization of a degradable polymeric bone adhesive containing hydrolysable fillers and interpretation of anomalous mechanical properties, Acta Biomater. 5(6) (2009) 2072-2083.
[565] C. Heiss, R. Kraus, F. Peters, W. Henn, M. Schnabelrauch, A. Berg, T. Pautzsch, J. Weisser, R. Schnettler, Development of a bioresorbable self-hardening bone adhesive based on a composite consisting of polylactide methacrylates and β-tricalcium phosphate, J. Biomed. Mater. Res. B: Appl. Biomat. 90B(1) (2009) 55-66.
[566] K. Gellynck, E.A. Abou Neel, H. Li, N. Mardas, N. Donos, P. Buxton, A.M. Young, Cell attachment and response to photocured, degradable bone adhesives containing tricalcium phosphate and purmorphamine, Acta Biomater. 7(6) (2011) 2672-2677.
[567] M. Waselau, V.F. Samii, S.E. Weisbrode, A.S. Litsky, A.L. Bertone, Effects of a magnesium adhesive cement on bone stability and healing following a metatarsal osteotomy in horses, Am. J. Vet. Res, 68(4) (2007) 370-378.
[568] S. Rammelt, H. Zwipp, Calcaneus fractures: facts, controversies and recent developments, Injury 35(5) (2004) 443-461.
[569] S. Rausch, K. Klos, U. Wolf, M. Gras, P. Simons, S. Brodt, M. Windolf, B. Gueorguiev, A biomechanical comparison of fixed angle locking compression plate osteosynthesis and cement augmented screw osteosynthesis in the management of intra articular calcaneal fractures, Int. Orthop. 38(8) (2014) 1705-1710.
[570] Y. Taniwaki, R. Takemasa, T. Tani, H. Mizobuchi, H. Yamamoto, Enhancement of pedicle screw stability using calcium phosphate cement in osteoporotic vertebrae: in vivo biomechanical study, J. Orthop. Sci. 8(3) (2003) 408-414.
[571] H. Yamamoto, S. Niwa, M. Hori, T. Hattori, K. Sawai, S. Aoki, M. Hirano, H. Takeuchi, Mechanical strength of calcium phosphate cement in vivo and in vitro, Biomaterials 19(17) (1998) 1587-1591.
[572] K.S. Leung, W.S. Siu, S.F. Li, L. Qin, W.H. Cheung, K.F. Tam, P.P.Y. Lui, An in vitro optimized injectable calcium phosphate cement for augmenting screw fixation in osteopenic goats, J. Biomed. Mater. Res. B: Appl. Biomat. 78B(1) (2006) 153-160.

[573] M. Yazu, A. Kin, R. Kosaka, M. Kinoshita, M. Abe, Efficacy of novel-concept pedicle screw fixation augmented with calcium phosphate cement in the osteoporotic spine, J. Orthop. Sci. 10(1) (2005) 56-61.
[574] C.J. Stankewich, M.F. Swiontkowski, A.F. Tencer, D.N. Yetkinler, R.D. Poser, Augmentation of femoral neck fracture fixation with an injectable calcium-phosphate bone mineral cement, J. Orthop. Res. 14(5) (1996) 786-793.
[575] K. Ishikawa, S. Takagi, L. Chow, Y. Ishikawa, Properties and mechanisms of fast-setting calcium phosphate cements, J. Mater. Sci. - Mater. Med. 6(9) (1995) 528-533.
[576] M. Bohner, G.H. van Lenthe, S. Grünenfelder, W. Hirsiger, R. Evison, R. Müller, Synthesis and characterization of porous -tricalcium phosphate blocks, Biomaterials 26(31) (2005) 6099-6105.
[577] F.C.M. Driessens, M.G. Boltong, O. Bermudez, J.A. Planell, Formulation and setting times of some calcium orthophosphate cements: a pilot study, J. Mater. Sci. - Mater. Med. 4(5) (1993) 503-508.
[578] J. Galante, W. Rostoker, R.D. Ray, Physical properties of trabecular bone, Calc. Tis. Res. 5(1) (1970) 236-246.
[579] H. Ohta, S. Wakitani, K. Tensho, H. Horiuchi, S. Wakabayashi, N. Saito, Y. Nakamura, K. Nozaki, Y. Imai, K. Takaoka, The effects of heat on the biological activity of recombinant human bone morphogenetic protein-2, J. Bone. Miner. Metab. 23(6) (2005) 420-425.
[580] K. Ishikawa, Calcium phosphate cement: regulations in anti-washout property, in: B. Ben-Nissan (Ed.), Advances in calcium phosphate biomaterials, Springer, Berlin Heidelberg, 2014, pp. 216–217.
[581] A. Cipitria, A. Skelton, T.R. Dargaville, P.D. Dalton, D.W. Hutmacher, Design, fabrication and characterization of PCL electrospun scaffolds-a review, J. Mater. Chem. 21(26) (2011) 9419-9453.
[582] F. Chen, G. Hochleitner, T. Woodfield, J. Groll, P.D. Dalton, B.G. Amsden, Additive manufacturing of a photo-cross-linkable polymer via direct melt electrospinning writing for producing high strength structures, Biomacromolecules 17(1) (2016) 208-214.
[583] B. Sun, X.-J. Jiang, S. Zhang, J.-C. Zhang, Y.-F. Li, Q.-Z. You, Y.-Z. Long, Electrospun anisotropic architectures and porous structures for tissue engineering, J. Mater. Chem. B 3(27) (2015) 5389-5410.
[584] T.D. Brown, P.D. Dalton, D.W. Hutmacher, Direct writing by way of melt electrospinning, Adv. Mater. 23(47) (2011) 5651-5657.
[585] P.D. Dalton, C. Vaquette, B.L. Farrugia, T.R. Dargaville, T.D. Brown, D.W. Hutmacher, Electrospinning and additive manufacturing: converging technologies, Biomater. Sci. 1(2) (2013) 171-185.
[586] L.F. Brooke, D.B. Toby, U. Zee, W.H. Dietmar, D.D. Paul, R.D. Tim, Dermal fibroblast infiltration of poly(ε-caprolactone) scaffolds fabricated by melt electrospinning in a direct writing mode, Biofabrication 5(2) (2013) 025001.
[587] G. Hochleitner, T. Jüngst, T.D. Brown, K. Hahn, C. Moseke, F. Jakob, P.D. Dalton, J. Groll, Additive manufacturing of scaffolds with sub-micron filaments via melt electrospinning writing, Biofabrication 7(3) (2015) 035002.
[588] T.D. Brown, A. Slotosch, L. Thibaudeau, A. Taubenberger, D. Loessner, C. Vaquette, P.D. Dalton, D.W. Hutmacher, Design and fabrication of tubular scaffolds via direct writing in a melt electrospinning mode, Biointerphases 7(1) (2012) 13.
[589] S. Zaiss, T.D. Brown, J.C. Reichert, A. Berner, Poly(ε-caprolactone) scaffolds fabricated by melt electrospinning for bone tissue engineering, Materials 9(4) (2016) 232.
[590] M. Shin, O. Ishii, T. Sueda, J.P. Vacanti, Contractile cardiac grafts using a novel nanofibrous mesh, Biomaterials 25(17) (2004) 3717-3723.
[591] O. Ishii, M. Shin, T. Sueda, J.P. Vacanti, In vitro tissue engineering of a cardiac graft using a degradable scaffold with an extracellular matrix–like topography, J. Thorac. Cardiovasc. Surg. 130(5) (2005) 1358-1363.
[592] W.-J. Li, R.L. Mauck, J.A. Cooper, X. Yuan, R.S. Tuan, Engineering controllable anisotropy in electrospun biodegradable nanofibrous scaffolds for musculoskeletal tissue engineering, J. Biomech. 40(8) (2007) 1686-1693.
[593] W.-J. Li, R. Tuli, C. Okafor, A. Derfoul, K.G. Danielson, D.J. Hall, R.S. Tuan, A three-dimensional nanofibrous scaffold for cartilage tissue engineering using human mesenchymal stem cells, Biomaterials 26(6) (2005) 599-609.
[594] A.A. Bulysheva, G.L. Bowlin, A.J. Klingelhutz, W.A. Yeudall, Low-temperature electrospun silk scaffold for in vitro mucosal modeling, J. Biomed. Mater. Res. A 100(3) (2012) 757-767.
[595] M.F. Leong, M.Z. Rasheed, T.C. Lim, K.S. Chian, In vitro cell infiltration and in vivo cell infiltration and vascularization in a fibrous, highly porous poly(D,L-lactide) scaffold fabricated by cryogenic electrospinning technique, J. Biomed. Mater. Res. A 91A(1) (2009) 231-240.
[596] C. Vaquette, J.J. Cooper-White, Increasing electrospun scaffold pore size with tailored collectors for improved cell penetration, Acta Biomater. 7(6) (2011) 2544-2557.
[597] D. Grafahrend, K.-H. Heffels, M.V. Beer, P. Gasteier, M. Möller, G. Boehm, P.D. Dalton, J. Groll, Degradable polyester scaffolds with controlled surface chemistry combining minimal protein adsorption with specific bioactivation, Nat. Mater. 10(1) (2011) 67-73.
[598] D. Grafahrend, K.-H. Heffels, M. Möller, D. Klee, J. Groll, Electrospun, biofunctionalized fibers as tailored in vitro substrates for keratinocyte cell culture, Macromol. Biosci. 10(9) (2010) 1022-1027.
[599] M.D. Weir, H.H.K. Xu, C.G. Simon, Strong calcium phosphate cement-chitosan-mesh construct containing cell-encapsulating hydrogel beads for bone tissue engineering, J. Biomed. Mater. Res. A 77A(3) (2006) 487-496.
[600] C.M. Chan, T.M. Ko, H. Hiraoka, Polymer surface modification by plasmas and photons, Surf. Sci. Rep. 24(1) (1996) 1-54.
[601] A. Martins, E.D. Pinho, S. Faria, I. Pashkuleva, A.P. Marques, R.L. Reis, N.M. Neves, Surface modification of electrospun polycaprolactone nanofiber meshes by plasma treatment to enhance biological performance, Small 5(10) (2009) 1195-1206.

[602] H.-S. Yu, J.-H. Jang, T.-I. Kim, H.-H. Lee, H.-W. Kim, Apatite-mineralized polycaprolactone nanofibrous web as a bone tissue regeneration substrate, J. Biomed. Mater. Res. A 88A(3) (2009) 747-754.
[603] L. Ghasemi-Mobarakeh, M.P. Prabhakaran, M. Morshed, M.H. Nasr-Esfahani, S. Ramakrishna, Bio-functionalized PCL nanofibrous scaffolds for nerve tissue engineering, Mater. Sci. Eng.: C 30(8) (2010) 1129-1136.
[604] A. Oyane, M. Uchida, C. Choong, J. Triffitt, J. Jones, A. Ito, Simple surface modification of poly(ε-caprolactone) for apatite deposition from simulated body fluid, Biomaterials 26(15) (2005) 2407-2413.
[605] Z. Ma, W. He, T. Yong, S. Ramakrishna, Grafting of gelatin on electrospun poly(caprolactone) nanofibers to improve endothelial cell spreading and proliferation and to control cell orientation, Tissue Eng. 11(7-8) 1149-1158.
[606] C.X.F. Lam, M.M. Savalani, S.-H. Teoh, D.W. Hutmacher, Dynamics of in vitro polymer degradation of polycaprolactone-based scaffolds: accelerated versus simulated physiological conditions, Biomed. Mater. 3(3) (2008) 034108.
[607] C.X.F. Lam, D.W. Hutmacher, J.-T. Schantz, M.A. Woodruff, S.H. Teoh, Evaluation of polycaprolactone scaffold degradation for 6 months in vitro and in vivo, J. Biomed. Mater. Res. A 90A(3) (2009) 906-919.
[608] C.X.F. Lam, S.H. Teoh, D.W. Hutmacher, Comparison of the degradation of polycaprolactone and polycaprolactone–(β-tricalcium phosphate) scaffolds in alkaline medium, Polym. Int. 56(6) (2007) 718-728.
[609] Y. Yuan, T.R. Lee, Contact angle and wetting properties, in: G. Bracco, B. Holst (Eds.), Surface science techniques, Springer Berlin Heidelberg, Berlin, Heidelberg, 2013, pp. 3-34.
[610] F. Tamimi, D.L. Nihouannen, D.C. Bassett, S. Ibasco, U. Gbureck, J. Knowles, A. Wright, A. Flynn, S.V. Komarova, J.E. Barralet, Biocompatibility of magnesium phosphate minerals and their stability under physiological conditions, Acta Biomater. 7(6) (2011) 2678-2685.
[611] E. Graf, J.W. Eaton, Antioxidant functions of phytic acid, Free Radic. Biol. Med. 8(1) (1990) 61-69.
[612] H. Bieth, P. Jost, B. Spiess, C. Wehrer, Effect of the alkali-metal cations on the protonation constants of myo-inositol hexakis(phosphate), Anal. Lett. 22(3) (1989) 703-717.
[613] H. Bieth, B. Spiess, P. Jost, Complexation studies on inositol-phosphates. I. Ca(II) and Mg(II) complexes of D-myo-inositol 1,2,6-trisphosphate, J. Inorg. Biochem. 39(1) (1990) 59-73.
[614] M.H. Alkhraisat, J. Cabrejos-Azama, C.R. Rodríguez, L.B. Jerez, E.L. Cabarcos, Magnesium substitution in brushite cements, Mater. Sci. Eng.: C 33(1) (2013) 475-481.
[615] Z. Meleti, I.M. Shapiro, C.S. Adams, Inorganic phosphate induces apoptosis of osteoblast-like cells in culture, Bone 27(3) (2000) 359-366.
[616] P. Ekholm, L. Virkki, M. Ylinen, L. Johansson, The effect of phytic acid and some natural chelating agents on the solubility of mineral elements in oat bran, Food Chem. 80(2) (2003) 165-170.
[617] H.S. Mahanti, R.M. Barnes, Determination of major, minor and trace elements in bone by inductively-coupled plasma emission spectrometry, Anal. Chim. Acta 151 (1983) 409-417.
[618] S.C. Weber, M.W. Chapman, Adhesives in orthopaedic surgery. A review of the literature and in vitro bonding strengths of bone-bonding agents., Clin. Orthop. Rel. Res. 191 (1984) 249-261.
[619] T. Şekercíoğlu, H. Rende, A. Gülsöz, C. Meran, The effects of surface roughness on the strength of adhesively bonded cylindrical components, J. Mater. Process. Tech. 142(1) (2003) 82-86.
[620] S. Budhe, A. Ghumatkar, N. Birajdar, M.D. Banea, Effect of surface roughness using different adherend materials on the adhesive bond strength, Appl. Adhes. Sci. 3(1) (2015) 20.
[621] R.A. Gittens, R. Olivares-Navarrete, Z. Schwartz, B.D. Boyan, Implant osseointegration and the role of microroughness and nanostructures: Lessons for spine implants, Acta Biomater. 10(8) (2014) 3363-3371.
[622] P. Habibovic, F. Barrère, C.A. Van Blitterswijk, K. de Groot, P. Layrolle, Biomimetic hydroxyapatite coating on metal implants, J. Am. Ceram. Soc. 85(3) (2002) 517-522.
[623] J.C. Keller, E.P. Lautenschlager, G.W. Marshall, P.R. Meyer, Factors affecting surgical alloy/bone cement interface adhesion, J. Biomed. Mater. Res. 14(5) (1980) 639-651.
[624] K. Ishihara, N. Nakabayashi, Adhesive bone cement both to bone and metals: 4-META in MMA initiated with tri-n-butyl borane, J. Biomed. Mater. Res. 23(12) (1989) 1475-1482.
[625] M. Bohner, G. Baroud, A. Bernstein, N. Döbelin, L. Galea, B. Hesse, R. Heuberger, S. Meille, P. Michel, B. von Rechenberg, J. Sague, H. Seeherman, Characterization and distribution of mechanically competent mineralized tissue in micropores of β-tricalcium phosphate bone substitutes, Mater. Today 20(3) (2017) 106-115.
[626] M. Bohner, S. Matter, Brushite hydraulic cement stabilized with a magnesium salt, Mathys Dr H C Stiftung, Synthes USA LLC, 2004.
[627] S.C. Cox, S. Patel, U. Gbureck, A.J. Wright, L.M. Grover, A cohesive premixed monetite biocement, J. Am. Ceram. Soc. 100(3) (2017) 1241-1249.
[628] Y. Li, S.-K. Chen, L. Li, L. Qin, X.-L. Wang, Y.-X. Lai, Bone defect animal models for testing efficacy of bone substitute biomaterials, J. Orthop. Translat. 3(3) (2015) 95-104.
[629] K. Takafumi, U. Takao, S. Masao, The synthesis of Mg3(PO4)2·8H2O and its new polymorphism, Bull. Chem. Soc. Jpn. 52(12) (1979) 3713-3717.
[630] M. Catti, M. Franchini-Angela, G. Ivaldi, A case of polytypism in hydrated oxysalts: the crystal structure of Mg3(PO4)2 · 22 H2O-II, Z. Kristallog. – Cryst. Mater., 1981, pp. 53-64.

[631] L. Chen, Y. Shen, A. Xie, F. Huang, W. Zhang, S. Liu, Seed-mediated synthesis of unusual struvite hierarchical superstructures using bacterium, Cryst. Growth Des. 10(5) (2010) 2073-2082.
[632] A.E. Jakus, A.L. Rutz, S.W. Jordan, A. Kannan, S.M. Mitchell, C. Yun, K.D. Koube, S.C. Yoo, H.E. Whiteley, C.-P. Richter, R.D. Galiano, W.K. Hsu, S.R. Stock, E.L. Hsu, R.N. Shah, Hyperelastic “bone”: A highly versatile, growth factor–free, osteoregenerative, scalable, and surgically friendly biomaterial, Sci. Transl. Med. 8(358) (2016) 358ra127-358ra127.
[633] S. Van Vlierberghe, P. Dubruel, E. Schacht, Biopolymer-based hydrogels as scaffolds for tissue engineering applications: A review, Biomacromolecules 12(5) (2011) 1387-1408.
[634] S.J. Kalita, S. Bose, H.L. Hosick, A. Bandyopadhyay, Development of controlled porosity polymer-ceramic composite scaffolds via fused deposition modeling, Mater. Sci. Eng.: C 23(5) (2003) 611-620.
[635] J.-T. Schantz, A. Brandwood, D.W. Hutmacher, H.L. Khor, K. Bittner, Osteogenic differentiation of mesenchymal progenitor cells in computer designed fibrin-polymer-ceramic scaffolds manufactured by fused deposition modeling, J. Mater. Sci. - Mater. Med. 16(9) (2005) 807-819.
[636] M.J. Mondrinos, R. Dembzynski, L. Lu, V.K.C. Byrapogu, D.M. Wootton, P.I. Lelkes, J. Zhou, Porogen-based solid freeform fabrication of polycaprolactone–calcium phosphate scaffolds for tissue engineering, Biomaterials 27(25) (2006) 4399-4408.
[637] L. Shor, S. Güçeri, X. Wen, M. Gandhi, W. Sun, Fabrication of three-dimensional polycaprolactone/hydroxyapatite tissue scaffolds and osteoblast-scaffold interactions in vitro, Biomaterials 28(35) (2007) 5291-5297.
[638] K. Jinku, M. Sean, T. Brandi, A.-U. Pedro, S. Young-Hye, D.D. David, L.S. Victor, E. Hoda, O. Joo, O.H. Jeffrey, Rapid-prototyped PLGA/β-TCP/hydroxyapatite nanocomposite scaffolds in a rabbit femoral defect model, Biofabrication 4(2) (2012) 025003.
[639] B. Perissutti, J.M. Newton, F. Podczeck, F. Rubessa, Preparation of extruded carbamazepine and PEG 4000 as a potential rapid release dosage form, Eur. J. Pharm. Biopharm. 53(1) (2002) 125-132.
[640] N. Venkataraman, S. Rangarajan, M.J. Matthewson, B. Harper, A. Safari, S.C. Danforth, G. Wu, N. Langrana, S. Guceri, A. Yardimci, Feedstock material property – process relationships in fused deposition of ceramics (FDC), Rapid Prototyping J. 6(4) (2000) 244-253.
[641] Q. Zhu, L.S. Taylor, M.T. Harris, Evaluation of the microstructure of semicrystalline solid dispersions, Mol. Pharm. 7(4) (2010) 1291-1300.
[642] H. Li, M.A. Huneault, Effect of nucleation and plasticization on the crystallization of poly(lactic acid), Polymer 48(23) (2007) 6855-6866.
[643] J. Engstrand Unosson, C. Persson, H. Engqvist, An evaluation of methods to determine the porosity of calcium phosphate cements, J. Biomed. Mater. Res. B: Appl. Biomat. 103(1) (2015) 62-71.
[644] S.N. Danilchenko, O.G. Kukharenko, C. Moseke, I.Y. Protsenko, L.F. Sukhodub, B. Sulkio-Cleff, Determination of the bone mineral crystallite size and lattice strain from diffraction line broadening, Crys. Res. Technol. 37(11) (2002) 1234-1240.
[645] L. Alexander, H.P. Klug, Basic aspects of X-ray absorption in quantitative diffraction analysis of powder mixtures, Anal. Chem. 20(10) (1948) 886-889.

Acknowledgements

Zunächst möchte ich mich bei Prof. Jürgen Groll für die Möglichkeit, am Lehrstuhl für Funktionswerkstoffe der Medizin und der Zahnheilkunde meine Doktorarbeit durchführen zu können, sowie für die Begutachtung der Dissertation, bedanken. Bei Prof. Matthias Lehmann möchte ich mich ebenfalls dafür bedanken, dass er sich die Zeit zur Begutachtung meiner Arbeit genommen hat. Meinem Doktorvater Prof. Uwe Gbureck danke ich für seinen Ideenreichtum, seine Betreuung und permanente Diskussionsbereitschaft.

Für den angeregten Informationsaustausch danke ich Prof. Alexander Kübler und PD Uwe Klammert von der Mund-Kiefer-Gesichtschirurgie, sowie PD Stefanie Hölscher-Doht und Dr. med. Martin Jordan von der Unfallchirurgie des Universitätsklinikums Würzburg. Bei den Kooperationspartnern Dr. Berthold Nies, Dr. Andreas Höß und Dr. Sascha Heinemann von InnoTERE in Radebeul bedanke ich mich für die Bereitstellung präfabrizierter Pasten und die gute Zusammenarbeit. Letzteres gilt ebenso für Prof. Friedlinde Götz-Neunhoeffer, Prof. Jürgen Neubauer und Dr. Katrin Hurle des Lehrstuhls für Mineralogie der Friedrich-Alexander-Universität Erlangen-Nürnberg, sowie Prof. Sarit Bhaduri der Abteilung für Chirurgie der Universität in Toledo, USA.

Der Bayerischen Forschungsallianz und Dr. Elke Vorndran danke ich für die Finanzierung des Forschungsaufenthalts in Montréal, Kanada. An dieser Stelle bedanke ich mich auch bei Prof. Jake Barralet der Abteilung für Zahnheilkunde der McGill Universität für die freundliche Aufnahme. Ich danke außerdem dem Bundesministerium für Bildung und Forschung, sowie der Deutschen Forschungsgemeinschaft für die Finanzierung meiner Doktorarbeit.

Für die Unterstützung am Rasterelektronenmikroskop bedanke ich mich bei Dr. Claus Moseke, Apothekerin Michaela, Dipl.-Phys. Philipp Stahlhut und Judith Friedlein. M. Sc. Markus Meininger danke ich für seine Hilfe bei der energiedispersen Röntgenspektroskopie. Des Weiteren gilt mein Dank der Deutschen Forschungsgemeinschaft für die Finanzierung des Rasterelektronenmikroskops unter der Förderungsnummer INST 105022/58-1 FUGG. M. Sc. Julia Blöhbaum danke ich für ihre Hilfestellung im Syntheselabor; Prof. Paul Dalton, M. Eng. Hochleitner und Apothekerin Laura Wistlich bei der Bereitstellung sowie Unterstützung bei der Herstellung von elektrogesponnenen Materialien. Bei Dr. Andrea Ewald, M. Sc. Kathrin Hahn, M. Sc. Carina Blum, Maria Aniolek und Simone Werner möchte ich mich dafür bedanken, dass sie mir während meiner Aufenthalte in den Biolaboren mit Rat und Tat zur Seite standen. Den Kollegen Anton Hofmann und Harald Hümpfer aus der Werkstatt danke ich für die Bereitstellung von Metalloberflächen, -prüfkörpern und Werkzeugen jeglicher Art, sowie speziellen Prüfaufbauten für die mechanische Testung. Harald Hümpfer danke ich besonders für seinen permanenten Einsatz bei IT-Problemen. Zuletzt bedanke ich mich bei Dr. habil. Jörg Teßmar, Dr. Martha Schamel, Dipl.-Chem. Simone Schäfer, M. Sc. Susanne Meininger, Isabell Biermann und Tanja Dambach für ihr stets offenes Ohr. Bei allen anderen Arbeitskollegen, die hier nicht namentlich erwähnt wurden, möchte ich mich ebenfalls für die gemeinsame Zeit an der FMZ bedanken!

Meiner Familie und meinen Freunden gebührt ein besonderer Dank, da sie immer an mich geglaubt und mir den Rücken gestärkt haben! Danke Lukas, Mama & Papa!